NASA/ OHIO SPACE GRANT CONSORTIUM

2022-2023 ANNUAL STUDENT RESEARCH SYMPOSIUM PROCEEDINGS XXXI

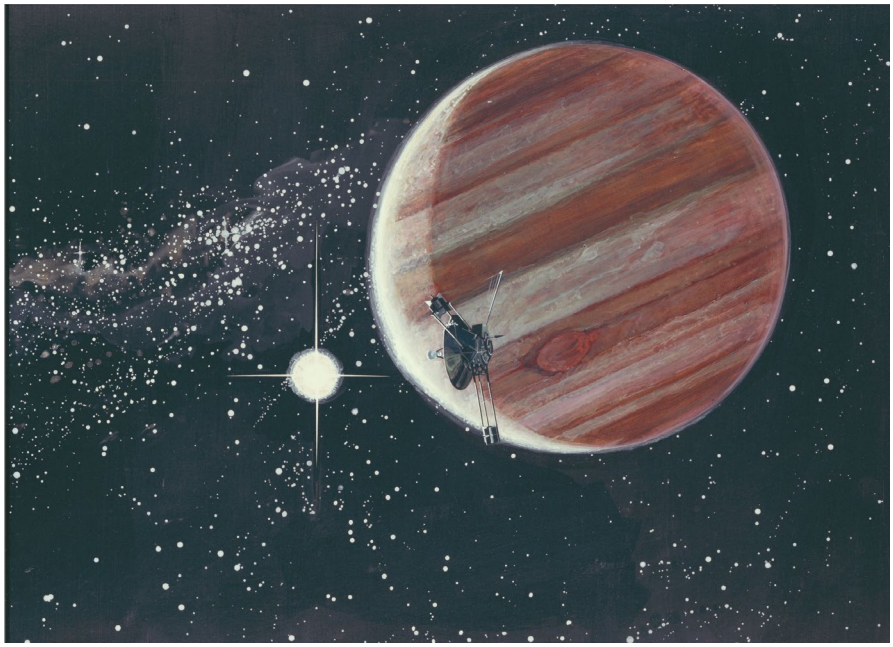

The Pioneer 10 spacecraft passes by the gas giant planet Jupiter. The spacecraft's primary goal was to explore Jupiter, its satellites, its magnetic field, and trapped radiation belts. Pioneer 10 was the first satellite to pass through an asteroid belt and the first spacecraft to obtain detailed images of Jupiter and its moons.

Photo Courtesy of NASA

March 31, 2023
Held at the Ohio Aerospace Institute
Cleveland, Ohio

Follow OSGC on:

Just click on any name, and it will link you to the page immediately!

TABLE OF CONTENTS

FOREWORD

The Ohio Space Grant Consortium (OSGC), a member of the NASA National Space Grant College and Fellowship Program, awards graduate fellowships and undergraduate scholarships to students working toward degrees in Science, Technology, Engineering and Mathematics (STEM) disciplines at OSGC-member universities. The awards are made to United States citizens, and the students are competitively selected. Since the inception of the program in 1989, over 1,455 undergraduate scholarships and 288 graduate fellowships have been awarded.

Matching funds are provided by the 24 member universities/community colleges, the Ohio Aerospace Institute (OAI), and the Ohio Department of Higher Education (State of Ohio).

By helping more students to graduate with STEM-related degrees, OSGC provides more qualified technical employees to industry. The research conducted for the Master's fellowship must be of interest to NASA. A prime aspect of the scholarship program is the undergraduate research project that the student performs under the mentorship of a faculty member. This research experience is effective in encouraging U. S. undergraduate students to attend graduate school in STEM. The Education scholarship recipients are required to attend a workshop conducted by NASA personnel where they are exposed to NASA educational materials and create a lesson plan for use in their future classrooms.

Research reports of students from the following schools are contained in this publication:

Affiliate Members

- The University of Akron
- Baldwin Wallace University
- Cedarville University
- Central State University
- Cleveland State University
- University of Dayton
- Kent State University
- Marietta College
- Miami University
- Ohio Northern University
- The Ohio State University
- Ohio University
- University of Cincinnati
- Wilberforce University
- Wright State University
- Youngstown State University

Community Colleges

- Cincinnati State Technical and Community College
- Lorain County Community College

MEMBER INSTITUTIONS

Affiliate Members	***Campus Representative***
• Baldwin Wallace University	James W. McCargar, Ph.D.
• Case Western Reserve University	Roger D. Quinn, Ph.D.
• Cedarville University	Robert Chasnov, Ph.D., P.E.
• Central State University	Augustus Morris, Jr., Ph.D., P.E.
• Cleveland State University	Wei Zhang, Ph.D.
• Kent State University	Joseph D. Ortiz, Ph.D.
• Marietta College	Dr. Andrew Beck
• Miami University	Jeong-Hoi Koo, Ph.D.
• Ohio Northern University	Jed E. Marquart, Ph.D., P.E.
• The Ohio State University	Dr. Mo Samimy
• Ohio University	Dr. Roxanne Male'-Brune
• The University of Akron	Dr. Julie Zhao
• University of Cincinnati	Dr. Kelly Cohen
• University of Dayton	Dr. Robert J. Wilkens
• The University of Toledo	Dr. Lesley M. Berhan
• Wilberforce University	Deok Hee Nam, Ph.D.
• Wright State University	Mitch Wolff, Ph.D.
• Youngstown State University	Byung-Wook Park, Ph.D.

Community Colleges	***Campus Representative***
• Cincinnati State Technical and Community College	Professor Abigail Yee
• Columbus State Community College	Professor Jeffery M. Woodson, M.S., I.E.
• Cuyahoga Community College	Prof. Michelle S. Davis
• Lakeland Community College	Professor Rick Bartlett
• Lorain County Community College	Regan L. Silvestri, Ph.D.
• Sinclair Community College	Eric C. Dunn

NASA Glenn Research Center - Representatives

- Dr. M. David Kankam
- Ms. Susan M. Kohler

ACKNOWLEDGMENTS

Thank you to all who helped with the OSGC's 31st Annual Research Symposium!

OSGC Alumni Panel:

★ Joshua Allen, NASA Glenn Research Center

★ Eleana Cintron, Case Western Reserve University

★ Robert Wilson, Swagelok

★ Em Williams, Lorain County Community College

Campus Representatives – 4-Year Universities

- Dr. James W. McCargar, Baldwin Wallace University
- Dr. Roger Quinn, Case Western Reserve University
- Robert Chasnov, Ph.D., P.E., Cedarville University
- Augustus Morris, Jr., Ph.D., P.E., Central State University
- Wei Zhang, Ph.D., Cleveland State University
- Dr. Joseph D. Ortiz, Kent State University
- Dr. Andrew Beck, Marietta College
- Jeong-Hoi Koo, Ph.D., Miami University
- Jed E. Marquart, Ph.D., P.E., Ohio Northern University
- Dr. Mo Samimy, The Ohio State University
- Dr. Roxanne Male'-Brune, Ohio University
- Dr. Julie Zhao, The University of Akron
- Dr. Kelly Cohen, University of Cincinnati
- Dr. Robert J. Wilkens, University of Dayton
- Dr. Lesley M. Berhan, The University of Toledo
- Deok Hee Nam, Ph.D., Wilberforce University
- Mitch Wolff, Ph.D., Wright State University
- Dr. Byung-Wook Park, Youngstown State University

Campus Representatives - Community Colleges

- Professor Abigail Yee, Cincinnati State Technical and Community College
- Professor Jeffery M. Woodson, M.S., I.E., Columbus State Community College
- Professor Michelle S. Davis, Cuyahoga Community College
- Professor Rick Bartlett, Lakeland Community College
- Regan L. Silvestri, Ph.D., Lorain County Community College
- Eric C. Dunn, Sinclair Community College

Special thanks go out to the following:

- Dr. John Sankovic, President and CEO – OAI, for supporting the OSGC and hosting this event.
- Mark Cline, Senior Manager, Information Technology – OAI, whose expertise made the hybrid medium not only possible, but a huge success!
- Robert Romero, Director – OSGC, for his enthusiasm and vigor in leading the Ohio Space Grant Consortium.
- Em Williams, Program Assistant – OSGC, for pulling together our rockstar panel and providing a fresh perspective to the program.
- Sam Santos, Program Assistant – OSGC who is on the spot to assist team and students alike throughout the day.
- Jill Marconi, K-12 Specialist – OSGC, who brings in the inner child out in the team and the STEM professional out of our pre-college students.
- All of our presentation evaluators providing insight to our students: Michelle Davis, Scott Halfhill, Dr. Dave Kankam, Susan Kohler, Dr. Roxanne Male'-Brune, Jill Marconi, Mike Marconi, Dr. James McCargar, Christopher Morris, Devon Sheehy, and Dr. Mitch Wolff.

31st Annual OSGC
Student Research Symposium

The 2023 Student Research Symposium was held in-person at the Ohio Aerospace Institute.

2023 OSGC STUDENT RESEARCH SYMPOSIUM
Hosted By: Ohio Aerospace Institute (OAI)
22800 Cedar Point Road • Cleveland, OH 44142
• (440) 962-3000
Friday, March 31, 2023

AGENDA

8:00 AM – 8:30 AM	Sign-In / Continental Breakfast / Student Portraits (30 minutes) ..... Lobby
8:35 AM – 8:40 AM	Welcome to OAI (5 minutes) ..... Forum (Lobby Level) *Dr. John Sankovic* President and Chief Executive Officer, Ohio Aerospace Institute
8:40 AM – 8:45 AM	Welcome and Introductions (5 minutes) *Robert Romero* Director, Ohio Space Grant Consortium
8:45 AM – 8:50 AM	Symposium Logistics (5 minutes) *Tim Hale* Program Manager, Ohio Space Grant Consortium
8:50 AM – 9:00 AM	Group Photograph (10 minutes) ..... Lobby / Atrium Stairwell
9:00 AM – 11:00 AM	Student Oral Presentations – Senior Scholars and Fellows (120 minutes) •Group 1 ..... Forum (Lobby Level) •Group 2 ..... Presidents' Room (Lower Level) •Group 3 ..... Industry Room (2nd Floor) •Group 4 ..... Board Room (2nd Floor)
11:00 AM – 12:15 PM	Various Displays (75 minutes) •Student Poster Presentations ..... Lobby Junior, Community College, and Pre-Service Teacher (Education) Scholars •Industry Displays ..... Lobby
12:15 PM – 1:15 PM	Luncheon Buffet (60 minutes) ..... Atrium / Sunroom (Lower Level)
1:15 PM – 2:15 PM	Panel Discussion and Q&A (60 minutes) ..... Forum (Lobby Level) *"Launching a STEM Career"*
Panel Members:	
2:15 PM – 2:30 PM	Presentation of Best Poster Awards (15 minutes) ..... Forum
2:30 PM	Symposium Adjourns

SENIOR & FELLOWSHIP PRESENTATIONS

OHIO AEROSPACE INSTITUTE

OHIO SPACE GRANT CONSORTIUM

Lauren Meisberger (Cedarville University) demonstrates her project “Recovery System for a High Powered Rocket”.

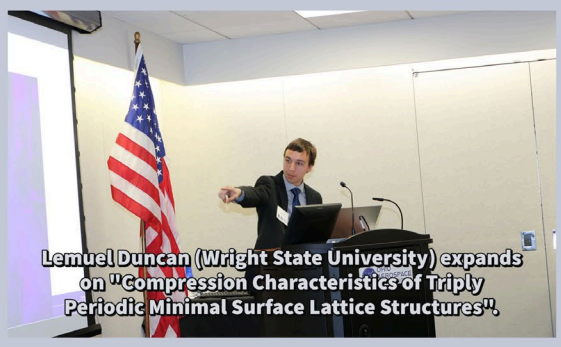

Lemuel Duncan (Wright State University) expands on "Compression Characteristics of Triply Periodic Minimal Surface Lattice Structures".

Alexandra Filiatraut (Miami University) elaborates her project "Machine Learning-Based Study of Building Block Interactions and Material Properties of Soft Matter Systems".

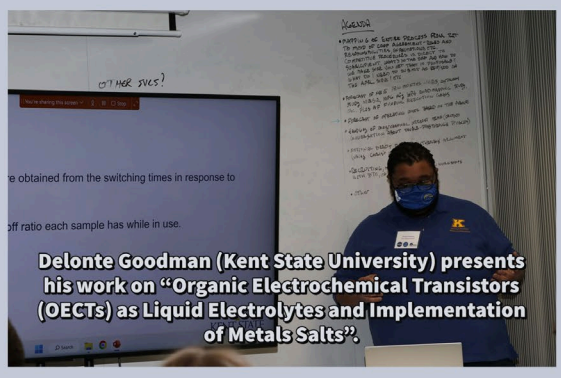

Delonte Goodman (Kent State University) presents his work on “Organic Electrochemical Transistors (OECTs) as Liquid Electrolytes and Implementation of Metals Salts”.

Calvin Coffin (Ohio University) shares his study "Characterizing Transcription Factor Activity at the Heart of the Arabidopsis Gravity Response".

Rebecca Gilligan (University of Cincinnati) reveals her work on "Characterizing Transcription Factor Activity at the Heart of the Arabidopsis Gravity Response".

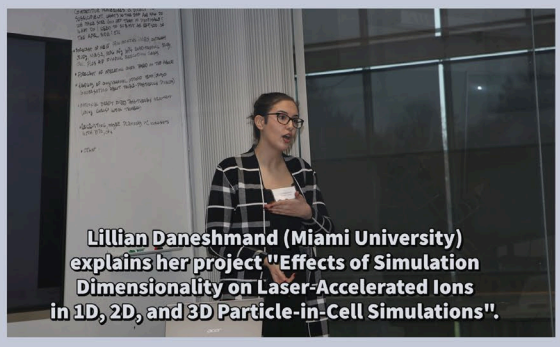

Lillian Daneshmand (Miami University) explains her project "Effects of Simulation Dimensionality on Laser-Accelerated Ions in 1D, 2D, and 3D Particle-in-Cell Simulations".

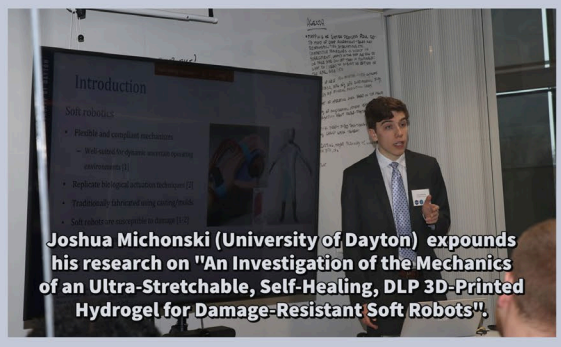

Joshua Michonski (University of Dayton) expounds his research on "An Investigation of the Mechanics of an Ultra-Stretchable, Self-Healing, DLP 3D-Printed Hydrogel for Damage-Resistant Soft Robots".

SENIOR & FELLOWSHIP PRESENTATIONS

OHIO AEROSPACE INSTITUTE

OHIO SPACE GRANT CONSORTIUM

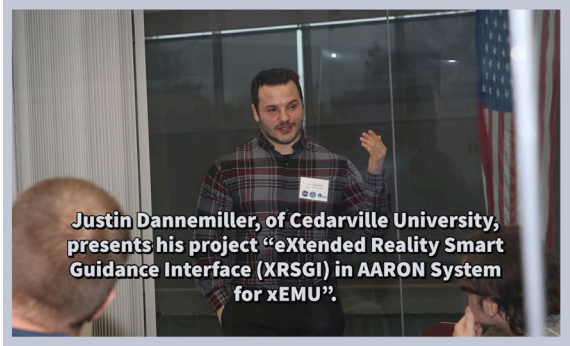

Justin Dannemiller, of Cedarville University, presents his project “eXtended Reality Smart Guidance Interface (XRSGI) in AARON System for xEMU”.

Abhilash Yarlagadda, of The Ohio State University, displays his aim on "Directivity of Far-Field Noise in Supersonic Rectangular Twin Jets".

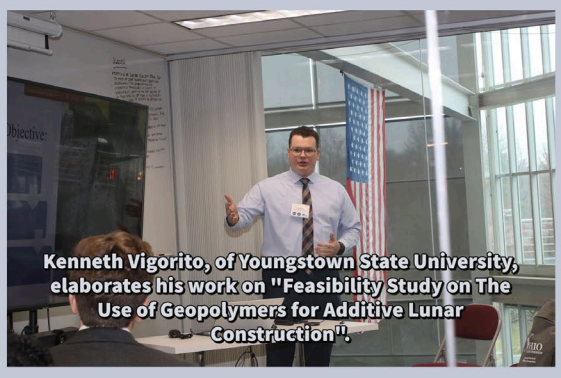

Kenneth Vigorito, of Youngstown State University, elaborates his work on "Feasibility Study on The Use of Geopolymers for Additive Lunar Construction".

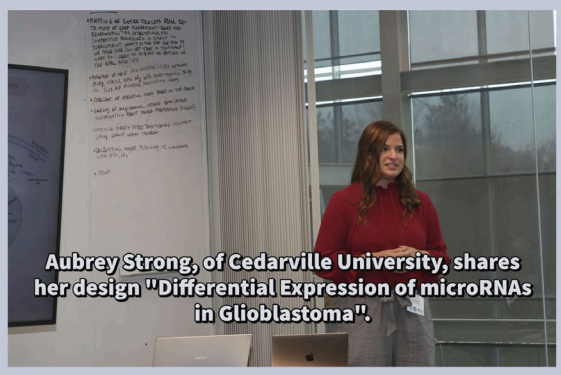

Aubrey Strong, of Cedarville University, shares her design "Differential Expression of microRNAs in Glioblastoma".

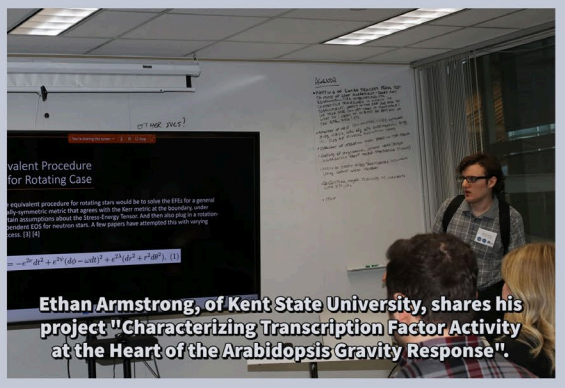

Ethan Armstrong, of Kent State University, shares his project "Characterizing Transcription Factor Activity at the Heart of the Arabidopsis Gravity Response".

Grant Guggenbiller, of Ohio University, presents his work on “Electrospinning Photopolymer Fibrous Mats Derived From Salicylic Acid With Tunable Morphology".

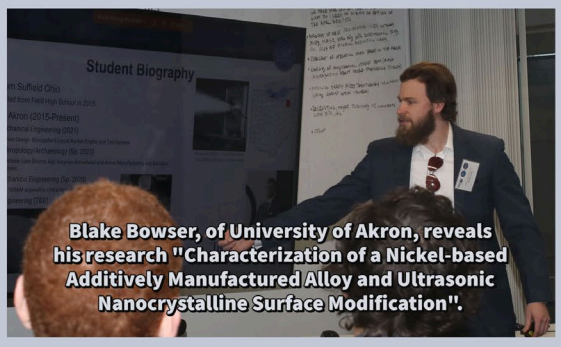

Blake Bowser, of University of Akron, reveals his research "Characterization of a Nickel-based Additively Manufactured Alloy and Ultrasonic Nanocrystalline Surface Modification".

Alyssa Reinhardt, of Kent State University, shines light on her effort "Using Remote Sensing to Predict Seasonal Controls on Soil Respiration and Weathering Across a Watershed".

STEM, EDUCATION, & COMMUNITY COLLEGE PRESENTATIONS

OHIO AEROSPACE INSTITUTE

OHIO SPACE GRANT CONSORTIUM

Tyreese Bernard (Wilberforce University) displays his work on “Space Radiation Protection for Space Travel”.

Emily Bursk (Cincinnati State Technical and Community College) shares her project "Discovering the Distant Universe Using Strong Gravitational Lensing".

Anya zurBurg (Cedarville University) presents her lesson design on "Bottle Rockets and Trajectory".

Chaz Stump (University of Cincinnati) reveals his lesson "Levels of Engagement, Prediction, and Discussion for Students with Disabilities When Given a Lesson on Deep Space ".

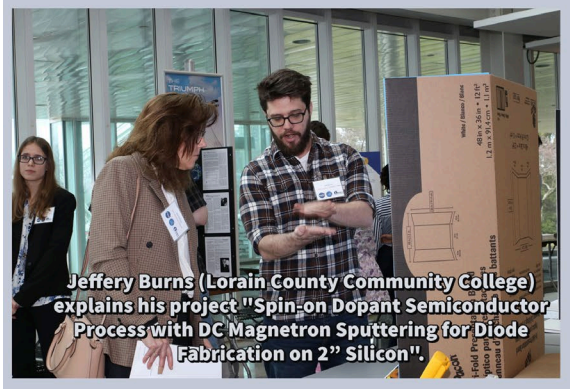

Jeffery Burns (Lorain County Community College) explains his project "Spin-on Dopant Semiconductor Process with DC Magnetron Sputtering for Diode Fabrication on 2” Silicon".

Cora Gill (The University of Cincinnati) exhibits her lesson on “Creating an Ecosystem on Another Planet".

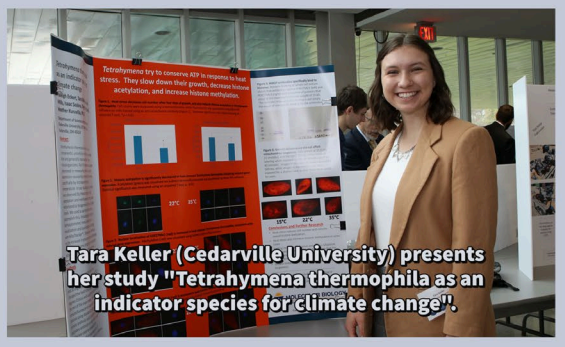

Tara Keller (Cedarville University) presents her study "Tetrahymena thermophila as an indicator species for climate change".

Matthew Ripple (The University of Akron) unveils his lesson build on "The Human Impact on Global Climate".

Fellows

Characterization of a Nickel-based Additively Manufactured Alloy and Ultrasonic Nanocrystalline Surface Modification

Student Researcher: Blake A. Bowser

Advisor: Dr. Gregory N. Morscher

The University of Akron
Mechanical Engineering and Materials Science

Abstract

Jet propulsion and gas turbine engines are presently extraordinary systems that require materials that can withstand high load, temperature, and highly corrosive environments. Considering this, components within these propulsive systems can be highly complex and made from advanced materials and alloys. When repairs are needed, it can cause significant downtime for a flight vehicle due to component lead times as well as a consistently high cost of replacement when using conventional manufacturing techniques for advanced materials. With the advent of additive manufacturing (AM), methodologies such as Directed Energy Deposition (DED) can be used to provide repairs on an existing wrought component, significantly reducing repair lead times, and considerably decreasing cost of service. Due to this, Nickel-based superalloys optimized for additive manufacturing processes are of high interest regarding this application. The Nickel-based superalloy (ABD-900AM) provided by the Air Force Research Lab (AFRL) will be analyzed using Non-Destructive Evaluation (NDE) techniques such as acoustic emission (AE), digital image correlation (DIC), and electrical resistance (ER) to characterize flaw propagation for the materials in various build orientations and manufacturing techniques under uniaxial tension and fatigue testing. The microstructural properties of the material will also be characterized via SEM, digital microscopy, and other analysis techniques.

Project Objectives

The purpose will be to characterize the materials via mechanical testing with the associated NDE techniques and analyze the intrinsic differences in mechanical properties in differing build orientations similar to Shrestha et al. [1]

Methodology

Mechanical testing was completed in uniaxial tension, high cycle fatigue, and FCG testing for each material. ABD-900AM Nickel-based samples specifically will be tested. Once completed, test data will be compiled, and fracture propagation data will be extracted from the NDE techniques presented and fracture propagation characteristics will be enumerated and cross-examined for each orientation type. Digital microscopy and SEM will also be completed to analyze the microstructure of each build orientation, as well as fractography to analyze fracture characteristics.

Results

Tensile testing and high cycle fatigue testing was completed on three different build orientations of ABD-900AM. Vertically, horizontally, and 45-degree built specimens were manufactured by laser powderbed manufacturing. 45-degree specimens showed the highest performance in HCF as well as uniaxial tensile testing, while horizontal and vertical specimens showed varying performance. More specimens will be required to provide a higher accuracy in understanding mechanical properties for the material in the different build orientations. Due to project timeline constraints, fatigue crack growth

(FCG) testing will be completed after the completion of this report writing for OSGC. Fractography on specimen fracture surfaces indicated tendencies for intergranular fracture. In the case of 45-degree specimens, this causes high amounts of crack branching in comparison to vertical and horizontal specimens, which increases strain to failure and yield/ultimate tensile strength for 45-degree specimens and coincidentally provides higher performance in fatigue.

Figures

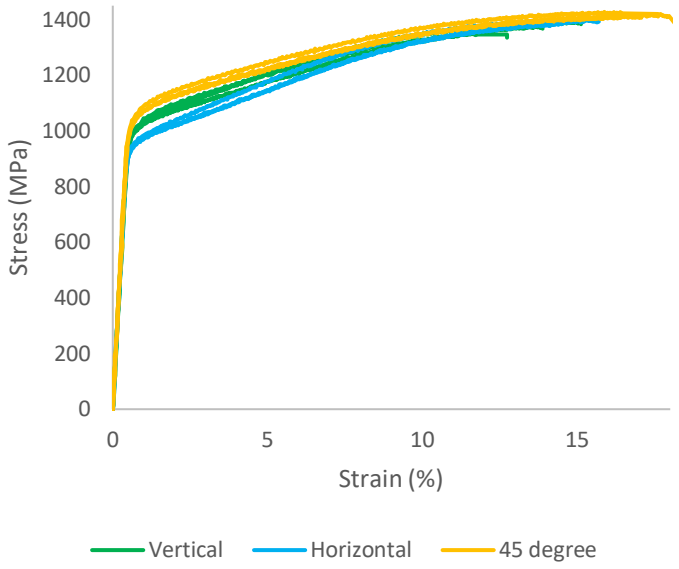

Figure 1 - Stress over Strain curve indicating higher performance for 45-degree built specimens compared to vertically and horizontally built specimens.

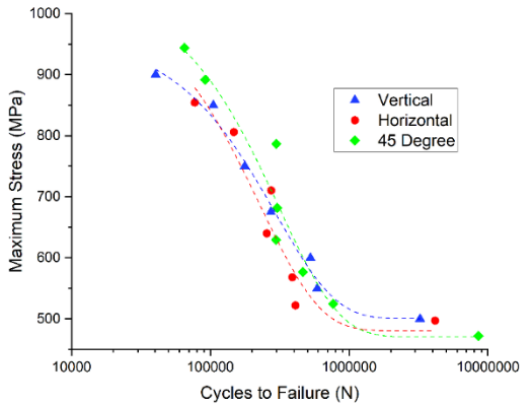

Figure 2 - High cycle fatigue (HCF) stress over cycles to failure curve

References

[1] Shrestha, Sulochana, et al. "In-situ fatigue life analysis by modal acoustic emission, direct current potential drop and digital image correlation for steel." *International Journal of Fatigue* 142 (2021): 105924.

Characterizing Transcription Factor Activity at the Heart of the Arabidopsis Gravity Response

Student Researcher: Calvin Coffin

Advisor: Dr. Sarah Wyatt

Ohio University
Department of Environmental and Plant Biology

Abstract
Gravity is among the most critical of environmental cues in shaping plant growth; however, its ubiquity on Earth limits available options in the study of the plant gravity response. NASA has circumvented this obstacle by hosting experiments in the microgravity environment of the International Space Station. The collection of gene expression data via RNAseq and microarray analyses of Arabidopsis seedlings grown in space has provided a wealth of data regarding how plants respond to this unique gravity condition. When intersected with similar expression data from terrestrial plants exposed to an alternate gravity stimulus - a new gravity vector - several novel components in the gravity signaling pathway have been implicated. Of particular interest in the analysis were transcription factors, for their role in regulating downstream expression patterns. Two transcription factors were identified at this basal level of the Arabidopsis gravity response: ERF104, which is upregulated on earth in response to a new gravity vector and downregulated in microgravity, and IQD21, which displays the inverse expression pattern. A third gene, CIB1, was shown to be upregulated in both scenarios. Phenotypic characterizations of mutant lines of each of these genes show significant gravity sensitivity in the root tip and/or shoot, confirming their gravitropic role. Human Influenza Hemagglutinin (HA) tagged fusion lines of each of these proteins have been generated and placed under the control of a constitutive promoter. These lines are enabling chromatin immunoprecipitation followed by sequencing (ChIP-Seq) to identify the binding sites of these three transcription factors in the Arabidopsis genome, and consequently to infer their downstream targets. Paired with qPCR analyses targeting the expression patterns of each protein in response to gravistimulation, this research will help to contextualize and clarify the gravity response pathway as well as shed light on the complex web of interconnected signaling events it entails.

Project Objectives
Aim 1. We will use ChIP-seq to identify the DNA-binding sites of the TFs CIB1, ERF104, and IQD21 on the Arabidopsis genome.
Aim 2. By identifying genes downstream of these binding motifs, we will generate a list of genes potentially regulated by each of these three TFs.
Aim 3. qRT-PCR analysis of the expression patterns of each target protein in root tissue post-reorientation will provide an understanding of the dynamic transcriptional environment resulting from a gravitational stimulus.

Methodology Used
The regulatory role of TFs makes them attractive targets in clarifying signaling pathways. One of the most powerful technologies available in TF characterization is chromatin immunoprecipitation followed by sequencing (ChIP-seq). To this end, human influenza hemagglutinin (HA) tagged fusion constructs of each of our TFs have been transformed into their respective mutant backgrounds, to avoid competition with endogenous WT protein. These fusion proteins will be chemically crosslinked on their DNA binding sites in the Arabidopsis genome, DNA extracted and sonicated to shear the chromatin into small fragments. Those fragments bound to the TFs of interest will be precipitated using anti-HA antibodies, and the protein/chromatin complex chemically disassociated. The DNA fragments will then be sequenced and aligned to the Arabidopsis genome, providing valuable clues as to the regulatory action of these fundamental actors in the plant gravity response.

Regarding the qRT-PCR, specialized primers have been designed against transcripts of each of the three TF targets. RNA extractions were performed on Arabidopsis roots at the 2, 5, 10, and 30 minute timepoints post reorientation. The plants extracted from were plated on MS media and grown vertically for 5 days, after which the plates were reoriented 135 degrees against the vertical vector.

Results Obtained

Though the ChIP-seq protocol is still ongoing, preliminary results to confirm the eventual efficacy of the procedure have been done. These involve PCR analyses to confirm the presence of the HA-tagged constructs within the Arabidopsis genome, RT-PCR analyses to confirm transcription of the insert, Western blotting to confirm protein expression and viability of the anti-HA antibody in finding and pulling down these tagged proteins, and complementation assays to determine if my fusion lines can rescue the gravitropic mutant phenotypes in their respective knockout lines.

Significance and Interpretation of Results

RT-PCR analysis shows mRNA transcripts are being produced that correspond with the expected lengths of each of the HA-tagged fusion constructs (Figure 1). Translation into protein, and the ability of the anti-HA antibody to find these tagged TFs, was confirmed via Western blot (Figure 2). Complementation assays observing the gravitropic phenotypes of the lines were carried out demonstrating rescue of the mutant phenotype (Figure 3). These analyses were necessary to ensure that the eventual results of the ChIP could be trusted – if my fusion lines were not able to rescue the mutant phenotype, it would indicate that the proteins being expressed are not acting as they would in a wild-type plant – that is to say, they are not binding to the correct sites on the chromatin or regulating expression in the same way, rendering me unable to infer their proper targets from my eventual results.

Figures

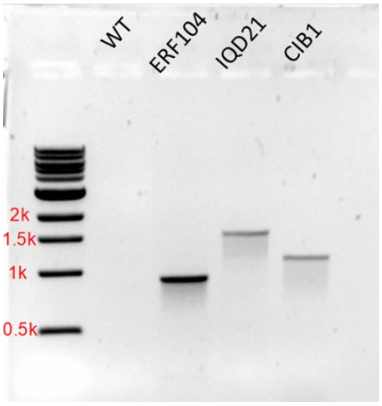

Figure 1: RT-PCR analysis showing mRNA bands corresponding to the expected length of each fusion construct

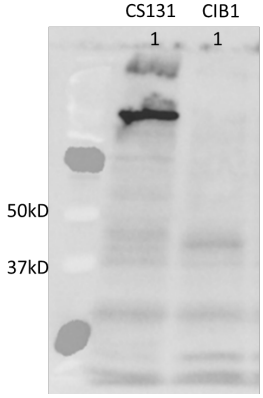

Figure 2: Western blot demonstrating expression of CIB1 fusion protien (38kDA). CS131 is a triple HA tagged GI line used as a positive control

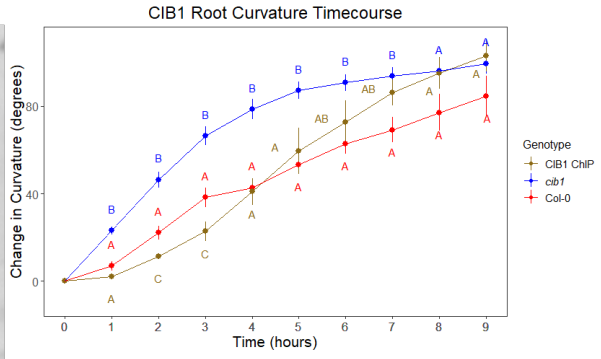

Figure 3: Complementation assay of root curvature in response to reorientation in the cib1 mutant, wild-type, and CIB1 ChIP line, respectively.

Acknowledgements

I would like to acknowledge Dr. Wyatt, as well as contributing Wyatt lab members Dr. Colin Kruse, Bailey Erickson, and Wafa Aziz. I would also like to thank funding sources NASA/GeneLab (grant #80NSSC22K0366) and the Ohio Space Grant Consortium.

Impedimetric Determination of Cortisol Levels Using Gold Nanoparticles Functionalized Laser Induced Graphene Electrode for Smart Wound Dressing Application

Student Researcher: Kyle C. Duke

Advisor: Dr. Byung-Wook Park

Youngstown State University
Chemical Engineering

Abstract

Wearable biosensors have become an important tool for their promising applications in personalized medicine. Cortisol is a biomarker for various diseases and plays an important role in metabolism, blood pressure regulation, and glucose levels. In this study, we fabricated a BSA/AB/MPA/AuNP/LIG laser-induced graphene (LIG) biosensor for the non-faradaic impedimetric detection of cortisol in sweat. Surface characterization of the LIG was performed at each step of modification by Electrochemical impedance spectroscopy (EIS) in a phosphate buffered saline (PBS) solution containing a 5 mM Fe(CN)63-/4- (1:1) redox couple. Further characterization of the modified LIG electrode was achieved through Scanning electron microscope (SEM), surfaced-enhanced Raman spectroscopy (SERS), and X-ray diffraction (XRD). The detection experiment using EIS was carried out in increasing concentrations of cortisol (0.1 pM-100 nM) in PBS. The Z_{Mod} decreased logarithmically (R^2=0.89) with a 1.83 nM limit of detection. Reproducibility was examined by percent change of Z_{Mod} at 100 nM and a 10.21 %RSD (n=5) was observed . Additional analysis of sensor specificity and interference studies showed no substantial effect on detection. This research establishes the feasibility of using the gold nanoparticle decorated LIG electrode for flexible, wearable cortisol sensing devices, which would pave the way towards an end-user easy-to-handle biosensors as point-of-care diagnostics.

Objective

The objective of this project is to fabricate and then evaluate the sensors performance through various experiments. The overall goal is to incorporate the sensor into a wearable sensor platform for point-of care applications.

Methodology Used

Fabrication of bare LIG and gold nanoparticle (AuNP) modified LIG electrodes

The LIG electrode was obtained by subjecting PI to CO_2 laser cutter. After the LIG formation ,the LIG/PI film was rinsed with acetone and 2-propanol followed by oxygen plasma treatment for 30 seconds to increase wettability on the surface[1]. Each LIG electrode was individually treated with a copper foil tape placed over the connection point, and the body of the electrode was insulated with a 5-minute epoxy. To obtain the gold nanoparticle (AuNP) modified laser induced graphene (LIG) electrode, gold nanoparticles (AuNP) were electrochemically deposited on the LIG surface via cyclic voltammetry (CV) for 10 cycles in a 1 mM $HAuCl_4$ in 0.1 M KNO_3 solution.

Immobilization of cortisol antibody on AuNP-LIG

To immobilize anti-cortisol antibody on the AuNP sites on the LIG electrode, thiol chemistry was used. The self-assembled monolayer of MPA was formed on the AuNP by incubating the LIG in a 10 mM MPA in ethanol for 1 hour at room temperature followed by a rinse with ethanol and DI

water. Next, the terminal carboxylic acid groups of the MPA were activated to immobilize anti-cortisol antibody through incubation in a 0.1 M MES buffer containing 40 mM EDC and 100 mM Sulfo-NHS for 1 hour at room temperature. To obtain the antibody immobilized AuNP-LIG electrode, the activated electrode was incubated in an anti-cortisol antibody solution at 5 μg/mL in 10 mM PBS for 2 hours. Lastly, to minimize undesired unspecific adsorption on the surface of the LIG, the electrode was incubated in a 1 % BSA in 10 mM PBS.

Electrochemical characterizations using EIS

To verify the LIG underwent surface modification, EIS was performed with a Gamry Interface 1010E Potentiostat. A three-electrode system in a conventional glass-made cell was used for EIS measurements with the modified LIG electrode as a working electrode, a platinum wire as a counter electrode, and saturated calomel electrode (SCE) as a reference electrode. The EIS measurements were carried out in 5 mM $Fe(CN)^{3-}/Fe(CN)^{4-}$ PBS solution as a supporting electrolyte. Impedance spectra were collected in the frequency range from1 Hz to 100 kHz with a potential amplitude of 10 mV rms at 10 points per decade. EIS results were analyzed by fitting the experimental impedance data to electrical equivalent circuit models.

SEM/EDX

The JIB-4500 MultiBeam integrated with SEM-EDS was used for SEM imaging and EDX analysis on LIG and AuNP/LIG. SEM images were collected at an electron energy of 15kV for 15,000x, 500x, and 100x magnifications for morphology characterization and verification of AuNP electrodeposition. EDS characterization was carried out at 5000x magnification with an electron energy of 138 eV for the elemental analysis of the LIG and AuNP/LIG.

XRD

XRD was performed with a Bruker X8 Prospector Ultra (Billerica, MA, USA) via Cu radiation to characterize the structures of the samples. XRD spectra of PI film, LIG, and AuNP were obtained, and the peaks were analyzed to show the degree of graphitization and defect after formation of the graphitic structure, and further verify the presence of electrodeposited AuNP on the LIG surface.

Raman spectroscopy

Raman spectroscopy is a commonly used technique to examine chemical structure and crystallinity. In this study, Raman spectra were collected using the Horiba iHR320 (Kyoto, Japan) at 531.4 nm laser with a 1800g/mm diffraction gratings to examine the degree of graphitization on the PI film.

Detection of cortisol

EIS of the BSA/Ab/EDC/NHS/AuNP/LIG exposed to increasing cortisol concentrations (0.1 pM-100 nM) in 10mM PBS was conducted using a 3-electode set up comprised of the modified LIG (working electrode), platinum wire (counter electrode), and a saturated calomel electrode (SCE) (Reference electrode). After each cortisol injection, the solution was incubated for 30 minutes, after which EIS was taken 3 times to obtain an average with a standard deviation. Z_{mod} values at 200 Hz were collected at each concentration for calibration.

Results and discussion

Electrochemical characterization for surface modification

The electrochemical characterization of the different electrodes (LIG, AuNP/LIG, Ab/AuNP/LIG, and BSA/Ab/AuNP/LIG) was carried out using EIS from 1-100000 Hz. The AuNP/LIG electrode showed the lowest R_{ct} (30.98 ±3.59 Ω), indicating electrodeposition of AuNP effectively increased the conductivity of the surface. Following the AuNP/LIG, EDC/NHS/AuNP had a R_{ct} of 34.83 ± 7.38 Ω indicating SAM immobilization of 3-MPA, followed by the attachment of EDC/NHS. Incubation of the anti-cortisol antibody saw an increase of 144% (46.32 ± 2.43), signifying the bonding of large amounts of the antibody to the surface. All steps leading to antibody immobilization resulted in a lower R_{ct} than the bare LIG (50.42± 11.02) further supporting AuNP electrodeposition effectively increased the sensors overall conductivity, thus improving its overall sensitivity and functionality. Finally, the addition of the blocking agent BSA to the Ab/AuNP/LIG saw a further 168% increase in R_{ct} (77.84 ± 4.04) indicating a large portion of the unmodified surface was successfully covered.

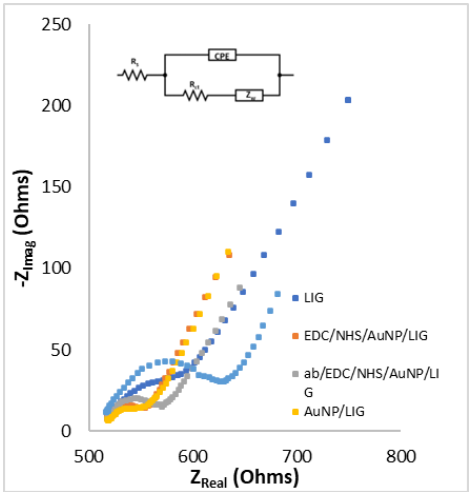

Figure 1. Nyquist plot of each step-in surface modification (n=3).

SEM-EDX

The morphology of the LIG and AuNP/LIG surface was examined through SEM imaging at various magnifications with further analysis of the elemental composition achieved by EDX. The porous 3D structure of LIG and AuNP/LIG is clearly exhibited in (Figure 2 A-D). Bright spots were shown (Figure 2D) after the formation of AuNP via electrodeposition.

Results from EDS characterization for LIG and AuNP/LIG are shown in (Figure 3). The fabricated LIG is comprised of 100 wt% carbon with AuNP/LIG comprised of 93.54 wt% carbon with the remaining 6.46 wt% gold, further conforming successful electrodeposition of AuNP's. The absence of other elemental peaks indicates a pristine surface with undetectable traces of contaminants.

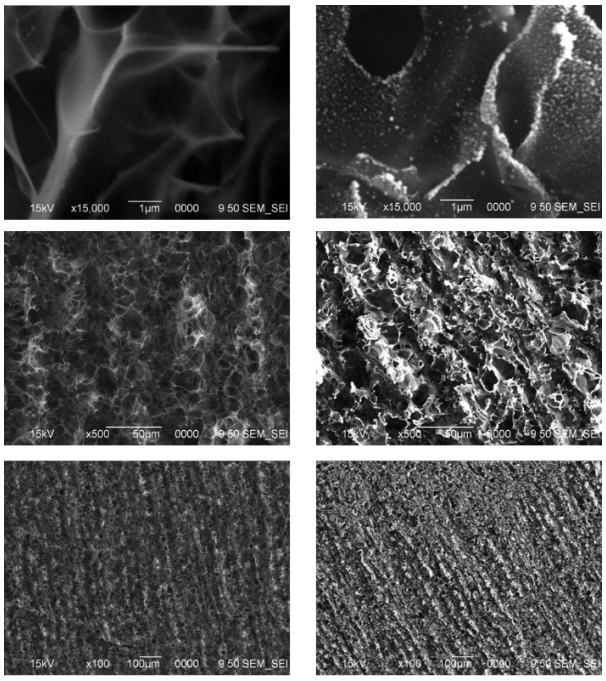

Figure 2. SEM of LIG and AuNP-LIG

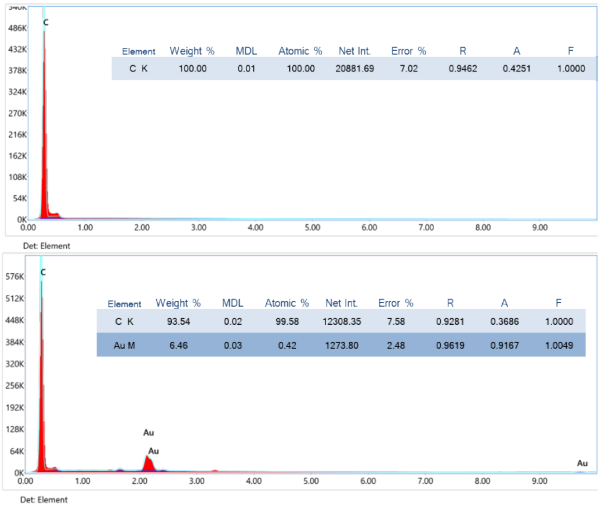

Figure 3. EDS of LIG and AuNP/LIG electrodes.

XRD

Successful graphene formation, and deposition of Au on the LIG is confirmed by X-ray diffraction (XRD). Shown in (Figure 4A) LIG exhibited a short peak at ~26 ° which is attributed to low crystallinity and low diffraction [2]. AuNP/LIG exhibited reflections of Au face-centered cubic crystallographic structure (38°, 44°, 64°, and 77°) signifying AuNP were successfully deposited on the LIG [3, 4]. The short peak observed at ~26 ° is indicative of a highly graphitized surface, thus increasing the surface area and consequently the available bonding sites for reagents.

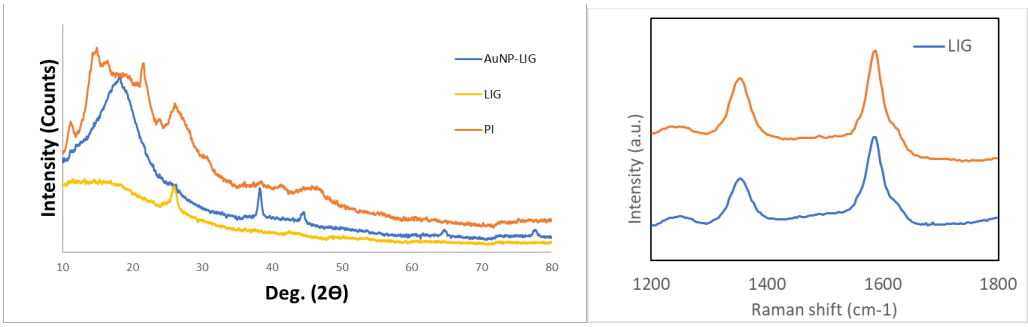

Figure 4. XRD (Left) and Raman spectra (Right of PI, LIG, and AuNP/LIG

Raman Spectroscopy

Raman spectra of LIG and AuNP/LIG shows both D (defect states) and G (graphitic states) bands at around 1350 cm^{-1} and 1590 cm^{-1} respectively (Figure 4B). The intensity ratio, I_D/I_G, represents the degree of graphitization that occurred, and was found to be 0.475 and 0.548 for LIG and AuNP/LIG. The increase in intensity is the result of interactions between the gold nanoparticles and graphene surface with an increase in disorder of the graphitic structure [5].

Detection of cortisol

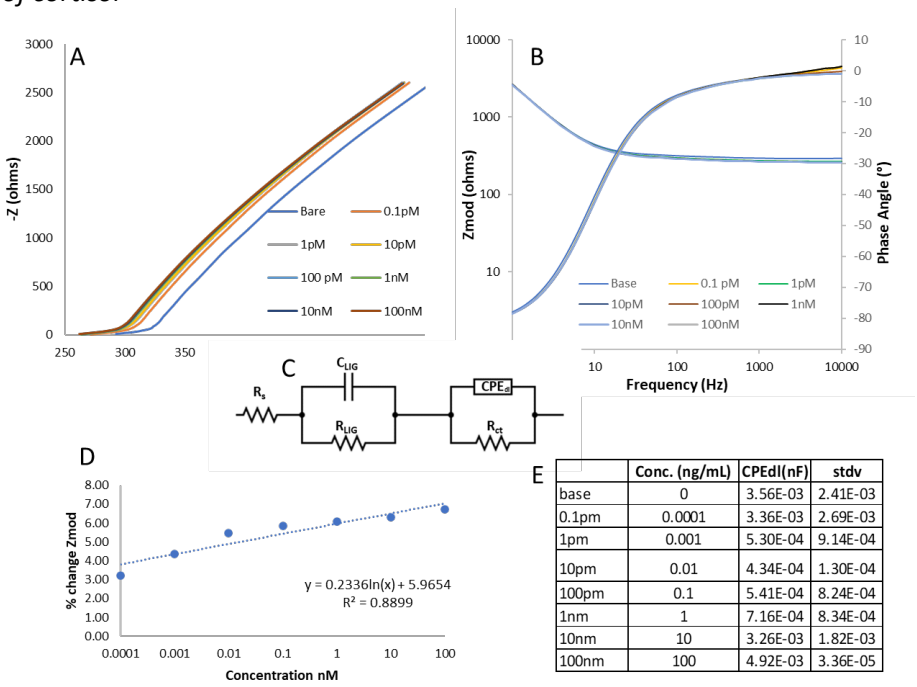

	Conc. (ng/mL)	CPEdl(nF)	stdv
base	0	3.56E-03	2.41E-03
0.1pm	0.0001	3.36E-03	2.69E-03
1pm	0.001	5.30E-04	9.14E-04
10pm	0.01	4.34E-04	1.30E-04
100pm	0.1	5.41E-04	8.24E-04
1nm	1	7.16E-04	8.34E-04
10nm	10	3.26E-03	1.82E-03
100nm	100	4.92E-03	3.36E-05

Figure 5. (A) Nyquist plot and (B) Bode plot for increasing cortisol concentrations. (C) LIG equivalent circuit model. (D) Cortisol dose response and corresponding CPE_{dl} values (E).

The Nyquist plot in (Figure 5A) shows how the BSA/Ab/AuNP/LIG EIS response changed with respect to increasing dose of cortisol (0.1pM-100 nM). As cortisol dose concentration increases, the formation of the cortisol-antibody complex increases the capacitive reactance (CPE_{dl}) and causes the observed shift in the Nyquist plot and Bode plot in (Figure 5B). The Z_{mod} value at 200

Hz was taken for each concentration and the percent change was calculated for (Figure 5D). The sensor exhibited a logarithmic response with an overall 6.74% change in Z_{mod} over the tested range. However, a near linear response (R^2=0.8104) with a sensitivity of 518.02 Ω/nM and a limit of detection (3σ/S) of 0.015 nM was observed from 0.1 pM-10 pM. The modified Randal's equivalent circuit in (Figure 5C) was used to obtain the CPE_{dl} values [6]. As concentration increased, the . EDL values of the capacitance (C_{LIG} & CPE_{dl}) increased after each successive injection.

EIS was ran at an applied sine wave potential of 10 mV over a frequency range of 1-100,000 Hz for increasing cortisol concentrations [0.1 pM-100 nM]. At lower frequencies around 10 Hz, diffusion driven mechanisms dominate[7]. As such, Zmod values were taken at the higher frequency of 200 Hz. Under non-faradaic conditions, parameters associated with electron transfer such as charge transfer resistance (R_{ct}) and Warburg impedance are negligible as they become infinite due to slow electron transfer [8, 9]. Therefore, imaginary impedance is inversely proportional to the electrical double layer capacitance, represented as (CPE_{dl}). Furthermore, the interaction between the immobilized anti-cortisol antibody and cortisol at the electrode surface Ab/AuNP/LIG and BSA/Ab/AuNP/LIG samples creates a change in capacitance at the electric double layer. This phenomenon can be observed in (Figure 5A) where decrease in imaginary impedance at 200 Hz is observed with increase in the concentration of cortisol [10]. Consequently, the decrease in impedance and increase in CPE_{dl} can be explained by the increase in cortisol [11].

Due to LIG's 3D graphitic structure the surface is rough and heterogeneous creating the appearance of a CPE global impedimetric response at high frequencies, resulting in a phase angle that is independent of frequency[12]. Consequently, modeling of electrical double layer capacitance is represented by CPE_{dl} in the modified Randle's circuit (Figure 5C).

Reproducibility/Repeatability

To examine the efficacy of the modified electrode, reproducibility was performed by independently incubating five BSA/Ab/AuNP/LIG in 100 nM of cortisol for 30 minutes and comparing the percent change in Z_{mod} before incubation. The low RSD of 10.24 % shows no significant deviation in sensor response and demonstrates its potential for real world applications.

Under the experimental conditions for cortisol dose response, the repeatability of the BSA/Ab/AuNP/LIG was investigated by three replicant measurements to obtain Z_{mod} at 200 Hz for each concentration (0.1pM-100nM). The corresponding %RSD values in Table 1 display the biosensors excellent repeatability. A maximum of only 0.41 %RSD observed at 1pM, representing an outstanding analytical performance when compared to recent works [6, 13].

Concentration	%RSD
0.1 pM	0.17
1 pM	0.41
10 pM	0.25
100 pM	0.19
1 nM	0.13
10 nM	0.19
100 nM	0.02

Table 1. Repeatability (n=3) for Z_{mod} values obtained at 200 Hz.

References

1. Cheng, C., et al., *Bisphenol A Sensors on Polyimide Fabricated by Laser Direct Writing for Onsite River Water Monitoring at Attomolar Concentration.* ACS Applied Materials & Interfaces, 2016. **8**(28): p. 17784-17792.
2. Saleem, H., M. Haneef, and H.Y. Abbasi, *Synthesis route of reduced graphene oxide via thermal reduction of chemically exfoliated graphene oxide.* Materials Chemistry and Physics, 2018. **204**: p. 1-7.
3. Sneha, K., et al., *Yucca-derived synthesis of gold nanomaterial and their catalytic potential.* Nanoscale research letters, 2014. **9**: p. 627.
4. Li, Y., et al. *Intrinsic Catalytic Activity of Gold/Multi-Walled Carbon Nanotubes Composites in Squaric Acid-Iron(II/III) System*. Catalysts, 2018. **8**, DOI: 10.3390/catal8050187.
5. Yang, X., et al., *Graphene uniformly decorated with gold nanodots: in situ synthesis, enhanced dispersibility and applications.* Journal of Materials Chemistry, 2011. **21**(22): p. 8096-8103.
6. Kinnamon, D., et al., *Portable biosensor for monitoring cortisol in low-volume perspired human sweat.* Scientific Reports, 2017. **7**(1): p. 13312.
7. Nguyen, T.Q. and C. Breitkopf, *Determination of Diffusion Coefficients Using Impedance Spectroscopy Data.* Journal of The Electrochemical Society, 2018. **165**(14): p. E826.
8. Daniels, J.S. and N. Pourmand, *Label-Free Impedance Biosensors: Opportunities and Challenges.* Electroanalysis, 2007. **19**(12): p. 1239-1257.
9. Bogomolova, A., et al., *Challenges of Electrochemical Impedance Spectroscopy in Protein Biosensing.* Analytical Chemistry, 2009. **81**(10): p. 3944-3949.
10. Tanak, A.S., et al., *Non-faradaic electrochemical impedimetric profiling of procalcitonin and C-reactive protein as a dual marker biosensor for early sepsis detection.* Analytica Chimica Acta: X, 2019. **3**: p. 100029.
11. Upasham, S., O. Osborne, and S. Prasad, *Demonstration of sweat-based circadian diagnostic capability of SLOCK using electrochemical detection modalities.* RSC Advances, 2021. **11**(13): p. 7750-7765.
12. Mark, E., et al., *The Apparent Constant-Phase-Element Behavior of an Ideally Polarized Blocking Electrode.* Journal of the Electrochemical Society, 2007. **154**: p. C81.
13. Kim, K.S., et al., *Highly sensitive and selective electrochemical cortisol sensor using bifunctional protein interlayer-modified graphene electrodes.* Sensors and Actuators B: Chemical, 2017. **242**: p. 1121-1128.

Burner Rig Optimization for High Temperature Materials and Coating Systems

Student Researcher: Christopher Ferguson

Advisor: Dr. Gregory Morscher

The University of Akron
Mechanical Engineering

Abstract

At the University of Akron (UA), the capability of extreme environment testing of ceramic matrix composites (CMCs) and CMC/coating systems needed to be expanded to include accurate temperature control for high temperature, high stress, and high velocity testing in a combustion environment. CMCs are traditionally used in the internal components of a jet turbine engine and will experience different stress and temperature conditions based on what stage in the cycle the aircraft is at. An automated two-axis positioner was created for the pre-existing combustion facility at UA [1] allowing for a more realistic simulation of an aircraft's typical flight cycle. This system was affordably built from two linear ball screws, two stepper motors, a microcontroller (Teensy 4.0), and a laptop to run the custom-built software. Flight stages include ground idle, take-off, climb, cruise, flight idle, approach, reverse thrust, and a return to ground idle [2]. Each stage requires a different temperature and stress condition that could not previously have been tested in the current facility. Using a two-color pyrometer to measure temperature, and a timer to sync the MTS program with the positioner, temperature-based programs can be created to iteratively hit unique setpoints of stress and temperature. Automating the position of the torch allows for more complex temperature cycles, including thermomechanical fatigue tests of SiC/SiC [3].

Project Objectives

The goal of this project is to create an automated positioner that can move the high velocity oxygen fuel (HVOF) torch both automatically, through a user created program, and manually, for simple tests, to precisely change the temperature experienced at the surface of the sample.

Methodology Used

As a project, the hardware, software, and validation testing are the three main stages necessary to build a reliable testing system. The hardware was created first using two linear ball screws attached to custom machined aluminum plates that acts as the structure for the positioner. Two axes were chosen: one to move the torch perpendicular to the sample (Z-Axis), used to change the temperature experienced, and one parallel to the sample (Y-Axis), used to center the flame on the material.

The software of the torch positioner was split into two separate codes: a microcontroller script written in C, and a desktop application written in C# using Visual Studio 2019. A microcontroller is needed to communicate directly with the stepper motor drivers to rapidly send out step and direction signals which the desktop cannot handle alone. The C# application allows for ease of operation as all interactions between the user and system is based out of a graphic user interface (GUI).

Testing was required to validate the system to perform the required cycles accurately and repeatably using both the positioner and the MTS in tandem. Square wave, variable ramp rate, and quench cycles were completed to measure the performance of the system to better design future testing.

Results

The hardware was built to move the torch 176 mm in the Z direction and 112 mm in the Y direction at speeds ranging from 0.25 mm/s to 15 mm/s. 2.0 Nm stepper motors were used to provide torque to move the torch in 0.02 mm increments. That increment is based on the pitch of the ball screw (5.08 mm/rev) and the number of steps needed per revolution (200 steps/rev) for the stepper motors. The completed system is labeled in Figure 1 though the two-color pyrometer is not included. This pyrometer measures the temperature of the sample and feeds that data back to the system to adjust the torch position based on the given setpoint.

Complementing the hardware is the software built in Visual Studio 2019 using the .NET Framework with Windows Form as the application builder. As seen in Figure 2, it allows for both manual and automatic control of the torch in two directions, allowing for complex programs to be built. In automatic mode, the software executes an iterable plan from an array of sample distances or temperatures and the required dwell times in between each setpoint. Sample distance, time, temperature and axis location data is recorded which is plotted in real time on the main page of the software. All data can be exported into a CSV file at the end of the test.

A number of validation tests were ran including a variable ramp rate test, from 0.25-15 mm/s, a quench test, and a one hour long square wave test. This does not include all validation testing completed, but is the most pertinent for the purpose of demonstrating its capabilities. For the variable ramp rate tests, the positioner was able to heat the specimen from 800-1200°C and hit temperature ramp rates from 2 to 90°C/s depending on the torch speed used, increasing or decreasing the severity of the test. Next, the quench cycle consists of going to a set max temperature, and then automatically moving the torch off the specimen using the Y-axis to quickly cool the sample before applying the flame back on after a dwell period. This represents a cyclic condition that is found to be severe for certain coatings on CMCs. Lastly, a simple square wave test was run for one hour that uses the automatic mode of the positioner to cycle between two setpoints, 800 and 1200°C while applying a load that corresponds to 40 and 80 MPa of stress. This test, as seen in Figure 3, proves the long-term stability of the system and its ability to sync the automated positioner with the MTS program.

Figures

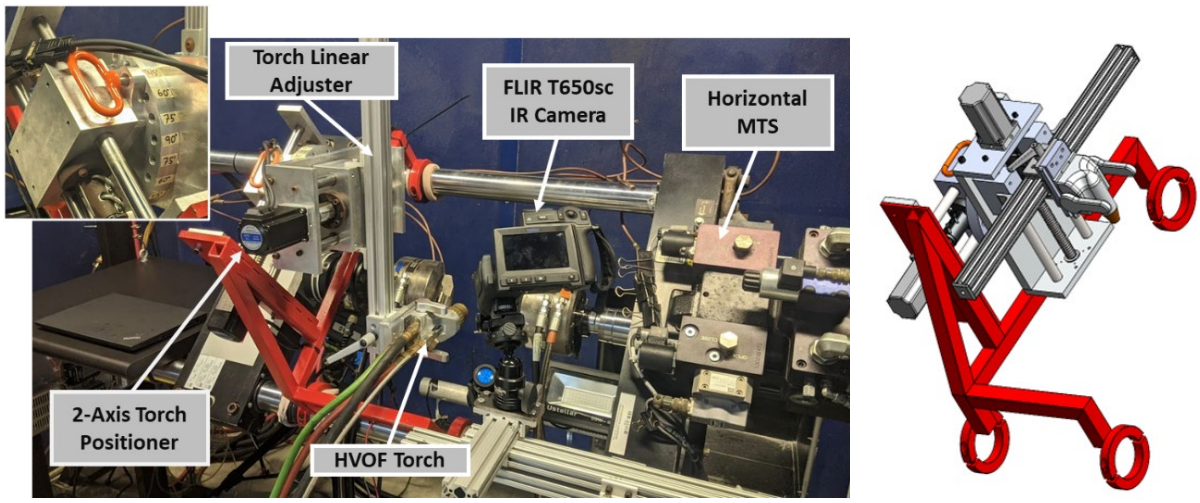

Figure 1: Current Burner Rig Hardware

Figure 2: *Custom Built Desktop Application*

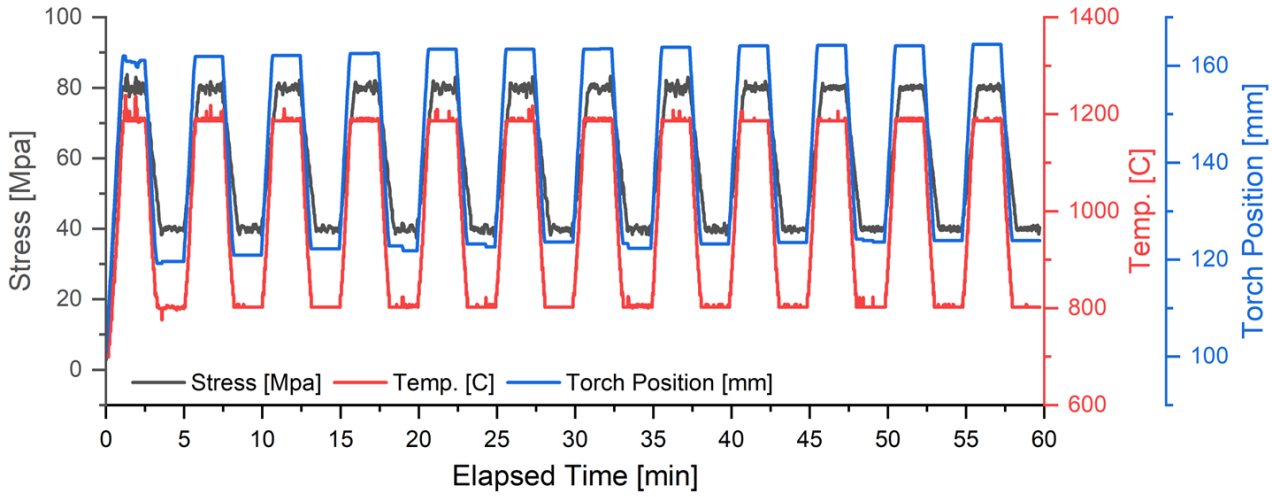

Figure 3: Validation Testing using a Simple Square Wave

References

1. G. Morscher, R. Panakarajupally, L. Hoffman, “The Versatility of HVOF Burner Rig Testing for Ceramic Matrix Composite Evaluation”, J. Compos. Sci., 2021, vol 5.

2. R.C. Reed, “The Superalloys Fundamentals and Applications”, Cambridge University Press (2006)

3. Panakarajupally, Ragav P., Michael J. Presby, K. Manigandan, Jianyu Zhou, George G. Chase, and Gregory N. Morscher. 2019. "Thermomechanical Characterization of SiC/SiC Ceramic Matrix Composites in a Combustion Facility" Ceramics 2, no. 2: 407-425. https://doi.org/10.3390/ceramics2020032

Machine Learning-Based Study of Building Block Interactions and Material Properties of Soft Matter Systems

Student Researcher: Alexandra N. Filiatraut

Advisor: Dr. Mehdi Zanjani

Miami University
Department of Mechanical and Manufacturing Engineering

Abstract
In recent years, the field of materials science has increasingly turned to machine learning techniques to aid in complex research applications. This study seeks to utilize such techniques to further the understanding of soft matter systems, in particular colloidal particle assemblies and dynamically crosslinked networks, which consist of polymer backbones and crosslinking agents that interact with one another in unique and complex ways. This study utilizes a Convolutional Neural Network (CNN) and Graph Convolutional Neural Network (GCNN) to learn and predict the relationship between polymer network architecture and the resultant mechanical properties of crosslinked polymer composites. Additionally, this study uses a dense neural network to learn and predict fundamental interactions that occur at the particle-level within colloidal particle assemblies using a particle's network of nearby neighbors.

Project Objectives
The objectives of this study are two-fold: to use CNN and GCNN techniques for the prediction of physical properties based on the system architecture of a dynamic polymer system and to create a dense neural network capable of predicting particle-level interactions of colloidal particle assemblies based on a particle's neighbor network.

Methodology
Two important components of this study to discuss are the data set and the machine learning algorithms. All data used within this study were molecular dynamic (MD) simulations of coarse-grained, micro-scale soft matter systems, as coarse-gained models reduce the level of computational resources that atomistic resolution models would require. This study employed two distinct data sets to accomplish the objectives listed above. The first data set consists of approximately 2,400 dynamicallycrosslinked polymer MD simulations and the second data set consists of approximately 480,000 particles from colloidal particle assemblies for investigation into particle-level interactions. The first data set features unique architectures of dynamic polymer systems generated by varying system parameters such as the number of crosslinker arms, length of the crosslinker arms, length of the FMIDA backbone chain,number of bonding sites located on each backbone chain, and ratio of percent crosslinkers to backbone chains within the system. The secondary data set features four system types that are distinguished by their number of particle types; this data set consists of one, two, and three particle-type systems as well as a two particle-type system with differing radii.

To learn the relationship between system architecture and properties of a dynamic polymer system, this study uses two types of machine learning algorithms - an image-based CNN and a graph-based GCNN. Both of these types of models are largely praised for their abilities to handle complex, three-dimensional inputs [3]. The image-based CNN uses a voxel representation of the simulation cell as input, whereas the GCNN model uses a graph representation made up of nodes (representing particles) and edges (representing bonds). The voxel array or graph is then fed into the corresponding 3D CNN and GCNN machine learning models that predict the system's overall Young's modulus (see schematic outlines in

Figure 1 below). The final machine learning technique is a dense, neural network used to predict the particle-level interactions within a colloidal particle assembly. This machine learning model learns to predict these interactions using a particle's "neighbor network" - graph-based [1] quantification of the relationship between a particle and its nearby neighbors shown in Figure 2 below. This study created twelve separate models to predict each number of neighbors successfully which by feeding inputs through a series of fully connected, dense layers that predict the desired output - particle forces in the x, y, and z directions. Force prediction on a particle level is incredibly important to a system and can help determine particle trajectory and assembly behavior for these colloidal particle systems.

Results Obtained

This current study is still ongoing. The data set of dynamic polymer assemblies is still in the process of being collected, therefore there are no results to present at this time on the first objective of this study, investigating dynamic polymer network property prediction based on initial system architecture. The secondary data set of this study has been completed and is used to predict particle-level interactions of colloidal particle assemblies. The machine learning algorithms used to predict particle-level interactions from a particle's neighbor network have also been completed, trained, and tested. In total, this study created 48 machine learning models to predict particle properties of four system types - one, two, two multi-size, and three particle type systems - with twelve numbers of neighbors. Each machine learning model was identical in architecture but varied slightly in dimensionality of input. Overall, the machine learning model proved successful in its predictions and can be used as a tool to predict particle-level interactions of colloidal particle assemblies. Figure 3 below shows examples of training and validation curves per epoch - a measure of the accuracy of the machine learning models during training. Exponentially decreasing trends that converge to a value of loss are indicative of a well-trained model that is neither over- nor underfitting data. After the machine learning models were trained, they were tested with an unbiased data set to gain a measure of how well the trained models perform. Our preliminary results show an average overall testing loss for particle-level force prediction was at or below 0.04 MAE for all particle systems - a low enough testing error to call this model successful.

Significance and Interpretation of Results

This study has successfully built, trained, and presented a machine-learning model capable of predicting particle-level interactions of colloidal particle systems. Prediction of particle-level interactions provides insight into particle trajectories and overall system behavior which is an important component as these particle-level interactions often remain "hidden" within colloidal particle assemblies. Prediction of these interactions occurring at a particle level will better the understanding of these systems as a whole and provide a unique tool for material scientists to predict system interactions at the particle level.

Acknowledgments

The author would like to thank her advisor, Dr. Mehdi Zanjani for his support and guidance throughout this project as well as the Department of Mechanical and Manufacturing Engineering at Miami University for their resources and support throughout the author's undergraduate and graduate education. The author would also like to thank the Ohio Space Grant Consortium for their partnership and funding that helped the continuation of this study. Finally, the author would like to thank her family and friends for their love, support, and encouragement throughout this and every chapter of her life.

Figures/Charts

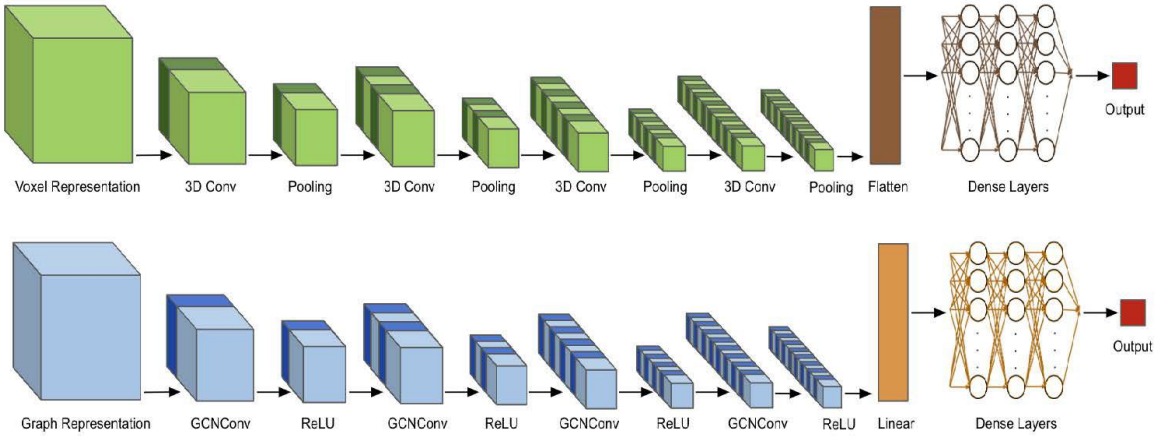

Figure 1. Machine Learning Model Architecture for CNN (top) and GCNN(bottom).

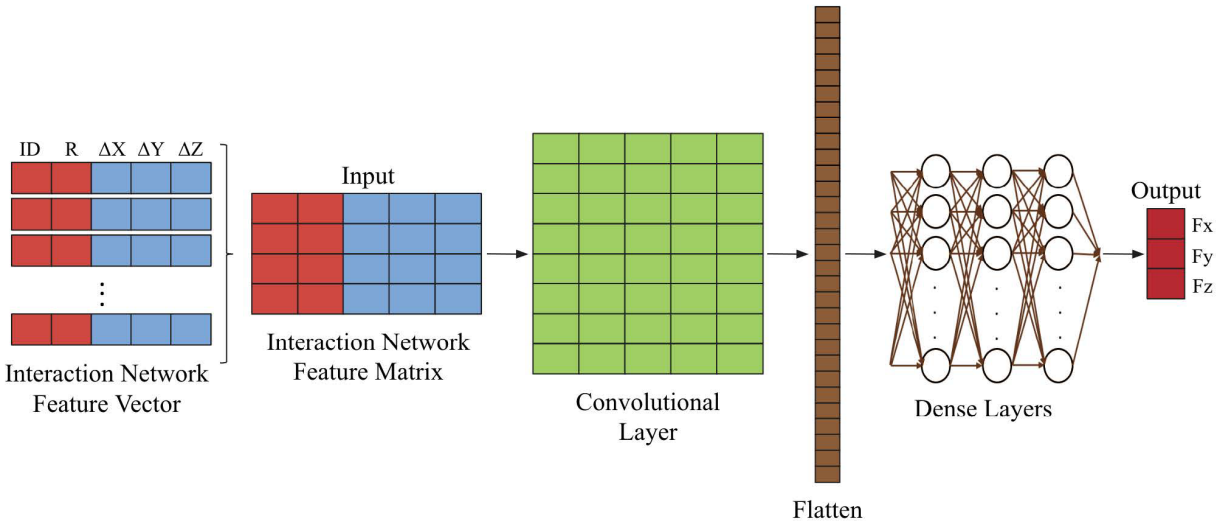

Figure 2. Schematic Representation of a Particle Neighbor Network and the Dense Neural Network.

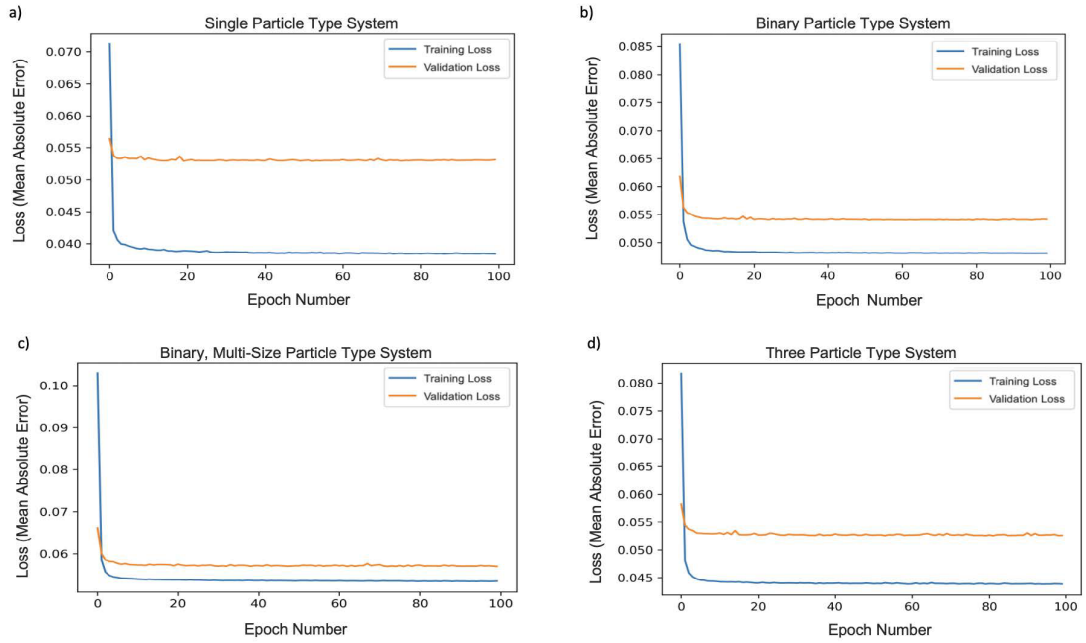

Figure 3. Training and Validation Loss Curves per Epoch for Particles with Three Nearby Neighbors of a) One Particle Type Systems, b) Two Particle Type Systems, c) Two Multi-Size Particle Type Systems, and d) Three Particle Type Systems.

References

[1] Battaglia, Peter W., et al. *Interaction Networks for Learning about Objects, Relations and Physics*. arXiv, 1 Dec. 2016. *arXiv.org*, http://arxiv.org/abs/1612.00222.

[2] *Close Packed Structures: Fcc and Hcp | Physics in a Nutshell*. https://www.physics-in-a-nutshell.com/article/11/close-packed-structures-fcc-and-hcp. Accessed 1 Apr. 2023.

[3] Heidari, Negar, et al. "Graph Convolutional Networks." *Deep Learning for Robot Perception and Cognition*, Elsevier, 2022, pp. 71–99. *DOI.org (Crossref)*, https://doi.org/10.1016/B978-0-32-385787-1.00009-9.

Uncertainty Propagation in Low-Thrust Trajectory Design

Student Researcher: Zachery S. Fitzgerald

Advisor: Dr. Ye Lu

Kent State University
College of Aeronautics and Engineering

Abstract

The current mission design process considers the optimal trajectories and Monte Carlo analysis separately. The state-of-the-art onboard guidance algorithms tend to find a single optimal solution based on the current navigation knowledge, which is then used for reference tracking. This research focuses on robust low-thrust trajectory design methods that integrate uncertainty propagation to provide a probabilistically optimal trajectory. A nominal optimal low-thrust trajectory is generated using basic polynomial collocation to convert the optimization problem to a nonlinear programming problem where it will then be solved with commercial nonlinear programming software. The statistical performance of the solution will then be analyzed using Monte Carlo simulation. Using the nominal trajectory generated as a baseline comparison for the research, uncertainty propagation will then be implemented into the problem formulation. The results from each solution method will then be analyzed and compared to determine the cost and benefits of implementing uncertainty propagation into trajectory optimization.

Objectives

The first objective is to use a direct method of optimization with basic polynomial collocation to generate a nominal optimal low-thrust trajectory, followed by a Monte Carlo analysis to evaluate the statistical performance of the nominal optimal trajectory. Modified equinoctial orbital elements will be used in the problem formulation to avoid fast changing dynamics of cartesian variables and the ambiguity issues with the conventional Keplerian orbital elements. This nominal optimal low-thrust trajectory was obtained using General Purpose Optimal Control Software (GPOPS-II). This trajectory will act as a baseline comparison for the result. The state variables from each segment can then be used as the parameters for a nonlinear programming problem and the number of points evaluated at each segment can be easily changed to achieve a desired level of accuracy. Next, Monte Carlo analysis of the optimized trajectory will be done to evaluate the performance and the results will be used as a baseline for comparison with uncertainty propagation results. Uncertainty propagation will be formulated in the integration step of the nonlinear programming problem. The objective function of the optimization will depend on the mean and variance of the state and control variables. To make the problem tractable, this work focuses on the uncertainty of the thrust throttle and pointing. The final task will be to compare the results of the two methods. The goal will be to show the improvement of implementing nonlinear uncertainty propagation into trajectory design when compared to the current method of trajectory optimization that does not include a form of uncertainty propagation.

Methodology

The entirety of this research will be done in MATLAB. GPOPS-II is a software package developed in MATLAB. GPOPS-II includes a low-thrust trajectory example that is used as the foundation of the research. The problem will be reformulated to include thrust uncertainties and the MATLAB scripts will be altered to model such.

Results

The uncertainty propagation method Unscented Transformation (UT) has been modeled and compared to the Monte Carlo analysis with the nominal optimal low-thrust trajectory. Both results only include an initial covariance. This was done to show that UT was performing as expected. Future results will include uncertainties over the course of the trajectory. This is where it will be shown if implementing uncertainty propagation into low-thrust trajectory design is a viable option.

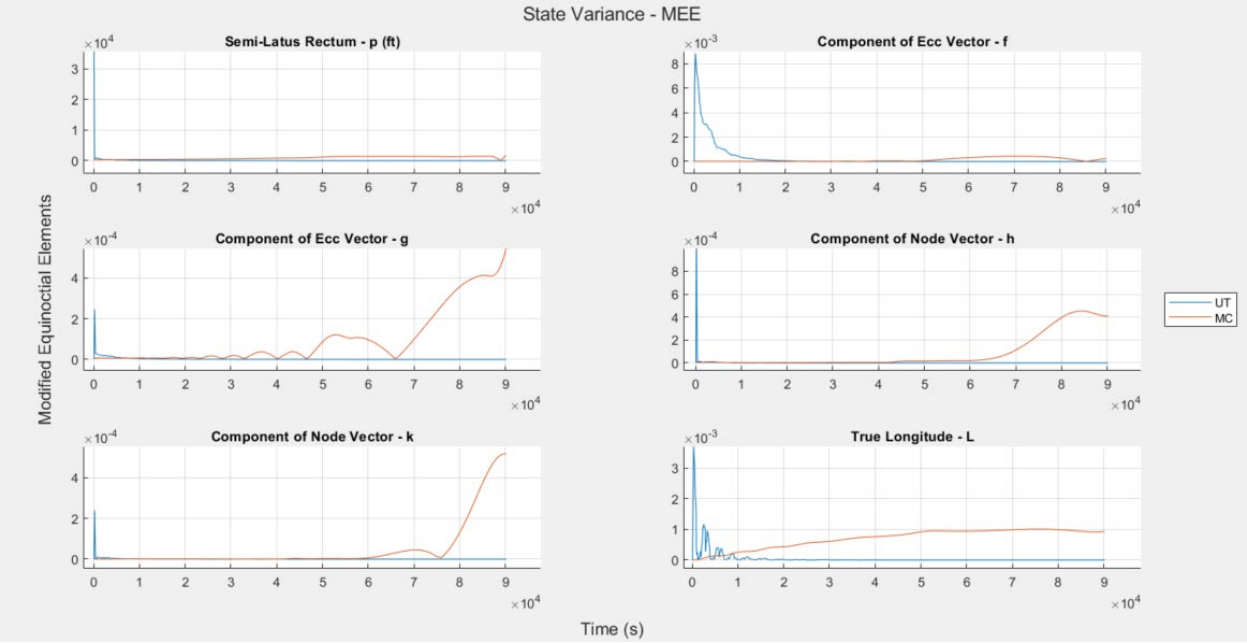

Figure 1: Pictured above is the state variance for each modified equinoctial elements. The Monte Carlo (MC) analysis was done using only an initial covariance. The unscented transform (UT) was also done using only an initial covariance. The figure shows that UT has results similar to MC and the research can move forward to include uncertainties throughout the trajectory.

Acknowledgements

I would like to thank my advisor, Dr. Ye Lu, for guiding me throughout the entirety of this research project. The support from the Ohio Space Grant Consortium was greatly appreciated as it gave me the ability to give this research the time and focus needed.

References

A. Shirazi, J. Ceberio, and J. A. Lozano, “Spacecraft trajectory optimization: A review of models, objectives, approaches and solutions,” Progress in Aerospace Sciences, vol. 102, pp. 76–98, 2018.

J. T. Betts, “Optimal low-thrust orbit transfers with eclipsing,” Optimal Control Applications and Methods, vol. 36, no. 2, pp. 218–240, 2014.

N. Ozaki, S. Campagnola, R. Funase, and C. H. Yam, “Stochastic differential dynamic programming with unscented transform for low-thrust trajectory design,” Journal of Guidance, Control, and Dynamics, vol. 41, no. 2, pp. 377–387, 2018.

Y.-zhong Luo and Z. Yang, “A review of uncertainty propagation in Orbital Mechanics,” Progress in Aerospace Sciences, vol. 89, pp. 23–39, 2017.

Electrospinning Photopolymer Fibrous Mats Derived From Salicylic Acid With Tunable Morphology

Student Researcher: Grant W. Guggenbiller

Advisor: Dr. Andrew C. Weems

Ohio University

Biomedical Engineering Program - Department of Chemical and Biomolecular Engineering

Abstract

Micro and nano sized materials are significant in the biomedical space when considering how to design for tissue infiltration and healing upon implantation of new devices. Electrospinning offers a unique opportunity as a processing method that is compatible with a wide array of polymers and conditions that may all be tailored to produce similar morphologies in the resultant 3D porous scaffolds. An additional benefit of electrospinning is the ability to incorporate external stimuli, such as light, to drive in situ reactions including thiol-ene photoclick reactions to produce thermoset polymer network fibers during the jetting process (the fiber forms simultaneously with the network as the liquid jet moves from the nozzle to the plate and is irradiated along the pathway). Here, a series of bioderived, pro-drug photopolymers, derived from salicylic acids, are photocrosslinked, in the presence of polystyrene and silver sulfate, during jetting to achieve a series of composite fibrous mats. The mats were examined for physical properties to determine the role of the polystyrene, silver sulfate, and fiber morphology. Of specific note, these materials display shape memory, allowing for minimally invasive medical device opportunities, as well as cytocompatibility and antimicrobial behaviors. Ultimately, these composite fibrous mats display excellent promise for both implantable tissue scaffolds as well as for medical devices including face masks or wound coverings.

Project Objectives

This project aimed to use the electrospinning method to process a biomaterial candidate for use in burn and soft tissue wound recovery. The salicylic acid component in commodity anti-inflammatory was chosen to be functionalized due to its pro-drug behaviors. With functionalized salicylic acid a photopolymer network can be formed with the help of photo cross linking agents Pentaerythritol tetrakis(3-mercaptopropionate) (PETMP) and Triallyl-s-triazine-2,4,6(1H,3H,5H)-trione (Trione). With the help of known biomaterial polystyrene and antimicrobial silver sulfate a range of materials were screened with different ratios of the salicylic acid network and silver sulfate. Seeing how the amounts of compositing affected the morphology of the fibers. Finally, cell viability and bacterial interactions were observed for potential for wound healing device.

Methodology Used

Salicylic acid was functionalized into a salicylic acid-derived polymer network using thiol-ene crosslinking, referred to as SEE.[2] The SEE network material was then electrospun with the help of polystyrene and with the composite additive of silver sulfate. Silver sulfate was used given silver's anti-microbial properties. The materials were screened based on percent SEE polymer network and a trend resolved to see if a trend in morphology is present with photopolymer content. Furthermore, to study silver sulfate content, polystyrene with increasing loading percentages of silver sulfate was screened also attempting to view morphological changes. The fibers were measured using scanning electron microscopy (SEM) to image and measured using the FIJI ImageJ. Materials were then tested for cell viability using human corneal fibroblasts and an MTS assay for viability over a 7-day period with images taken of the cells on the 7th day with confocal microscopy. A final preliminary test was done with the material exposure to bacteria testing the fibers in media with *staphylococcus aureus* over a 3-day period to see how they reacted in the presence of the different formulations.

Significance and Interpretation of Results

SEE photopolymer networks, in composite with polystyrene and silver sulfate, can be successfully electrospun at different ratios to achieve fibrous results. With the help of SEM fibers were imaged and with the ImageJ software measurements on fiber diameters led to interesting results. In systems with photopolymer it has been interpreted that the more SEE photopolymer network added the more cylindrical the fibers become, as shown in figure 1 as the aspect ratio approaches 1. Furthermore, in the only silver containing system, as more silver sulfate was added the less uniform, and more ribbon-like the fibers become, the aspect ratio becomes farther away from 1 as silver content increases. Finally, in a joint system a trend showed that the SEE network was more in control of the morphology than the silver sulfate with a trend similar to an only SEE network containing system, further represented in figure 1. Finally, biological considerations were analyzed with fibroblasts finding the cell viability to be positive over a 7-day period and that over a 3-day period the photopolymer network is able to keep bacteria away when it contains the silver sulfate. These devices have a significant chance to be utilized as a burn wound and soft tissue wound healing device given the green nature, cytocompatibility, and morphological control we can obtain over the system.

Figures/Charts

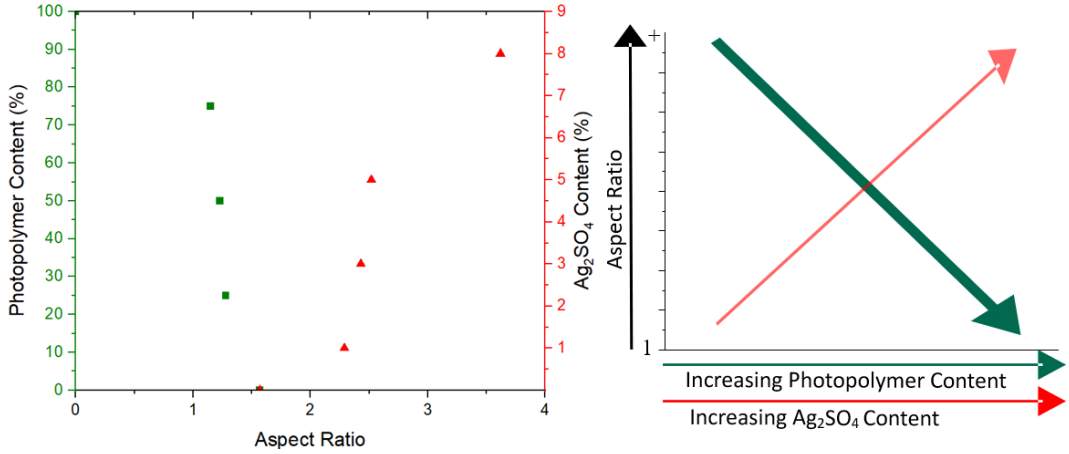

Figure 1. The demonstration of aspect ratio as the composite concentration is changed.

Acknowledgments and References

Thank you to my advisor Dr. Andrew Weems for his guidance, my fantastic lab mates and a very special thank you to the OSGC.

1. Guggenbiller, G. King, O. Weems, A.C. “Tunable Morphology Photopolymer Electrospun Fibrous Mats Derived From Natural Product Pro-Drug Salicylic Acid” 2023, Manuscript in Progress

2. King, O. M.; Pérez-Madrigal, M. M.; Murphy, E. R.; Dove, A. P.; Weems, A. C., “4D Printable Salicylic Acid Photopolymers for Sustained Drug-Releasing, Shape Memory, Soft Tissue Scaffolds” *Biomacromolecules,* 2023, submitted

The Effects of Active Control on Near-Field Pressure Fluctuations in Supersonic Rectangular Twin Jets

Student Researcher: Ryan P. Leahy

Advisor: Prof. Mo Samimy

The Ohio State University
Department of Mechanical Engineering

Abstract
The application of supersonic rectangular twin jets (RTJ) is of interest to current and future generations of tactical aircraft. Previous studies and application of supersonic twin jets have shown that increased far-field (FF) noise severely affect the personnel near these aircraft, while their near-field (NF) pressure fluctuations are of concern due to potential structural fatigue of aircraft aft components. The primary objective of this work in the study of RTJ, with an aspect ratio of 2 and a design Mach number of 1.5, was to characterize unheated baseline flows and to apply active control via localized arc filament plasma actuators (LAFPAs) for understanding of the key physics. In this work the effect of twin jet coupling on near field pressure fluctuations are of focus. The use of NF microphone azimuthal array allowed for measurement of NF pressure fluctuations using the calculated overall sound pressure level (OASPL) as well as the detection of the coupling mode by processing signals using a wavelet-based phase and coherence technique.

Project Objectives
Today, supersonic jets exhausting from current tactical aircraft pose issues for both the community and personnel around them, as well as the design and structural well-being of the aircraft. The future generation of tactical aircraft requires that exhaust systems have advancements to meet increasing complexity of operational performance parameters. Some of these parameters are lower drag allowance and simpler mechanical options for thrust vectoring, as well as greater control over the mixing and entrainment of the exhaust into ambient conditions. Rectangular jets offer a route to meet these increasingly complex requirements [1,2]. Supersonic jets' effect on aircraft structures is of prime importance to understand and mitigate. Past configurations of twin jets (e.g., the B1-A and F15-E test programs) demonstrated failure of the aircraft nozzle flaps due to elevated NF pressure fluctuations [3,4]. Localized arc filament plasma actuators (LAFPAs) were developed at Ohio State and have shown strong control authority in a wide variety of flows. The overall project objectives are to investigate the physics of screech and coupling of supersonic rectangular twin jets, utilizing LAFPAs to control coupling and effect near-field pressure fluctuations in supersonic RTJ.

Methodology
For the present work, the same RTJ assembly and setup shown in Leahy et al. [5] was utilized. The nozzle pressure ratio was set at 2.97 for an overexpanded desired jet Mach number of 1.35 (Mj = 1.35). The microphones were positioned at an axial location of x/De = 0 and radially (measured normal to the twin jets major axis) at r/De = 2 (for microphones 4 & 3) and r/De = 4 (for microphones 1 & 2). Microphones 1 & 2 were utilized to assess the twin jets' coupling mode and strength at baseline and controlled conditions. This was accomplished by calculating the Morlet wavelet coherence (magnitude and phase) between the signals from the two microphones. Then the time-averaged coherence and phase of the time traced signals were averaged for total number of blocks recorded (note coherence and phase were set to zero when the coherence magnitude was below 0.7). Microphones 4 & 3 were used to measure

NF pressure fluctuations in the inter-nozzle region (z/De = 0) and over one of the jets (z/De = +1.125), respectively. Overall sound pressure level (OASPL) in decibels was determined by integrating the PSD, as performed in previous literature [6]. LAFPAs were fired in the jets natural flapping motion for in-phase (IP) and out-of-phase (OOP) coupling of the jets. For more information on experimental setup please refer to Leahy et al. [5].

Results & Discussion

Figure 1 below shows the effect of coupling mode on near field pressure fluctuations. Figure 1a depicts the time averaged phase and coherence for the baseline Mj = 1.35 case. Where the black coherence curve suggest strong coupling (~1) at natural screech frequency of Sts = 0.40. The phase of this coupling is out-of-phase (~-π rad). The large error bars suggest an unsteady, intermittently coupled case. To summarize, the baseline is shown to have a strongly, intermittently out-of-phase coupling mode. Excited cases in the bottom two rows show LAFPAs control authority on coupling and its effect on near-field pressure fluctuations. The IP case (Figure 1b&d) show the LAFPAs have altered the coupling to a strong (coh ~ 1) consistent IP (phase~0) case. This has increased the internozzle near field pressure fluctuations as shown by the increase of ~4dB in microphone 4 in the ΔOASPL (relative to the baseline). The OOP coupling (Figure 1c&e) shows the strong control authority to couple the jets OOP (phase ~--π rad), consistently in time (low phase bars). This has an effect of drastically decreased internozzle pressure fluctuations (relative to baseline) of ~8 dB in microphone 4. Reasoning for this internozzle pressure fluctuations being effected by IP or OOP coupling is based either on constructive (IP) or destructive (OOP) interference of acoustic feedback waves in this region. More explanation and other cases of this are shown in Leahy et al. [5] and Samimy et al. [7].

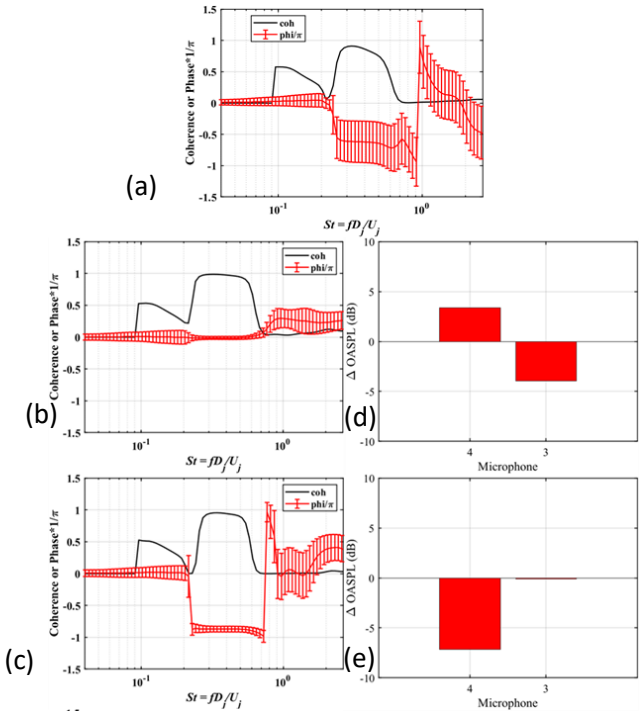

Figure 1. Wavelet phase and coherence and ΔOASPL of (a) Baseline Jet, excited at natural screech frequency ($St_e = St_s$) for (b&d) in-phase, (c&e) out-of-phase

Acknowledgements and References
The office of Naval Research (Steve Martens) as well as the Ohio Space Grant Consortium are gratefully acknowledged.

[1] Dusa, D., Speir, D., Rowe, R., and Leavitt, L. Advanced Technology Exhaust Nozzle Development. In *19th Joint Propulsion Conference*, AIAA paper 1983-1286, 1983.
[2] Wiegand, C. F-35 Air Vehicle Technology Overview. Presented at the 2018 Aviation Technology, Integration, and Operations Conference, Atlanta, Georgia, AIAA paper 2018-3368, 2018.
[3] Berndt, D. E. *Dynamic Pressure Fluctuations in the Internozzle Region of a Twin-Jet Nacelle*. Publication 841540. SAE International, Warrendale, PA, 1984.
[4] Walker, S. H. *Twin Jet Screech Suppression Concepts Tested for 4.7 Percent Axisymmetric and Two-Dimensional Nozzle Configurations*. 1990.
[5] Leahy, R. P., Ghassemi Isfahani, A., Webb, N. J., and Samimy, M. The Effects of Active Control on Near-Field Pressure Fluctuations in Supersonic Rectangular Twin Jets. In *28th AIAA/CEAS Aeroacoustics 2022 Conference*, American Institute of Aeronautics and Astronautics, 2022.
[6] Brès, G. A., Ham, F. E., Nichols, J. W., and Lele, S. K. "Unstructured Large-Eddy Simulations of Supersonic Jets." *AIAA Journal*, Vol. 55, No. 4, 2017, pp. 1164–1184. https://doi.org/10.2514/1.J055084.
[7] Samimy, M., Webb, N., Esfahani, A., and Leahy, R. "Perturbation-Based Active Flow Control in Overexpanded to Underexpanded Supersonic Rectangular Twin Jets." *Journal of Fluid Mechanics*, Vol. 959, 2023, p. A13. https://doi.org/10.1017/jfm.2023.139.

Fuzzy Logic SHAP for interpretability in high input engineering data applications

Student Researcher: Lynn K. Pickering

Advisor: Dr. Kelly Cohen

University of Cincinnati College of Engineering and Applied Sciences
Department of Aerospace Engineering and Engineering Mechanics

Abstract

This project extends efforts of AI coupled with game theory. SHAP is a novel unified approach for interpreting the predictions of models. It makes use of an explainer model, which is an interpretable approximation of the original model. The novelty of SHAP was unifying six explanation models from the literature: LIME, DeepLIFT, Layer-Wise Relevance Propagation, classic Shapley regression values, Shapley sampling values, and Quantitative Input Influence. The theory behind SHAP is based on the concept of Shapley values from game theory, where Shapley quantifies the contribution of each player to a game. In this work, SHAP is applied to fuzzy logic to further increase the interpretability of fuzzy logic for large input engineering applications. Interpretability has many aspects, of which understanding the impact of input variables on the final output of a classification task for an engineering application is one. Furthermore, in a fuzzy logic system, the input variables are partitioned into fuzzy sets, which allows this work to extend the typical work done applying SHAP to a system and analysing input variables, to analysing input variable fuzzy partitions on a finer scale.

Project Objectives

The objective of this project was to train a fuzzy logic system using a Genetic Algorithm on a high input engineering application, and then use SHAP to quantify the input features with the highest impact in the system to achieve further interpretability of the model.

Methodology Used

A genetic algorithm trains a fuzzy logic model on a high input engineering application. The application here is a ship breaking application to predict whether a ship has reached the end of its life and will be disposed of. There are 15 inputs, and the dataset is unbalanced in that for every ship that is at the end of its life, there are 9 ships that are not at the end of their life. A level of unbalance this high is difficult for a machine learning model to train on. The data is provided by the Human Environment and Transport Inspectorate (Inspectie Leefomgeving en Transport, ILT) in the Netherlands [2]. First, a cascaded fuzzy system is designed that makes sense to a human user given the input data as seen in Fig. 1, to retain the interpretability of a fuzzy logic system while the number of inputs is high. After the system has been trained using a genetic algorithm, Kernel SHAP [1] is applied to analyse the impact of the input features on the final output of the system.

Results Obtained

The precision recall curve of the trained fuzzy system is given in Fig. 2, and compared with a random forest model and a decision tree model the same depth as the fuzzy system. While the random forest outperforms the model trained here, the model does achieve similar results to the decision tree. The results of the SHAP analysis are given in Fig. 3, although due to data privacy, the input names may not be shared.

Significance and Interpretation of Results:

The trained fuzzy system performs well given how unbalanced the dataset, but more work will be done in the future to improve the accuracy of the model. This accuracy is achieved with many constraints on the system to maintain interpretability of the system. The SHAP results show that about 6 or 7 inputs had the majority of the impact on the model output, while the remaining inputs

were not as consequential. Initial comparisons of the fuzzy model SHAP to the random forest SHAP show very different impactful inputs. In future work, SHAP will be run on the fuzzy model for more test points, and at the linguistic input level. A framework to bring the interpretability tools together will be developed.

Figures/Charts

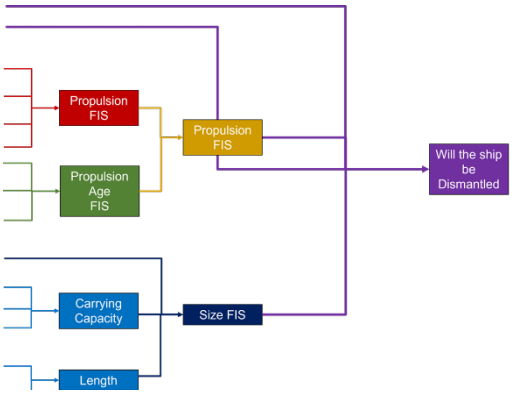

Figure 1. Structure of the fuzzy logic model

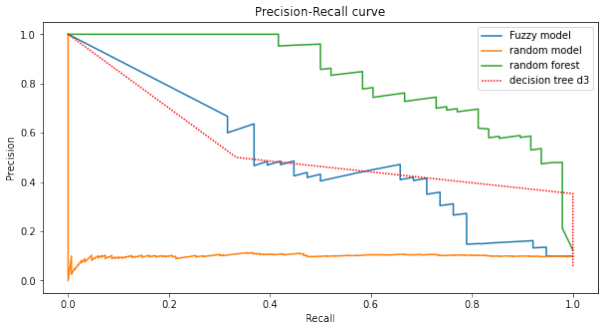

Figure 1. Precision-Recall curve of the trained model, compared to other machine learning methods used on the same dataset

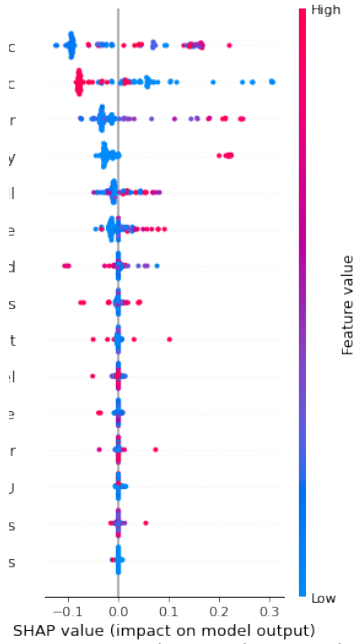

Figure 3. SHAP analysis on the trained fuzzy logic system

Acknowledgments

This work would not have been possible without the support of the Ohio Space Grant Consortium and my advisor, Dr. Kelly Cohen. Thank you!

References

1. Lundberg, S.M., Lee, S.I., 2017. A unified approach to interpreting model predictions, in: Proceedings of the 31st International Conference on Neural Information Processing Systems, Curran Associates Inc., Red Hook, NY, USA. p. 4768–4777. URL: https://dl.acm.org/doi/10.5555/3295222.3295230.

2. “'Beaching' of Vessels for Shipbreaking – Legal, Illegal or Somewhere in between?” Home, https://www.gard.no/web/updates/content/26050185/beaching-of-vessels-for-shipbreaking-legal-illegal-or-somewhere-in-between.

Structural Health Monitoring of Aerospace Structures Using a Passive Guided Wave Approach

Student Researcher: Natalie A. Reed

Advisor: Dr. Joseph Corcoran

University of Cincinnati College of Engineering and Applied Sciences
Department of Aerospace Engineering & Engineering Mechanics

Abstract
The uptake of structural health monitoring in aerospace has been limited by the practicality of piezoelectric transducers and the lengths of their associated cables. The use of fiberoptic strain sensors that can be integrated into or onto aerospace assets such as fuselages, wing structures, or pressure vessels presents a potential solution. However, a conventional structural health monitoring approach is to use guided waves sent and received between an array of transducers. This presents an issue for the use of fiberoptic sensors which are not capable of excitations and only detection. To solve this problem it is proposed that existing ambient vibrations (the 'noise') are used as a preexisting source of ultrasound. This provides a passive modality, where the desired signal can be created though advanced signal processing on data harvested simply by the fiberoptic sensors. The aim if this research is to produce a proof-of-concept prototype monitoring system. This system would allow for the construction of a close approximation of a traditional active signal (with ultrasonic excitation) through advanced processing on a passive signal (without ultrasonic excitation). In order to construct this system, this work will focus on creating a better understanding of the means by which an active signal can be reconstructed. This understanding will then be used to better define hardware limitations and data processing techniques required to build a reliable prototype.

Project Objectives
The ultimate goal of this project was to determine the feasibility of a fully passive ultrasonic technique. This included defining the requirements for data acquisition (e.g. transducers, amplifiers, filtering). In addition, the contributions of different signal components (e.g. acoustic noise, thermal vibrations, electrical noise) were explored for systems which allowed for successful passive measurements. Replication of past studies [1][2] was performed to verify the validity of a fully passive technique using both bulk and guided waves.

Methodology Used
Fully passive (no excitation) and semi-passive (excitation with very low amplitude random noise) measurements were taken using a variety of transducers and piezoelectric disc. Bulk wave measurements were taken on an aluminum block and guided wave measurements were taken on an aluminum plate. Autocorrelation was performed on bulk wave measurements from one receiver to recover the desired pulse-echo A-scan. Cross-correlation was performed on guided wave measurements from two receivers in an attempt to recover the desired pitch-catch A-scan. Measurements were taken with multiple frequencies, capture times, and sample rates to optimize the quality of the a-scan recovered.

Results Obtained
Figure 1 shows an example of a successful a-scan recovery from a semi-passive data capture from the aluminum block. A successful a-scan recovery was also achieved from a fully passive measurement on the block. Currently, measurements on the aluminum plate using guided waves have been unsuccessful in recovering the desired pitch-catch a-scan.

Significance and Interpretation of Results

Previous studies [1][2] have proposed that the success of fully passive ultrasonic techniques is due to thermal fluctuations generating a diffuse ultrasonic field. Results in this research suggest that this diffuse ultrasonic field may be the result of low-level excitation from the receiving transducers. This low-level excitation is the result of electrical noise causing a mechanical response in the piezoelectric material. Although this strays from the previously suggested theory, the results of this research can still be considered as a successful passive ultrasonic method that requires no excitation. However, these results suggest that use of this methodology with fiberoptic strain sensors is limited as they cannot “self-excite” like piezoelectric discs.

Figures/Charts

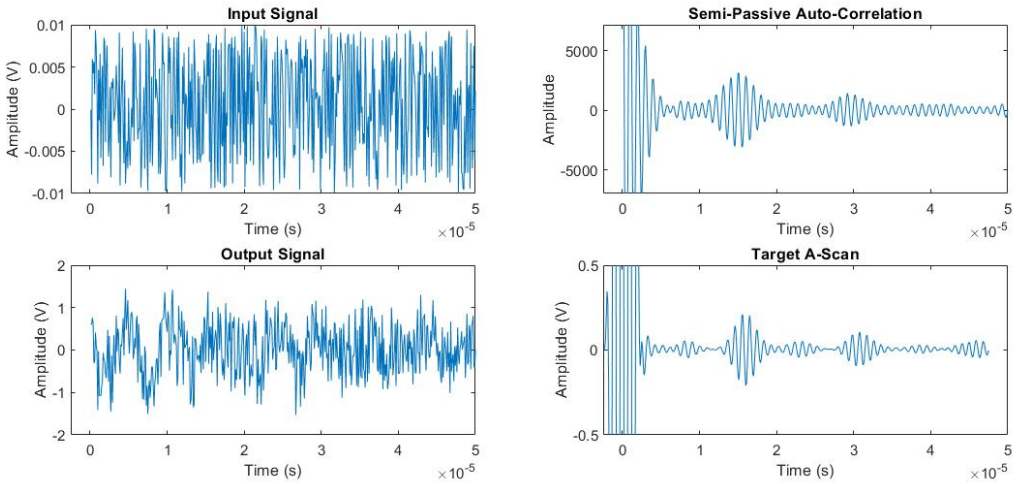

Figure 1. Example of a successful semi-passive a-scan replication using bulk waves

Acknowledgements and References

The author would like to thank the Ohio Space Grant Consortium for their support during the 2022/2023 academic year. Additionally, this work wouldn’t have been possible without the support and guidance of thesis advisor Dr. Joseph Corcoran.

[1] Oleg I. Lobkis and Richard L. Weaver , "On the emergence of the Green’s function in the correlations of a diffuse field", The Journal of the Acoustical Society of America 110, 3011-3017 (2001) https://doi.org/10.1121/1.1417528

[2] Tom Druet, Bastien Chapuis, Manfred Jules, Guillaume Laffont, and Emmanuel Moulin , "Passive guided waves measurements using fiber Bragg gratings sensors", The Journal of the Acoustical Society of America 144, 1198-1202 (2018) https://doi.org/10.1121/1.5054015

Aligning Functional Analysis Processes to Designers' Natural Cognitive Flow to Improve Creativity and Reduce Effort

Student Researcher: Hunter S. Reeling

Advisor: Dr. Jinjuan She

Miami University
Mechanical and Manufacturing Engineering

Abstract
In the field of engineering design for developing new products, balancing creativity with a structured approach is a critical challenge. While researchers strive to optimize the process, each stage is analyzed to enable designers to create superior products in a cost-effective manner. One approach to improve product development is by incorporating Human-centered Design into functional analysis. However, some critics of these methods argue that they require too many resources, restrict creativity, and impose high demand on the design teams. This research aims to address these concerns by incorporating theories from both cognitive research and Human-centered Design into the functional analysis process. The proposed method, termed Natural Cognitive Flow Functional Analysis (NCFFA), is designed to promote the designers' creative freedom, enhance the quality of the function model of the design space, and be accessible to engineering students and industry professionals alike.

Project Objectives
Functional decomposition is a widely taught practice in engineering curricula today[1,2]. Research has shown that it is a useful step in breaking down complex high-level issues into smaller, more manageable problems that can be addressed during the design process[2,3]. Integrating the consideration of user needs and interactions with the product into this process can result in more comprehensive and successful outcomes. However, the time and effort required for functional analysis, along with its perceived lack of creativity, have limited its application in practice[4,5,6]. Further research is necessary to effectively integrate Human-centered Design into functional analysis in a way that suits the needs of designers. Industry interviews conducted by Miami University's Human-centered Design Lab suggest that engineers and their companies do not place a high value on functional decomposition tasks. The proposed methods aim to address these concerns and promote improved design practices that appeal to both academia and industry, thereby bridging the gap between the two. The objective of this research is to develop a more effective approach that overcomes the limitations of traditional functional analysis methods while promoting the benefits of Human-centered Design in the engineering design process.

This research 1) proposes a novel strategy to overcome the challenges associated with functional decomposition, as discussed previously, by integrating concepts of Dual-Process Theory[7], Fuzzy Trace Theory[8], the benefits of incorporating Human-centered Design elements into functional analysis[9], and the function interaction model[10]. The effectiveness of this strategy is being assessed through a 2) between-subject study, comparing its impact on the design process and outcome to the traditional approach. It is expected that this proposed approach will help improve creativity in functional analysis, make the process more accessible to engineering students, and more appealing to experienced engineers, ultimately improving the design process.

Methodology
In a typical design environment, designers usually start by identifying the needs or requirements for the design. In consumer product design, this typically takes the form of a basic user requirements list for the end product. NCFFA proposes a Process Flow by modifying the User Workflow and FIM[10]. In this context, a process flow combines product actions, user actions, and user-product interactions to display the complete functional process flow the product will undergo. A user workflow is similar to the proposed process flow, except that passive actions from FIM are divided into user actions and user actions that interact with a product function. Previous functional analysis methods required designers to immediately enter a structured decomposition step following a review of the product requirements. However, critiques of this approach cited strict structure and rules, such as syntax and solution neutrality, as major hindrances to designers' creativity, making the stage feel laborious. The proposed process separates the generation of ideas from their evaluation, following research on brainstorming that suggests this separation can promote a mode of thinking closer to System 1[7,11], which can increase creativity and reduce

perceived cognitive effort. To avoid negative consequences such as design fixation[12] and other issues associated with a flimsy model structure, NCFFA includes an intermediate housekeeping step to refine the functions so they are in optimal form, verb-noun, and solution-neutral. These refined functions then enter a decomposition step, where the designer breaks down larger primary functions into smaller sub-functions that are simpler to design for. The most common strategy is to build a function tree, where the functions are organized in a hierarchical manner, with primary functions at the top and sub-functions below. This strategy is preserved when developing a function model with NCFFA. Novices previously had struggled with generating these functions, focusing on compositional rules, and building the tree simultaneously. With NCFFA, the functions have already been developed and refined to meet user requirements and design rules, making it easier for novice designers to assemble the hierarchical function tree, break down sub-functions where necessary, and focus on understanding interactions between certain functions.

To test the efficacy of the proposed Natural Cognitive Flow Functional Analysis (NCFFA) method in addressing the identified and achieving the goals outlined in the previous section, a between-subject study was conducted with undergraduate engineering students representing novice engineers. A case product, a power-screwdriver, was selected due to the suitable level of complexity for functional analysis but not too complex as to be overly abstract or take too much time to complete the activity. The experiment had one group using the NCFFA method and the other group using a traditional method. Both groups received the same information, including a user persona, list of user needs, and a process flow, but the experimental group was guided through the NCFFA steps. Data was collected through analysis of the completed function models and the post-activity survey. The function models are currently being evaluated for depth, breadth, and coverage by measuring the total unique functions, total levels, and average number of functions per level. Additionally, a novelty measure is being calculated based on the frequency of function mentions across participants as a measure of creativity. Functions mentioned frequently receive a lower novelty score, while those mentioned less frequently have a higher value. The mean novelty score of each function tree is being computed and used for comparisons. The study also collected information on familiarity with functional analysis (FA) as a balancing variable, perceived effort, and creative flow state using the Flow State Scale (FSS) self-assessment which has been tied in research to be a successful measure of creativity during a process[13]. By utilizing these measures, the study aims to draw conclusions about the effectiveness of NCFFA compared to traditional functional analysis in terms of improving the function model, enhancing designer creativity, and reducing the effort required to complete design tasks.

Results

The main objective of the proposed Natural Cognitive Flow Functional Analysis (NCFFA) method is to assist novice engineers in developing a comprehensive function model. To assess the effectiveness of the NCFFA method, the depth, breadth, and extent of coverage of the functional model in the design space is being evaluated. This evaluation will involve analyzing the function trees to determine the total number of unique functions, total levels, and average number of functions per level. The depth of the function model will be approximated by measuring the number of hierarchical levels in the function tree. Additionally, the breadth of the function model will be estimated by determining the number of functions across the width of each level of the function trees. Processing these trees and analyzing the results is taking some time, however initial indicators have been positive. Student participants appear to be generating larger decompositions, with more creative functions, and preserving NCFFA as similar or less difficult in comparison to the traditional method. The major contribution to this point, at the time of this conference, has been the literature review, proposed strategy, and design of the between-subject study. More final results and interpretations will be finalized in the coming weeks and submitted as part of Hunter Reeling's final M.S. thesis.

Acknowledgments and References
This research would not be possible without the funding from the Ohio Space Grant Consortium (OSGC) and NASA. Additionally, thank you to the Miami University Undergraduate Research Association and Graduate School for the support and necessary resources to complete the studies in this research.

[1] Ulman, D.G. (2008), *Mechanical Desgin Process*, *Higher Education*.

[2] Ulrich, K. T., & Eppinger, S. D. (2012). Product Design and Development: Fifth Edition. In McGraw-Hill.

[3] Pahl, G., Beitz, W., Feldhusen, J., & Grote, K. H. (2007). Engineering design: A systematic approach. In Engineering Design: A Systematic Approach. https://doi.org/10.1007/978-1-84628-319-2

[4] Booth, J. W., Reid, T. N., Eckert, C., & Ramani, K. (2015). Comparing Functional Analysis Methods for Product Dissection Tasks. Journal of Mechanical Design, Transactions of the ASME, 137(8). https://doi.org/10.1115/1.4030232

[5] Caldwell, B.W., Ramachandran, R. and Mocko, G.M. (2012), "Assessing the use of function models and interaction models through concept sketching", *Proceedings of the ASME Design Engineering Technical Conference*, Vol. 7, available at: https://doi.org/10.1115/DETC2012-71374.

[6] Eckert, C., Alink, T., Ruckpaul, A., & Albers, A. (2011). Different notions of function: Results from an experiment on the analysis of an existing product. Journal of Engineering Design, 22(11–12). https://doi.org/10.1080/09544828.2011.603297

[7] Kahneman, D. (2011), *Thinking, Fast and Slow.*, *Thinking, Fast and Slow.*, Farrar, Straus and Giroux, New York, NY, US.

[8] Reyna, V.F. (2012), "A new intuitionism: Meaning, memory, and development in fuzzy-trace theory", *Judgment and Decision Making*, Vol. 7 No. 3.

[9] She, J., Belanger, E., Bartels, C. and Reeling, H. (2022), "Improve Syntax Correctness and Breadth of Design Space Exploration in Functional Analysis", *Journal of Mechanical Design*, Vol. 144 No. 11, available at: https://doi.org/10.1115/1.4054875.

[10] Ramachandran, R. (2011), *Understanding the Role of Functions and Interactions in the Product Design Process*, *Department of Mechanical Engineering*.

[11] Kannengiesser, U. and Gero, J.S. (2019), "Design thinking, fast and slow: A framework for Kahneman's dual-system theory in design", *Design Science*, Vol. 5, available at: https://doi.org/10.1017/dsj.2019.9.

[12] Jansson, D.G. and Smith, S.M. (1991), "Design fixation", *Design Studies*, Vol. 12 No. 1, available at: https://doi.org/10.1016/0142-694X(91)90003-F .

[13] Yang, X., Cheng, P.-Y., Lin, L., Huang, Y. M., & Ren, Y. (2018). Can an Integrated System of Electroencephalography and Virtual Reality Further the Understanding of Relationships Between Attention, Meditation, Flow State, and Creativity? Journal of Educational Computing Research, 57(4), 846–876. https://doi.org/10.1177/0735633118770800

Using Remote Sensing to Predict Seasonal Controls on Soil Respiration and Weathering Across a Watershed

Student Researcher: Alyssa N. Reinhardt

Advisor: Dr. Timothy Gallagher

Kent State University
Department of Earth Science

Abstract

Acid Mine Drainage (AMD) is an environmental concern commonly linked to spoils from coal mines. The oxidation of the mineral pyrite is a major contributor to this issue, and its chemical reaction consumes soil oxygen[1]. This gas consumption can obfuscate gas signals associated with soil respiration, known as the Apparent Respiratory Quotient (ARQ) in which the relation of O_2 consumed to CO_2 produced is theoretically 1:1[2]. This research investigates whether the oxidation of pyrite affects soil ARQ measurements, how seasonal moisture impacts these gas measurements, and whether there is a gas-moisture relationship that can be upscaled over the entire study area of the Huff Run Watershed in southeast Ohio.

Project Objectives

The objectives of this research were to a) track soil gas signals in the Huff Run Watershed seasonally, b) link gas signals to moisture patterns using remote sensing to create a Normalized Difference Moisture Index (NDMI), and to c) assess the possibility of upscaling relationships between soil gas signals and soil moisture over the Huff Run Watershed as a whole.

Methodology Used

Soil gas samples were collected from two sub-watersheds in the southwest corner of the Huff Run Watershed in December 2021, August 2022, October 2022, and February 2023. The samples were collected via steel wells that were drilled into the mine spoils at a maximum depth of 80 cm. Gas was extracted from these wells using a syringe and evacuated gas bags that were taken back to the lab for geochemical analysis. A Sable Systems Field Metabolic System (FMS) was used to ascertain the percentage of carbon dioxide and oxygen in each soil sample, and then ARQ values were calculated for each sample relative to the overlying atmosphere on the day of sampling.

A Normalized Difference Moisture Index was calculated with Landsat 8 data using the calculation (Band 5 – Band 6)/(Band 5 + Band 6)[3]. The NDMI's were created using QGIS and the Semi-Automatic Classification Plugin. Indices from each sample month were compared to their respective soil gas data.

Results Obtained

The NDMI results show that surface moisture was highest during August and October of 2022 and lowest during December 2021 and February 2023. Soil gas signals taken during August and October of 2022 reflect signals that are typical of a soil with gas signals dominated by soil respiration, while the gas data from December 2021 and February 2023 show deviations from this signature.

Significance and Interpretation of Results

The occurrence of typical gas signals (aligning with the 1:1 soil respiration relationship) during wetter months indicates that moisture likely does play a role in the measurement of both respiration and pyrite

oxidation signals. Although there is proof of AMD year-round, the pyrite oxidation signal seems to be lost during wetter months, suggesting that the infiltration of moisture into the soil (perhaps through precipitation) could cause the homogenization of deeper oxidation signals and shallower respiration signals. It is also possible that the soil respiration occurring during the more biologically productive months of the year (summer and autumn) could outpace oxidation in scale, thus making the oxidation signal relatively minimal and difficult to measure. Overall, this research shows the potential for using soil gas measurements and remote sensing to detect regional and seasonal patterns in soil gas processes and fluxes.

Figures/Charts

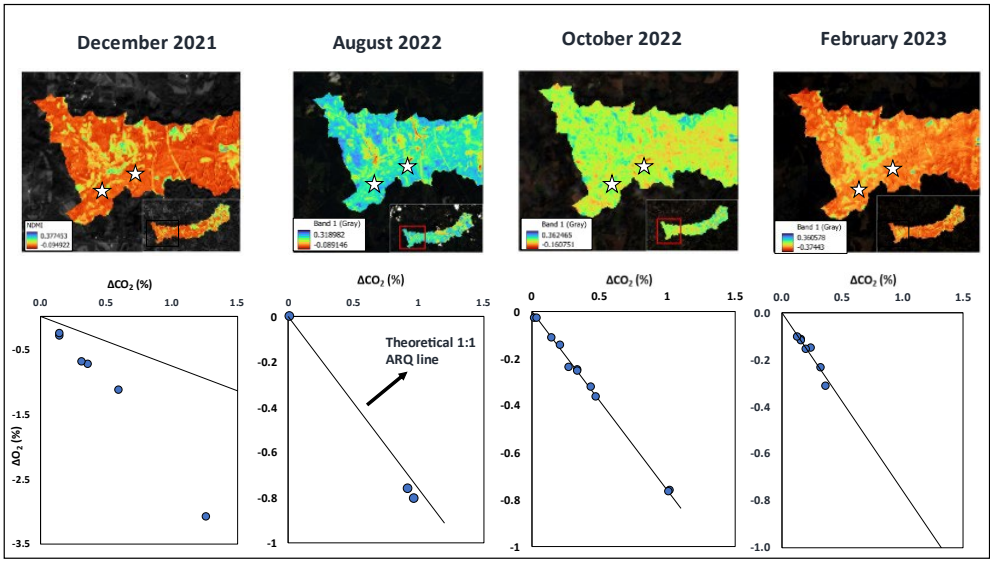

Figure 1. NDMI images for the Huff Run Watershed for each sampling month (top row) and their corresponding soil gas measurements relative to the theoretical 1:1 ARQ line representing soil gases controlled by respiration only (bottom row).

Acknowledgements and References

The author would like to thank the Ohio Space Grant Consortium for funding this research and the Ohio Aerospace Institute for hosting the symposium. They would also like to thank their thesis committee and the students of the Kent State University Earth Science Department for their support.

1. Chandra and Gerson. The mechanisms of pyrite oxidation and leaching: A fundamental perspective. *Surface Science Reports*, Volume 65(9), pp. 293-315 (2010).
2. Angert et al. Using O_2 to study the relationships between soil CO_2 efflux and soil respiration. *Biogeosciences*, Volume 12(7), pp. 2089-2099 (2015).
3. Landsat Missions. Normalized Difference Moisture Index. *USGS (https://www.usgs.gov/landsat-missions/normalized-difference-moisture-index)*, (2021).

Scholars

Predicting Gravitational Collapse with the Einstein Field Equations

Student Researcher: Ethan R. Armstrong

Advisor: Dr. Aloysius Bathi Kasturiarachi

Kent State University
Department of Mathematical Sciences

Abstract
A star's final mass at the end of its life determines if the pressure it generates is enough to resist the force of gravity. If it's light enough, it will leave behind a white dwarf or neutron star. If its final mass is over around 2 solar masses, the so-called TOV (Tolman Oppenheimer Volkoff) limit which comes from General Relativity, it will collapse into a black hole. This limit comes from the TOV equation and applying an Equation of State for a neutron star that relates its pressure to its density. Determining the proper equation of state is an active area of interest. Another complication on top of finding the right EOS is accounting for the rotation of a star, as the TOV equation is for non-rotating stars. The TOV limit can increase for rotating stars, as the centrifugal force produced by their rotation can further resist gravity.

Objectives
Our goal is to use Einstein's Gravitational Field Equations to predict whether certain stars will collapse into black holes at the end of their lives. Specifically, we will be using the bounds on neutron star mass given by the TOV equation, which describes a spherically symmetric body of isotropic material in gravitational equilibrium. We will apply it to the predicted final masses of several nearby stars, taking into account their mass, metallicity, and angular momentum.

Methodology Used
Because a star's remnant is determined by its final mass, it's a matter of predicting the star's final mass from its initial properties like mass, metallicity and angular momentum. A function that takes in initial mass and other properties and gives the final mass of the star is called an IFMR (initial final mass relationship). Heger et al. [2] used previous work on IFMRs and supernovae to predict what remnant a star would leave behind, accounting for its mass and metallicity, but not its rotation. Plotted below are various nearby stars with their masses and metallicities, as well as the boundaries between remnant types. An IFMR (taken from [1]) which does not take into account rotation was applied to the three stars above around 25 solar masses to check that their final masses were still all above the maximally increased TOV limit for a fast-spinning neutron star, which is known to be around 2.6 solar masses by observation [5].

Results Obtained
The three stars Rho Cygni, Zeta Puppis, and Rho Cassiopeiae should all form black holes based on their mass and metallicity, according to the chart below (Figures 1 and 3). Their final masses given by the applied IFMR were all significantly above 2.6 solar masses, lending further confidence that they would form black holes. All other stars were below the threshold to produce black holes.

Significance and Interpretation of Results
While the results would imply that the three heaviest stars listed will form black holes, there are substantial uncertainties in the full effects of rotation on the IFMR. A rotating star's mass loss rate and stellar wind can be affected by its rotation, which is not fully understood. Ideally, an IFMR would take into account a star's mass, metallicity and angular momentum. Care should be taken still in assuming these stars will produce black holes. Another interesting avenue of research would be an equivalent to the TOV equation for rotating stars based on the Kerr metric and an EOS that considers rotation. Some papers have attempted this with varying success, such as [3] and [4] below.

Figures

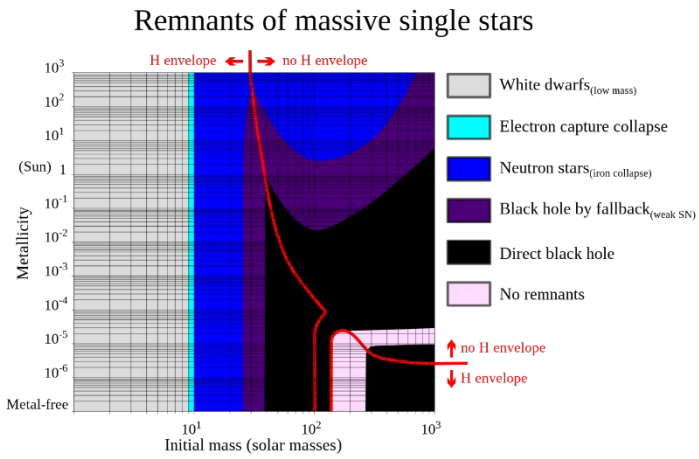

Figure 1 – from Heger et al. a chart of how initial mass and metallicity affect the stellar remnant left behind.

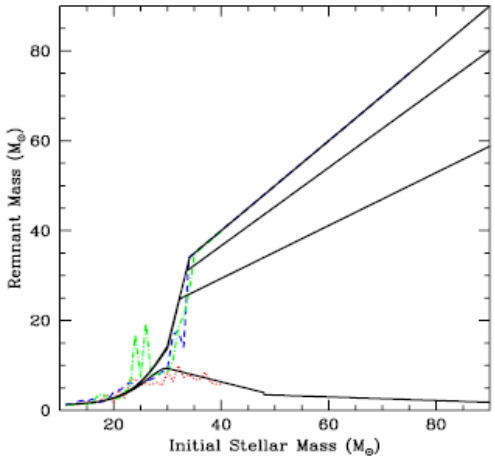

Figure 2 – IFMRs from Fryer et al.

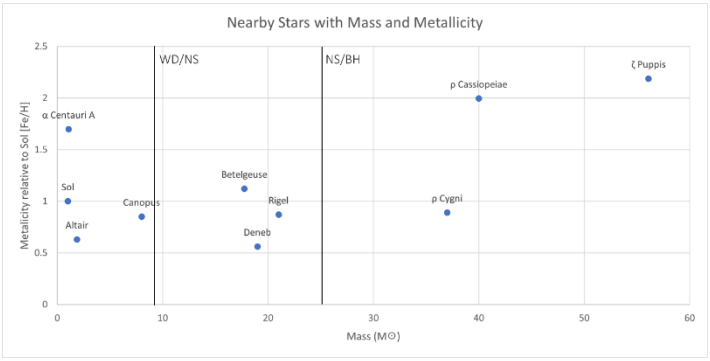

Figure 3 – Well known nearby stars with their masses and metallicities. Also given are the mass cut-offs for white dwarves and neutron stars for approximately solar metallicity from Heger et al.

Acknowledgments and References

Thank you to the OSGC and NASA for sponsoring the author's research, and to his advisor Dr. Kasturiarachi for his guidance, as well as to Kent State and the professors and faculty who facilitated his participation in the OSGC.

1] Fryer, C., Belczynski, K., Wiktorowicz, G., Dominik, M., Kalogera, V., & Holz, D. (2011). COMPACT REMNANT MASS FUNCTION: DEPENDENCE ON THE EXPLOSION MECHANISM AND METALLICITY. The Astrophysical Journal, 749(1), 91. https://doi.org/10.1088/0004-637x/749/1/91

[2] Heger, A., Fryer, C. L., Woosley, S. E., Langer, N., & Hartmann, D. H. (2003). How Massive Single Stars End Their Life. The Astrophysical Journal, 591(1), 288–300. https://doi.org/10.1086/375341

[3] Hernández-Pastora, J. L., & Herrera, L. J. (2017). Interior solution for the Kerr metric. Physical Review, 95(2). https://doi.org/10.1103/physrevd.95.024003

[4] Ravi, A., & Banerjee, N. (2018). An exact interior Kerr solution. New Astronomy. https://doi.org/10.1016/j.newast.2018.04.003

[5] Rezzolla, L., Most, E. R., & Weih, L. R. (2017). Using Gravitational-wave Observations and Quasi-universal Relations to Constrain the Maximum Mass of Neutron Stars. The Astrophysical Journal, 852(2), L25. https://doi.org/10.3847/2041-8213/aaa401

Phenotypic Characterization of Plants via Clinorotation

Student Researcher: Wafa O. Aziz

Advisor: Dr. Sarah Wyatt

Ohio University
Chemistry & Biochemistry Department

Abstract

How does gravity affect plant growth? Or rather the absence of it? To help answer these questions, some NASA spaceflights allow for plant experimentation in the microgravity environment of the International Space Station (ISS). One such experiment, Biological Research in Canisters (BRIC) 20 flown in 2015 by the Wyatt lab at Ohio University, led to the discovery of three transcription factors (TFs) that had altered expression in spaceflight as compared to ground controls. TFs control downstream gene expression and are often a control point for physiological responses. These three TFs, Ethylene-responsive transcription factor 104 (ERF104), IQ-domain 21 (IQD21), and Cryptochrome-interacting basic-helix-loop-helix 1 (CIB1), were selected for further study via chromatin immunoprecipitation sequencing (ChIP-seq) to identify the DNA binding sites of the transcription factors and subsequent genes they regulate (ChIP-seq project of MS student Calvin Coffin).

Transgenic *Arabidopsis thaliana* plants homozygous for each tagged transcription factor (ERF104, IQD21, and CIB1) will be genotyped and phenotyped via root and shoot curvature. The results will determine whether the constructs, inserted into the respective mutant background, will yield wild-type responses to reorientation (effectively "rescuing" the phenotype). Phenotyping of these mutants will be continued using a novel approach, clinorotation. A clinostat allows for plant growth while rotating the plants in three dimensions, effectively simulating microgravity, and it also has the ability to capture images of the growing seedlings. Although this is not the true microgravity environment a spaceflight allows for, industry and the academic community utilizes the mimicked environment provided by clinorotation to study plant responses to microgravity.

Objectives

Use the SciSpinner to phenotypically analyze roots and stems of homozygous mutant lines. Once homozygous lines defective in ERF104, IQD21, and CIB1 have been confirmed, the regulation of each transcription factor in simulated microgravity will be assessed using the clinostat. Specifically, the root and stem behavior of the seedlings homozygous for deletion of each transcription factor and those transgenics that "rescue" the mutant phenotype will be compared to that of wild-type Arabidopsis. This will provide a unique dataset on the effects of these transcription factors under simulated microgravity.

Methodology Used

Arabidopsis seeds were surface sterilized with 95% ethanol and placed on 1% agar MS plates. Using forceps and a microscope, each seed was arranged to turn the micropyles downward. Plates were wrapped in micropore tape and placed upside down for 2 days in 4°C for stratification. Plates were then moved to a growth chamber and grown vertically for 9 days. Plates were moved to the clinostat after 9 days where specific parameters were altered.

With all other parameters kept the same, only the direction of rotation of the inner compartment was varied. When the inner barrel rotates left (or counterclockwise), the roots rotate left. When the inner barrel rotates right (or clockwise), the roots rotate right (Figure 1).

Figures/Charts

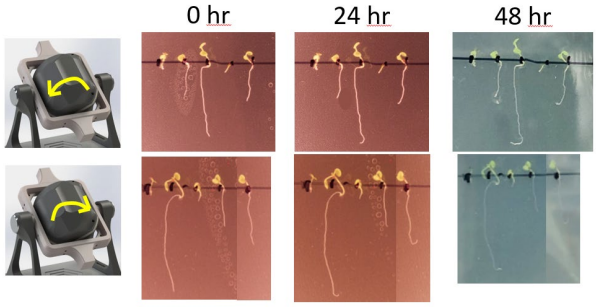

Figure 1: root curvature as a response to inner barrel rotation.

With all other parameters kept the same, only the direction of rotation of the plate of seeds was varied. Plate orientation confuses root curvature and more experimentation is still needed to discern a pattern (Figure 2).

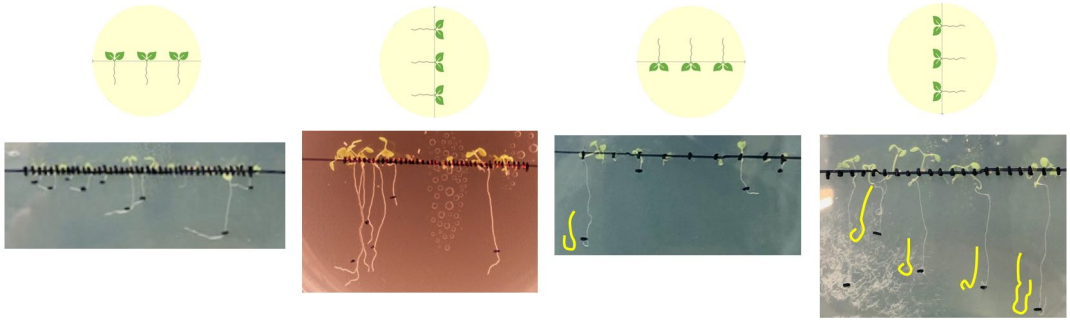

Figure 2: root curvature as a response to plate orientation.

With all other parameters kept the same, only the photoperiod the seedlings were exposed to was varied. Seedlings grown in a 1 hour on/1 hour off photoperiod displayed no curvature compared to seedlings grown in a 16 hour on/8 hours off photoperiod, indicating that exposure to light induces root curvature (Figure 3).

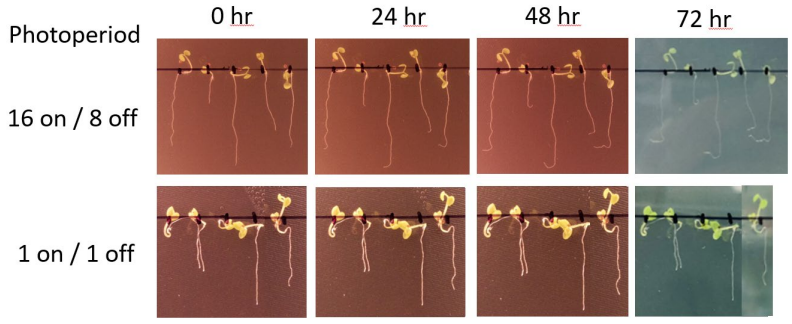

Figure 3: root curvature as a response to photoperiod.

Acknowledgments
Thank you to Dr. Sarah Wyatt for her continued guidance. This research was supported by The Ohio Space Grant Consortium.

Space Radiation Protection for Space Travel

Student Researcher: Tyreese Bernard

Advisor: Deok H. Nam, Ph. D.

Wilberforce University
Electrical Engineering

Abstract
Recently, many national space agencies are planning a human mission to space travel including the moon and Mars. The dangers of radiation from space travel are serious since the research of space radiation protection is to study the dangerous long-term side effects. In addition, if it is continuing to explore deeper outer space with crewed ships, more research about studying the dangers of radiation caused by space travel is required. Humans are safe from this harmful radiation on planet Earth by theearth's protective magnetic bubble which is called the magnetosphere that deflects most solar particles.Many national space agencies are planning a human mission to space travel including to the moon andMars. Radiation is simply a form of energy that is emitted in the form of rays, electromagnetic waves, and particles. One of the potential issues is how efficiently to protect the space radiation during space travel such as recognizing space radiation with high uncertainty on the risk of radiation-induced morbidityand the lack of simple countermeasures to reduce the exposure.

Project Objectives
the dangers of radiation from space travel are serious and if we want to keep continuing to explore deeper outer space with manned ships we need to study more about the dangers of radiation caused by space travel. On planet Earth we humans are safe from this harmful radiation. Due to earth's protective magnetic bubble that is called the magnetosphere that deflects most solar particles. Many national spaceagencies are planning a human mission to space travel including to the moon and Mars. Radiation is simply a form of energy that is emitted in the form of rays, electromagnetic waves, and particles. One of potential issues is how efficiently to protect the space radiation during space travel such as recognizing space radiation with high uncertainty on the risk of radiation-induced morbidity and the lack of simple countermeasures to reduce the exposure. The research of space radiation protection is to study the longterm side effects which are really dangerous. To find a better alternative to shielding radiation will be studied by comparing the existing technologies. Since researching and seeing if expanding our human civilization to another planet is really worth it or not, this research provides a method to lower the levels of radiation more efficiently while traveling through space.

Methodology Used
The project examines the various methods to protect space radiation from reduced exposure, and how efficiently to shield the space radiation. With the simplest physical countermeasure, and how to assess additional protection in the spacecraft. Space radiation protection is how each of the several different technologies works with the types being Immune modulation, hydrogen shielding, Active radiation shielding, Passive radiation shielding, and radioprotectors. With the study, you'll make a comparison of how each one works and all the pros and cons of everyone. Space travel is starting to become a big industry with small and major companies being developed every day. Protection from radiation is a big and serious topicthat needs to be discussed. New space radiation technology is being developed right now and has not been tested. In the future we could develop a solution that could stop it indefinitely there is simply more work that needs to be.

Results Obtained

Astronauts who stay on the ISS (International Space Station) for 1 year will receive on average 300 mSvof radiation, equivalent to approximately 50 chest CT scans. The crew of the Apollo Moon missions recorded a moderate dose of close to 5 mSv for each astronaut like a single chest CT scan & The average annual amount of exposure from cosmic radiation is 0.33 mSv (33) or 11% of a person's yearly orientation due to all-natural sources of radiation.

Significance and Interpretation of Results

Elon Musk predicts a crewed flight mission to mars by 2029 and also wants to expand 7 cultivate the planet mars for the human race. With it taking almost a year to get to the big red planet that is a lot of radiation that the astronauts will have to endure for a very long period of time. Then there are questions like once we get there how bad will the effects from radiation be, if we choose to expand and grow the human race will the mutated genes from space travel have an effect on the children we choose to make. Also will the life expectancy be lower due to the serious side effects like cardiovascular disease. Astronauts now use hydrogen, boron, and nitrogen to shield from radiation but is there anything else we could use? Truly no one knows what lies ahead in the future but is thereanyway we could block any and all radiation from space travel. The cardiovascular system plays a bigpart in our body. Is it really worth messing with it knowing all the side effects that come along with ist?.Some earlier work by past scientists and research has been done studying space radiation levels including.

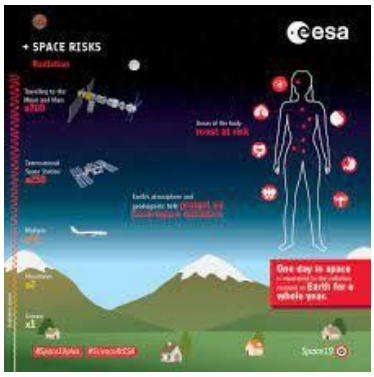

Figure 1. Flowchart of Space Radiation to body

Table 1. Comparison of Radiation Protection Methods

	Immune Modulation	Hydrogen shielding	Active radiation shielding	Passive radiation shielding	Radioprotectors
How the Radiation protection works.	Drug therapy that astronauts undergo.	A layer of hydrogen gas around the spacecraft.	Deflect and trapped portions of the incoming space radiation.	Placing some sort of physical material in between a prison and the source of radiation.	Radiation therapy that astronauts undertake before a flight.

Acknowledgements and References

Many thanks to Ohio Space Grant Consortium and OAI for the academic scholarship program. Special thanks to Dr. John Sankovic, Mr. Robert Romero, Mr. Tim Hale, and my advisor, Dr. Deok Nam.

[1] https://www.nasa.gov/analogs/nsíl/why-space-íadiation-matteís Oct 8, 2019, titled "Why Space íadiation matteís"

[2] https://stemíad.com/blocking-space-íadiation-in-deep-space/ Dec 22, 2021, titled "Blocking space íadiation in deep space"

[3] https://www.nasa.gov/analogs/nsíl/why-space-íadiation-matteís Oct 8, 2019, titled "Why Space íadiation matteís"

[4] https://www.cdc.gov/nceh/íadiation/cosmic.html :~:text=ľhe%20aveía#e%20annual%20dose%20oí,fíom%20thíee%20chest%20x%2Díays. Dec 7, 2015, titled Radiation from Space (Cosmic Radiation)

Welding's Practicality in the Space Environment

Student Researcher: Grant I. Brautigam

Advisor: Dr Jed E. Marquart

Ohio Northern University
Department of Mechanical Engineering

Abstract
With the accessibility of space increasing, manufacturing in the space environment will eventually be necessary for repairs and construction of bigger structures. Welding is a fundamental aspect of any large scale project thus knowing what kinds of welding are practical in the harsh environment of space is key for a safe a successful execution. Traditional arc welding poses different hazards that less-common types of welding such as friction and electric beam welding may be able to combat. In-space manufacturing can increase the scale and limit on what kinds of structures can be put into orbit.

Objective
The objective of this research was to compile different information on possible problems and solutions to in-space welding.

Methods
Documentation were searched for using internet search engines. Prior research and experiments were reviewed for content to include in this report.

Results
In recent years the accessibility of space has greatly increased. Soon In-space manufacturing will be necessary for large scall projects. Welding is a key aspect of large-scale fabrication projects and thus it will be needed for construction of big orbital structures. Current welding techniques pose problems when placed in the space environment. However, some less common techniques can potently combat these problems and allow for in-space fabrication.

The most common type of welding is traditional arc welding. This kind of welding poses multiple problems when considering it in the space environment. The first problem is gravity. During arc welding the filler material needs to mix with the existing material to form a strong bond. When in the microgravity of space, this is much harder to accomplish as there is no relative acceleration pulling the weld bead down towards the part. Additionally, the fumes and particles that arc welding produces could be harmful to astronauts in the surrounding environment as well as hard to filter out of the air. The filtering process could harm and degrade the life support equipment that the astronauts rely on. Another problem is with cooling. With there being no ambient air or bulk fluid, convection is no longer an available mode of heat transfer. This allows the weld to experience the aneling temperature for longer which could change the overall material properties of the welded area [1].

One type of welding that may be a more practical solution for the space environment is electric beam welding. In electric beam welding, electrons are fired on to the workpiece to introduce the energy needed to heat up the part and fuse them together. The one big problem with electric beam welding is that it must be done in a vacuum. This poses an expensive and time-consuming barrier to cross when this type of welding is used on the ground. However, in space this is not a huge consideration as a

vacuum is already present. Electric beam welding requires a high level of precision to run however that precision is preserved in the product and thus creates a time and cost-effective means of welding [2].

One of the more common welding techniques for the aerospace industry is friction stir welding. This type of welding is a non-fusion-based technique. A spinning head heats up the workpiece though friction until the material is soft enough to spin with the head and mix together. This type of welding is commonly used for aluminum since arc welding does not work well with most alloys. One problem with deploying friction stir welding in space is that it is not a portable process. Advancements in the technology are allowing for friction stir welding to be more accessible, but currently it would be very difficult to execute the process in a space setting as lots of support equipment would need to be sent up in cargo supply missions [3].

Large scale manufacturing in space will only become practical with the introduction of in-space welding. Having the ability to repair spacecrafts is also a major advantage that in-space welding would bring. Welding is the next hurdle for in-space manufacturing and with it the possibilities of future missions and research will push the boundaries of what mankind can accomplish.

References

1. N. Naden and T. J. Prater, et al. (2020). *A Review of Welding in Space and Related Technologies* [Online]. Available: https://ntrs.nasa.gov/api/citations/20200002259/downloads/20200002259.pdf
2. J. DeLalio. (Aug 2, 2016). *Electron beam or laser beam welding?* [Online]. Available: https://www.thefabricator.com/thefabricator/article/laserwelding/electron-beam-or-laser-beam-welding-
3. W. R. Longhurst. (2016). *Development of Friction Stir Welding Technologies for In-Space Manufacturing* [Online]. Available: https://www.osti.gov/servlets/purl/1360043

Simulating Fluid Flow through Quantum Computing

Student Researcher: Marek D. Brodke

Advisor: Dr. Prashant Khare

University of Cincinnati
Aerospace Engineering and Engineering Mechanics

Abstract
Recent advances in quantum computing hardware and its increased availability has made it possible for researchers to explore its potential. While this emerging area has been investigated by researchers in several different fields of inquiry, there is a lack of literature demonstrating its viability in simulating classical fluid flows. In this research effort, we build on previous work that showed the viability of solving the Navier-Stokes equations using classical-quantum algorithms. Specifically, we implemented a quantum amplitude amplification and estimation circuit and successfully demonstrated that it can be combined with classical algorithms to simulate fluid dynamic flows. This hybrid quantum-classical algorithm is then applied to investigate quasi-1D flow through a converging-diverging nozzle. Our results are in excellent agreement with the theoretical calculations for the flow through the nozzle. This evidence-based assessment is an important step to demonstrate the viability of applications of quantum computers to simulate fluid dynamic phenomena.

Project Objectives
In the present research effort, we build upon the algorithm mathematically demonstrated in [1] by implementing it into a quantum circuit and linking it to the classical portion of the algorithm. We then used the entirety of the algorithm to study quasi-1-D flow through a converging-diverging nozzle with a shock present. The working fluid for this flow is air and is approximated as a calorically perfect gas. The inlet conditions are nondimensional, with the inlet mass flow being 0.579. The temperature and pressure are based on this mass flow but have a random shift applied to them (see the supplementary information for [1] for more on the initial conditions as well as the boundary conditions). To ensure our implementation of the algorithm was effective, we compared our results with the variable area quasi-1D flow equations.

Methodology Used
We constructed the simulation using a classical algorithm based on [1], with minor optimizations and modifications. Our contribution was implementing the quantum algorithm directed by [1], which is constructed in [2]. Memory constraints on current quantum devices and simulators prevent directly implementing [2] due to the large number of qubits needed to match the large data sets generated by the classical portion of the algorithm. However, the underlying algorithm (i.e., the quantum amplitude amplification and estimation algorithm [3]) can be implemented without compromising the effectiveness of [2]. A thorough explanation can be found in our AIAA publication soon. For a diagram of the circuit that we used, see Figure 1.

Results

The raw results of our implementation, raw as in no computational tricks on the output such as interpolation, can be found in Figure 2. As you can see, the result of our implementation has low error except for the shock region. We also used interpolation to reduce the error in other implementations of our algorithm. Details on these can be found in our AIAA publication soon.

Significance and Interpretation of Results

The results of our implementation of the algorithm by [1] agree with the quasi-1D flow equations. This demonstrates that a hybrid quantum-classical algorithm is capable of simulating fluid flows. However, there is a concerning phenomenon that we observed with this algorithm. If the quantum portion of the algorithm is bypassed, then the results do not significantly change. This will be further explored in a future research effort.

Figures/Charts

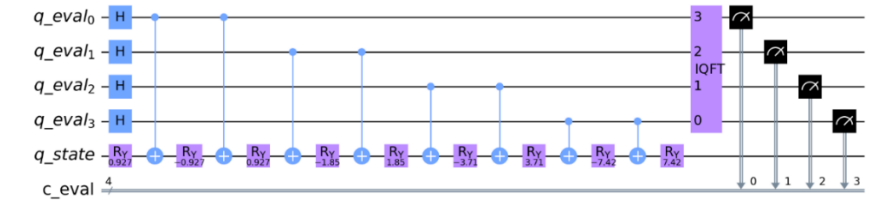

Figure 1. The quantum circuit used in our implementation.

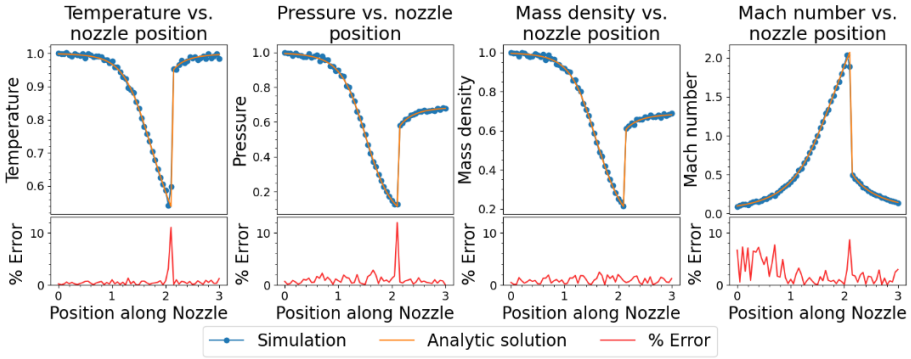

Figure 2. Results of our implementation plotted against the analytical solution of the flow.

Acknowledgments and References

Thank you to my advisor Dr. Prashant Khare, none of this would be possible without him. Also, a big thanks to OSGC for their support, it has given me the ability to pursue this research.

[1] F. Gaitan, "Finding flows of a navier–stokes fluid through quantum computing," *npj Quantum Information,* vol. 6, 2020.

[2] E. Novak, "Quantum Complexity of Integration," *Journal of Complexity,* vol. 17, pp. 2-16, 3 2001.

[3] Brassard, Gilles et al., "Quantum amplitude amplification and estimation," *Contemporary Mathematics,* p. 53–74, 2002.

Micro Electrical Discharge Machining of Aerospace Materials

Student Researcher: Collin R. Butler

Advisor: Dr. Muhammad Jahan

Miami University
Department of Mechanical and Manufacturing Engineering

Abstract
Electrical-Discharge Machining (EDM) is a non-contact machining technique that harnesses the electrical arc between a tool and workpiece in dielectric fluid to produce a spark, which removes material. The non-contact nature of EDM has many advantages, such as creating more options for machining materials that are very small or notoriously difficult to conventionally machine. This project investigates techniques of creating micro-scale electrodes that can create very small features and the practical limits of microscale machining. Different electrode machining parameters were tested, and finished electrodes were measured. This research aims to explore more options for creating micro-scale features on products and parts in a world where miniature, lightweight components are a key goal in manufacturing and design.

Project Objectives
Due to inherent imperfections in manufacturing processes, all machine tools have some sort of spindle run-out, which causes a slight off-axis rotation. In conventional, macro-scale machining, the incredibly small run-out on many machines (~10 micron) is much smaller than specified tolerances and therefore is a nonfactor. However, in micro-scale machining, 10 microns can cause serious deviations from intended dimensions and render tools and workpieces unusable. This study aimed to determine the best techniques to fabricate high aspect ratio micro-electrodes that can be used to create the small features that are increasingly sought after in the aerospace, computer, and other manufacturing industries. The experiment was designed to first determine appropriate machining parameters for the electrode manufacturing process, and then use those parameters to fabricate ultra-high aspect ratio electrodes of an acceptably consistent diameter.

Methodology Used
The self-drilled hole technique [1] was used on the Mikrotools DT-110 Integrated Micro-Machining Machine Tool using pure tungsten electrodes at a starting diameter of 500µm (0.5 mm). Shown in **Figure 1,** The self-drilled technique best compensates for any minute inconsistencies originating from a slightly slanted workpiece or spindle run-out compared to other electrode-reduction techniques. To carry out the technique, first a hole is drilled in a piece of sheet metal, which in this case was 1mm titanium, using conventional polarity (workpiece positive). Then, the electrode was offset a specified amount based on the diameter reduction desired, the polarity is reversed to make the tool positive, and the electrode is fed into the hole again. The offset means that a portion of the electrode is fed into the sheet metal, and the reversed polarity causes the workpiece to erode the electrode. This reduces the diameter by approximately the offset amount. The operation is then repeated until the desired electrode diameter and length is achieved.

One of the most important determinations to make when using EDM on micro-scale applications is the capacitance to set the machine at. Using more of the machine's capacitors will create a more powerful spark and therefore erode material faster, but this can cause the plate to erode and make the self-

drilled technique ineffective, or cause the electrode to break. Through initial experimentation, it was found that using 3 of the DT-110's capacitors (for a total capacitance of 1000pF) resulted in the plate staying intact during the reverse polarity phase of machining, and was therefore used for the duration of the experiment. For drilling the holes with conventional polarity, 10nF of capacitance was used for faster machining time. Using these two capacitances between the two machining phases, an intermediate voltage setting of 110V, and a spindle speed of 1500 RPM, which allowed for maximal debris clearing and therefore less short-circuiting, the electrodes were fabricated.

Results Obtained

Using the parameters detailed above, an electrode with a diameter of 38.1µm and length of 4.21 mm, for an aspect ratio of 110.5 (**Figure 2**), was fabricated. This electrode demonstrated a high degree of straightness and consistency that is difficult to obtain using other EDM techniques, and the process was shown to be repeatable in subsequent trials.

Significance and Interpretation of Results

This technique gives manufacturers a route to create ultra-small tools and use them to manufacture miniature features on any number of applications. Industry has a continuous and accelerating need for smaller-scale precision machining techniques, and while conventional machining is still an option, smaller tools will eventually not be able to withstand the high mechanical loadings required of them. For true micro and nano-scale applications, EDM and other non-contact machining techniques will need to be researched and developed to make them efficient, sustainable, and precise, and this study aimed to do just that. Using the parameters discussed earlier, electrodes with unique shapes could be fabricated for any number of desired features or applications. Non-contact machining will allow for smaller-scale computers and biological applications, and future manufacturing will look for affordable, efficient, and repeatable methods to do so.

Figures

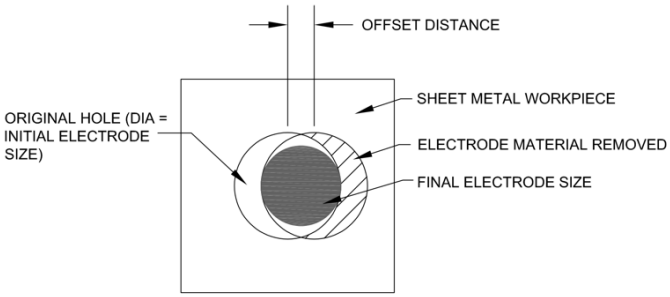

Figure 1: Schematic of Self-Drilled Hole Technique

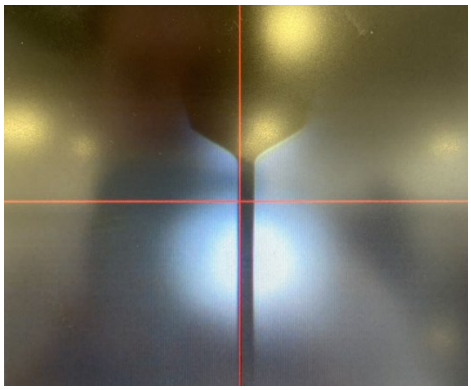

Figure 2: Finished Electrode (Φ = 38.1µm)
**Entire length of electrode not shown*

References

[1] Yamazaki, Minoru, et al. "EDM of Micro-Rods by Self-Drilled Holes." Journal of Materials Processing Technology 149, 2004.
[2] Mikrotools PTE LTD, "Operation Manual: DT-110." Mikrotools, 2012.
[3] Kibria, Golam, et al. "Micro Electrical Discharge Machining Processes." Springer, 2019.

Asymmetric Control of Subsonic Axisymmetric Jet Aerodynamics using Plasma Actuators

Student Researcher: Ethan C. Cartwright

Advisor: Dr. Mo Samimy

The Ohio State University
Department of Mechanical and Aerospace Engineering

Abstract

Improved aircraft performance is a continually active area of research. Altering the angle of jet thrust, known as thrust vectoring (TV), is particularly interesting for its impact on aircraft maneuverability and required takeoff/landing distance. Thrust vectoring is traditionally achieved by mechanical manipulation of nozzle exit geometry, which involves added weight and complexity to the aircraft. An alternative method Coanda-based Thrust Vectoring (CTV), exploits the Coanda effect to attach jet flow to a fixed surface at the nozzle exit which curves away from the jet axis (i.e., a "reaction surface"). This is accomplished by injecting high velocity flow into the exhaust flow shear layer which comes at the cost of a high bleed air requirement.

Localized arc-filament plasma actuators (LAFPAs) manipulate natural instabilities in jet flows to control shear layer behavior which could be used, similar to CTV, to attach the jet flow to a curved reaction surface, deflecting the exhaust thrust along the surface. LAFPAs may be particularly suited for this application due to their rapidly variable operational state and low power requirement. LAFPAs have demonstrated success in establishing shear layer control authority for various flow control objectives, but have yet to be applied to thrust vectoring.

Project Objectives

The unification of the demonstrated flow control authority of the LAFPAs and the impact of TV on maneuverability and takeoff/landing distance is promising in terms of the potential aircraft performance gains available. This work serves as a preliminary exploration of jet response to LAFPA/reaction surface control in a broad parameter space, as well as the particular potential of LAFPA operation in thrust vectoring. This is done by sweeping through excitation frequencies and spatial modes of LAFPAs and reaction surface configuration, and documenting jet behavior with pressure measurements, schlieren imaging, and PIV.

Methodology

The Kelvin-Helmholtz instability is an inherent sensitivity of shear layer flows (regions of high velocity gradient) to small perturbations of velocity, temperature, and pressure [1] that cause the shear layer to roll up into large scale structures (LSS) [2]. LAFPAs operate by striking a high voltage arc across pin electrodes which produce local thermal perturbations (1000s of Kelvin) with a relatively low input power (10s of Watts) at a controlled frequency [3,4]. These perturbations are amplified into LSS by the Kelvin-Helmholtz instability, allowing for control authority over LSS formation and development within the shear layer [5]. LSS formation in jet shear layers play a dominant role in several processes such as mixing and entrainment. Past works have applied the control authority over LSS formation afforded by LAFPA's in areas of jet acoustics [6,7], and mixing enhancement [5]. Gonzalez et al. [8,9] demonstrated the LAFPAs' ability to induce asymmetric mixing in a supersonic axisymmetric jet with a straight exit geometry (i.e., no CTV-like reaction surface).

Here, a CTV inspired curved nozzle outlet geometry is paired with embedded LAFPAs to explore the TV capability of the LAFPAs by means of attaching exhaust flow to the curved reaction surface. A 1-inch diameter jet nozzle with a curved reaction surface (depicted in Fig. 1) is installed in subsonic jet facility where experiments exploring LSS' physics were conducted. This nozzle is embedded with 8 azimuthally spaced LAFPAs, as well as pressure taps within the reaction surface. A backward facing step was included to generate a distinct shear layer as flow passes the step. Spatial excitation modes were explored by altering the number and azimuthal position of active LAFPAs, while the effects of variously sized LSS were explored by altering actuator control frequency. The effect of control on the jet flow was assessed with embedded pressure taps and schlieren imaging (a method of capturing density gradients in fluid flows).

LAFPAs are expected to initiate LSS formation in the shear layer that forms at the step. These LSS naturally entrain fluid as they propagate downstream, but instead attach to the curved reaction surface due to its proximity. An actuation frequency dependent response is expected in the LSS development behavior. At low actuation frequency, LSS are expected to grow naturally as they propagate downstream, while at high actuation frequency, reduced spacing between LSS is expected to cause growth interference and reduce ultimate size. LSS' entrainment—and therefore jet attachment/thrust vectoring capability—is higher for large, coherent structures than for small, rapidly dissipating structures, allowing manipulation of jet attachment location. Using different actuation frequencies for different LAFPAs, LSS size at particular azimuthal locations

can be independently controlled, causing an asymmetry in fluid entrainment and subsequent jet attachment/thrust vector deflection along a specified direction.

Results

Excitation was asymmetrically introduced across a range of frequencies and number of active actuators. Results in Fig. 2 highlight the azimuthal static pressure profile caused by either 3 or 4 adjacent active actuators at a jet Mach number of .48 and .90, respectively. The horizontal axis displays the azimuthal measurement location with the origin as the relative center of the active actuators, while the vertical axis represents a negative coefficient of pressure (suction) reported by the static pressure array. An expected significant asymmetric static pressure distribution is observed for both cases with low frequencies demonstrating increased suction toward active actuators (termed "attachment mechanism") and high frequencies demonstrating increased suction away from active actuators (termed "detachment mechanism"). Future work is required to understand the relatively less asymmetric pressure profile present at the higher Mach number, as well as measurement techniques including schlieren imaging and PIV to validate control mechanisms and confirm and quantify thrust vectoring.

Figures

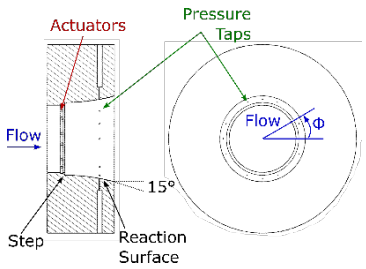

(a) (b)

Figure 1: Subsonic axisymmetric jet with reaction surface: (a) Side view (flow left-to-right) of actuators, static pressure taps, and reaction surface contour and (b) Front view (flow out-of-the-page) highlighting static pressure tap azimuthal distribution.

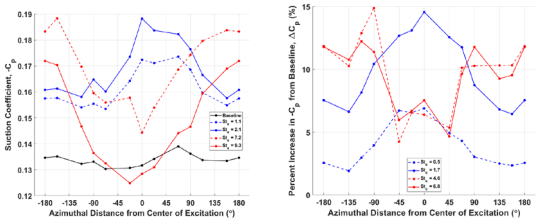

(a) (b)

Figure 2: Azimuthal distribution of suction coefficient ($-C_p$) for jet excited by a group of active LAFPAs (centered at 0°) at various excitation frequencies (St_e): (a) 4 active LAFPAs, M_j = 0.48 and (b) 3 active LAFPAs, Mj = 0.90

References

[1] Moore, C. "The Role of Shear-Layer Instability Waves in Jet Exhaust Noise." Journal of Fluid Mechanics 2 (1977): 321–67.

[2] Michalke, A. "On Spatially Growing Disturbances in an Inviscid Shear Layer." Journal of Fluid Mechanics 3 (1965): 521–44.

[3] Samimy, M., I. Adamovich, B. Webb, J. Kastner, J. Hileman, S. Keshav, and P. Palm. "Development and Characterization of Plasma Actuators for High-Speed Jet Control," Experiments in Fluids, Vol. 37, No. 4 (2004): 577-588.

[4] Samimy, M., N. Webb, and M. Crawley, "Excitation of Free Shear-Layer Instability in High-Speed Flows," AIAA Journal (Invited Paper), Vol. 56, No. 5 (2018): pp. 1770-1791.

[5] Samimy, M., J.-H. Kim, J. Kastner, I. Adamovich, and Y. Utkin. "Active Control of High-Speed and High-Reynolds-Number Jets Using Plasma Actuators." Journal of Fluid Mechanics 578 (2007): 305–30. https://doi.org/10.1017/S0022112007004867.

[6] Kearney-Fischer, M., J.-H. Kim, and M. Samimy. "Noise Control of a High Reynolds Number High Speed Heated Jet Using Plasma Actuators." International Journal of Aeroacoustics 5–6 (2011): 635 – 658.

[7] Kim, J.-H., M. Kearney-Fischer, M. Samimy, and S. Gogineni. "Far-Field Noise Control in Supersonic Jets Using Conical and Contoured Nozzles." ASME Journal of Engineering for Gas Turbine and Power 133 (2011): 081201. https://doi.org/10.1115/1.4002811.

[8] González, D., D. Gaitonde, and M. Lewis. "Large-Eddy Simulation of Plasma-Based Asymmetric Control of Supersonic Round Jets." International Journal of Computational Fluid Dynamics 29, no. 3–5 (2015): 240–56. https://doi.org/10.1080/10618562.2015.1053877.

[9] González, D., D. Gaitonde, and M. Lewis. "Under-Expanded Round Jet Receptivity to Asymmetric Active Control," 2016–1105:1–26. San Diego, CA: AIAA Paper, 2016. https://doi.org/10.2514/6.2016-1105.

How Parabens Affect Cholesterol Content of Melanoma Cells

Student Researcher: Kennedy L. Couch

Advisor: Dr. Suzanne Parsons

Marietta College
Department of Chemistry and Biochemistry

Abstract
Parabens are preservative chemical compounds found in many everyday cosmetic products and are used in this research project to treat melanoma cells. This project was completed in order to determine if there is a correlation between the treatment of melanoma cells with paraben and cell cholesterol content. Heptylparaben and mononitroparaben, novel parabens used in different concentrations, were used and have the potential to be a preliminary treatment for melanoma, the deadliest form of skin cancer. Trends in data were determined to identify if cholesterol levels, which are critical to cell life, were affected by the treatment of such chemical compounds. Cell culture, paraben treatment, cell lysis, Bradford assay, and cholesterol assay were important methods utilized to collect viable data.

Project Objectives
Preliminary studies revealed paraben treatment of M624 human melanoma cells were shown to initiate apoptotic cellular death through the presence of caspase-3. Cholesterol content levels within the membrane of M624 human melanoma cells before and after paraben treatment can reveal the mechanism of cell death initiation as changes in cholesterol are linked with lipid rafts and extracellular signaling. Lipid rafts located within a cell's plasma membrane are composed of glycoproteins, involved in cell signaling, and have been implicated as master regulators of signal transduction and apoptotic signaling specifically in cancer cells. The object of this project was to determine if heptylparaben and mononitroparaben changed cholesterol content of the cell membrane in M624 melanoma cells.

Methodology Used
M624 human melanoma cells were cultured with DMEM media containing 10% Fetal Bovine Serum and 1% Penicillin Streptomycin. Once cells were grown to 70-95% confluency, they were treated with the following parabens: heptyl and mononitro. Heptyl was added to the cells in concentrations of 0-0.25 mM for one hour, and mononitroparaben was added in concentrations ranging from 0-10 mM for twelve hours as determined from previous LC50 values. Cells were washed, centrifuged, and added to buffer with a protease inhibitor. Cells were sheared with a 23-gauge needle and a syringe and frozen in order to induce membrane lysis. A Fujiform Medical Systems USA Cholesterol E kit was used with a spectrophotometer plate reader at 595 nm to determine cholesterol concentration. A standard Bradford assay dilution series was created, and samples were read in a spectrophotometer plate reader at 595nm to determine the total protein concentration in each sample.

Results Obtained
Results indicated no statistically significant change in cholesterol concentrations with heptylparaben or mononitroparban treatment. Research conducted in Dr. Parson's lab revealed a positive correlation between paraben treatment of M624 human melanoma cells and caspase-3 which indicated cells were undergoing apoptosis, a form of mediated cell death. This data paired with cholesterol concentration levels suggests that mononitroparaben and helptylparaben induced apoptosis independent of changes in the membrane lipid raft content.

Figures/Charts

a.

b.

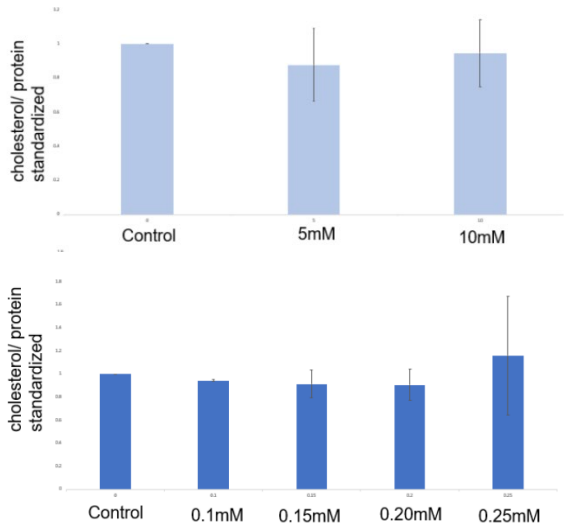

Figure 1. Cholesterol concentration (standardized to protein) after treatment of mononitroparaben (a) and heptylparaben (b)

Significance and Interpretation of Results

In order to investigate if paraben-treatment has potential to be a topical therapy for melanoma in the presence of normal skin cells. Cholesterol and caspase-3 assay results of normal HaCat human epithelial cells will be conducted as an extension of this project. If melanoma cells are shown to have increased apoptotic activity with treatment of methylparben, mononitroparaben, and heptylparaben, while not affecting normal epithelial cells, then parabens may have potential as a topical treatment of melanoma cells. Caspase-3 assays will provide data that shows evidence of desired form of apoptotic cell death activity and will be used as an indicator to determine cell death concentration at LC50 paraben levels in melanoma and normal skin cells.

Acknowledgments and References

Thanks to Dr. Suzanne Parsons for her advisement, support, and guidance on this project. Thanks to the Department of Chemistry and Biochemistry at Marietta College for their financial support. A special thanks to the Ohio Space Consortium for funding this project.

Cabaleiro, N; Calle, I; Bendicho, C; Lavilla, I. An overview of sample preparation for the determination of parabens in cosmetics. Trends in Analytical Chemistry. 2014, 57. 34-46.

Lopes, J.; Rodrigues, C. M. P.; Gaspar, M. M.; Reis, C. P. Melanoma Management: From Epidemiology to Treatment and Latest Advances. Cancers (Basel) 2022, 14 (19), 4652. https://doi.org/10.3390/cancers14194652

eXtended Reality Smart Guidance Interface (XRSGI) in AARON System for xEMU

Student Researcher: Justin M. Dannemiller

Advisor: Dr. Jong-Hoon Kim

Kent State University
Department of Computer Science

Abstract

Contemporary space missions rely on a simple communication approach wherein ground crew personnel relay task-pertinent information to astronauts to assist them in the completion of their missions. Such an approach, however, will not be feasible in future explorations of the Moon, Mars, and beyond. In such missions, the substantial distances between astronauts and their supporting personnel would result in temporally prohibitive communication delays. Future systems envision addressing this issue by incorporating intelligent support into spacesuits and nearby robotic agents.

This paper presents one such module, the eXtended Reality Smart Guidance Interface (XRSGI). The XRSGI is designed for potential incorporation in NASA's xEMU for the assisting of astronaut missions by recognizing and highlighting task-pertinent objects with which the astronaut must interact. The XRSGI achieves recognition through the deployment of the YOLOv5 instance segmentation algorithm to recognize objects of interest. Furthermore, highlight visualization is achieved through a custom-designed Unity application running on a MagicLeap augmented reality (AR) headset. Through the real-time recognition and highlighting of objects related to the astronaut's mission, the XRSGI affords greater autonomy to the astronaut in the completion of their mission, an imperative capability for the distant space missions of the future.

Project Objectives

The distant nature of future space missions, such as the human-led exploration of the Moon and Mars, requires that communication between astronauts and their support personnel and system be transformed. Specifically, to avoid excessive communication delays and to offer greater autonomy, support must be integrated locally around the astronaut. This project was developed in light of these interests: to design and develop a system to recognize and highlight environmental task-pertinent objects to aid an astronaut in the completion of their mission. For instance, the XRSGI could be used to assist in the repair of a rover by recognizing and visually highlighting malfunctioning components. Moreover, the Advanced Telerobotics Research (ATR) Laboratory supporting this project previously developed an AR-leveraging system, the Assistive Augmented Reality Operations and Navigation System (AARON) for potential integration in NASA's future Exploration Extravehicular Mobility Unit (xEMU) (Cardenas et al., 2021). As such, the secondary objective of this project was to further enhance the autonomous capability of the AARON system through the integration of the XRSGI.

Methodology

The implementation of the XRSGI relies on several subcomponents, namely an instance segmentation model, an Intel RealSense RGB-D depth camera, Unity visualization scripts, and a MagicLeap AR headset. An instance segmentation model was trained using the You Only Look Once (YOLOv5) instance segmentation algorithm (Redmon et al.). More specifically, the instance segmentation model was trained using *yolov5l-seg.pt* pretrained checkpoint for 300 epochs using images of rovers, the ISS, and other such space systems labeled using Roboflow annotation software. This instance segmentation model provides spatial highlighting of peripheral objects, and these highlighted objects are viewed using a depth camera and MagicLeap AR headset.

Specifically, the Intel RealSense RGB-D depth camera was used to capture three-dimensional point cloud data of the environment. This point cloud data is then converted into a 3D spatial model using visualization scripts

written in Unity Game engine through a Robot Operating System (ROS) and Unity bridge. Moreover, the labeled pixels obtained from the instance segmentation model are then used to highlight objects in the 3D Unity environment in accordance with the instance segmentation model's predictions. Finally, the resulting 3D environment is ported to MagicLeap AR headset to provide a view of the environment with any detected objects augmented on the visual display.

Results

The trained instance segmentation model showed considerable accuracy in its classification and localization of objects, demonstrating a mean average precision score (mAP50) of 97.8% on the testing set. The results of this model are further illustrated in the figure 1 below which shows the attempted highlighting of the Mar Curiosity Rover's Rover Environmental Monitoring Station (REMS), ChemCam, and mobility unit wheels. The 3D environmental model component also showed considerable potential, as high fidelity, 3D environmental models were successfully created from the 3D point cloud data.

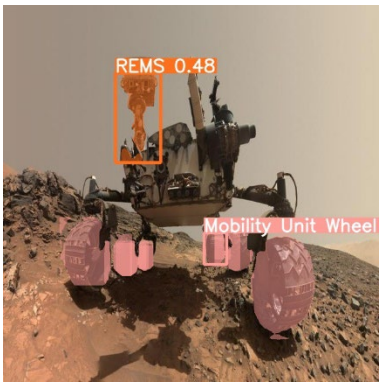

Figure 1. Highlighting of Mars Curiosity Rover Components by Instance Segmentation Model

Discussion

Despite the project's promising preliminary results, there were several limitations that need addressed in future developments. First, the dataset used to train the model was very small. This is due to the fact that images capturing rovers or other space systems are quite limited. As such, the generalizability of the trained model is inherently limited, and future work should address this issue by leveraging image harmonization to generate more images for both training and testing the model. Furthermore, due to the computational complexity of the segmentation model and constructing a 3D map from 3D point cloud data, real-time projection of detected environmental objects could not be achieved. As such, other, more efficient methods should be leveraged to afford a real-time system. Despite these limitations, however, the project's results are promising, and the ongoing development efforts could establish the XRSGI as a critical mission support system.

Acknowledgements and References

I would like to thank the Ohio Space Grant Consortium for providing the transformative opportunity to engage in this exciting research project and my advisor, Dr. Jong-Hoon Kim, for all the support and guidance he provided along the way.

[1] Cardenas, I.S. *et al.* (2021). AARON: Assistive Augmented Reality Operations and Navigation System for NASA's Exploration Extravehicular Mobility Unit (xEMU). In: Singh, M., Kang, DK., Lee, JH., Tiwary, U.S., Singh, D., Chung, WY. (eds) Intelligent Human Computer Interaction. IHCI 2020.

[2] Joseph Redmon, Santosh Divvala, Ross Girshick, Ali Farhadi; Proceedings of the IEEE Conference on Computer Vision and Pattern Recognition (CVPR), 2016, pp. 779-788

Plasma Assisted Combustion of Hydrocarbon Fuels in Extreme Fuel Lean Conditions for the Study of Combustion Kinetics and Intermediate Chemical Reactions

Student Researcher: Alexander G. Demagall

Advisor: Dr. Igor Adamovich

The Ohio State University
Department of Mechanical and Aerospace Engineering

Abstract

A supersonic flow wind tunnel is coupled with a heated plasma flow reactor to study chemical reactions that occur during combustion of hydrocarbon fuels, at extreme "fuel-lean" conditions. In the reactor, which serves as the wind tunnel plenum, the fuel-oxidizer flow is diluted in argon is heated by passing through a thermal energy storage system (a container filled with ceramic beads and placed in a tube furnace), and then expanded through a converging-diverging nozzle into a supersonic test section. Between the thermal storage and the nozzle, there is an electric discharge section, to generate reactive radicals not present in the fuel-oxidizer reactant mixture. The heated and reacting flow excited in the plasma is expanded through the nozzle into the supersonic test section. This wind tunnel / heated flow reactor will be used by graduate research assistants, to measure the reaction products in the supersonic test section using laser diagnostics. The rapid supersonic expansion to low pressure and temperature will stop the chemical reactions, such that the reaction products in the flow can be analyzed. This wind tunnel / heated flow reactor will be used for the measurements of the reaction products in the test section, specifically CO2, CO, and H2O. The reaction products will be measured by infrared absorption spectroscopy, already fully operational, using a tunable Quantum Cascade Laser (QCL).

Project Objectives

There is limited knowledge on the kinetics of radicals and the intermediate species formed during the combustion of hydrocarbon fuels at extreme "fuel-lean" conditions. Therefore, the aim of this project is to develop a deeper understanding of these phenomena, using a new experimental facility where these species are generated in the flow by an electric discharge plasma, and measured spectroscopically after a supersonic expansion. This facility will be used in several research projects at the Nonequilibrium Thermodynamics Laboratories (NETL). The potential outcomes of these projects include the improved jet engine performance, improved supersonic combustor performance, and the development of safe and efficient plasma assisted combustion methods. The main objective of this project is the design, development, and testing of the new facility, a heated plasma flow reactor combined with a supersonic test section for in situ spectroscopic diagnostics.

Methodology

To accomplish the project objectives, two thrusts were performed in parallel. The first is the construction and testing of the supersonic plasma reactor. The flow through the reactor is made up of 0.2% Ethylene, 1% Oxygen, and Argon. Argon is used as a buffer gas to lower the reaction rate and prevent an uncontrolled reaction. The mixture then enters a ThermCraft tube furnace and heated to T = 600-900 K. Once heated, the flow enters the electric discharge section. The purpose of the plasma sustained in the electric discharge section is to generate highly reactive radicals, mainly O atoms, out of relatively non-reactive O_2 molecules in the mixture. This is done with a 30 kV plasma with a 25 kHz pulse rate for 10 ms. This approach produces a volume-filling diffuse plasma, as has been shown in previous work at NETL [1]. The production of these radicals initiates chemical reactions with the fuel, such as occur in conventional combustion. Some of the species taking part in these reactions, such as (CH_4, C_2H_4), reaction intermediates (HO_2, CH_2O, CH_3O_2, $C_2H_5O_2$), and reaction products (CO, CO_2, and H_2O) can

be measured in the flow using laser diagnostics, such as absorption spectroscopy. For these measurements, it is critical to expand the flow to low temperatures and pressures. The expansion effectively "freezes" the chemical reactions and greatly simplifies the identification of different species, since the spectral lines become narrow and do not overlap. The expansion must be rapid, such that the target species would not have time to decay. In the present work, the expansion occurs in a converging-diverging nozzle, bringing the flow to M =3.9, followed by a straight diagnostic section and a supersonic diffuser. The flow heated in the thermal storage unit and excited in the plasma passes through the nozzle, test section, and diffuser, before exhausting into a vacuum chamber. The steady state run time of the reactor is approximately 10 seconds.

The second thrust of this project focuses on the laser diagnostics needed to measure radical products. To employ the diagnostics a simpler setup was used which sent a flow of 2.5% CO_2 and Nitrogen gas. The flow is hit with the same plasma as is implemented in the supersonic plasma reactor, a 30kV plasma with a 25kHz pulse rate for 10 ms. An infrared laser was sent through the plasma to detect CO and CO_2. The raw absorption spectra was analyzed to find the vibrational and rotational temperature of CO, as well as the number density of CO.

Results

The reactor itself has been built, assembled, and tested. The pressure upstream of the supersonic nozzle has been measured to be 590 torr and the temperature was measured at 700 kelvin (the temperature was measured with the plasma off). The pressure downstream of the supersonic nozzle was measured to be 9.5 torr. This pressure ratio gives a Mach number of 3.9. Using the vacuum chamber available in Dr. Adamovich's lab a steady state run time of around 10 seconds was achieved. The plasma created was relatively diffuse, however it could be stronger and more diffuse. Future work will involve improving the plasma, perhaps by using smaller electrodes to increase the electric field.

Absorption laser spectroscopy was successfully employed in the simpler setup. Several CO lines were detected, and vibrational temperature, rotational temperature, and CO number density were calculated. The laser diagnostics system is ready to be used for the reactor. Future work will involve using this laser diagnostics method on the reactor, adjusting the method to look at different species, and employing cavity ring down spectroscopy (a method in which the laser beam is trapped between two mirrors, greatly increasing the length of the absorption path) to look at lower population species.

Significance and Interpretation of Results

A heated, supersonic flow plasma reactor has been developed and tested. This involves a mixture of 0.2% Ethylene, 1% Oxygen, and Argon flowing through a furnace and into a plasma chamber. The heated mixture (around 700K) is hit with a 30kV plasma with a 25kHz pulse rate for 10 ms. The flow is sent through a supersonic nozzle to freeze reactions and create ideal conditions for laser diagnostics. Said laser diagnostics has been tested and employed for CO number density and temperature measurements. Future work will involve creating a more diffuse plasma and implementing laser diagnostics on the reactor, making use of cavity ring down spectroscopy.

Acknowledgements and References

The support of NASA and the Ohio Space Grant Consortium is gratefully acknowledged.

1. E.R. Jans, I. Gulko, D.C.M. van den Bekerom, T.A. Miller, and I.V. Adamovich, "Measurements of Metastable $N_2(A^3\Sigma_u^+,v)$ Molecules in Nonequilibrium Supersonic Flows", Journal of Thermophysics and Heat Transfer, vol. 36, 2022, p.196

Development of a Microbial Fuel Cell

Student Researcher: Braddon A. Dennison

Advisor: Paul Penko

Baldwin Wallace University
Department of Engineering

Abstract
Electrical energy is a central aspect of today's society. Global energy consumption has increased dramatically over the last seven decades (Ritchie & Roser, 2020). Many traditional energy solutions involve obtaining energy from non-renewable energy sources such as fossil fuels, which are particularly detrimental to the environment due to the emission of carbon dioxide and other gases contributing to global climate change. Thus, there is a clear need for sustainable power sources. The primary focus of this project was to design, fabricate, test, and optimize a microbial fuel cell as a means of producing renewable energy. Microbial fuel cells utilize naturally occurring bacteria that decompose and oxidize organic material to generate electricity and could be potentially employed as a power source in a latrine or waste treatment plant, or even on a space mission. Throughout this project a laboratory prototype was repeatedly tested and modified with the intent of increasing the power production of the fuel cell.

Additionally, a theoretical design was created that could be implemented outside of the laboratory in such places as composting latrines in developing countries. The research showed that although the power generation of the prototype was limited, the microbial fuel cell reliably produced a small amount of power and modifications led to a significant increase it the power output. Several methods of increasing the fuel cell's power output are being pursued including using different substrates and increasing the volume of the fuel cell. The results demonstrate a clear need for further interdisciplinary investigation of the fuel cell. Provided that the problem regarding the limited power output is solved, the proposed design would be a practical and convenient way to provide electricity to people in remote locations that lack reliable access to electricity.

Objectives
The first objective of this project was to build and research a microbial fuel cell, which utilizes naturally occurring bacteria that decompose and oxidize organic material to generate electricity, as a feasible and affordable means of producing renewable energy. The second objective was to create a practical, sustainable design of the microbial fuel cell that could be used to power or charge an LED light for reading, doing homework, crafts, and other household tasks. Electrical energy is paramount to the functioning of today's society. The use of fossil fuels as a source of energy is particularly detrimental to the environment due to the emission of carbon dioxide and other gases, which contributes to global climate change that endangers all of humanity. Although access to power has been increasing, 940 million people around the world still lack reliable electricity (Ritchie & Roser, 2020). Thus, there is a need for sustainable power sources, particularly in regions with unreliable electricity. Although microbial fuel cell technology has improved significantly over the last couple of decades, there are still significant limitations, so further research is warranted. The power generation is the most significant limitation of the microbial fuel cell. Current microbial fuel cell technology does not generate enough power to meet an entire household's electricity needs.

Researchers are consistently looking for ways to improve power output. While microbial fuel cells have many different parameters that can be manipulated to attempt to improve power output, two of the principal factors that influence the performance of microbial fuel cell are the electron shuttle from the anode compartment to the circuit and permeability of the proton exchange membrane (Rahimnejad et al., 2009). Modifying these aspects of the microbial fuel cell can improve its performance so that it will have a significant impact as a source of electrical energy.

Methodology Used
The engineering design process was followed to complete this project and design an energy

solution. First, the need for an energy solution was recognized and research was conducted. An iterative process was followed in order to determine the feasibility of the microbial fuel cell as an alternative energy source. A single chamber PVC laboratory prototype was designed, built, tested, and modified. In order to maximize power output, ideal resistance was estimated using Ohm's Law: V/I = R. Power was determined using Watt's Law: $VI = P$. Then, a practical solution was conceptualized and designed. The final design was evaluated, and more research was performed to optimize the design. Onshape software was used to create CAD engineering drawings for all the designs, and sustainability was assessed using the Economic Input-Output Life Cycle Assessment Tool from Carnegie Mellon University (2022). Finally, the results were presented as a poster presentation.

Results Obtained

The first objective was to research the feasibility of the microbial fuel cell as an alternative energy source. The research prototype had a maximum open circuit voltage of 377mV and a peak power generation of 144nW. Although the tested microbial fuel cell did not meet the objective of generating enough power for an LED, the research showed that the microbial fuel cell could reliably produce power for more than a week proving that it is a feasible energy source provided that its power output can be increased. As can be observed in Figure 1, the modifications increasing the surface area of the electrode and the proton exchange membrane led to a significant increase in the current and power output of the fuel cell.

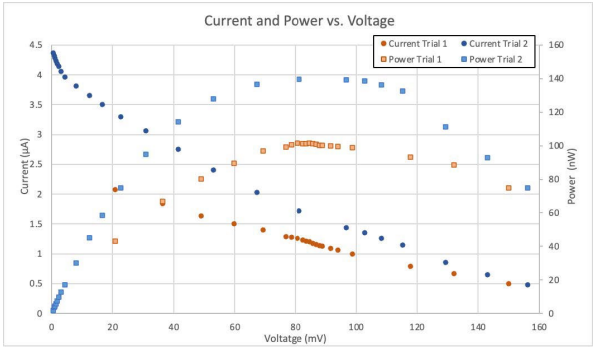

Figure 1: Power Graph with Resistances from 10 $k\Omega$ to 300 $k\Omega$

The second objective of designing a practical microbial fuel cell that could be used to generate power beyond the laboratory was successful. The final design could be installed in developing countries and as well as other locations around the world in places such as a latrine, a pond, or a waste treatment plant. The design was affordable, and the solution should be readily adoptable in developing countries where composting latrines are already accepted technology. The design was sustainable based on the analysis using the Economic Input-Output Life Cycle Assessment Tool from Carnegie Mellon University (2022).

The results showed that there is a clear need for further research concerning microbial fuels cells. The research prototype was capable of sustaining electricity generation for more than a week and modifications led to improved power generation, which show the fuel cell to be a promising source of alternative power. The fuel cell's power output may be improved in several ways such as by using different substrates and increasing the volume of the fuel cell. Provided that the problem regarding the limited power output is solved, the final design would be a practical and convenient way to provide electricity to people in remote locations that lack reliable access to electricity.

References

Carnegie Mellon University Green Design Institute. (2022) Economic Input-Output Life Cycle Assessment (EIO-LCA) US 2007 (388 sectors) Producer model [Internet], Available from: http://www.eiolca.net/ [Accessed 22 Nov, 2022]

Rahimnejad, M., Adhami, A., Darvariab, S., Zirepour, A., & Oh, S. (2015). Microbial fuel cell as new technology for bioelectricity generation: A review. *Alexandria Engineering Journal*, *54*(3), 745–756. https://www.sciencedirect.com/science/article/pii/S1110016815000484

Ritchie, Hannah and Roser, Max. (2020). "Energy". *Published online at OurWorldInData.org.* Retrieved November 1, 2021 from https://ourworldindata.org/energy

Powder Bed EDM, Additively Manufactured Ti-6Al-4V Property and Surface Treatment Analysis

Student Researcher: Ryan P. Dippolito

Advisor: Dr. Manigandan Kannan

The University of Akron
Mechanical Engineering Department

Abstract

Grinding is a simple and affordable process typically done in most metallic manufacturing centers, primarily for precision and surface improvement. Currently, the grinding process of titanium alloys generally requires flood coolant application. Grinding is a major secondary process applied to additively manufactured metals, but with the current methodologies, grinding may impart tensile residual stress on the surface, and thus the performance of the material under fatigue conditions is reduced. In this paper, a targeted cutting fluid application approach for grinding an additively manufactured titanium alloy is used to possibly impart a compressive residual stress upon the subsurface while also providing an improved surface roughness. This study uses samples ground with a traditional flood coolant and samples with targeted cutting fluid applications developed by the researchers. The study is performed on the additively manufactured Ti6Al4V material used in various rotating components in jet engines. The results show that the targeted grinding cooling fluid application induced compressive subsurface residual stresses and reduced the average surface roughness.

Project Objectives

The objectives of the project are to evaluate different surface treatment methods on additively manufactured titanium and compare their imparted residual stresses on the surface. For improved fatigue life, an imparted compressive residual stress and smooth surface finish is desired. The overall goal of this study is to see which grinding method imparts the largest compressive residual stress and smoothest surface finish so it can be further analyzed in a future study.

Methodology Used

For this study, a 6" x 6" sheets of Ti-6Al-4V were manufactured by Avalign Additive using the Powder Bed EDM process. Specimens were then machined using a face mill to make parts into a flat shape. The Ti6Al4V plate was machined into rectangular specimens with dimensions 140 mm long, 27 mm wide, and 2.5 mm thick, and specimens were machined in such a way that the build direction was parallel to the loading direction for the specimens (vertically oriented). This sample manufacturing took place at the mechanical engineering machine shop at the University of Akron. All test surfaces prior to the grinding application were machined surfaces. To test the hypothesis, two samples were ground with each cutting fluid condition, namely flood fluid condition, targeted minimum quantity coolant (MQC), and targeted compressed air on an Okamoto Grind X surface grinding machine with a maximum speed of 40m/s. See figure 1 for a visual representation of the sample and grinding process. The grinding itself was completed at M.K. Morse and is pictured in Figure 2. For comprehending the surface integrity post grinding, residual stress profiles and surface roughness are analyzed at the University of Akron.

A Keyence VHX 7000 is a high-resolution digital microscope that uses a non-contact measurement method for surface roughness measurement was used to analyze surface roughness in this study. The digital microscope uses 3D imaging technology and a 4K optical system to capture digital images of a sample surface. Then, surface roughness can be quantified by analyzing the captured images and calculating various surface topographical parameters such as average surface roughness (Ra), maximum peak-to-valley height (Rt), etc. This study uses the hole drilling method to measure the machining-induced surface residual stresses. The hole-drilling method is typically used in the industry for measuring residual stresses. The residual stresses are measured by drilling (at increments of .025 mm) a small (less than 2.5 mm in diameter) hole through the material (with an EA-06-062RE-120/LE strain gage mounted on the sample), and the material's change in dimensions caused by the material's removal is measured to calculate the residual stresses. The strain gauge values are reported to ©H-Drill Software which converts the values to imparted residual stress data.

Results Obtained

The targeted air (at 0.62 MPa pressure) cutting fluid condition produced compressive maximum and minimum principle residual stresses on the subsurface (at 5 microns) shown in figure 3. However, the flood fluid condition and the targeted MQC (with a lower pressure of 0.4 MPa) produced a tensile residual state at 5 microns subsurface (Figure 3). Shown in Figure 4, the surface roughness measurement shows that the targeted air samples produced better surface parameters than the other cutting fluid conditions in this study.

Significance and Interpretation of Results

Since the targeted air method proved to be Future work includes performing fatigue tests of the ground samples (two for each condition) and use nano hardness measurement to understand the thermal effect of different cutting fluid applications. Also, a more detailed microstructural study is recommended to better understand the impact of target cutting fluid effects. Also, a more comprehensive study validating the effects of pressure, fluid quantity, and composition on the machining-induced surface integrity is suggested.

Figures/Charts

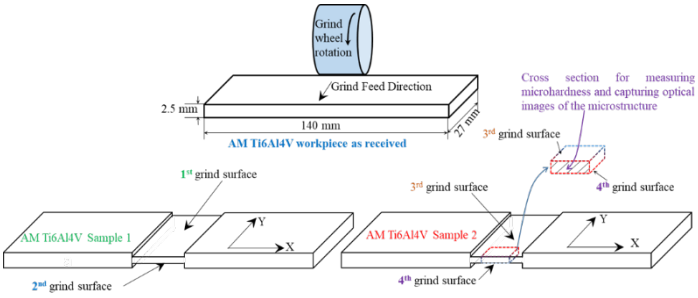

Figure 1. Grinding Methodology

Figure 2. Grinding Setup at M.K. Morse

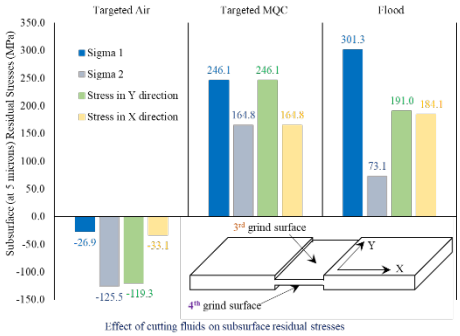

Figure 3. 5 Micron Subsurface Residual Stress Measurements

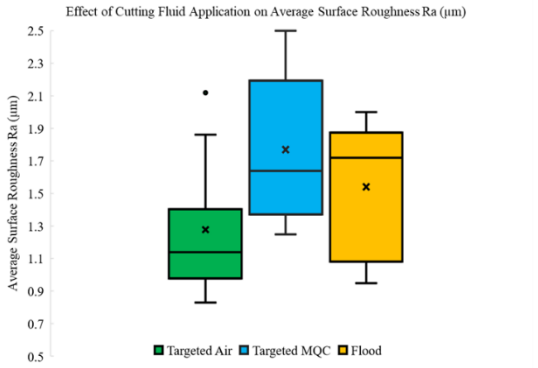

Figure 4. Surface Roughness Measurements

Acknowledgements and References

I'd like to thank Dr. Manigandan Kannan for taking me as an undergraduate research assistant, Julie Zhao for being my sponsor towards the OSGC scholarship, and the University of Akron Department of Mechanical Engineering. Also, I'd like to thank Sekhar Rakurty, Nithin Rangasamy, Satya Kakaraparthi, and M.K. Morse for their support on the project. Lastly, I'd like to thank Blake Bowser for his continued mentorship in the research realm, and Riley Myers for her support as an undergraduate researcher for Dr. Kannan as well.

Compression Characteristics of Triply Periodic Minimal Surface Lattice Structures

Student Researcher: Lemuel A. Duncan

Advisor: Dr. Ahsan Mian

Wright State University
Mechanical and Materials Engineering

Abstract
In recent years, interest in the behavior of complex lattice structures has increased significantly due to new advancements in 3D printing technology which allow for the manufacturing of parts possessing complex geometry [1-3]. In this study, three types of triply periodic minimal surface (TPMS) lattice structures possessing various gradient features are manufactured and tested in compression to determine the possible advantages they may hold regarding energy absorption. The three lattice types investigated are Primitive, Diamond, and Gyroid as seen in the rows of Figure 1 [4]. For each lattice type a comparison is made between their uniform, relative density gradient, and cell size gradient variations. A total of nine lattice samples are tested. Results from the study are inconclusive as to which type of gradient allows for best energy absorption. However, it is confirmed that the Diamond lattice type consistently outperforms the other lattice types regardless of their gradient characteristics.

Project Objectives
The main objective of the study is to find lattice configurations that result in the highest energy absorption. Energy absorbed by a structure in compression is defined as the integral of the force-displacement curve. By compressing nine lattice samples to their densification point, a comparison of their energy absorption can be made by applying the trapezoid rule to the force displacement plots obtained. In this study interest is also expressed in the modes of deformation present between the different samples. Deformation footage is captured throughout the compression of each sample and analyzed using a hybrid optical flow software in MATLAB.

Methodology Used
Each lattice sample was designed using an application for MATLAB called MS-Lattice [5]. The amount of material used to manufacture all the samples is held constant to make the results comparable. Each cubic lattice sample is designed with dimensions of 25 mm. A process of linear interpolation is utilized to hit the target material volume for each sample. The lattice designs are printed on the Open Additive PANDA available in the Wright State additive manufacturing lab. Separate bulk and contour parameters are used to optimize the prints per [6]. The resulting samples are depicted in Figure 1. After removing the lattice samples from the build plate via EDM, they are individually tested using the Instron 5500R equipped with a 150 kN load cell. The test is set at a rate of 2 mm/min in accordance with [7]. A high-resolution camera is set up to record footage normal to the face of the lattice as it is compressed.

Results Obtained
The compression tests yield force vs. displacement data plots. By accounting for the nominal dimensions of the lattice samples, a plot of the Engineering Stress vs. Engineering Strain is developed for each sample as seen in middle of Figure 2. There are two quantities of interest that can be obtained from the stress vs. strain curve: those being the Young's Modulus, E_m, and the Yield Strength, σ_y. E_m is calculated as the slope of the initial linear region of the curves whereas σ_y for the material is determined using the typical 0.2% offset method which can be seen as the short red line visible Figure 2.
Energy absorbed, E, is calculated as the integral of the force vs. displacement curve up to the densification strain. To find the densification strain, ε_d, the derivative of the stress vs. strain is obtained numerically and plotted as seen at the bottom of Figure 2. The portion towards the end of the derivative plot, where it suddenly increases, is ε_d. Each lattice sample's mass is also recorded and used to determine specific values for each of the quantities above. By dividing each of the lattice's properties by their mass, the error resulting from material volume differences is accounted for to make the results more comparable. Table 1 contains the comprehensive results from all nine tests. Some challenges were encountered in interpreting data from some of the plots. For example, The CSG gyroid sample does not exhibit a dramatic change in its derivative plot toward the end which adds significant uncertainty in defining ε_d which in turn makes the calculation of E unreliable. Unknown and unreliable quantities are clearly marked in Table 1.
The displacement analysis is carried out on frames from the footage that are 30 seconds apart during the initial stages of each test. The hybrid optical flow program inspects the translation of distinguished brightness patterns that can be correlated between the two frames [8]. The result is a vector field displaying the magnitude and direction of each object in the field of view. Figures 3-5 depict the hybrid optical flow results for the primitive lattices.

Significance and Interpretation of Results

All the data trends can be quickly obtained by an inspection of the results outlined in Table 1. The primitive lattice structures provided the most complete set of data. The trend for the three primitive samples is that the application of gradients, decrease their ability to absorb energy. For the primitive samples, the uniform variation absorbed 194.6 J/g whereas the relative density and cell size gradients absorbed only 169.2 J/g and 145.2 J/g respectively. This observation is supported by a comparison of the plots obtained for the three primitive samples as seen in Figure 6. Here, the data for the three primitive samples are plotted together on the same axes exhibiting very similar stress vs. strain curves which was unexpected because of prior research results. A more distinct difference can be seen in their energy absorption plots where the uniform's E is consistently higher than the other's. In Figure 7, for the different relative density samples, it is noted that the diamond lattice type significantly outperforms the other lattice types in terms of stiffness, yield strength, and energy absorption. These observations are supported by an inspection of Table 1 and hold true for the data in Figure 8 as well.

The optical flow results provided valuable information regarding the deformation behavior of each sample. Figures 3-5 depict the deformation of the primitive samples. A comparison of the three vector magnitude plots reveals significant differences in the way by which the samples deform. It is seen that deformation in the uniform lattice sample is distributed evenly through its height by considering that the base of the lattice is stationary. In Figure 3, a definite boundary at roughly 45° is visible where the lattice experiences the effects of shear stress. In Figures 4 and 5, the deformation is concentrated to the first two or three layers of lattice cells. This was the expected result seeing as the top layers in the gradient lattice structures are the weakest.

Conclusions that can be drawn from this research are minimal because the results discovered here do not match what is expected and are not comparable to results obtained by previous studies in similar experiments [7, 9-11]. Only one sample for each variation was tested so, more samples should be tested to reduce uncertainty. However, it is very clear that the diamond lattice structures consistently exhibit higher structural properties than the primitive and gyroid types. According to the optical flow results, one can control the deformation behavior and stress distribution in a lattice by designing specialized gradient features.

Figures & Charts

Table 1: Lattice Characteristics

Lattice Type	Mass (g)	Modulus (MPa)	Specific Modulus (MPa/g)	Densification Strain	Energy Abs. Pre-densification (J)	Specific Energy Abs.	Yield Strength (MPa)	Specific Yield Strength (MPa/g)
P UNI	40.860	1564.750	38.295	0.694	7953.233	194.646	73.511	1.799
P RDG	41.200	1571.260	38.137	0.697	6970.209	169.180	57.060	1.385
P CSG	40.760	1544.150	37.884	0.645	5919.709	145.233	61.114	1.499
D UNI	48.530	2375.620	48.952	Unknown	Unknown	Unknown	97.845	2.016
D RDG	45.890	1858.360	40.496	Unknown	Unknown	Unknown	72.223	1.574
D CSG	31.060	1762.720	56.752	0.490	3901.830	125.622	68.348	2.200
G UNI	31.820	1554.640	48.857	0.463	2938.118	92.336	59.439	1.868
G RDG	44.930	1846.460	41.096	Unknown	Unknown		64.938	1.445
G CSG	31.900	1424.610	44.659	0.438	2756.257	86.403	61.213	1.919

Source: Author

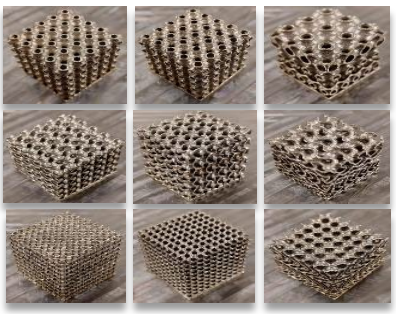

Figure 1: Completed Lattice Sample Prints
Source: Author

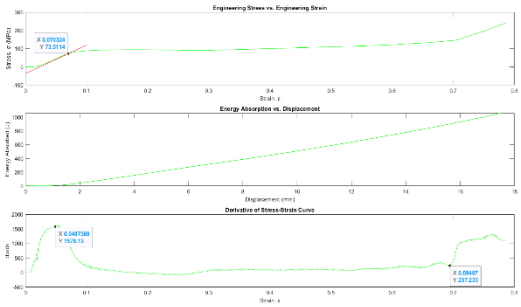

Figure 2: Data Plots for Primitive Uniform Sample
Source: Author

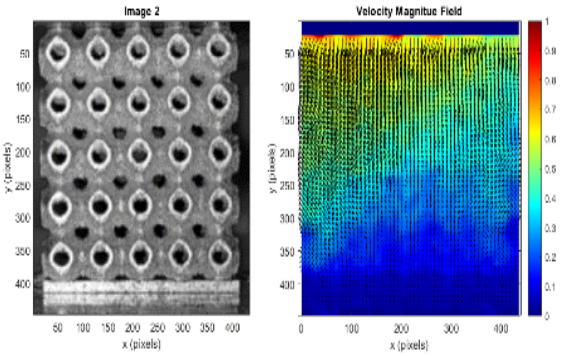

Figure 3: Optical Flow for Primitive Uniform Sample

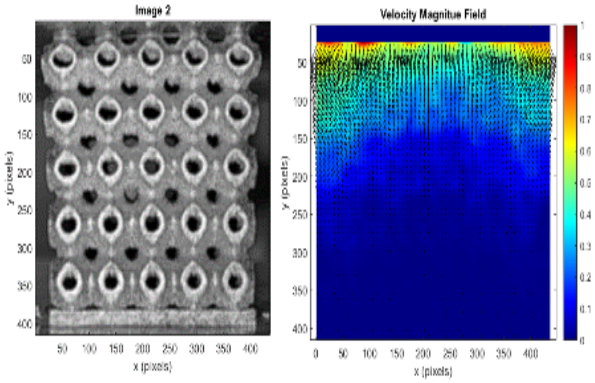

Figure 4: Optical Flow for Primitive Relative Density Sample

Source: Author

Source: Author

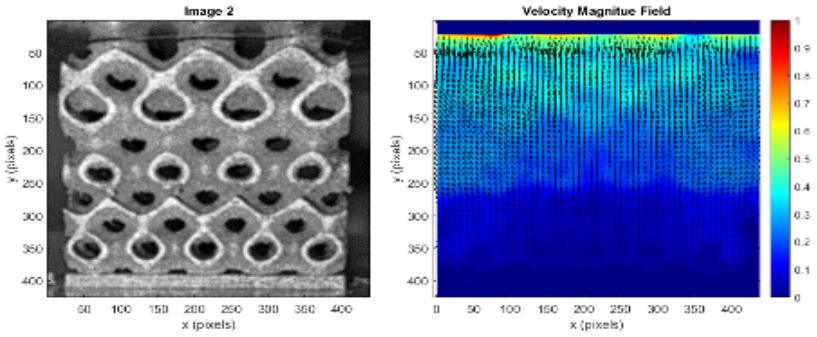

Figure 5: Optical Flow for Primitive Cell Size Gradient Sample. Source: Author

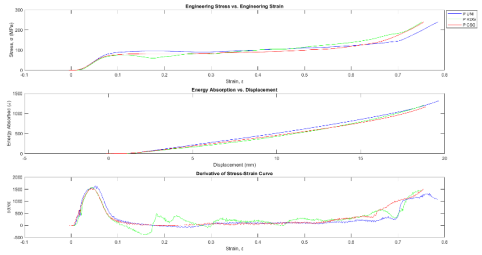

Figure 6: Data Plots for the Three Primitive Samples. Source: Author

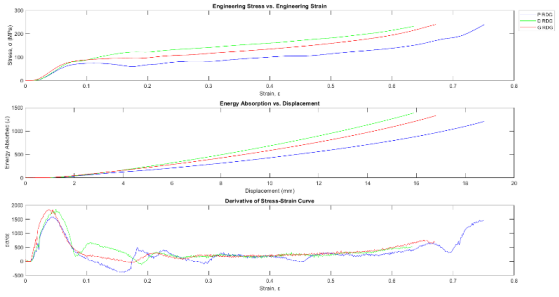

Figure 7: Data Plots for Primitive, Diamond, & Gyroid Relative Density Gradient Samples. Source: Author

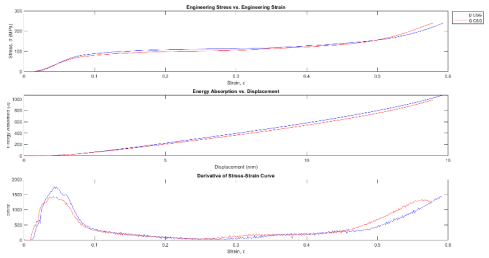

Figure 8: Data Plots for Diamond & Gyroid Cell Size Gradient Samples. Source: Author

Acknowledgments and References

Special thanks to Dr. Ahsan Mian for his invaluable support of this research. With his help I was able to gain access to state-of-the-art equipment and acquire the required materials for the experiments.

[1] I. Maskery, L. Sturm, A. O. Aremu, A. Panesar, C. B. Williams, C. J. Tuck, R. D. Wildman, I. A. Ashcroft, and R. J. Hague, "Insights into the mechanical properties of several triply periodic minimal surface lattice structures made by polymer additive manufacturing," *Polymer*, 15-Dec-2017. [Online]. Available: https://reader.elsevier.com/reader/sd/pii/S0032386117311175?token=C70966C6D9F99429E9BA9F1802A11564FAEF39BD766E7A05746AC5F442236AC00DEF7B3F61FCCEF251D5771673CD4A1F&originRegion=us-east-1&originCreation=20221111151215. [Accessed: 11-Nov-2022].

[2] R. Santiago, S. Almahri, D.-W. Lee, H. Alabdouli, O. Banabila, H. Ramos, M. Alteneiji, Z. Guan, and M. Alves, "Mechanical characterization and numerical modeling of TPMS lattice structures subjected to impact loading," *EPJ Web of Conferences*, 09-Sep-2021. [Online]. Available: https://www.epj-conferences.org/articles/epjconf/abs/2021/04/epjconf_dymat2021_02005/epjconf_dymat2021_02005.html. [Accessed: 11-Nov-2022].

[3] H. Peng, F. Gao, and W. Hu, "Design, modeling and characterization on triply periodic minimal surface heat exchangers with additive manufacturing," *TexasScholarWorks*, 01-Jan-2019. [Online]. Available: https://repositories.lib.utexas.edu/handle/2152/90564. [Accessed: 11-Nov-2022].

[4] S. T. Hyde, V. Robins, and S. J. Ramsden, "Triply periodic minimal surfaces," *Mathematics of The EPINET Project*, 2009. [Online]. Available: http://epinet.anu.edu.au/mathematics/minimal_ surfaces. [Accessed: 16-Oct-2022].

[5] O. Al-Ketan and R. K. Abu Al-Rub, "MSLattice: A free software for generating uniform and graded lattices based on triply periodic minimal surfaces," Material Design & Processing Communications, vol. 3, no. 6, Oct. 2021.

[6] A. Dunn, "Effect of build geometry and build parameters on microstructure, fatigue life, and tensile properties of additively manufactured alloy 718," OhioLINK ETD: Dunn, Anna, 2022. [Online]. Available: https://etd.ohiolink.edu/apexprod/rws_olink/r/1501/10?clear=10&p10_accession_num=wright1661548523389679. [Accessed: 03-Apr-2023].

[7] Z. Minting, Z. Wie, X. Huifeng, L. Yinjing, and W. Zhigang, "Double-level energy absorption of 3D printed TPMS cellular structures via wall thickness gradient design," National Library of Medicine, 2021. [Online]. Available: https://pubmed.ncbi.nlm.nih.gov/34771788/. [Accessed: 17-Nov-2022].

[8] T. Liu and D. M. Salazar, "Tianshu-Liu/openopticalflow_piv_v1: MATLAB code for a hybrid optical-flow-cross-correlation method for piv," GitHub, 18-Dec-2019. [Online]. Available: https://github.com/Tianshu-Liu/OpenOpticalFlow_PIV_v1. [Accessed: 28-Mar-2023].

[9] L. J. Gibson, "Mechanical Behavior of Metallic Foams," *EBSCO Host*, 01-Aug-2000. [Online]. Available: https://content.ebscohost.com/ContentServer.asp?T=P&P=AN&K=6533520&S=R&D=bth&EbscoContent=dGJyMNHr7ESep7E4zOX0OLCmsEqep7RSsau4SLKWxWXS&ContentCustomer=dGJyMPGuskiurK9JucPfgeyx43zx. [Accessed: 13-Nov-2022].

[10] U. Ramamurty and A. Paul, "Variability in mechanical properties of a metal foam," *Acta Materialia*, 06-Nov-2003. [Online]. Available: https://www.sciencedirect.com/science/article/pii/S1359645403006384. [Accessed: 13-Nov-2022].

[11] L. Zhang, S. Feih, S. Daynes, S. Chang, M. Y. Wang, J. Wei, and W. F. Lu, "Energy absorption characteristics of metallic triply periodic minimal surface sheet structures under compressive loading," *Additive Manufacturing*, 04-Aug-2018. [Online]. Available: https://www.sciencedirect.com/science/article/pii/S2214860418304688. [Accessed: 17-Nov-2022].

Application of Magneto-Rheological Fluids for Replicating a Range of Radial Pulses

Student Researcher: Miranda E. Eaton

Advisor: Dr. Jeong-Hoi Koo

Miami University
Department of Mechanical and Manufacturing Engineering

Abstract
Radial pulses, measured at the terminal region of the wrist, are used extensively to determine one's health. Two specific areas where they are used are in Oriental Medicine (OM) with the three-finger technique and wearable technology such as noninvasive blood pressure monitors. However, the three-finger technique is subjective to each physician, and the sensor accuracy in wearable technology can be greatly improved [1-3]. A pulse generator capable of reliably and continuously simulating the human radial pulse can play an important role for training physicians and calibrating sensors. There does not exist a system that can continuously reproduce a human pulse at a low cost. Therefore, the goal of this study is to develop a system which can continuously replicate a wide range of radial pulses.

Project Objectives
The primary goal of this project is to replicate radial pulses that represent a wide range of in vivo pulse waveforms. This project intends to employ a "smart" fluid called Magneto-Rheological (MR) fluid whose behavior can be controlled by a magnetic field in order to simulate radial pulses. A base pulse will be shaped to match a variety of *in vivo* pulses to evaluate the success of the experimental set-up.

Methodology Used
The experimental set up shown below in Figure 1 was used to generate the results, including the CAM pulse generator which sends the base pulse to the MR fluid chamber. Under an applied magnetic field, MR fluid will change its properties. Therefore, the chamber sits atop an electromagnet, and the MR fluid inside the chamber surrounds the tubing to control the expansion of the tube. A laser sensor is placed above the frictionless plunger assembly to measure the displacement of the plunger.

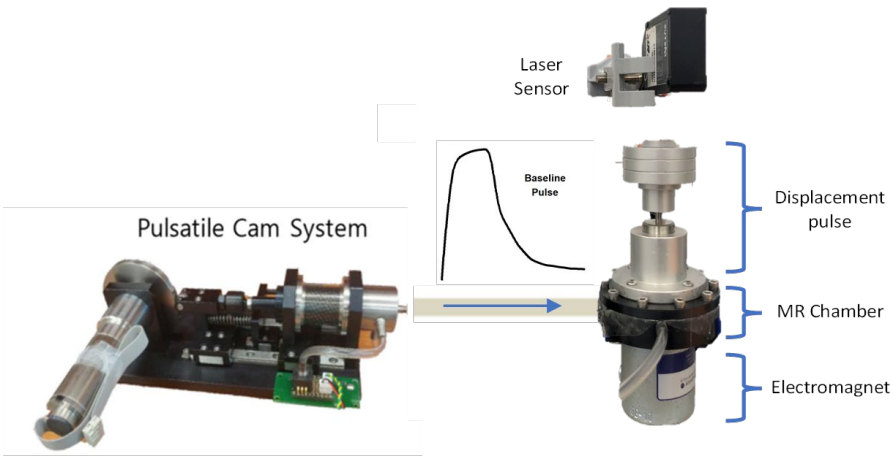

Figure 1. Experimental set-up depicting CAM pulse generator and plunger assembly

The control of the electromagnet will be discussed below. The electromagnet placed beneath the MR chamber was controlled via pulse width modulation (PWM). First, duty values were input into a driver board to create the PWM signals. These signals were then sent to the electromagnet to generate a magnetic field. The magnetic field then changed the MR fluid to shape the base pulse into a range of radial pulses. Therefore, the goal was to shape the base pulse into a variety of age-related *in vivo* pulses.

Significant Results Obtained

The experimental set-up worked well and was used to shape several pulses. For the brevity of this paper, two results are shown. Figure 2(a) shows the results of shaping the base pulse to a 20yr-old *in vivo* pulse, and Figure 2(b) shows pulse shaping to an 80yr-old *in vivo* pulse. The blue solid line is the *in vivo* pulse while the orange dotted lines are the results from shaping the base pulse using the experimental set-up. The base pulse was able to be shaped well to a 20 and 80yr-old. The set-up could create the initial sharp peak of the 20yr-old and the complexities of the waveform during diastole. Furthermore, the set-up can also create a wider initial peak similar to that of an 80yr-old peak and smooth out the rest of the waveform during diastole.

To quantitatively evaluate the system, the root mean square error (RMSE) was calculated. The RMSE was found by finding the difference between the experimental and *in vivo* values and dividing by the total number of data points. The RMSE for the 20yr-old shaping was 3.7% and 2.9% for the 80yr-old. It was expected for the 80yr-old to have the least amount of error because the base pulse was most similar to an 80yr-old *in vivo* pulse. The range of ages from 20-80 was representative of the lifespan of a human. Because the system can shape to a 20 and 80yr-old, it can be implied any ages within that gap can be shaped as well. Therefore, based on these low error values, it was determined the system was able to successfully shape a range of ages.

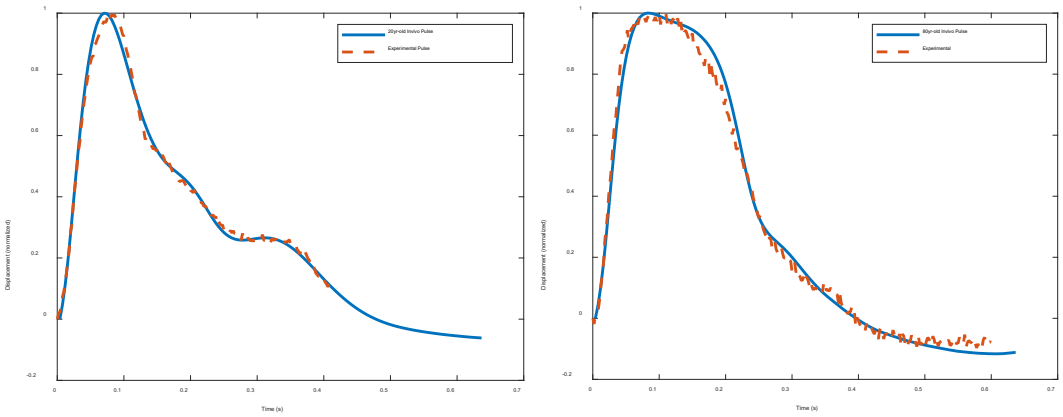

(a) (b)

Figure 2. Shaping base pulse to 20yr-old *in vivo* pulse

Conclusion and Future Work

In this study, the construction and experimental evaluation of MR fluids was conducted and found it successful to replicate human radial pulse waveforms. A CAM pulse generator was used to send a baseline pulse to be shaped using MR fluid. The set-up was able to shape the pulse reliably and continuously to a range of age-related pulse with minimal error. The findings of this project are a foundation for developing standards in oriental medicine to train healthcare professionals. Furthermore, this research could lead to developments in the sensors used in smart watches to measure blood pressure.

Acknowledgements

The author would like to thank the Ohio Space Grant Consortium for the opportunity and support in this project. Their generosity has helped fund the research and studies. Additionally, the author is thankful for the support and guidance of her mentor Dr. Jeong-Hoi Koo.

References

[1] J.-J. Shu and Y. Sun, "Developing classification indices for Chinese pulse diagnosis," Complementary Therapies in Medicine, vol. 15, no. 3, pp. 190-198, 2007.

[2] Young, C.C., Mark, J.B., White, W. et al. Clinical evaluation of continuous noninvasive blood pressure monitoring: Accuracy and tracking capabilities. J Clin Monitor Comput 11, 245–252 (1995). https://doi.org/10.1007/BF01617519

[3] Y.-F. Chung, C.-S. Hu, C.-C. Yeh and C.-H. Luo, "How to standardize the pulse-taking method of traditional Chinese medicine pulse diagnosis, "Computers in Biology and Medicine, vol. 43, no. 4, pp. 342-349, 2013.

Simulator Based Study of Vehicle Control Performance

Student Researcher: Molly E. Fenik

Advisor: Megan Reissman

University of Dayton
Department of Mechanical Engineering

Abstract

The ability of humans to consistently perform precise motor control tasks is one of the most missions critical aspects of human space exploration. Under aerospace conditions humans must frequently perform these tasks with limited visual information and under conditions where vestibular sensory function is compromised. Continuing the "Effects of Hypoxia on Vehicle Motor Control during Matched and Mismatched Vestibular feedback" [2] research 7 additional subjects have been collected. These subjects completed Day B of this procedure where the subjects performed motor control tasks under hypoxic (10% O_2) and normoxic (21% O_2) conditions.

Additionally, in alignment with the Human Exploration and Operation Directorate, I proposed to study human-vehicle interactions (motor control tasks) focused on coupled motion tasks in an environment consistent with space travel where there are minimal orientation ques (starfield). I planned to examine factors of task information motion (motion vs. no motion) and of vestibular sensory information (physical rotation rate different from visual rate). The coupled motion tasks will include roll tilt and yaw that is consistent with aircraft heading changes.[1] This is a multiaxial study where participants will perform repeated motor control tasks in a starfield environment by tilting to a displayed tilted bar that will cause the yaw motion to happen. The subjects will then be presented with a vertical bar where they will have to counter the tilt input to come out of the tilt to achieve the vertical bar location.

Project Objective

The purpose of both studies is to examine the impact and effect the vestibular system can have on the performance of a motor control task. In addition, examining the performance under different oxygen conditions to determine where the greatest variability in performance is.

Methodology

Using virtual reality the "Effects of Hypoxia on Vehicle Motor Control during Matched and Mismatched Vestibular feedback" [2] study participants(n = 7) performed a training set of all four types of trials (no motion solid target, no motion flashed target, motion solid target and no motion solid target) with target at ±20° and ±10° angles. After the training set the participants performed the same four trials under hypoxia and normoxia with a break in between. When under hypoxic conditions the participants breathed 10% oxygen which is equivalent to oxygen at 14,000ft and under normoxia the participants breathed 21% oxygen which is equivalent to room air. During the collection the participants were wearing a VR headset, breathing mask, transcranial doppler, finger photoplethysmography, and blood pressure cuff and all data was recorded.

For the multiaxial study of roll tilt and yaw the specific methodology has not yet been confirmed with the anticipated test plan of biases added to the roll tilt and yaw. These biases would be +-5°/s for yaw and +-1°/s for roll tilt with different combinations for both motion and no motion trials.

Results

After completing the collection for the "Effects of Hypoxia on Vehicle Motor Control during Matched and Mismatched Vestibular feedback" study, two main takeaways were found. The first main finding was that the larger roll tilt angles resulted in oxygen level and motion being significant factors ($p=0.021$ and $p<0.001$)The participants undershot their roll tilt target under hypoxic conditions. The next key takeaway was that when under hypoxic conditions the solid no motion trials had the lowest variability compared to all other conditions ($p<0.0054$).

Figure: 1 Virtual reality environments with the Yaw Motion Simulator set up.

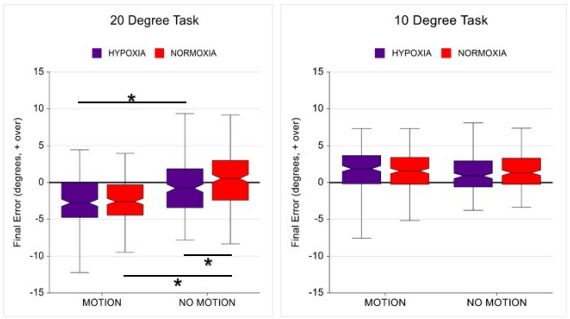

Figure 2: Roll tilt angles of 20 and 10 degrees with final error for all trials

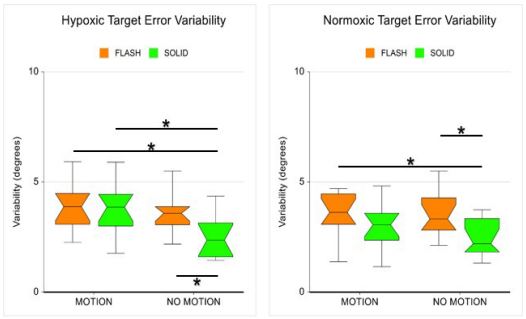

Figure 3: Target variability in hypoxic and normoxic oxygen conditions for all trials

Acknowledgements and References

The author would like to thank Dr. Reissman, her advisor, for all her guidance and support throughout this project. The author would also like to thank Dr. Crecelius from the Department of Health and Sport Sciences for helping with the collections of the physiological data and for always being an extra resource. Finally, the author would also like to thank the other students in the lab that helped make this project happen.

[1] Day, Richard E. *Coupling Dynamics in Aircraft: A Historical Perspective*. National Aeronautics and Space Administration, Office of Management, Scientific and Technical Information Program, 1997.

[2] Klausing, Lanna Nicole. "Impact of Motion and Visual Presentation on the Performance of a Vehicle Roll-Tilt Task in a Virtual Reality and Motion Simulator System." *University of Dayton*, 2022

Comparing Flow Over a Surface Numerically vs Experimentally

Student Researcher: Olivia F. Galigher

Advisor: Jed E. Marquart, Ph.D., P.E.

Ohio Northern University
Dr. Carl D. Clay and H. Jane Clay Department of Mechanical Engineering

Abstract
Understanding how flow over a specific surface happens is really valuable information, however it is not always feasible to construct a full-scale model of something and test it. Numerical software like Computational Fluid Dynamics (CFD) allows you to take a 2D or 3D model and simulate flow under various conditions. Another option is testing it experimentally, using a small-scale model in a wind tunnel. In order to better understand the benefits of both methods and determine which contains more accuracy, a comparison of the flow results over a sphere from both numerical and experimental techniques can be completed and conclusions drawn.

Project Objectives
The following goals were set for this project: Compute flow over a sphere numerically using Computational Fluid Dynamics (CFD); Compute flow over a sphere experimentally using a wind tunnel; Compare the accuracy of the two methods.

Methodology Used
To collect the experimental data, a three-inch diameter sphere was mounted in a wind tunnel, with the input control being the fan motor frequency, in Hertz. The immediate output was differential pressure in inches of water, also known as the head. There were six different cases varying the fan motor – 25, 30, 35, 40, 45, and 50 Hz. Two sets of data were collected for each of these cases. Each case outputs a head value in inches of water, h, and the computer software outputs axial force, F_D, which was time averaged over 10 seconds. The head output from the wind tunnel was used to calculate differential pressure, Δp, as shown in equation 1:

$$\Delta p = \rho_{H20} g h \tag{1}$$

where ρ_{H20} is the density of water at 70°F and g is the gravitational constant.
Differential pressure was used to calculate velocity, V, as shown in equation 2:

$$V = \sqrt{\frac{2\Delta p}{\rho_{air}}} \tag{2}$$

where ρ_{air} is the density of air at 70°F.
The velocity was then used to calculate Reynolds number, Re, Coefficient of Drag, C_D, and Mach number, Ma, in equations 3, 4, and 5 respectively:

$$Re = \frac{\rho_{air} V D}{\mu} \tag{3}$$

$$C_D = \frac{F_D}{\frac{1}{2}\rho_{air} V^2 A} \tag{4}$$

$$Ma = \frac{V}{c} \tag{5}$$

where D is the diameter, μ is the dynamic viscosity of air, A is the cross-sectional area, and c is the speed of sound.
CFD is a numerical method of solving fluid flow using a computer. The geometry was modeled after the sphere in a wind tunnel, with a three-inch diameter sphere in a 18” by 18” block, with a 9” by 9” wake block. *Pointwise* was used to generate the grid with points on the connectors concentrated at the front end, closer to the sphere on the wake block to concentrate more cells in that area. T-Rex cells were also used coming off the sphere to increase the accuracy of the results. *Pointwise* generates a boundary condition file in which

Solid Wall Adiabatic No Slip condition was used for the sphere and Farfield Modified Riemann Invariants were used for the Outer Edges (the sides of the block). Six different job files were created for each of the cases in which units, reference area, and Mach number were modified, with Mach number the value differing in each of them. *Cobalt* was used to run the job. In order to get the results to converge, it was run for a total of 26,000 iterations changing the time step a couple of different times. *Cobalt* was set to output time averaged data over the last 6,000 iterations, as well as transient data with files outputting every 100 iterations.

Results Obtained

The Coefficient of Drag for all six Reynolds numbers are shown in Figure 1 for both the experimental and numerical data. The two sets of experimental data were very close and were averaged to show in the chart. The experimental and numerical results were compared to the accepted values found in a fluid mechanics textbook, which are shown in Figure 2.

Significance and Interpretation of Results

The experimental data was more accurate of the two methods based on the data collected. The wind tunnel produces data that is very close to the accepted values. There are a couple of reasons for the discrepancies with the numerical data. First, the grid quality was only 90.22 percent. If the grid quality increases, the numerical data should get closer to the accepted value. The tradeoff with increasing the grid quality is the increased computational time. The second possible reason for the discrepancy is the boundary condition of the outer edges. If Solid Wall Slip condition was used instead of Farfield Modified Riemann Invariants, it may better simulate what was happening in the wind tunnel.

Figures/Charts

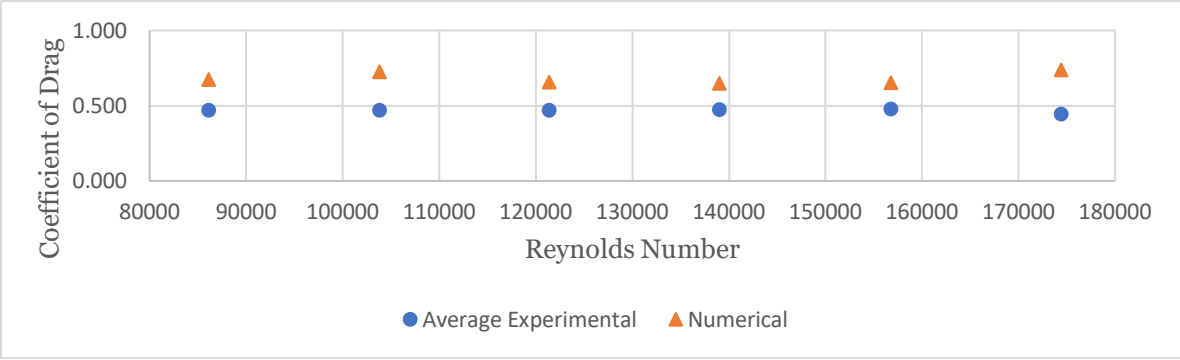

Figure 1. Coefficient of Drag vs Reynolds Number

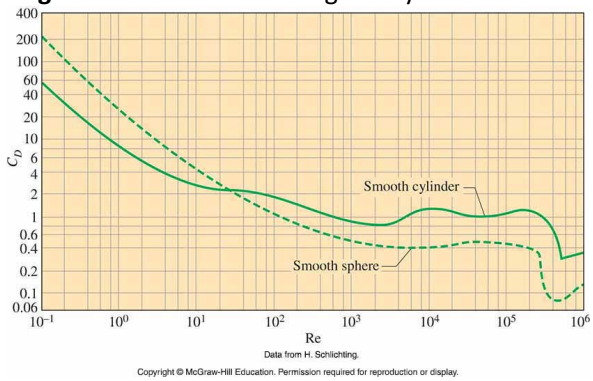

Figure 2. Avg. drag coefficients for cross-flow over a smooth circular cylinder and a smooth sphere [1]

Acknowledgements and References

[1] Y. A. Cengel, J. M. Cimbala, and H. Schlichting, "Figure 11-34," in *Fluid Mechanics: Fundamentals and Applications*, 4th ed., New York, NY: McGraw-Hill Education, 2018.

Fine-Grained Air Quality Sensing with IoT

Student Researcher: Julia M. Gersey

Advisor: Dr. Brian Krupp

Baldwin Wallace University
Department of Computer Science

Abstract
Air quality is an important factor for human health. The World Health Organization states there are "4.2 million deaths every year as a result of exposure to ambient (outdoor) air pollution". Additionally, they report that "9 out of 10 people worldwide live in places where air quality exceeds WHO guideline limits". For Cuyahoga County, an area of 459.07 square miles and a population of 1,245,337 (as of 2020), only one air quality sensor monitors Particulate Matter 2.5 levels, proven to be the most dangerous kind for humans to breathe. Particulate Matter 2.5 (PM 2.5) are inhalable particles with a 2.5-micrometer diameter and pose the most significant risk to humans as they can penetrate human lungs and the bloodstream. Long-term exposure can lead to asthma and lung cancer, among other health conditions. With that large area to cover, the EPA cannot provide communities with a solid sense of the air they breathe. By using Internet-of-things (IoT) devices, a network of sensors could capture fine-grained air quality, specifically PM 2.5 levels, and report it to a web dashboard.

Project Objectives
This project aims to deploy a network of low-cost air quality sensors throughout Cleveland to capture more fine-grained air quality data throughout the city. Additionally, we are looking to create a K-12 Computer Science Curriculum and partner with local schools so they can learn about air quality and important computer science topics.

Sensor Prototype and Testing
Our sensor units were made with four main factors in mind: low-cost, low-power, generally available boards, and accuracy. Commercial-off-the-shelf air quality sensors cost ~$200, and ours cost around $40 per sensor. We also focused on making our sensors low power because power is expensive and limits where these sensors could be placed. Next, we used generally available boards such as Raspberry Pi's and Arduino's, because both are easy for younger computing students to learn. Lastly, accuracy is important in capturing trends in Cleveland's air quality. Although low-cost sensors are not as precise as higher-cost alternatives, they can still accurately show general trends in air quality.

Our sensor units active in the field are made up of a Raspberry Pi and Plantower PMS5003 2.5 sensor, and we programmed them to start reporting their PM 2.5 readings to our web dashboard once they have power and connectivity. We partnered with a Cleveland company, PCsForPeople, who provides Wi-Fi hotspots and refurbished electronics to low-income neighborhoods. By leveraging their existing infrastructure and hotspots around Cleveland, we got both power and connectivity for our sensors. In Figure 1, the black dot is the EPA's sensor, and the blue, red, and green are ours. After calibrating our sensors in the robotics lab on campus for a week, we deployed our sensors in Cleveland, as shown in Figure 1, for around two months to serve as our pilot deployment and capture our initial air quality data.

Figure 1. Sensors in Cleveland

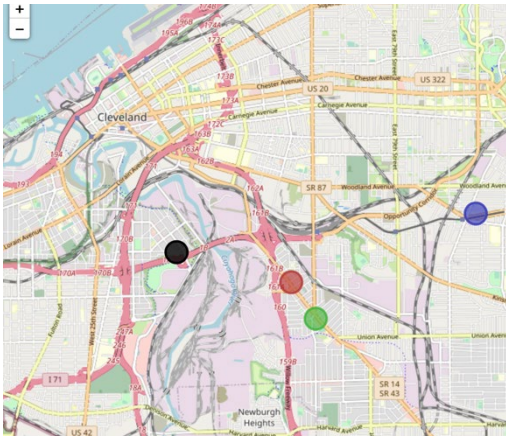

Figure 2. Test Deployment Results

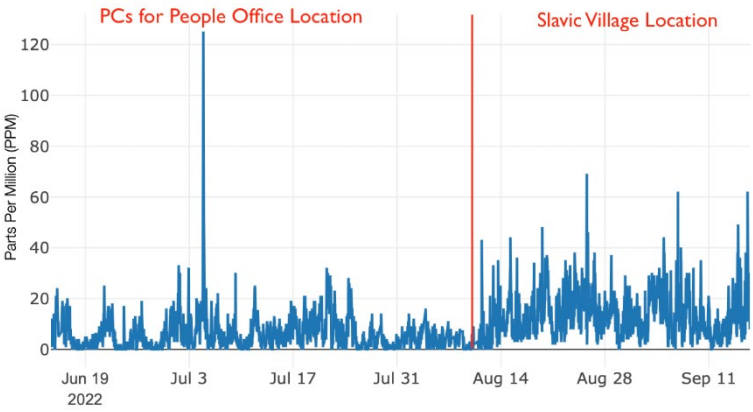

Deployment Results

In Figure 2, you will see a significant blue spike slightly after 'Jul 3', corresponding with Cleveland's Fireworks show for the 4th of July. Relatedly, when we moved our sensor from the blue dot (PCs for People Office Location) in Figure 1 to the red/green dots (Slavic Village Location), we saw that the average PM 2.5 level was more than twice the average reading at the blue dot, as shown in Figure 2. This meant that between a distance less than 4 miles, the PM 2.5 levels could be vastly difference, but without a fine-grained approach this would be unknown. The red portion of the Figure 1 map between the black dots and red/green dots is where the Steel Mill is located, and our data from August to September showed higher levels of PM 2.5 in the air than the EPA sensor was reporting, simply because the EPA sensor's location cannot capture the pollution from the Steel Mill with the wind coming off the lake. This proves the need for fine-grained air quality monitoring since one sensor cannot provide accurate data for Cleveland.

Future Work

Our future work is focused on a campus deployment, increasing our sensors around Cleveland, and building a K-12 Computer Science Curriculum. To lower the costs of our sensor for our campus deployment, we are using Raspberry Pi Pico W's, which cost $4 and will be housed in PVC pipe capsules while deployed around campus. If we see success with this deployment, it will help us lower the cost of our sensors even further. This leads to us increasing the number of sensors in Cleveland to support our goal of fine-grained monitoring. Lastly, we will be building a Computer Science Curriculum for K-12 kids so that they can build these sensors themselves. This will allow those kids to learn more about air quality and important computer science topics they otherwise wouldn't.

Acknowledgments and References

I want to thank my advisor, Dr. Brian Krupp, for his continued support and mentorship, PCsForPeople for their partnership and support for our project, and the Ohio Space Grant Consortium for helping make this project possible through their scholarship.

Testing Approach and Precision Landing for All-Terrain Aerial Robotic Interface (ATARI)

Student Researcher: Rebecca N. Gilligan

Advisor: Dr. Kelly Cohen

University of Cincinnati
Mechanical Engineering

Abstract
Combining the strengths of different autonomous vehicles in a multi-modal system creates opportunity to complete more complex missions through collaborative interaction. The development and testing of All-Terrain Aerial Robotic Interface (ATARI) builds on a previously funded OSGC project titled Integrating Unmanned Aerial Vehicle and Unmanned Ground Vehicle Collaborative Systems. ATARI consists of a collaborative unmanned aerial vehicle (UAV) and unmanned ground vehicle (UAV). The UAV features a precision landing system which is utilized to land on the levelling platform attached to the UGV. This allows the UGV to serve as a mobile landing platform for the UAV which can provide improved landing sites and enhance the flight time of the UAV. This phase of work focuses on the flight testing approach, precision landing system, and preliminary flight test results.

Project Objectives
The first design iteration of a collaborative UAV-UGV pair was part of a previous OSGC funded project in [1]. The ATARI concept and the designs were further developed in [2]. Work completed in the 2022-2023 academic year focused on tuning testing the precision landing system and the prototype vehicles further developed in [2]. A major goal was to validate the precision landing behavior of the UAV with ArduPilot firmware, determine the accuracy of the system, and to determine how precision landing interacts with failsafe behavior.

Methodology
The testing methodology followed a crawl-walk-run approach (Figure 1), beginning with basic flight testing and tuning, validating failsafe behavior, then validating and tuning the more complicated precision landing. Each test followed thorough flight test planning and procedures to ensure validation of requirements and behavior in flight testing assessments. Flight test plans also documented information such as wind conditions during flights as this could affect the precision landing accuracy and stability. A major risk in testing the precision landing capability for the ATARI system involves the UAV falling off of the elevated platform on the UGV, causing damage to one or both vehicles. Risk was mitigated by using a ground platform for initial tuning and determining the accuracy and precision of the precision landing functionality. In this case, should the vehicle miss it's target, it will still land safely on the ground, regardless of the strictness being tested.

Results
The results obtained are from summer and fall flight testing as once the weather became too cold, outdoor testing opportunities were scarce. Precision landing requires GPS and must be tested outdoors. In Figure 1, completed flight tests are denoted by green, and future tests in blue. The results of the

precision landing testing are shown in Figure 2, along with 2-D standard deviations. Based on the current data, the precision landing system beats the manufacturer specified accuracy and meets the stricter ATARI requirements shown in the figure (outer and inner blue circles, respectively). Many limitations of the precision landing system with ArduPilot were identified and the system will utilize PX4 firmware in the future as it is more development-friendly. Some of the limitations include that the precision landing system poses challenges for multi-vehicle systems, especially in cases where vehicles may have different landing requirements. Additionally, in ArduPilot, the precision landing functionality kicks in whenever any failsafe is activated which includes a landing flight mode. This is a problem as the purpose of the failsafe, battery for example, is to land the vehicle safely, while the precision landing, if in strict settings will prevent the vehicle from doing so if the beacon is not in sight.

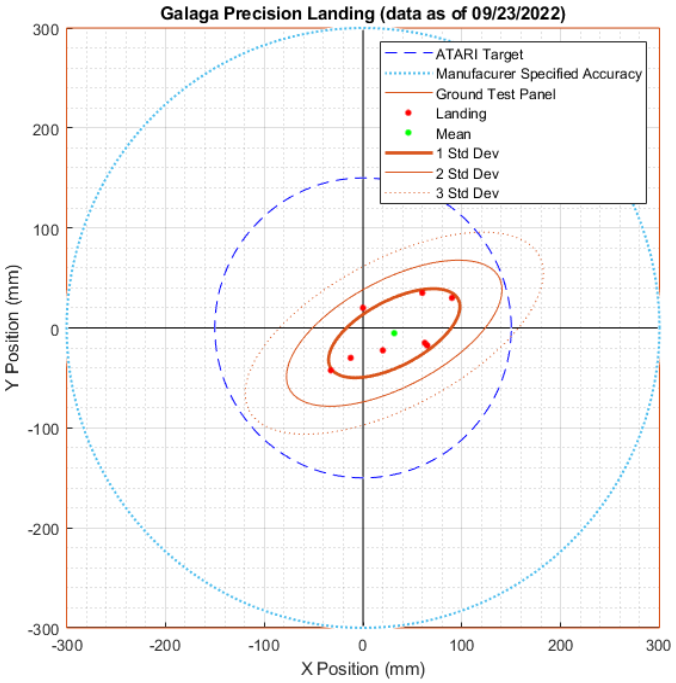

Figure 1. ATARI Precision Landing Results – ArduPilot (As of 09/23/2022)

Conclusion and Future Work

A transition to PX4 firmware for both vehicles will occur throughout the rest of the spring and summer semesters as PX4 has benefits for development and simulation. This helps future-proof the system for future development of the system in my graduate studies. Continued testing of precision landing with ArduPilot will resume in late March to obtain statistically significant data and constrain additional variables such as the yaw orientation during landing. This process will then be repeated for PX4 and allow for comparison between the precision landing for each firmware.

Acknowledgements

I would like to thank my advisor Dr. Kelly Cohen as well as Bryan Kowalczyk, Justin Ouwerkerk, and Austin Wessels for their guidance and support. I look forward to continuing testing through the summer and building upon this project for my graduate studies!

References

[1] Rebecca N. Gilligan. “Integrating Unmanned Aerial Vehicle and Unmanned Ground Vehicle Collaborative Systems”. In: NASA/ Ohio Space Grant Consortium 2020-2021 Annual Student Research Symposium Proceedings XXIX (Cleveland, Ohio). OSGC, Mar. 2021, pp. 126–130. url: http://osgc.org/wp-content/uploads/2021/09/2-Proceedings-PDF.pdf

[2] Rebecca N. Gilligan and Dr. Kelly Cohen. “Design of an All-Terrain Aerial Robotic Interface (ATARI) as a Collaborative Platform for UAVs”. In: National Harbor, MD.: International Student Competition at AIAA’s SciTech Forum, Jan. 2023. url: https://arc.aiaa.org/doi/10.2514/6.2023-0002.

Organic Electrochemical Transistors (OECTs) as Liquid Electrolytes and Implementation of Metals Salts

Student Researcher: Delonte E. Goodman

Advisor: Dr. Antal Jakli and Arwa Alyami

Kent State University
Physic Department

Abstract

The study was focused on investigating the influence and comparison of different metal salts in the creation of liquid electrolytes as Organic Electrolytes Chemical Transistors (OECTs). The effect of various metal salts such as (LiTFSI), $Mg(TFSI)_2$, and $Al(TFSI)_3$ (bis-trifluoromethane sulfonyl imide) was measured and analyzed regarding the electrical characteristics of the fabricated OECTs. The conducted experiments used different metal salts with different ratio sizes/valency cations. During the investigation, cations were varied utilizing Lithium, Magnesium, and Aluminum metals salts. In addition to varying metal salts sulfonates such as Chloroform ($CHCl_3$) and Tetrahydrofuran (C_4H_8O) were implemented to facilitate the creation of ionic liquid. Electrical characteristics such as transient measurements and steady-state measurements. Finally, the On and Off Ratio and Switching Times were compared between the three samples.

Project Objectives

Research during the academic year was based on previous experiments conducted with Organic Electrochemical Transistors (OECTs). This research focused on liquid electrolytes, which will be used to fabricate OECTs. The goal of the experiments was to investigate the influence of metal salts in liquid electrolytes for characteristics such as transient measurements. After obtaining the transient measurements, plots would be created to compare the three metal salts used in the experiments.

Methodology Used

The conducted experiments used different metal salts with different ratio sizes/valency cations. The anion known as TFSI was kept constant when creating the liquid electrolytes. As previously mentioned the following samples were created and electrical characteristics such as gate voltage, gate current, and drain current were measured. The $Al(TFSI_)_3$ was synthesized by a simple metal/acid reaction with trifluoromethane acid (HTFSI) and aluminum. The following mixture was dissolved in distilled water, stirred, and then evaporated, to create a white powder when all the water was removed.

During the experiment, there was an issue when mixing the ionic liquid with the metal salts. Due to dissimilar melting points the monomers within the ionic liquid evaporated before being mixed with the metal salts. To solve this problem sulfonates such as Chloroform ($CHCl_3$) were used with respect to each sample examined. Once the data for each sample were obtained a plot for the electrical characteristics of each sample were plotted with respect to time. To account for the high speed of the signals generated a time interval of zero to fifteen seconds was used. Finally, during the analysis stage of the experiments, a linear fit using an exponential decay function was used to help determine the switching times of each sample. Finally, using the switching times the time constant was plotted to be used as a graphical representation of the speed each sample signal exhibited.

Results Obtained

The results of the experiment showed that Magnesium had the fastest switch time, which indicated a very small time constant. These results were similar to the experiment conducted in the previous research conducted by the Jakli lab [1]. In the previous research time constants for the OECTs were created, which yielded approximately 0.3 s [1]. The results also showed that metal salts yielded a faster switching time and time constants than the previous experiments.

Significance and Interpretation of Results

The results from the research showed that the application of metal salts in ionic liquid was feasible and yielded results that showed improvement from previous experiments. Using the previous methods better transistors can be created to produce more efficient devices. Finally, more efficient OECTs can allow for more advancements in technology and the fabrication process of transistors.

Figures/Charts

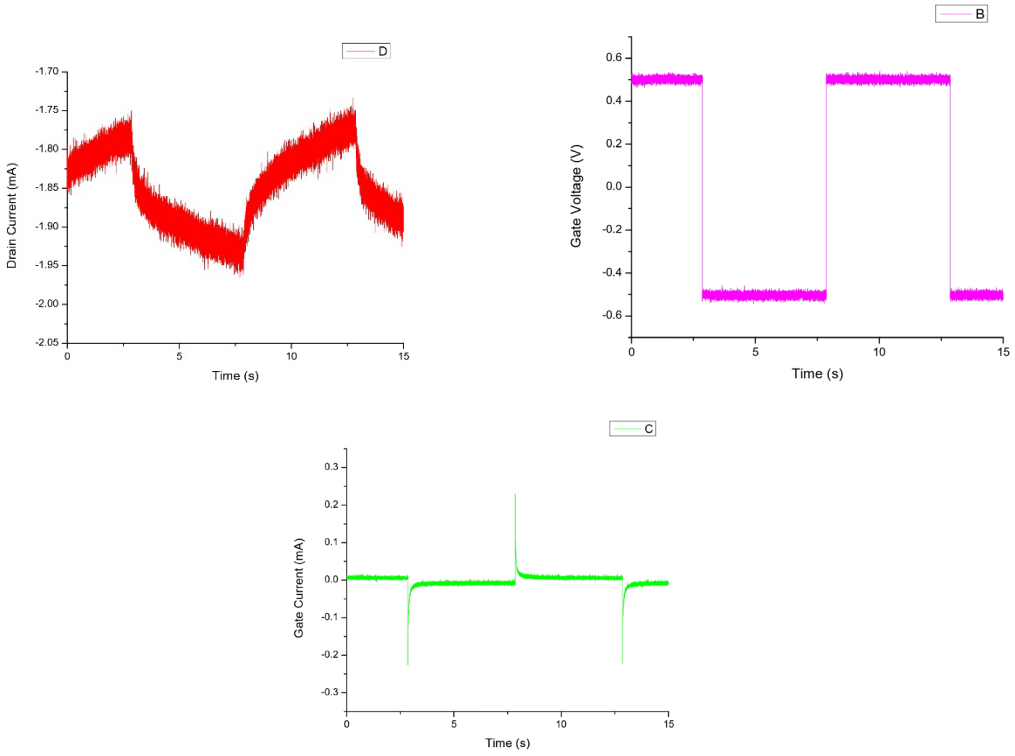

Figure 1: Li(TSFI) Transient Measurements

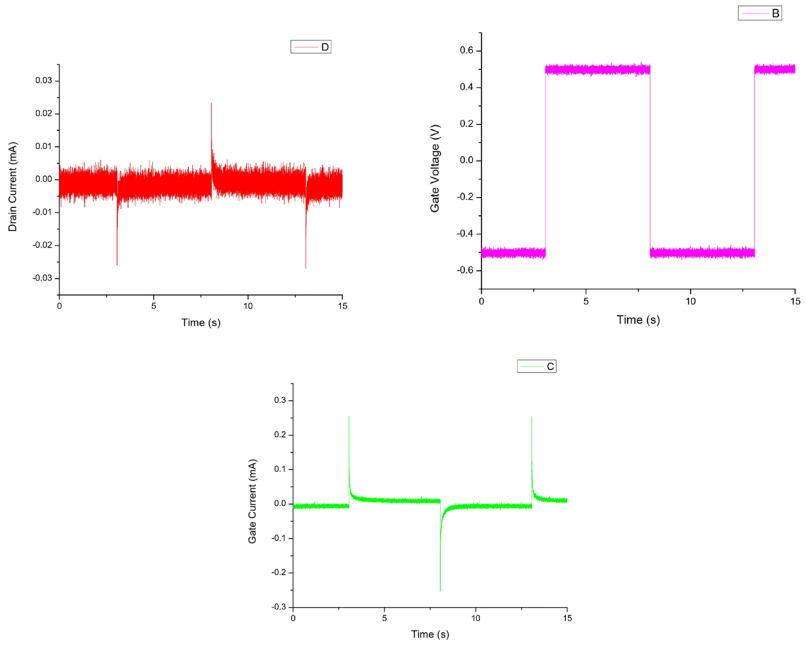

Figure 2: $Mg(TSFI)_2$ Transient Measurement

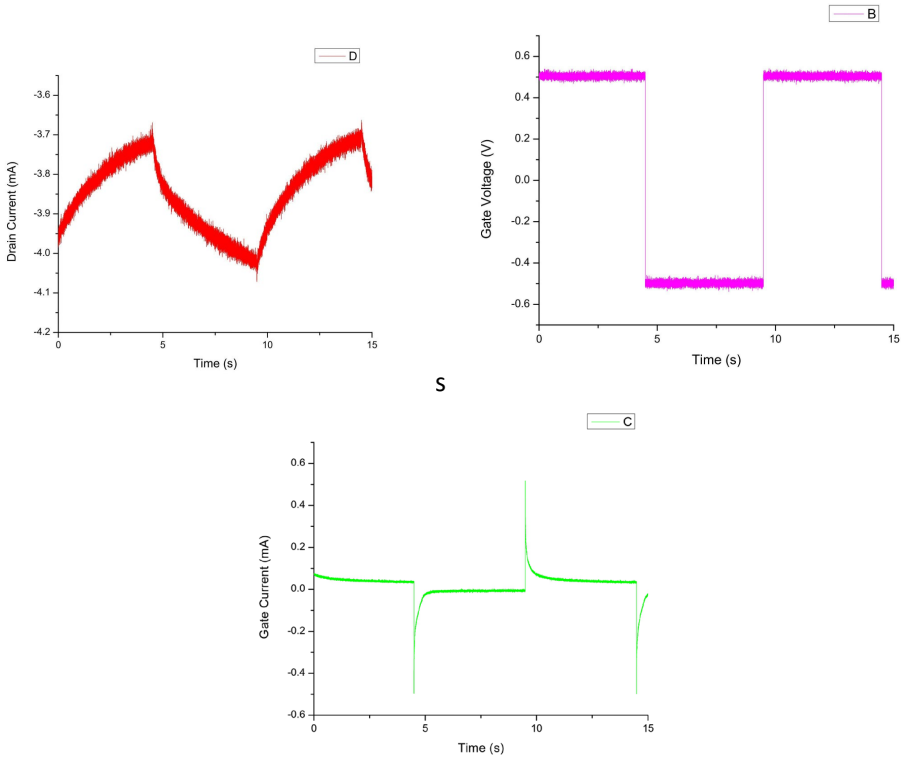

S

Figure 3: $Al(TSFI)_3$: Transient Measurements

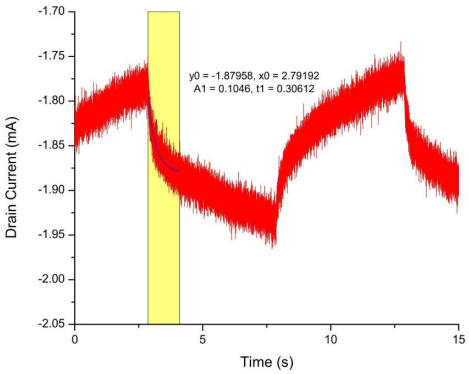

Figure 4: Li(TSFI): Switching Times

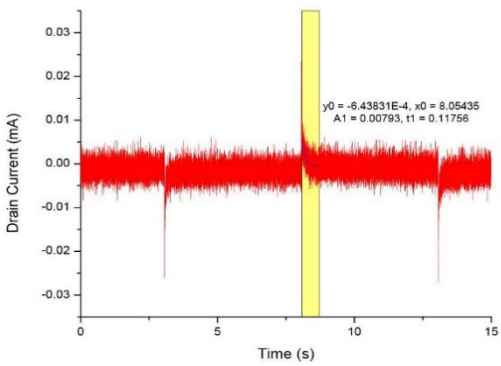

Figure 5: $Mg(TSFI)_2$ Transient Measurements

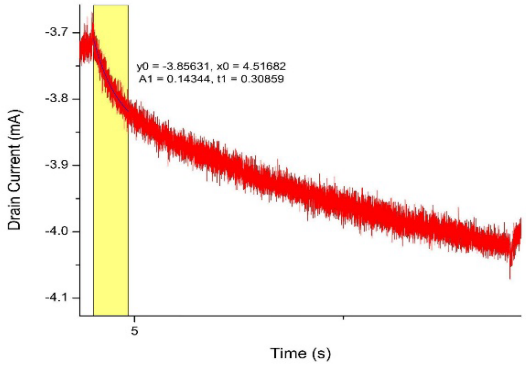

Figure 6: $Al(TSFI)_3$ Switching Times

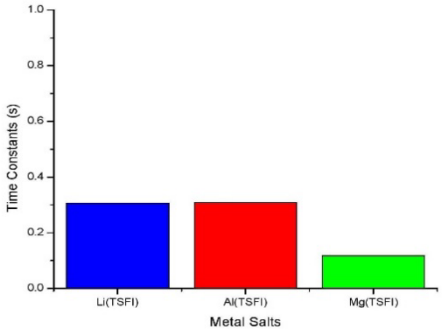

Figure 7: Time Constants Of All Samples

Acknowledgments and References

I would like to thank my mentors Dr. Jakli and Arwa Alyami for their help in completing this project.
I would also like to thank the Ohio Space Grant Symposium for providing me with the opportunity to share my work as well as a scholarship for my studies.

[1] Hemantha Rajapaksha, C. P., Paudel, P. R., Kodikara, P. M., Dahal, D., Dassanayake, T. M., Kaphle, V., Lüssem, B., & Jákli, A. (2022). Ionic liquid crystal elastomers-based flexible organic electrochemical transistors: Effect of director alignment of the solid electrolyte. Applied Physics Reviews, 9(1), 011415. https://doi.org/10.1063/5.0077027

Integrating UAV with sensors to monitor the Harmful Algal Blooms in the Ohio River

Student Researcher: Catherine J. Gottsacker

Advisor: Dr. Dongmei Feng

University of Cincinnati
Department of Chemical and Environmental Engineering

Abstract

Harmful algae blooms (HABs) in surface waters are a global environmental concern, threatening both human and environmental health. To control their impact, HABs must be monitored in a timely manner. While continuous monitoring of surface water is possible using monitoring stations equipped to measure chlorophyll concentration, establishing and maintaining the stations is a costly and labor-intensive endeavor. Chlorophyll data can also be detected in the field using sensors or by collecting water samples, but these methods are time consuming and require direct access to the water. The methods become dangerous and impractical in areas surrounded by cliffs or wetlands.

In this project, a flexible, efficient, and cost-effective approach for monitoring surface water quality is developed using Unmanned Aerial Vehicles (UAV), a water quality sensor, and a multispectral camera. A UAV platform is created to allow direct monitoring of chlorophyll concentration using a water quality sensor carried through the water, allowing monitoring of otherwise inaccessible water bodies. In future research, this platform will be deployed in tandem with a second UAV carrying a multispectral camera, to develop a concentration-reflectance rating curve for Chlorophyll as an indicator of HABs. The reflectance readings from the multispectral-carrying UAV alone can then be used to remotely collect water quality data on any surface water with high spatial and temporal resolutions.

Project Objective

This study aims to identify appropriate in-water sensors and create an integration method for the direct monitoring of HABs using UAV.

Methodology

To begin the project, a sensor able to measure chlorophyll concentration *in situ* and capable of continuous monitoring was needed. While selecting the sensor, attention was paid to the size and weight of the equipment, the capability to record and store data, and needed power supply. Commercially available sensors were researched, and a YSI EXO 3 Sonde was selected for the study (shown in figure 1).

The sonde was customized to include sensors for chlorophyll, which is present in all algae, phycocyanin, another pigment that is a specific indicator of blue-green algae, and temperature and conductivity, which help adjust the pigment calibrations and measurements. Both chlorophyll and phycocyanin fluoresce and can therefore be measured optically. The YSI sensors package a fluorometer into a probe, which emits a blue light at 470 nm to excite chlorophyll, and a second orange beam at 590 nm to excite phycocyanin. The excited compounds then emit light at a higher wavelength than the initial excitation beam, which is filtered and detected by the probe. The YSI sensor reports separate datasets for chlorophyll and phycocyanin containing both relative fluorescence units and µg/L of each.

Figure(s)/Chart(s)

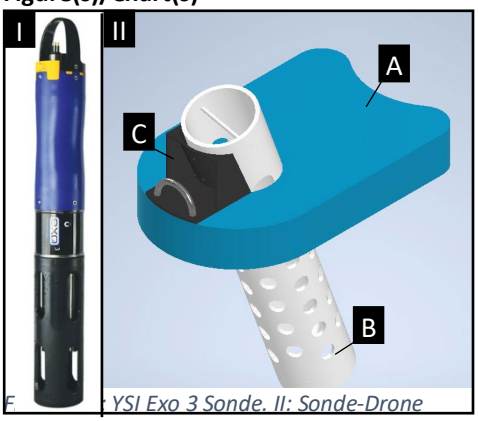

F : YSI Exo 3 Sonde. II: Sonde-Drone Integration Platform, including (A) foam boards, (B) sonde containment, and (C) stabilizer.

While cameras are often easily integrated with drones, in-water sensors are not. Therefore, a sonde-drone integration platform to securely connect the two was designed. The solution had to provide a consistent underwater submergence depth of sensors during measurement, the ability to be flown through air and water, protection against in-water obstacles, and easy access to the sonde for cleaning and data collection. In addition, no direct connections could be made to the sonde, which can be easily damaged and deformed by clamps.

The platform design is shown in figure 1, and includes foam boards, sonde containment, and a stabilizer. The closed-cell ethylene vinyl acetate (EVA) foam boards provide flotation for the sonde, decreasing load for the drone while ensuring a consistent submergence of the sonde. The sonde itself is contained in a 4-inch diameter PVC pipe with holes drilled to allow flow to the sensor. Stop bolts placed at the top and bottom of the pipe prevent the sonde from sliding out of the tube but keep an almost entirely open bottom to further maintain flow to the sensor. The containment tube protects the sensor from impact with debris in the water, allows an indirect connection between the sensor and the drone, and maintains easy access to the sonde when needed. Most of the weight of the sensor is carried below the board to increase stability of the platform, and the precise placement of the pipe into the board was calculated to align the center of mass of the angled sonde to that of the foam board. The black stabilizer piece, custom designed and 3D printed, connects the sonde containment and foam board together, and allows for the attachment of the drone to the platform using paracord.

Results

The sonde-drone integration will be tested in late spring and early summer of this year, in collaboration with the University of Cincinnati UAV Master Lab who have provided a pilot and drone for the study. The drone is expected to be able to take off from an area without direct water access, fly over a body of water, lower the platform to the surface, tow the platform through the water, and then return to the takeoff site. The testing will first be completed with a weighted platform, and then with the sensors recording live data. The sonde will be pre-programmed to record readings on a frequent interval, which can be time-correlated to the UAV navigation data to provide approximate position in post processing.

Significance and Interpretation of Results

In this project, a platform was designed for the direct monitoring of HABs in surface waters with UAV.
Future work will focus on the integration of a multispectral camera with a second drone, which will be flown in tandem with the sonde-carrying drone developed this year. Imagery from the camera will be correlated with sensor readings to develop a concentration-reflectance rating curve for Chlorophyll as an indicator of HAB.

Acknowledgements

I would like to thank the Ohio Space Grant Consortium for this scholarship opportunity, Dr. Dongmei Feng for her mentorship, and Bryan Kowalczyk and Justin Ouwerkerk for their guidance.

Motion Prediction of Birds to Prevent Bird Strikes with Low-Altitude Aircraft

Student Researcher: Katie M. Horn

Advisor: Dr. Syed A.M. Shihab

Kent State University
Department of Aeronautics and Aerospace Engineering

Abstract

Emerging low-altitude aircraft such as drones or UAS offer new possibilities for package delivery and passenger transportation below 400 m. However, bird strike risk with aircraft is highest at these low altitudes. Bird strikes pose significant flight safety risk for both UAS and birds and may result in fatalities. To prevent bird strikes with UAS, this research project develops: 1) regression models using GPS-based bird tracking data to model and predict bird movements; and 2) a deconfliction algorithm that assigns departure delays to aircraft based on bird movement forecasts to prevent collisions. Results demonstrate that this approach can prevent bird strikes and enhance the safety of air travelers and birds.

Project Objectives

In the US, birds are involved in 97% of all strikes with civil aircraft, with 15,400 reported in 2021 alone [1]. The annual cost of bird strikes to commercial airlines worldwide is approximately US$1.2 billion [2]. Despite the high number of incidents and critical safety and financial implications of bird strikes, research on methods to prevent bird strikes has not received significant attention. Past studies on bird strikes have typically concentrated on forecasting the number of incidents, identifying high-risk species and locations, assessing damages, and analyzing contributing factors [3, 4, 5]. This project focuses on preventing bird strikes by first developing linear and nonlinear regression models to predict future bird movement track latitudes and longitudes. Then, a strategic deconfliction algorithm is developed which uses these predictions to assign departure delays to flights to prevent collisions between aircraft and birds. This approach is shown in Figure 1.

Methodology Used

To develop the predictive models, bird movement data of Sparrows, a high-risk bird in aviation, was first gathered from MoveBank[6]. The bird tracking data collected includes the following features: time, latitude, longitude, and type of bird. The data was then preprocessed using interpolation and normalization. Then, a linear regression model and a fourth-order polynomial nonlinear regression model were trained with 80% of the data and tested with the remaining 20% of the data. The performance of the models were then evaluated using the mean squared error metric. Next, a deconfliction algorithm was developed based on the bird movement forecasts to prevent collisions. The algorithm first assigns a delay of up to five seconds if there is an intersection between the aircraft and bird flight paths. If the risk persists after five seconds, the algorithm will then assign an advancement of up to five seconds to prevent a collision.

Results Obtained

The study results demonstrate that the linear regression model have higher prediction accuracy in testing compared to the nonlinear regression model, as reflected by the lower mean squared error shown in Figures 2 and 3. This finding suggests that the linear regression model outperforms the nonlinear regression model for both latitude and longitude prediction. To test the deconfliction algorithm, flight paths of aircraft taking off from the Cleveland Hopkins Airport were simulated as shown in Figure 4. By assigning departure delays when an intersection is detected between the aircraft and bird flight paths, the deconfliction algorithm was able to prevent the collision, as depicted in Figure 5.

Significance and Interpretation of Results

To address the bird strike problem, we developed regression-based bird movement forecasting models and a delay-based deconfliction algorithm. The deconfliction algorithm uses the bird movement predictions from the forecasting model to assign departure delays to aircraft to prevent collisions between aircraft and birds. This approach can reduce the number of bird strikes, thus improving the safety of both air travelers and birds.

Figures/Charts

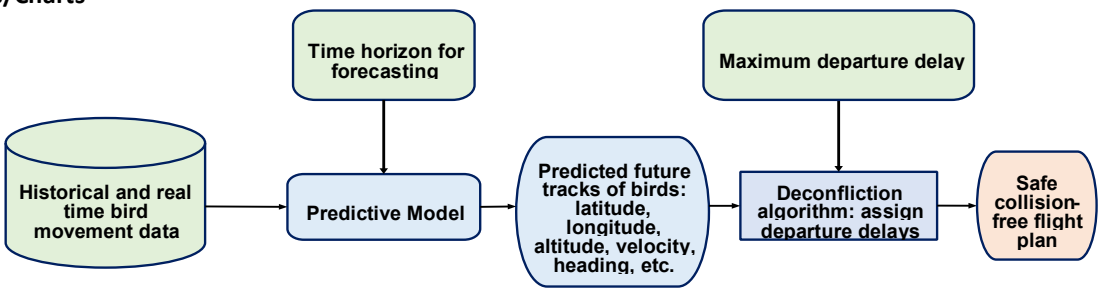

Figure 1: Safe collision-free UAS flight planning flowchart considering bird movement predictions

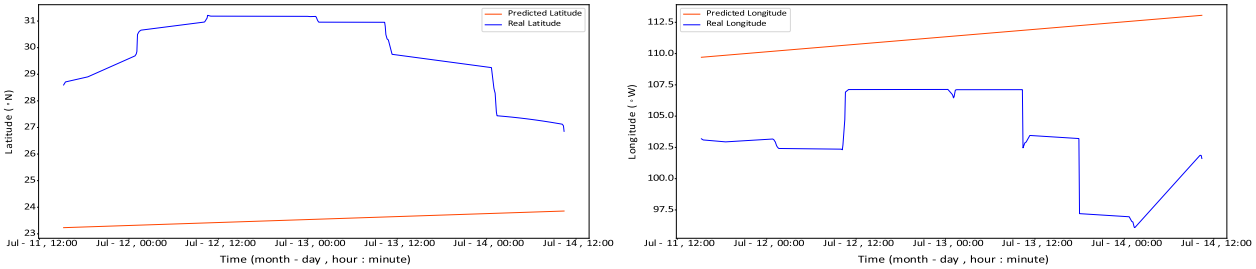

(a) Latitude prediction (b) Longitude prediction

Figure 2: Bird movement prediction by linear regression model during testing

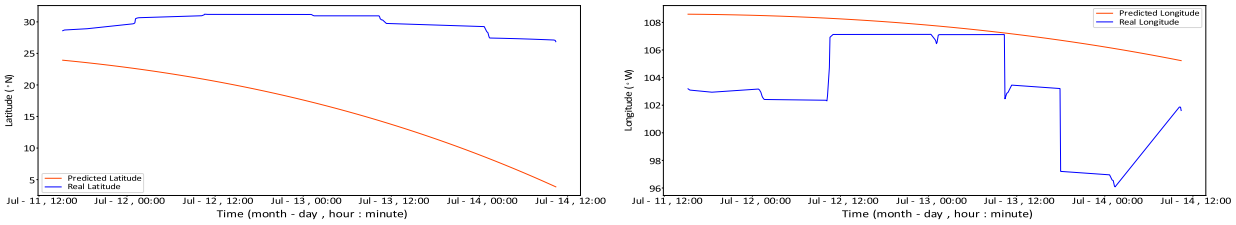

(a) Latitude prediction (b) Longitude prediction

Figure 3: Bird movement prediction by nonlinear regression model during testing

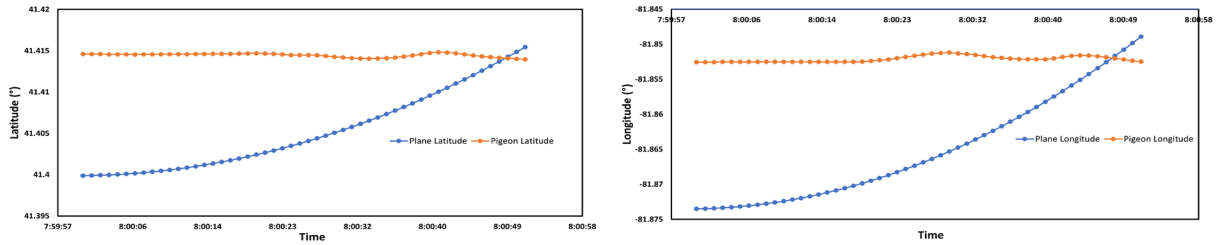

(a) Predicted bird latitude and the plane latitude (b) Predicted bird longitude and the plane latitude

Figure 4: A bird strike detected on the take-off path

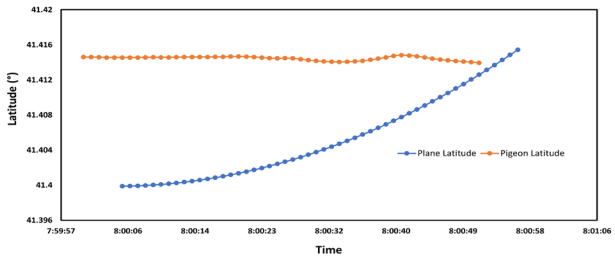

(a) Predicted bird latitude and the plane latitude

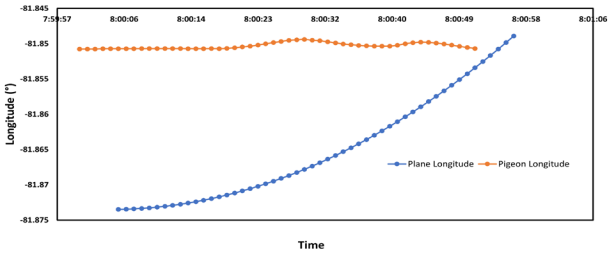

(b) Predicted bird longitude and the plane latitude

Figure 5: Predicted bird path and plane path after delaying departure time

Acknowledgements and References

I would like to express my gratitude to Dr. Syed A. M. Shihab, my faculty advisor, and Elaheh Sabziyan Varnousfaderani, a graduate student working with Dr. Shihab, for their guidance and help throughout this research. I would also like to gratefully acknowledge the support provided by OSGC for this research project.

[1] FAA. "FAA Wildlife Strike Database". In: (2023). URL: https://wildlife.faa.gov/home.

[2] John R Allan and Alex P Orosz. "The costs of birdstrikes to commercial aviation". In: *2001 Bird Strike Committee-USA/Canada, Third Joint Annual Meeting, Calgary, AB*. 2001, p. 2.

[3] Isabel C Metz et al. "The bird strike challenge". In: *Aerospace* 7.3 (2020), p. 26.

[4] Vijayakumar Mathaiyan, R Vijayanandh, and Dong Won Jung. "Determination of Strong Factor in Bird Strike Analysis using Taguchis method for Aircraft Manufacturing guide". In: *Journal of Physics: Conference Series*. Vol. 1733. 1. IOP Publishing. 2021, p. 012002.

[5] Quan Shao et al. "Key factors assessment on bird strike density distribution in airport habitats: Spatial heterogeneity and geographically weighted regression model". In: *Sustainability* 12.18 (2020), p. 7235.

[6] MoveBank. *Data*. 2022. URL: https://www.movebank.org/cms/movebank-main.

Continuously Variable Transmission Analysis

Student Researcher: Benjamin L. Jackson

Advisor: Mitch Wolff

Wright State University
Mechanical Engineering

Abstract

The main objective of a continuously variable transmission (CVT) is to provide an optimal gear ratio that will allow the engine to remain in a peak power output zone for any variable wheel speed. Due to the new implication of a fourteen-horsepower engine for the SAE Baja Team, the clutch design and tuning is different from previous years of only ten horsepower. A CVT clutch consists of many different internal components that affect the gear ratios it puts out. Different forms of testing will be conducted as well as calculations to maximize the efficiency of the clutch. The first test will consist of how the clutch will react to the RPM(Revolutions Per Minute) of the engine to get a baseline of how different the engine is from the past. The clutch will be installed as the engine will be run at various RPMs. To complete this a tachometer will monitor RPM while a video recorder will monitor the primary clutch sheave opening distance. The main variables that will decide this ratio will be the weights on the outer basket which apply the centrifugal force and the center spring which slowly resists that force creating a smooth gear ratio transition. After a baseline is met, calibration of weights and a spring will allow for changes to occur making the clutch more efficient for the new engine. Testing for belt strength is another key factor to limit slip in the drivetrain. Different lengths and width belts will be tested on the engine to see which size provides the least slip and allow the car to accelerate quicker when the throttle is hit. After all the tests and calculations are completed, the CVT clutch will be tuned to maximize efficiency and limit power loss. The ultimate goal is to supply a transmission setup that will allow the team to compete with an efficient CVT clutch setup.

Project Objective

The purpose of this project is to better understand and produce a continuously variable transmission that will allow Wright State's Baja Team to compete at their event in Wisconsin. As the Engine horsepower and torque was increased, changes to the CVT took place. The goal is to observe a baseline for the CVT and observe how it reacts in its manufactured form. After completing the testing, changes and tuning can take place.

Methodology

To complete the testing for this project a test stand had to be fabricated as one did not exist. To start, the stand was modeled in Solid Works to have a plan to follow as seen in Figure 1. Once designed, materials could then be gathered to start the fabrication process. While making the test stand, many different iterations took place to improve the setup. Rubber mounts were added to limit vibrations, an ATV master cylinder was used in place of a pedal style master cylinder to lock the brake, and a large through bolt was used to hold the rotor to prevent shearing. The brake was locked between 400-500 psi to apply load to the engine. A tachometer was used to monitor the RPMs while running the test. In order to calculate the high, mid, and low gear ratios and torque output of this CVT, measurements were taken of the primary and secondary clutch. The three measurements taken were RPMs, center of each clutch to the median thickness of the belt, and the engine horsepower supplied by the manufacturer as seen in Figure 2 .

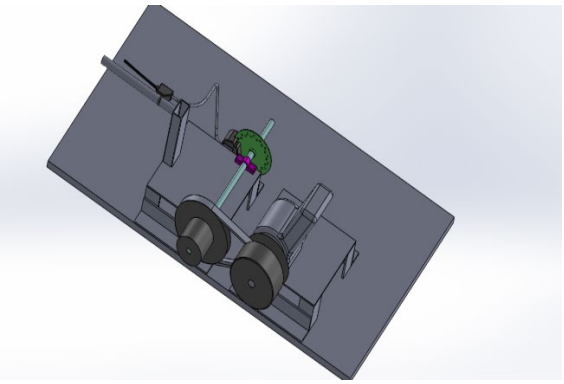

Figure 1: Final CAD rendering of test stand

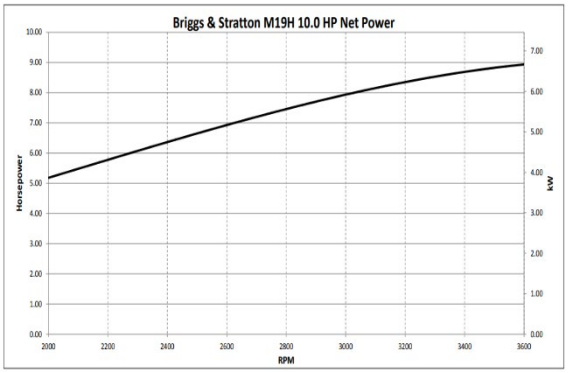

Figure 2: Horsepower per RPM for the engine

Results and Conclusions

While completing the testing, multiple points were made. Although the stock spring did not perform badly, it was observed that a higher spring force could be used. This result was made due to the engine sputtering at lower RPMs under load due to the primary sheaves not returning to fully open releasing the belt. The importance of the sheaves opening back up is to allow the engine to idle and the car not move. Another problem that can arise from this is gear grinding when going from neutral to drive due to the secondary clutch staying engaged from the sheaves not fully opening at the primary. Due to supply and financial concerns, the stronger spring did not come in time to complete its test on time. The 14hp Kohler engine did not arrive in time as well. The test will still be run for the Baja Team. But nonetheless, the project was still a success due to the amount of knowledge gained and the baseline of the CVT will allow for quick tuning in the upcoming weeks. Figure 3 shows the test stand to complete the experiment.

Figure 3: Test stand used to run the test

References

Renshaw, Jerry. *What's the difference between an automatic and a CVT transmission?.* Advanced Auto. 2018.https://shop.advanceautoparts.com/r/advice/car-technology/whats-the-difference-between-an-automatic-and-a-cvt-transmission

Briggs and Stratton Racing. https://www.briggsandstratton.com/content/dam/briggsandstratton/as/zh_cn/files/baja-sea-materials/M19%E5%87%80%E5%8A%9F%E7%8E%87%E6%9B%B2%E7%BA%BF%E5%9B%BE.pdf

DeGreenia, Timothy. The Continuously Variable Transmission: A Simulated Tuning Approach. Worcester Polytechnic Institute.file:///C:/Users/benja/Downloads/MQP_Timothy_DeGreenia_Edited_Jan19.pdf

Tetrahymena thermophila as an indicator species for climate change

Student Researcher: Tara R. Keller

Advisor: Dr. Heather Kuruvilla

Cedarville University
Molecular Biology

Abstract

Tetrahymena thermophila are free-living, nonparasitic unicellular eukaryotic organisms that are generally representative of other microorganisms. For this experiment, we were interested in measuring the change in gene expression caused by stressing *Tetrahymena*, specifically by increasing the culture temperature. In our studies, gene expression was observed by measuring mitotic rates, acetylation and methylation of histones, and mitochondrial biogenesis in response to heat shock. We used a variety of techniques to accomplish this, including cell counting via hemocytometer, immunofluorescence visualization and quantitation, and staining with MitoTracker™. *Tetrahymena*'s response to the increase in environmental temperatures could give us some insight into the effects of climate change on unicellular organisms.

Methodology Used

Cell counting was carried out using a hemocytometer after incubating cells at 22.2 and 30 degrees Celsius for 4 days. We then changed the heat stress cells incubation to 35 degrees Celsius and used this temperature for the rest of the experiment. Indirect and direct immunofluorescence was used to bind to the histones using standard 1:100 dilution of primary antibody and 1:100 dilution of secondary antibody on cells. MitoTracker™ staining was used to determine the upregulation and or downregulation of mitochondrial biogenesis in the cells. Western blotting was used to confirm that the antibodies were binding to histones. We used a standard 1:1000 dilution of primary antibody and 1:1000 dilution of secondary antibody in our Western blots.

Significance and Interpretation of Results

Cell counts were measured using a hemocytometer (Figure 1), while fluorescence was quantitated using Nikon NIS software on cells stained using an anti-acetyllysine antibody (Figure 2). Statistical significance was measured using an unpaired T-test, *p < 0.01. The results shown demonstrate that heat stress decreases cell number after four days of growth, and also reduces histone acetylation in *Tetrahymena thermophila.*

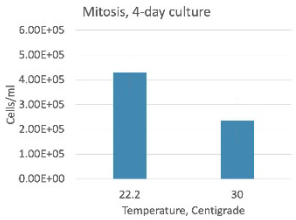

Figure 1. The effect of temperature on mitotic rates of Tetrahymena thermophila.

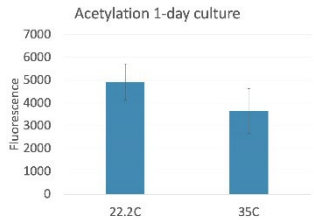

Figure 2. The effect of temperature on acetylation levels of *Tetrahymena.*

Methylation (red) was visualized using indirect immunofluorescence (Figure 3). Nuclear localization of H3K27Me1 (red) is increased in heat-stressed *Tetrahymena thermophila,* consistent with reduced gene expression demonstrated by the decreased acetylation levels shown prior. We obtained similar results when we visualized localization of H3K27Me3 in similar fashion.

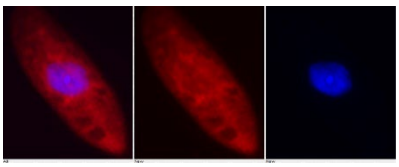

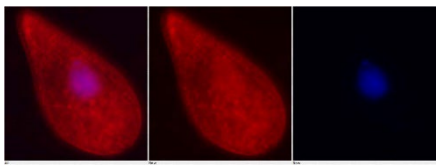

Figures 3 and 4. The blue staining indicates binding of the immunofluorescent antibody DAPI binding to DNA, allowing visualization of the organism's nucleus. The figure on the left is representative of our control group at 22°C. The figure on the right is representative of our test group at 35°C.

The observance of the abundance of antibody binding occurring outside of the nucleus was unusual to see because it was intended to bind to a nuclear protein. This led to the conduction of a Western Blot of the antibody to ensure that it was binding to the correct protein. Western blotting of whole cell extract shows that antibodies against H3K27Me1 (Figure 5) and H3K27Me3 (Figure 6) stain a doublet of proteins that occur at the expected molecular weight of 15 kD. This indicates that cytosolic staining is not simply the result of nonspecific binding by the antibodies.

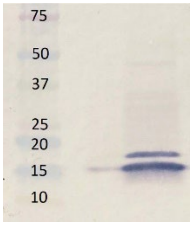

Figure 5. Western blot of H3K27Me1 compared to a standard.

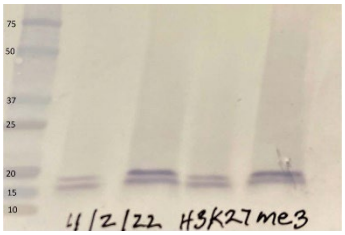

Figure 6. Several western blots of H3K27Me3 compared to a standard.

Our final results came from testing mitochondrial biogenesis. Cells grown at 15°C (Figure 7), 22°C (Figure 8), and 35°C (Figure 9) had similar levels of labeling when exposed to 100 nM MitoTracker™ for 40 minutes. This demonstrates that growth temperature did not affect mitochondrial biogenesis.

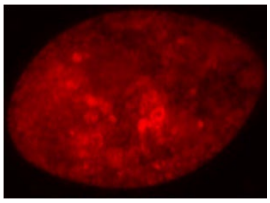

Figure 7. Mitochondria presence at 15°C.

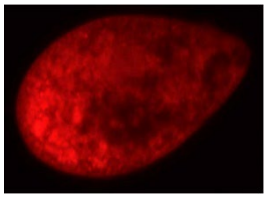

Figure 8. Mitochondria presence at 22°C.

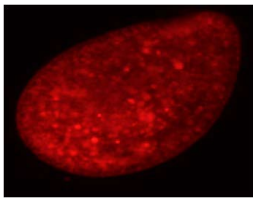

Figure 9. Mitochondria presence at 35°C.

In conclusion, heat stress reduces cell number and reduces overall histone acetylation. It was also observed that methylated histones in the cytoplasm unexpectedly occur, but our Western blot showed that the antibodies were binding to the histones at the expected molecular weight. Lastly, it was determined that growth temperature did not affect mitochondrial biogenesis. These results are helpful in broadening our understanding of the effects of climate change on microorganisms.

Acknowledgements and References

I would like to acknowledge my research partners, Haleigh Eckert, Katarina Mills, Isaac Seabra, and Taylor Strickland for their collaborative help, as well as my advisor Dr. Heather Kuruvilla for her involvement and guidance. I would like to additionally express gratitude to the Ohio Space Grant Consortium (OSCG) and Cedarville University for their generous financial support.

Tribological behavior of 3D Printed PEEK-PFA composites

Student Researcher: Anthony J. Krcik

Advisor: Mark A. Sidebottom

Miami University
[1]Department of Mechanical and Manufacturing Engineering

Abstract
In recent years, 3D printing has emerged as a powerful tool for the fabrication of complex parts and structures using a variety of materials. Polyetheretherketone (PEEK) and perfluoroalkoxy polymer (PFA) composites are among the materials that have gained considerable attention in aerospace applications due to their outstanding mechanical, thermal, and chemical properties. However, the wear and frictional properties of PFA and PEEK composites have yet to be tested. The objective of this research project is to investigate the tribological behavior of 3D printed PEEK and PFA composites, with a focus on their friction and wear properties. The main motivator for this research is the need to find alternatives to polytetrafluoroethylene (PTFE), a commonly used material in aerospace systems with low friction but limited manufacturability due to high melt viscosity.

Project Objective
This study aims to provide a better understanding of the tribological properties of PEEK and PFA composites, and their potential to be used in aerospace systems where low friction and wear resistance are critical factors.

Methodology
The materials used in this study were polyetheretherketone (PEEK) and perfluoroalkoxy (PFA) pellets. These pellets were mixed together using a single-screw extruder. After repalletizing, a filament ~2 mm in diameter was spooled for 3D printing. To develop the test samples, a fused filament fabrication (FFF) technique was used as a type of 3D printing. Four samples of materials were developed with the same ratio of 80% PEEK and 20% PFA by weight, however the fill rate of the material in the 3D printer was varied. The printer is continuously determining fill rate of the material, however we limited the fill rate to between 70% and 95% of the machines calculated fill percentage. For samples 1,2, and 4 the flow rate was kept constant whereas sample 3 was increased to 95% during the printing process to help produce more even parts.

Results Obtained
The tribometer used in this study was a four sample flat-on-flat tribometer. The applied load was a 250N load with 6.2 MPa pressure on the sample. The instrument uses load cells to measure friction and normal force, which were calibrated before the testing to ensure accurate measurements. These load cells were connected to a data acquisition (DAQ) system that recorded and processed the data in MATLAB to calculate the coefficient of friction. The tests consisted of 500,000 cycles, with each cycle consisting of two strokes of 25 mm, resulting in a total sliding distance of 25 km. The sliding velocity used during these tests was 50 mm/s and the samples were slid against polished 304 SS. Friction data was taken continuously at every cycle. Wear rate measurements were based off incremental mass measurements. The experiment was paused, samples were removed, massed, and reinstalled on the instrument. Polymer composite samples were blown with compressed air to remove any scraps that could have fallen off immediately during testing. The length of the test segments increased as the experiment continued until 25 km was reached. The results of these measurements were used to evaluate the tribological performance of the materials in wear rate calculations.

Figures/Charts

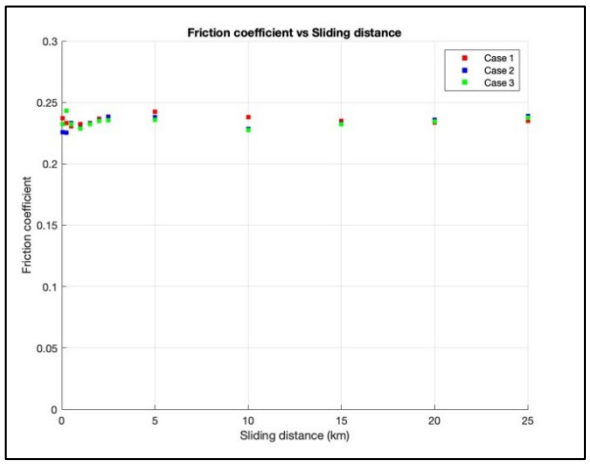

Figure 1: Friction coefficient versus sliding distance distance

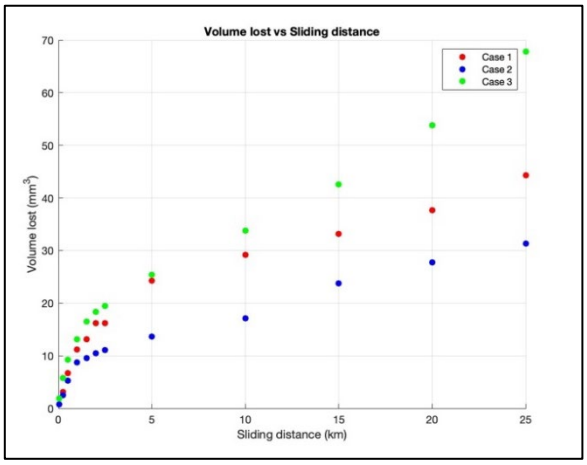

Figure 2: Volume lost as function of sliding

Table 1: 3D Printed PFA-PEEK Sample tribological results compared to unfilled PFA and unfilled PEEK

Sample	Print Fill Rate	Friction Coefficient (last 10km)	Wear Rate (last 10km) [mm^3/Nm]
PFA-PEEK (80|20) #1	80%	0.231±0.005	$4.4 \pm 0.2 \times 10^{-6}$
PFA-PEEK (80|20) #2	80%	0.234±0.005	$3.0 \pm 0.1 \times 10^{-6}$
PFA-PEEK (80|20) #3	80% ↑ to 95%	0.235±0.004	$1.0 \pm 0.3 \times 10^{-6}$
PFA-PEEK (80|20) #4	70 %	N/A	N/A
PEEK [1]	N/A	0.42	5.0×10^{-5}
PFA [2]	N/A	0.24	$6.6 \pm 0.6 \times 10^{-4}$

Significance and Interpretation of Results

Firstly, note that the fourth sample with a 70% flow rate could not withstand the loads under testing and became unstable after 0.2 km of sliding and sample 4 results were omitted from the plots. For the three remaining samples, friction coefficient stayed constant between 0.23 and 0.25 throughout testing (Figure 1), which is consistent with unfilled PFA and much lower than unfilled PEEK. Unfilled PEEK has a friction coefficient of around 0.42 [1] and unfilled PFA has a typical friction coefficient of 0.24 [2]. During the first 2 km of sliding all three samples experienced high wear rates ~ 10^{-5} mm^3/Nm (Figure 2). After 5 km of sliding, all samples held a relatively constant wear rate, with sample 3 experiencing the greatest rate of volume loss. The wear rate of all 3D printed PFA-PEEK composites shows a 100x improvement compared to unfilled PFA and about a 10x improvement over unfilled PEEK (Table 1).

References

[1] Lu, Z. P., & Friedrich, K. (1995). On sliding friction and wear of PEEK and its composites. *Wear*. https://doi.org/10.1016/0043-1648(95)90178-7

[2] Sidebottom, M. A., Pitenis, A. A., Junk, C. P., Kasprzak, D. J., Blackman, G. S., Burch, H. E., Harris, K. L., Sawyer, W. G., & Krick, B. A. (2016). Ultralow wear Perfluoroalkoxy (PFA) and alumina composites. *Wear*. https://doi.org/10.1016/j.wear.2016.06.003

Application of Pressure Sensitive Paint at the University of Dayton: Small Rotorcraft Applications

Student Researcher: Jacob Kulig

Advisor: Dr. Carson Running

University of Dayton
Department of Mechanical and Aerospace Engineering

Abstract

Traditional measurement of pressure on wind tunnel models requires individual pressure transducers or other discreet sensors. To provide advantageous data over an area or complex geometry, placing an adequate number of sensors can be cost prohibitive and physically challenging. Computational fluid dynamics (CFD) provides an alternate approach to such experiments, but often needs experimental verification. Pressure-sensitive paint (PSP) is a distinctive, appealing measurement technique for providing pressure measurements in these cases. By measuring the intensity of a specialized paint's luminescence, the pressure at almost all visible points on a test object can be found [1]. In some unsteady aerodynamic cases, the paint mixture is altered to provide faster response times, thus allowing rapidly changing phenomena to be analyzed [2]. This technique has been utilized for several decades [1]; however, it has been heretofore unused at the University of Dayton. This research provides the groundwork for the use of PSP in various applications at this university. The technique is then applied to analyze the ground effects of small rotorcraft blades [3]. This will assist in revealing the underlying characteristics of the unsteady flow that occurs between a small propeller and the ground, as may occur in unmanned arial vehicles.

Project Objectives

In this experiment, PSP is used to analyze the flow between a small rotorcraft blade and a flat plate, simulating how a small rotorcraft or drone's propulsion system may interact with the ground or other obstacle. It is expected that underlying trends and characteristics of the flow field can be uncovered with this method, increasing the ability to understand and predict how the propeller interacts with the ground or other large objects.

Methodology Used

To measure the pressure field under the rotorcraft blade, PSP formulated for unsteady flows [2] is applied to a piece of acrylic measuring approximately 0.75 by 0.75 meters. This plate is mounted four inches from a small rotorcraft propeller. Three pressure sensors are installed on this plate. The PSP is then illuminated from the opposite side with a blue laser and imaged with a high-speed camera, as shown in Figure 1. This data is then processed based on methods from [1], [2], [4], [5], and [6] to obtain pressure readings at each individual pixel and useful statistical or visual representations of this data.

Results Obtained

The Fast Fourier Transform (FFT) from one of the pressure sensors and an area of PSP near the transducer both show peaks in intensity at 162.1 Hz and 324.2 Hz. In addition, the pressure data collected by the paint and traditional sensors show a very similar oscillation, offset by a small timestep. Applying the FFT at all pixels and filtering the data spatially, a region of intense unsteady flow is seen in a ring shape midway along the radius of the prop (Figure 2). In addition, spatially filtered videos of the pressure data appear to show some swirling motions.

Significance and Interpretation of Results

The similarities between the FFT of the discreet pressure sensor and the PSP suggest the PSP is measuring the pressure field successfully. The frequency of this unsteady phenomenon matches that of the propeller, suggesting that the unsteady frequency is directly related to the propeller's speed. The global FFT also suggests that the strongest unsteady flow occurs in a ring midway from the center of the propeller, with the weakest unsteady flow near the center of the propeller. Future work should include understanding the asymmetries in the data, applying this technique to more trials, and interpreting the results in the context of small rotorcraft.

Figures/Charts

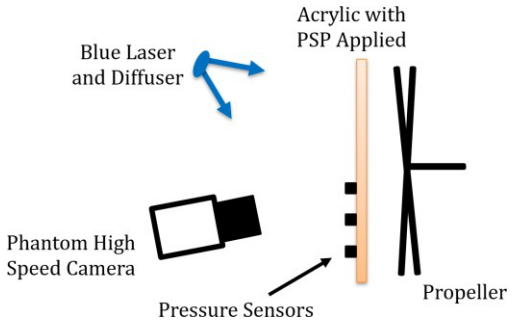

Figure 1: The PSP setup utilized in this experiment.

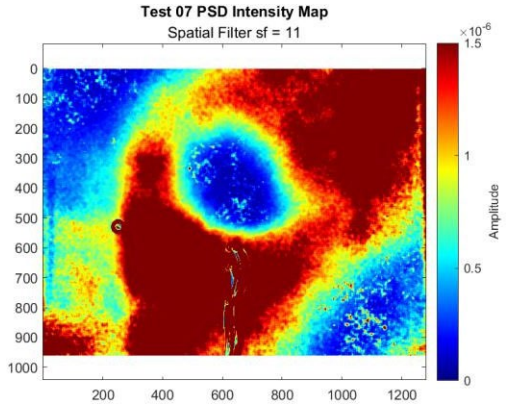

Figure 2: The intensity of the FFT signal over pressure field.

Acknowledgements and References

The author would like to thank Jacky Cai, graduate researcher at the University of Dayton, and Dr. Sidaard Gunasekaran, for providing the experimental case, setup, lab space, expertise, and advice; the Ohio Space Grant Consortium for their support; and the advisor for this research, Dr. Carson Running.

[1] Liu, T., Sullivan, J. P., Asai, K., Klein, C., and Egami, Y. *Pressure and Temperature Sensitive Paints*. Springer, Cham, 2021.

[2] Gregory, J. W., Sakaue, H., Liu, T., and Sullivan, J. P. "Fast Pressure-Sensitive Paint for Flow and Acoustic Diagnostics." *Annual Review of Fluid Mechanics*, Vol. 46, No. 1, 2014, pp. 303–330. https://doi.org/10.1146/annurev-fluid-010313-141304.

[3] Cai, J., Gunasekaran, S., and Ol, M. "Effect of Partial Ground and Partial Ceiling on Propeller Performance." *Journal of Aircraft*, 2022, pp. 1–14. https://doi.org/10.2514/1.C036974.

[4] Sakaue, H., Kakisako, T., and Ishikawa, H. "Characterization and Optimization of Polymer-Ceramic Pressure-Sensitive Paint by Controlling Polymer Content." *Sensors*, Vol. 11, No. 7, 2011, pp. 6967–6977. https://doi.org/10.3390/s110706967.

[5] Zare-Behtash, H., Lo, K. H., Yang, L., and Kontis, K. "Pressure Sensitive Paint Measurements at High Mach Numbers." *Flow Measurement and Instrumentation*, Vol. 52, 2016, pp. 10–16. https://doi.org/10.1016/j.flowmeasinst.2016.02.004.

[6] Running, C. L. "Global Measurements of Axisymmetric Hypersonic Shock-Wave/Boundary-Layer Interactions." 2020. https://doi.org/10.7274/G732D79515N.

An investigation of winglet design with limited computational cost, using an efficient optimization method and calculations.

Student Researcher: Suraju A. Lawal

Advisor: Dr. Augustus Morris

Central State University
Manufacturing Engineering

Abstract
The problem being addressed is design, analysis, multi-objective constrained optimization, construction, and experimental validation of multi-winglets. The main purpose of this project is to formulate an optimization procedure for a design that reduces computational cost while producing an optimum design. The optimization is carried out using a Response Surface Approximation with few design parameters and two objective functions. The optimum winglet will be tested at Central State University facility to compare experimental and computational results. The objective of this project includes designing and optimizing a multi-winglet configuration capable of increasing the lift-to-drag ratio by 4% with respect to the currently implemented blended winglets used.

Project Object
Winglets are vertical extensions of wingtips that improve an aircraft's fuel efficiency and cruising range. Designed as small airfoils, winglets reduce the aerodynamic drag associated with vortices that develop at the wingtips as the airplane moves through the air.

Winglets reduce wingtip vortices, the twin tornados formed by the difference between the pressure on the upper surface of an airplane's wing and that on the lower surface. High pressure on the lower surface creates a natural airflow that makes its way to the wingtip and curls upward around it. Current global environmental issues such as rising aviation fuel costs and global warming have forced airlines to adjust. In this way, manufacturers and commercial airlines will strive to minimize the environmental impact of aviation, and ideally improve the efficiency of the use of aviation fuel during flight. Airplanes are an efficient and fast means of transport and require a huge volume of fuel.

Therefore, aviation artists are increasingly paying more attention to how to reduce fuel consumption and improve flight efficiency. The key to achieving this goal is to reduce traction and increase lift. Reducing air resistance is an important aspect of improving the performance of large transport aircraft. Develop an aircraft configuration that uses less fuel.

Fuel consumption per seat mile is highly desirable. Aviation designers are working to improve the overall efficiency of aircraft, which will benefit aircraft manufacturers and airlines. One of the most difficult aspects of the aircraft design process is reducing the overall air resistance to a less acceptable level. There have been several studies of procedures to reduce the traction induced by abstraction. F.V. British scientist Lanchester invented the endoscope in the late 19th century.

The induction resistance can be reduced by using the plate technique. The fusion wing can effectively block airflow in the wing range and form a vortex. The structure of the vortex can be damaged, the induction resistance can be reduced, the air resistance can be reduced, aerodynamic efficiency can be improved, and vehicle fuel consumption can also be reduced Screens are one of the most notable fuel saving technologies in aviation. The wing, which is a small wing or a vertical projection of the knee, increases the efficiency of the aircraft by reducing the air resistance caused by the forward slope of the wing, which increases the lift-to-draft ratio (L/D).

Methodology
The process of model creation, including model creation and implementation, is called modeling. This model resembles a real system, allowing analysts to predict the effort required to fix the system. In other words, modeling is the process of creating a model that represents a system and its properties. Model design is more flexible as a wide range of software is available. Winglet was efficiently modeled and designed using Solid Edge

software. Most airplane winglets are made of **high-tech polymers**. They can be retrofitted to aircraft that were originally designed without them. Adding winglets to an aircraft extends its range.

Solid Edge is a computer aided design (CAD) computer aided engineering (CAE) and simulation software that is widely used in the modern world. Solid Edge is a solid mediator with a feature-based parametric approach. With my knowledge about the use of solid Edge software I will use my experience to design an up-to-date winglet that will be more accurate and more efficient to serve the purpose of this project.

With my experience as an aircraft Mechanic dealing with series of aircraft on daily basis, I am so interested and ready to dig deep in this project if I am given the opportunity.

Results

The data obtained will be analyzed using statistical techniques and software available in SPSS or MINITAB or MATLAB or other analysis code available in the Manufacturing Engineering Department. Data gathered from this project for different types of winglets were used to assess each winglet's efficiency which is related to L to D and how pressure is distributed over the upper surface of the wing. calculate lift and drag coefficients by using equations. However, lift and drag forces will be calculated using in-built expressions to describe force on y and x axis respectively, in which a variable wing will create that is located at pre-processing as "wing". The ratio was found using the absolute value of lift divided by drag.

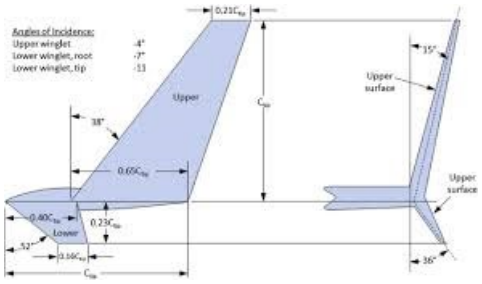

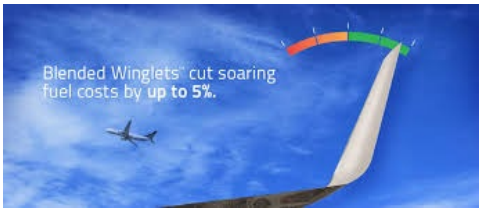

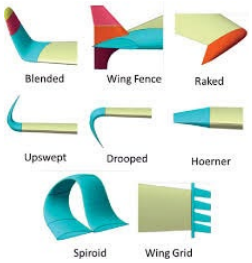

Acknowledgements and References

I would like to thank Dr. Augustus Morris for his mentorship which was invaluable during my research. I would like to thank Dr. Abayomi Ajayi-Majebi for his advice and the opportunity he gave me to validate my calculation and results at the department of Manufacturing Engineering Central State University. I would like to thank the Ohio Space Grant Consortium (OSGC) committee members for their generous contributions toward achieving my educational goals. Finally, I would like to thank my parents, and my course mate for their love and support.

1. Rominger WA, Maimon R (2020) Why does the air flow faster over the top of an air foil?. Link: https://bit.ly/3ey5cJ6
2. LeBlanc R (2020) Will Electric Airplanes Make Travel More Sustainable. Link: https://bit.ly/3euqUxA
3. Takenaka K, Hatanaka K, Yamazaki W, Nakahashi K (2008) Multidisciplinary Design Exploration for a Winglet. Journal of Aircraft 45: 1601-1611. Link: https://bit.ly/33vYxIQ
4. Toor Z, Abbas Z, Masud J (2016) Uncertainty Analysis of Various Design Parameters on Winglet Performance. 54th AIAA Aerospace Sciences Meeting. Link: https://bit.ly/2SuXmqS
5. Panagiotou P, Kaparos P, Yakinthos K (2014) Winglet design and optimization for a MALE UAV using CFD. Aerospace and science Technology.

Shape Memory Alloy Adaptive Wing Prototype Model

Student Researcher: James J. Lyons

Advisor: Dr. Nicholas Garafolo

The University of Akron
Mechanical Engineering

Abstract
This research is being conducted in support of a master's thesis project by University of Akron graduate student Ray Roos studying the development of an adaptive wing. Adaptive wings can improve aircraft performance in fuel efficiency, aerodynamic performance, and functionality, like a traditional flap system, with the added benefit of maintaining surface integrity and avoiding gaps in the wing surface. Hydraulically actuated adaptive wing systems utilize heavy and complex systems to manipulate the wing surface, which has historically added significant weight and drag to the aircraft. Shape memory alloy actuators are being explored as an alternative that is lighter, lower maintenance, and less complex than conventional hydraulic systems. SMAs exhibit mechanical memory whereby temperature manipulation results in a precisely controlled deformation to a "memorized" form that the sample has been trained to. The alloy can thus be implemented as an artificial muscle to manipulate the wing flap with integrated heating eliciting the desired articulation in the flap. A successful result offers desirable control authority of the adaptive wing with improvement in aircraft performance.

Project Objectives
The objective of this project is to develop an alternative adaptive wing technology known as a blended flap. The flap will utilize shape memory alloy actuation. This area of the project specifically focusses on the production of a physical prototype wind tunnel model to validate the results of ongoing aerodynamic simulations conducted by the graduate student. Upon completion of a successful test model and attainment of a satisfactory convergent CFD simulation, a wind tunnel test campaign will be conducted and compared to the simulated results. Following successful development of the scale model through iteration, a larger SMA blended flap will be produced and outfitted onto the Zips Aero Design Team RC plane **(Figure 1)** for flight testing to provide a practical, tangible proof of concept.

Methodology Used
Aerodynamic simulations are being computed using Ansys Fluent. The 3D model being tested is based on the wing of a past Zips Aero Design Team RC plane. To design a physical model the parameters were first selected as follows. A 24-inch model span was determined by the wind tunnel test section available at The University of Akron **(Figure 2)**. To determine the loads the model would be subject to, the wind tunnel airspeed was determined analytically. Zips Aero flight data was analyzed to find the original cruise speed of the full-scale plane. Original airspeed, atmospheric conditions, and the mean aerodynamic chord lengths of the small and full-scale wings were then input into the Reynolds number equation. A wind tunnel speed of 92 mph resulted as the design criteria of the model required to replicate the aerodynamics of the full-size wing. SolidWorks CAD was then used to develop a solid body 3D model by modifying and scaling the Zips Aero plane.
With the model designed, 3D-printing was chosen to achieve precise, strong airfoil contours. This method is significantly simple, cheaper, and faster to iterate than machining a model from metal or utilizing a composite construction. A 3-section assembly was selected due to printing volume and print orientation limits. Pins were designed to be inserted at the section joints ensure bending and torsional

rigidity. A trailing edge mounting tube was designed to interface with the wind tunnel sting mount. Upon achieving a successful solid model, it can be redesigned with vacancies for flexible flaps. To design flexible, SMA-actuated flaps, inspiration can be drawn from a past master's thesis project by Garrett McHugh, advised by Dr. Garafolo, which utilized silicone-embedded joule-heated SMA wire elements. **(McHugh)** The complete model can then be assembled and bench tested to obtain desirable actuation. At that time wind tunnel testing can begin.

Results Obtained

During the 2022-2023 research period, Ray has refined an aerodynamic simulation of the standard wing model and is currently simulating the experimental curved trailing edge and flaps. The 3D model of the wing prototype was completed **(Figure 3)** and production began. Manufacturing the model revealed many challenges of 3D-printing which resulted in numerous iterations. Print orientation, percent infill, filament selection, and slicer settings were adjusted, and the obstacles of assembly tolerance and support material removal were overcome to achieve a desirable result. Upon testing, wing chatter occurred at wind speeds well below 92 mph. The sting mount was redesigned, and a spar was added to enhance rigidity but vibration was still severe at aggressive angles of attack. The model was tested at neutral AoA and achieved the target test speed. As the objective of the project isn't to characterize the airfoil, the tests will be conducted at AoA close to 0 and the model can be used. A wing model with flap vacancies was designed, printed, and assembled. Next, a 2-piece mold was modeled, and 3D printed to cast silicone flaps from. A set of silicone flaps were successfully created and have been adhered into the model vacancies using Sil Poxy, a specialized silicone compatible epoxy.

Moving forward, The adhesion strength of the silicone flaps will be evaluated in the wind tunnel to ensure that they will remain attached during later testing. Next, joule-heated wire-wound SMA actuators will be developed with physical prototypes being prepared, evaluated, and iterated alongside simulations. The SMA elements will then be embedded within silicone flap castings which will be assembled into a wing model and bench tested. At that point, wind tunnel testing of the prototype will be performed to characterize performance and confirm simulation results. Finally, an SMA flap will be outfitted onto a Zips Aero RC plane for flight testing to provide a practical, tangible proof of concept.

Figures/Charts

Figure 1. Zips Aero RC Plane

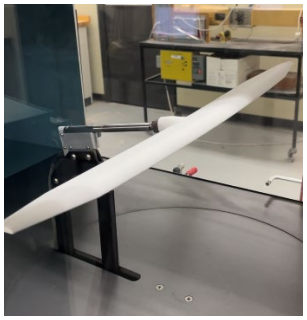

Figure 2. Wing Model in Wind Tunnel

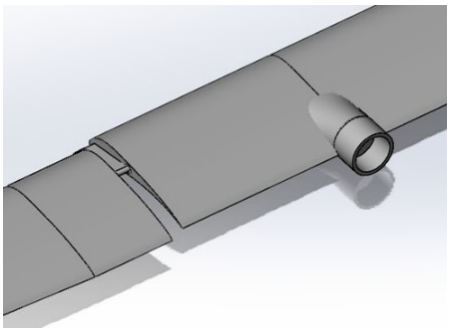

Figure 3. Prototype Wing SolidWorks Model

Acknowledgments and References

McHugh, G. R. (2016). *An Experimental Investigation in the Mitigation of Flutter Oscillation Using Shape Memory Alloys* [Master's thesis, University of Akron]. OhioLINK Electronic Theses and Dissertations Center. http://rave.ohiolink.edu/etdc/view?acc_num=akron1479119992818089

Effectiveness of Vortex Generators on Airfoil Performance

Student Researcher: Brandon M. Malahtaris

Advisor: Dr. C. Virgil Solomon

Youngstown State University
Mechanical Engineering

Abstract
Vortex generators play a critical role when a plane is in takeoff or landing by providing improved control and reduced stall speeds by organizing separated flow near the boundary layer of an airfoil. The goal of the project is to design and test a NACA 2412 used on a Cessna 172 with and without vortex generators to determine their effectiveness in flight at different velocities and angles of attack. The airfoil is scaled and designed with a 9" chord length for use with the wind tunnel available at Youngstown State University. The airfoil will be made using a vat photopolymerization 3D printer in three different pieces. Data will be gathered using pressure taps in 64 different locations around the airfoil. For collection, a 16-port data acquisition unit will be used and repeated four times to receive all values. After acquiring the data, the pressure will be plotted on a graph using Excel to examine the surface pressure distribution. XFOIL will then be used to validate the results without vortex generators. Data will be collected at 10, 15, and 30 m/s to analyze differences with and without vortex generators.

Project Objectives
The objective of this research is to examine the effectiveness of adding vortex generators to a common airfoil used in the aviation industry. The NACA 2412 airfoil was selected as it is used on a Cessna 172. Once designed, the airfoil will be placed in an open wind tunnel that will run at 10, 15, and 30 m/s. Additionally, the airfoil will be oriented with an angle of attack at 0°, 5°, and 10°. Once validated, a new airfoil with vortex generators would be tested to examine any differences between the two airfoils based on velocity and angle of attack.

Methodology Used
The airfoil was designed with a 9" chord length for use in an open wind tunnel provided by Youngstown State University. To interpret results, 64 different locations were observed using pressure taps that were heat pressed into the airfoil. A Scanivalve 16 port data acquisition unit was used to acquire readings based on each trial. Due to the airfoils data requirements, the experiment was conducted by reading 16 different locations and repeating the process four different times without disturbing the airfoils position or wind tunnels speed. Once validated using either XFOIL or CFD, a replicated wing was to be printed with the addition of vortex generators. Individual vortex generators were printed using a fused deposition modeling 3D printer and then adhered to the airfoil. Trials were to then be repeated using the airfoil with generators. Results would then be interpreted to find any differences in airfoil performance.

Results Obtained
Figure 1 shows results of the wind tunnel testing at the three different velocities described in the project objectives at an angle of attack of 5°. Figure 2 compares the experimental data to CFD results at 35 m/s at an angle of 5°. The effectiveness of the vortex generators would be determined with future testing.

Significance and Interpretation of Results

The results obtained by the experiment and CFD have a percent difference of less than 10% verifying the experimental results. The analysis of the vortex generators would be performed after airfoil assembly.

Figures/Charts

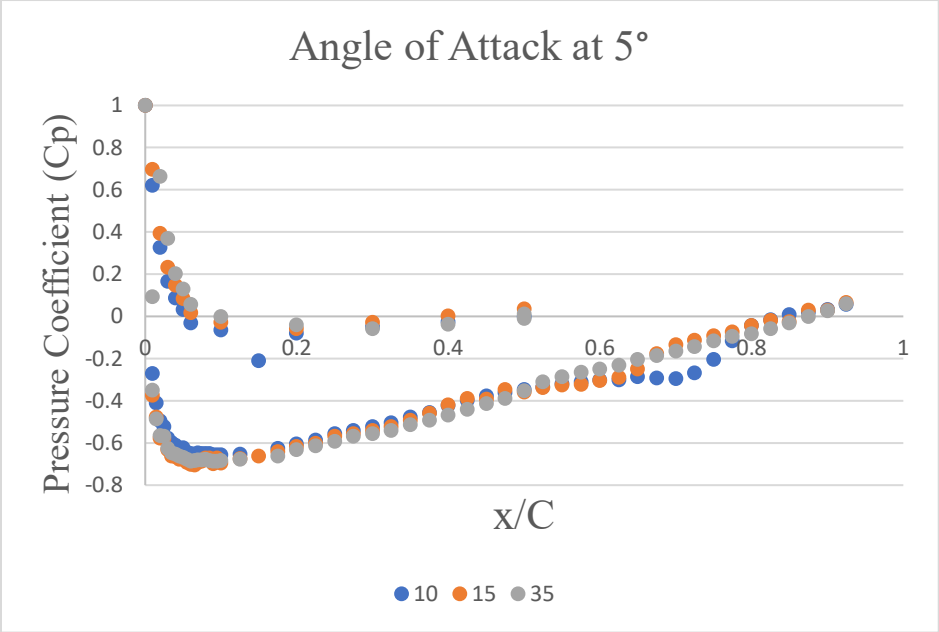

Figure 1. Wind Tunnel Testing at 10, 15, and 35 m/s at 5° Angle of Attack

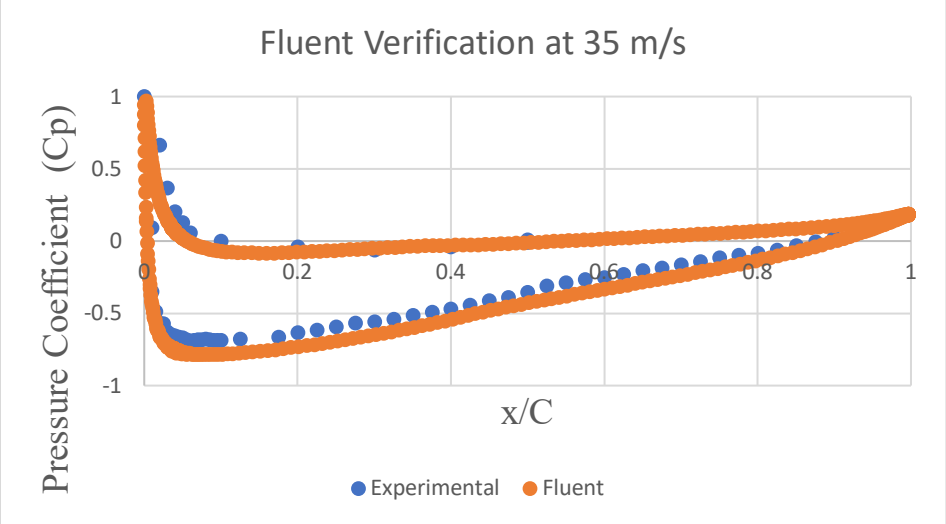

Figure 2. Comparison Between Experimental and Fluent Results at 5° Angle of Attack

Acknowledgements
Special thanks to Ohio Space Grant Consortium for providing the scholarship funding along with Sahaj Thapa and Eric Haake for providing guidance on the project.

Roux-en-Y Gastric Bypass Surgery Does Not Increase Preference for Low Concentrations of Ethanol in Cafeteria Diet-Fed Female Rats: How is Ghrelin Involved?

Student Researcher: Jacob G. Mansell

Advisor: Clare Mathes Ph.D.

Baldwin Wallace University
Department of Neuroscience

Abstract

Even though women are more prone to obesity than men and 80% of patients receiving bariatric surgery are female, most studies feature only male model organisms. Here we sought to characterize the impact of cafeteria diet-feeding followed by Roux-en-Y gastric bypass (RYGB) surgery on metabolic profiles and alcohol preference profiles of female rats. At weaning, female rats were provided either with chow only (n=12) or with chow and access to high-fat + high-sugar supplements (a "cafeteria diet"; n=24). By 20 weeks of age, the cafeteria diet induced weight gain and altered blood glucose responsivity to exogenous glucose. RYGB surgery (n=8) decreased body weight and fasting glucose levels of cafeteria diet-fed rats and blunted their responsivity to a glucose challenge compared to their sham-operated sisters (SHAM, n=11). The operated rats as well as unoperated female rats fed chow only (n=8) were then given ad libitum access to ethanol (2-8%) alongside water; intakes were measured across multiple days and preference calculated. The ethanol preference of female RYGB rats did not differ from that of SHAM female rats, which contrasts with previous results in male rats and reports from one lab in female rats. We sought to understand these contradictory results by assessing them against serum levels of acylated ghrelin, a "hunger" hormone that is positively correlated with desire for alcohol.

Project Objectives

The overarching study addresses a female rat model's physiological, behavioral, and neurohormonal changes induced by Roux-en-Y gastric bypass (RYGB) surgery. This weight loss surgery is currently the most effective therapy employed to treat obesity and its associated complications (e.g., 3). However, in contrast to its benefits, the RYGB procedure can increase alcohol consumption (e.g., 1,10). The majority (80.7%) of people who undergo this procedure are women (e.g., 11). However, most of the mechanistic research on this topic uses male model organisms, and so know little about how the surgery may impact female-specific physiology. Studies assessing alcohol intake after RYGB surgery with male rats replicate the human condition (i.e., after RYGB surgery, rats drink more alcohol; 2,4), but only one group has examined this in female rats and found similar increases (8,9). Therefore, here we sought to expand understanding in a female rat model by using a surgical procedure very similar to that used on humans and a clinically relevant obesigenic diet. Why individuals – male or female – who receive RYGB surgery are more likely to develop alcohol use disorder is not currently understood. One contributor may be the hormone ghrelin, which is produced by the stomach when it is empty and signals "hunger" when it travels through the blood to the brain. In humans, intravenous administration of ghrelin increased craving for alcohol intake (6). In male rats, ghrelin increases after RYGB and may facilitate the increased preference for alcohol seen following RYGB surgery (4). Thus, in the third part of the project, I hypothesize that a) we will see higher ghrelin levels in female rats given RYGB than in female sham-operated rats, and b) ghrelin levels will positively correlate with the alcohol preference displayed by the female rats.

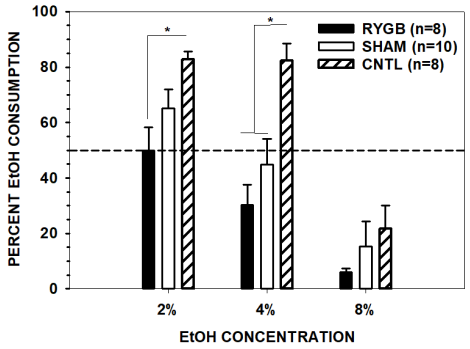

Figure 1. M +/- SE Percent ethanol preference (ethanol intake divided by total intake) calculated from the average of the last 3 days of access of female rats fed chow only (CNTL) or fed a cafeteria diet and on which RYGB surgery or SHAM surgery had been performed. Primary and follow-up ANOVA and t-tests revealed that CNTL rats preferred 2% and 4% ethanol more than either RYGB or SHAM rats.

Methodology Used & Results Obtained

The first project of our study series aimed to assess if 14 weeks of high-fat and high-sugar diet-feeding (starting at weaning) would induce obesity and metabolic disturbances, and if RYGB could correct this physiological profile. To note, a high-fat and high-sugar diet is commonly called a "cafeteria diet" and is meant to model the "western diet," which includes large amounts of "junk food" or "empty" calories in addition to a less palatable but full-nutrition diet. In the second part of the study series, we hypothesized that cafeteria diet-fed female rats given RYGB would show a higher preference for low concentrations of alcohol when offered ad libitum alongside water than cafeteria diet-fed female rats on which a sham operation had been performed, which is what has been seen in male (e.g., 3,4) and female (8,9) rats. We also included in this assessment a group of chow-fed control rats on which no surgery had been performed to assess the role of diet in ethanol preference as obesity may have protective effects against ethanol overconsumption (e.g., 5).

Our cafeteria diet regimen successfully induced weight gain and exacerbated responsivity to an injected glucose challenge. We conducted RYGB and sham surgeries (as per 7) on the cafeteria diet-fed female rats and found, as expected, that RYGB in these rats decreased body weight (a difference on average of 33 g) and restored glucose metabolism. We then found that the preference of female rats given RYGB (n=8) did not differ from that of female rats given sham surgery, but that maintenance diet strongly influenced ethanol preference as unoperated rats fed chow only preferred ethanol to a much higher degree than cafeteria diet-fed rats given either operation (Figure 1).

We then euthanized the cafeteria diet-fed female rats on which RYGB and sham surgeries had been performed and took blood via cardiac puncture. The blood was mixed with an anticoagulant and centrifuged, and the serum retained, mixed with a protease inhibitor, and stored at -80°C. We conducted an acylated ghrelin using an enzyme-linked immunoassay. We were able to construct a standard curve using the kit-provided standards however, our plasma samples contained too high of ghrelin levels and thus we were unable to interpolate a concentration.

Significance and Interpretation of Results

These data suggest that alcohol preference may not change after RYGB surgery in a female rat model as previously reported in male and female rats.

Acknowledgements and References

Alyssa Palumbo and Devon Stewart co-led these projects, and we were aided by Gregg DiNuoscio, Lily Gabriel, Sarah Kettleberger, Sydney Klingshirn, Melanie Mavroidis, Dave Revta, and Kristen Sperber. Funding for this study was provided in part by the Baldwin Wallace Faculty Development Committee (CMM), the Summer Scholars Program (AP & CMM), and the Ohio Space Grant Consortium (JM).

1. Briegleb, M., & Hanak, C. (2020). Gastric Bypass and Alcohol Use: A Literature Review. *Psychiatria Danubina*, *32*(Suppl 1), 176–179.
2. Davis, J. F., Tracy, A. L., Schurdak, J. D., Magrisso, I. J., Grayson, B. E., Seeley, R. J., & Benoit, S. C. (2013). Roux en Y Gastric Bypass Increases Ethanol Intake in the Rat. *Obesity Surgery*, *23*(7), 920–930.
3. Fisher, B. L., & Schauer, P. (2002). Medical and Surgical Options in the Treatment of Severe Obesity. *The American Journal of Surgery*, *184*(6), S9–S16.
4. Hajnal, A., Zharikov, A., Polston, J. E., Fields, M. R., Tomasko, J., Rogers, A. M., Volkow, N. D., & Thanos, P. K. (2012). Alcohol Reward Is Increased after Roux-en-Y Gastric Bypass in Dietary Obese Rats with Differential Effects following Ghrelin Antagonism. *PLoS ONE*, *7*(11), e49121.
5. Kleiner, K.D., Gold, M.S., Frost-Pineda, K., Lenz-Brunsman, B., Perri, M.G., & Jacobs, W.S. (2004). Body Mass Index and Alcohol Use. *Journal of Addictive Diseases*, 23(3), 105–118.
6. Leggio, L., Zywiak, W. H., Fricchione, S. R., Edwards, S. M., de la Monte, S. M., Swift, R. M., & Kenna, G. A. (2014). Intravenous Ghrelin Administration Increases Alcohol Craving in Alcohol-Dependent Heavy Drinkers: A Preliminary Investigation. *Biological Psychiatry*, *76*(9), 734–741.
7. Mathes, C. M., Letourneau, C., Blonde, G. D., le Roux, C. W., & Spector, A. C. (2016). Roux-en-Y Gastric Bypass in Rats Progressively Decreases the Proportion of Fat Calories Selected from a Palatable Cafeteria Diet. *American Journal of Physiology. Regulatory, Integrative and Comparative Physiology*, *310*(10), R952-959.
8. Orellana, E. R., Nyland, J. E., Horvath, N., & Hajnal, A. (2021). Vagotomy Increases Alcohol Intake in Female Rats in Diet Dependent Manner: Implications for Increased Alcohol Use Disorder After Roux-en-Y Gastric Bypass Surgery. *Physiology & Behavior*, *235*, 113309.
9. Orellana, E. R., Piscura, M. K., Horvath, N., & Hajnal, A. (2021). Differential Response in Ethanol Behaviors of Female Rats Given Various Weight Loss Surgeries. *Alcohol and Alcoholism*, *56*(5), 599–604.
10. Suzuki, J., Haimovici, F., & Chang, G. (2012). Alcohol Use Disorders After Bariatric Surgery. *Obesity Surgery*, *22*(2), 201–207.
11. Young, M. T., Phelan, M. J., & Nguyen, N. T. (2016). A Decade Analysis of Trends and Outcomes of Male vs Female Patients Who Underwent Bariatric Surgery. *Journal of the American College of Surgeons*, *222*(3), 226–231.

Testing Spaceflight Hardware (*C. elegans and D. melanogaster)*

Student Researcher: Anthony J. Marino

Advisor: Nathaniel Szewczyk

Ohio University
Biological Sciences

Abstract
Two different types of spaceflight hardware developed commercially will be used to understand the biological effects of various microgravity environments on the model organisms *C. elegans* and *D. melanogaster*. The first experiment is titled CBIOMES and will study how microgravity affects the microbiome of only *C. elegans*. The second experiment is titled iGCE and will study the genetic and molecular responses to altered gravity in both *C. elegans* and *D. melanogaster.* My involvement with these experiments is to test the hardware on the ground to ensure that data can be collected before it is used on the ISS. Unfortunately, the experiments have stalled selecting a candidate to create the hardware. While waiting, I studied and photographed flight *C. elegans* with mitochondrial GFP to better understand how they may respond to other microgravity environments.

Project Overview
My objective would be to ensure that data can be collected in a controlled environment on the ground. Due to the experiments staling I had to improvise; I have been studying *C. elegans* from previous flights that have been exposed to low gravity for extended periods of time. This will provide us with a better idea of what to do expect when we start running tests.

Methodology Used
A sample of frozen flight *C. elegans* was thawed out in 1ml of paraformaldehyde which helps preserve the worms. The worms are then pipetted into four eppendorf tubes and are placed into a centrifuge for 30-90 seconds. This forces all the worms to the bottom of the tube as they are denser. The worms are then pipetted onto a small slide with a coverslip placed on top. A Zeiss microscope with a camera is then used to study the mitochondria of the worms. The worms have a green mitochondrial GFP so that the mitochondria structure can be easily studied and assessed.

Results
The images show that the mitochondrial structure is significantly deteriorated. A healthy mitochondria would look like a system of connecting webs with no breaks in the shape of a rhombus. However, the flight worms have mitochondria with many breaks, lack of structure, and have collapsed in on themselves in some areas. This indicates that altered gravity environments do affect the health of *C. elegans* mitochondria.

Significance and Interpretation
The results from the imaging indicate that there will be some kind of affect when the actual experiments are conducted. This gives me a better idea of what to expect from those tests. This is not new information, it has been known that muscle health and even mitochondrial health are affected from altered gravity but this confirms it and provided me with some experience on the matter.

Figures

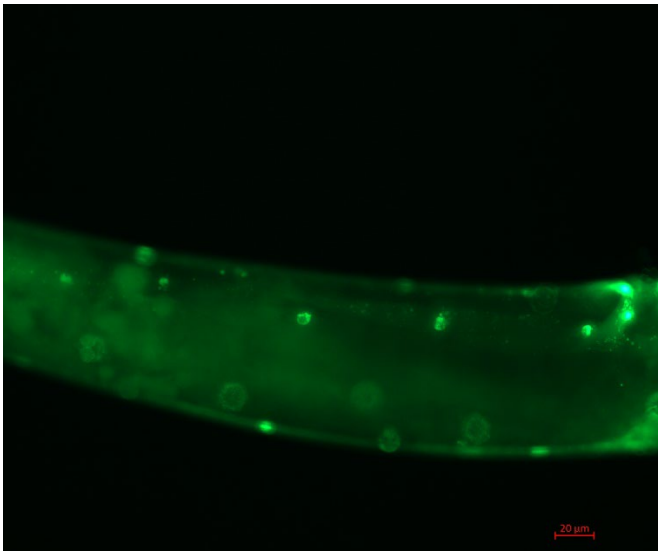

Figure 1. Example of healthy worm – the rhombus shaped mitochondria can be seen in the top right of the worm.

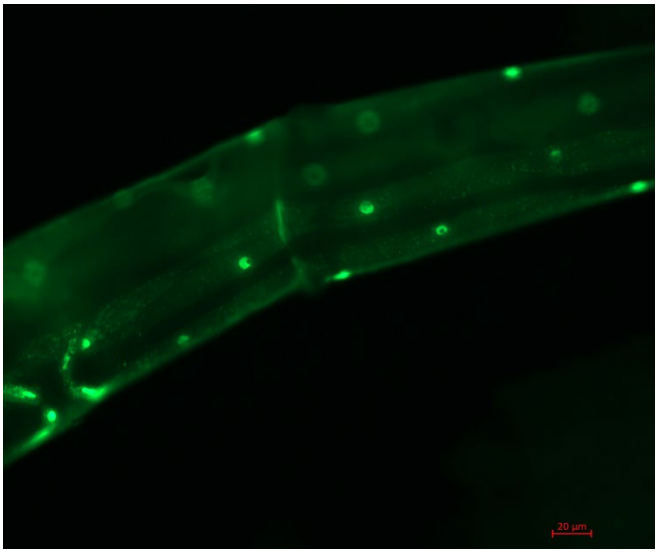

Figure 2. Example of unhealthy worm

Recovery System for a High Powered Rocket

Student Researcher: Laurin E. Meisberger

Advisor: Dr. Thomas Ward

Cedarville University
Mechanical Engineering

Abstract
In this project, I will overview the process of a high powered rocketry recovery system. I acted as recovery system lead for Cedarville University's NASA Student Launch Initiative team. Through this project I fully researched, designed, manufactured, and installed a recovery system that was adequate for our flight vehicle, Operation Trailblazer.

Project Objective
The overall goal of this project was to design a recovery system that will adequately and safety result in a successful launch and recovery of Trailblazer. In achieving this overall goal, I am to adhere to the NASA Student Launch requirements of a recovery system along with ensuring the reusability of the entirety of the flight vehicle.

Methodology Used
To begin my research, I compared the successes and results from last year's team and based on that I chose to design a dual bay recovery system. The components used in the recovery system include: bulkheads, U-bolts, quick links, shock cords, altimeters (with redundancy), shear pins, and black powder.

Results Obtained
To test my system, I utilized finite element analysis to analyze the strength of the bulkheads, this is shown in Figure 2. Part of the NASA Student Launch project is to design and launch both a sub-scale and full-scale high powered rocket. After testing Trailblazer in flight, one of the altimeters recorded the flight profile graph shown in Figure 3.

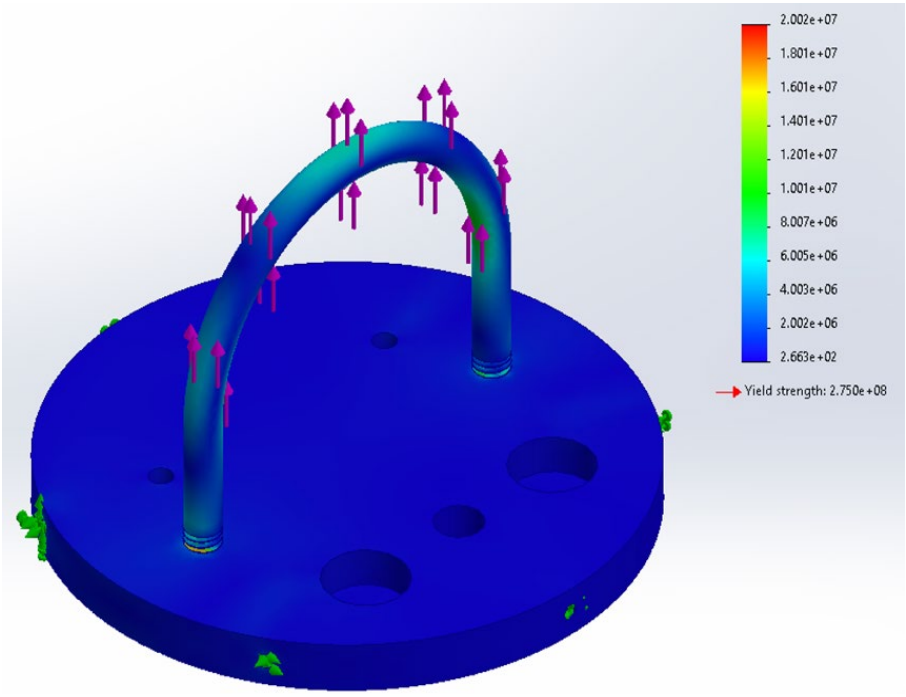

Figure 2. FEA results displaying von Mises stresses.

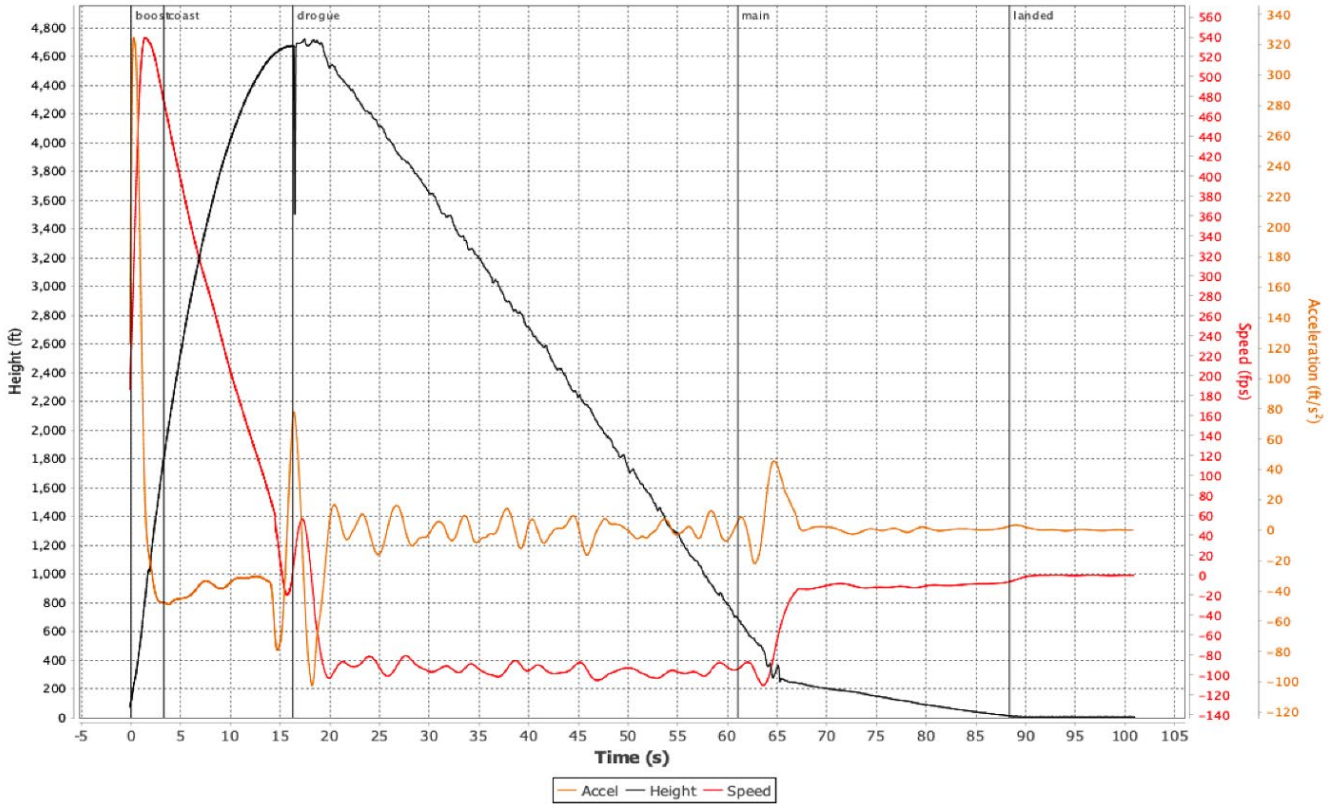

Figure 3. Flight profile graph recorded from on-board altimeter.

Significance and Interpretation of Results

After performing FEA on the bulkhead, I received confidence that the bulkheads would withstand the greatest in-flight force of the main parachute inflating. This force was calculated to be 275 N. As shown in Figure 2, the maximum von Mises stress that would be endured is 2.002e7 N/m^2. When using this value and the yield stress, I received a safety factor of 13.74 which is well within our design specifications. To analyze the success of the recovery system, Figure 3 should be viewed. From the flight profile graph, it can be observed that both the main and drogue parachutes deployed. The drogue parachute deployed at an apogee of 4,723 feet and the main parachute at 700 feet. The apogee recorded was very close to the predicted apogee of 4,730 feet. The main parachute was programmed to deploy at 700 feet and worked as it was programmed to.

Acknowledgements and References

I would like to thank OSGC for this opportunity to research and learn about rocketry, my advisor, Dr. Ward for supporting me throughout my project, and Cedarville Student Launch's team mentor, Dave Combs for being present at all launches and providing any rocketry advice when needed.

Analysis of Fuel Combustion

Student Researcher: Brooke N. Meyer

Advisor: Dr. Jed E. Marquart

Ohio Northern University
Department of Mechanical Engineering

Abstract
The goal of this research is to perform an analysis of fuel combustion. The fuels that will be analyzed are Jet A, Jet A-1, and SAF (Sustainable Aviation Fuel). Sustainable Aviation Fuel is also sometimes referred to as biofuel. Early biofuels used crops such as corn and soybeans but are now being produced using other, non-food sources such as cooking oil or grass. By analyzing the combustion of these fuels through balancing chemical equations and other processes that look at the fuel input and carbon dioxide output, a conclusion regarding the energy produced from various jet fuels and the future of them can be determined.

Project Objectives
The overall objective of this research is to analyze fuel combustion by looking at three types of jet fuels that can be used in airbreathing engines. Those fuels are Jet A, Jet A-1, and a SAF known as C1 GEVO ATJ (Alcohol-to-Jet). The fuel combustion of each of these will be analyzed and compared to each other in terms of fuel input, energy output from combustion, and carbon dioxide output.

Methodology Used
An analysis of fuel combustion of the fuels Jet A, Jet A-1, and SAF was performed. The analysis consisted of balancing the chemical equations of combustion for each of the fuels. An assumption was made that the products would only contain carbon dioxide, water, and nitrogen. From the balanced equations, the results showed the output of carbon dioxide of each of the three fuel sources when 1 kmol of fuel was combusted. Additionally, using the lower heating value of each of the fuels, an analysis of energy output was performed. This analysis used the molar weight of each fuel to obtain a value for the energy output of 1 kmol of fuel. The carbon dioxide output was analyzed similarly, comparing energy output to carbon dioxide output. The lower heating value (also known as net calorific value) of a fuel is defined as the amount of heat released by combusting a specified quantity (initially at 25°C) and returning the temperature of the combustion products to 150°C.

Results Obtained
Upon balancing each fuels' chemical equations, the resulting carbon dioxide output for each fuel is shown in table 1. Table 1 also shows the Lower Heating Values (LHV) for each of the three fuels [1]. Figure 1 shows the energy output obtained from the LHV. When using the LHV and molar weight for each fuel to obtain an energy output, ratios for the energy output to carbon dioxide output and carbon dioxide output to fuel input are shown in Figure 2 and Figure 3 respectively.

Significance and Interpretation of Results

As suspected [2], the results indicate that the C-1 GEVO (SAF) fuel is the most environmentally friendly in terms of overall CO2 emissions when compared to the energy output from fuel combustion. Additionally, the C-1 GEVO fuel had the lowest ratio of CO2 output to fuel input, meaning it produced the least number of emissions from a constant fuel input amount. Some possible future investigations include a more accurate fuel analysis with different products of combustion and looking at carbon monoxide output.

Figures/Charts

Table 1: Required Information & Results Obtained

Fuel	Chemical Formula	Molar Weight (kg/kmol)	LHV(MJ/kg)	Balanced Equation	CO2 Output (kmol)
Jet A-1	$C_{10.8}H_{21.6}$	151.9	43.2	$C_{10.8}H_{21.6} + 16.2(O_2 + 3.76N_2) \rightarrow 10.8CO_2 + 10.8H_2O + 60.912N_2$	10.8
Jet A	$C_{11.4}H_{21.7}$	158.6	43.1	$C_{11.4}H_{21.7} + 16.825(O_2 + 3.76N_2) \rightarrow 11.4CO_2 + 10.85H_2O + 63.262N_2$	11.4
C1 GEVO	$C_{12.5}H_{27.1}$	178	43.9	$C_{12.5}H_{27.1} + 19.275(O_2 + 3.76N_2) \rightarrow 12.5CO_2 + 13.55H_2O + 72.474N_2$	12.5

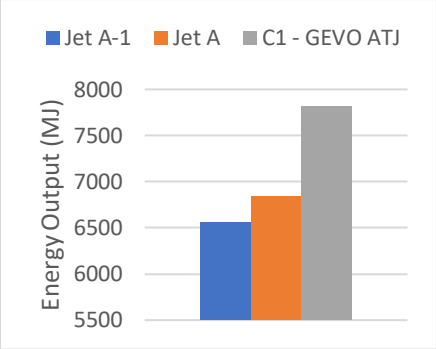

Figure 1: Energy Output from LHV

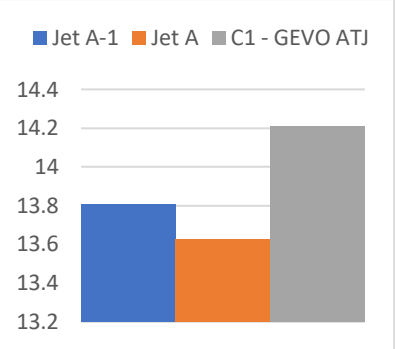

Figure 2: Ratio of Energy to CO2

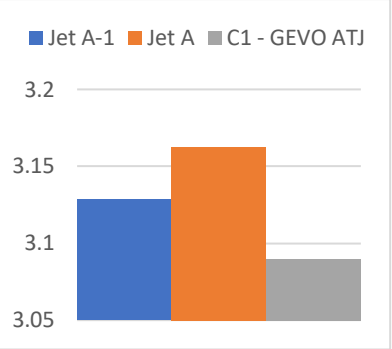

Figure 3: Ratio of CO2 Output to Fuel Input

Acknowledgments and References

I would like to thank OSGC for this scholarship. I would also like to thank Dr. Jed Marquart and the department of Mechanical Engineering at Ohio Northern University for providing me with many opportunities to learn and make my education possible.

[1] R. X. Hai Wang, “HyChem model,” HyChem Model. [Online]. Available: https://web.stanford.edu/group/haiwanglab/HyChem/pages/Home.html. [Accessed: 17-Apr-2023].

[2] “CO2 emissions,” Carbon Offset Guide, 22-May-2020. [Online]. Available: https://www.offsetguide.org/understanding-carbon-offsets/air-travel-climate/climate-impacts-from-aviation/co2-emissions/. [Accessed: 17-Apr-2023].

An Investigation of the Mechanics of an Ultra-Stretchable, Self-Healing, DLP 3D-Printed Hydrogel for Damage-Resistant Soft Robots

Student Researcher: Joshua Michonski

Advisor: Dr. Robert Lowe

University of Dayton
Department of Mechanical and Aerospace Engineering

Abstract

Inspired by nature, *soft robots* composed of compliant ("soft") materials are well-suited for uncertain, dynamic tasks requiring safe interaction between a robot and its environment.[1] Vat photopolymerization (VP) additive manufacturing (AM) processes such as digital light processing (DLP) have disrupted traditional manufacturing of soft devices, enabling the fabrication of soft robotic components with unprecedented speed, resolution, and complexity. Concurrently, the rapid development of novel *self-healing photo-curable soft materials* for VP-based AM has paved the way for soft robots with embedded healing of damage (e.g., perforations, tears) induced, for instance, by an unintended interaction with a sharp object in their operating environment. At present, however, the mechanical behavior (deformation and fracture) of self-healing photo-curable soft materials (elastomers and hydrogels) used for next-generation soft robots is not well understood. To address this compelling research opportunity, this work focuses on the design and execution of a mechanical testing program to characterize BeckOHflex, a novel self-healing photo-curable hydrogel synthesized using off-the-shelf chemicals. The large-strain elasticity of BeckOHflex is investigated through quasi-static uniaxial tension testing. Both virgin and self-healed mechanical properties are shown to be commensurate or superior to the best-performing self-healing hydrogels in the literature. Further, a suite of demonstration prints produced on a commercial VP 3D printer highlight the material's scalability and the ability to produce geometries with complex form factors.

Project Objectives

The scope of this research is to complete an experimental testing program for the mechanical characterization and functional demonstration of a novel self-healing photocurable elastomer called BeckOHflex.

Rapidly self-healing ultra-stretchable photo-curable elastomers, such as BeckOHflex, provide a uniquely aligned opportunity for soft robotics applications. The large and fully recoverable deformations of these materials allow soft robots to have a wide range of functions and use cases. However, in order to obtain optimized designs, rich mechanical data sets are required. Detailed mechanical testing creates these data sets which inform the design, control, and optimization of next-generation soft robots. Furthermore, to better understand the functional value of such a material, manufacturing methods and proof-of-concept models are investigated. The printability of the material are explored on a DLP 3D printer, and design capabilities were demonstrated in a simplified soft-robotics experiment.

Methodology Used

The BeckOHflex resin was synthesized using commercially available, off-the-shelf (COTS) acrylate-thiol-based hydrogel chemistry. ASTM D412 type C dogbone specimens were prepared for the mechanical characterization of the material. Fresh resin was prepared for all samples, and they were always cured within 24 hours in ambient conditions. Cast samples were cured using an Ecoflex (Smooth-On) silicone mold and a CF2000 UV LED source (365 nm) at 25% intensity for 4 minutes. Printed samples were cured using a 3D Systems Figure 4 Modular DLP printer that was "unlocked" by 3D Systems for use with experimental photopolymers. After curing, samples were stored in a UV-protected desiccator below 15% relative humidity. This was a particularly important element because BeckOHflex is a hydrogel that swells in the presence of water, and the ambient humidity varied greatly. After seven days, the fully cured specimens underwent quasi-static tensile testing on an Instron 3365 extended-height load frame with a long-travel clip-on extensometer. Self-healed samples were cut with a razor along the midpoint of the gauge section, left separated for 5 minutes to reduce residual stresses, and then realigned by hand. After resting for an additional 5 minutes, the specimens underwent tensile testing until fracture on the Instron 3365.

As the testing program unfolded, the original Ecoflex silicone mold presented difficulties with specimen extraction and ultimately fractured. As a result, a new mold was formed from PDMS silicone using the same ASTM D412 type C mold shape. The new mold both reduced specimen deformation during removal and proved to be compatible with

all material formulations. A new curing method that used a staggered application of 25% intensity UV light (10 s interval) with periods of no light (60 s interval) significantly improved specimen repeatability with alternative formulations. These formulation variations were used in control studies that analyzed the impact of specific components on material properties.

Results and Discussion

In terms of pristine mechanical properties, BeckOHflex appears to be a leading candidate in the field. The tensile strain at fracture is 458 ± 8 %, the ultimate tensile stress is 2.96 ± 0.13 MPa, and the toughness is 5.76 ± 0.43 MJ/m^3. The material is somewhat unique in that it does not require external stimuli (e.g., heat, light) to activate the self-healing mechanism — making it in a sense *autonomous*. Compared to other intrinsically self-healing photocurable elastomers, BeckOHflex exhibits the most rapid rate of healing per UTS reported in the literature, and with nearly instantaneous self-healing. Gomez et al. produced a material with a significantly higher elongation at tensile fracture, but the synthesis of the material was more complex like many other non-COTS chemistries.[2]

To validate the mechanics of BeckOHflex, a series of quasi-static uniaxial tension tests to quantify self-healing properties were conducted with varying amounts of dye, water, and thiol — as seen in **Figure 1**. The tensile strain at fracture for the virgin, water, and dye samples only varied in the range of 225-266% (and 0.67-0.79 MPa for the UTS), validating that both the dye and its water substitute do not meaningfully impact the mechanical properties or self-healing mechanism. However, in the third study, the non-thiol sample had a strain at fracture of only 46% and an UTS of 1.40 MPa, showing a much stiffer modulus and becoming much less tacky. This corroborates the crucial role thiol plays in the self-healing behavior. Based on the control studies, hydrogen bonding can conclusively be designated as the dominant self-healing mechanism.

To investigate its design capacity, the printability of BeckOHflex was explored on a commercially available 3D Systems Figure 4 printer in ambient conditions — and the prints were successful. The relatively low viscosity of the resin allowed for rapid resin refresh during layer-by-layer curing and increased print speeds. A rook, “Benchy” the boat, and an accordion-style soft robotic actuator with fully formed internal cavities were successfully 3D printed — with green food dye used to prevent over-penetration due to light scattering in the resin. Moreover, three soft robotic actuators were attached to a pneumatic triple gripper as seen in **Figure 2**, coated in Teflon to prevent adhesion, and then successfully lifted a 165 g beaker — demonstrating the functionality of the resin for soft-robot applications.

Figures/Charts

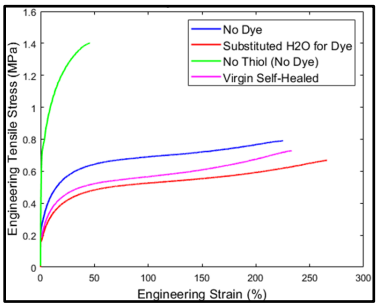

Figure 1. Instantaneous self-healing control gripper studies for aqueous and thiol-based formulations.

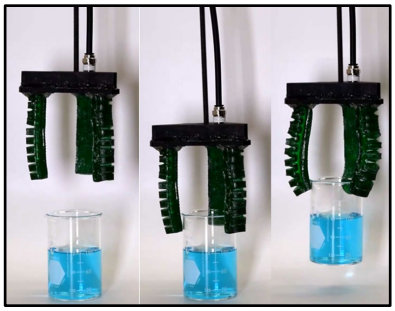

Figure 2. Pneumatic soft robotic triple demonstration with 165 g beaker.

Acknowledgments and References

I would like to thank the Ohio Space Grant Consortium, the University of Dayton School of Engineering, the Air Force Research Laboratory, the University of Dayton Research Institute, the Behavior of Advanced Materials and Structures (BAMS) Lab, and UES Inc. for supporting this research. Particular thanks to Dr. Robert Lowe, Dr. Chris Crouse, and Joseph Beckett for their support and guidance.

1. S. Terryn, J. Brancart, D. Lefeber, G. Van Assche, and B. Vanderborght. Self-healing soft pneumatic robots. *Sci Robot*. **2**(9), 2017.
2. E. Gomez et al. 3D-printed self-healing elastomers for modular soft robotics. *ACS Appl. Mater. Inter*. **13**(24), 28870-28877, 2021.

Development of a Paradigm of Software and Systems Engineering Processes for Aerospace Engineering

Student Researcher: Emmanuel Nshimiyimana

Advisor: Dr. Deok Nam

Wilberforce University
Electrical Engineering

Abstract

Development of a paradigm of software and systems engineering processes in engineering. The project presents a paradigm of software and systems engineering processes. The first plan of the system is started by assessing formal current software engineering practices. An action planis designed and developed for multi-functional working groups, which were tasked to define andfacilitate the implementation of software processes.[1] A second plan is initiated with the objective of designing and defining a system engineering process and integrating into the systems engineering process the software engineering process already in use. Finally, the project discusses how the developed protype can be interacted by the current industry systems engineering including various system design to understand what the phrase "Systems Design" means in the twenty-first century, aerospace system design with the significance and current development of systems engineering, the foundational elements of the aerospace engineering of the entire system, and the common problems and how the aerospace engineering can be related to system engineering in the present-day business environment.[3]

Project Objectives

The purpose of developing a paradigm of software and systems engineering processes in engineering is to provide a systematic approach for designing, developing, and maintaining complex software and systems. The development of a paradigm provides a framework for understanding the relationships among these activities and their roles in the development process. This can help to ensure that software and systems are developed in a consistent and repeatable manner, leading to higher quality products, improved productivity, and reduced development time and cost. [2] The development of a paradigm of software and systems engineering processes is a key step towards achieving effective and efficient software and systems development, which is essential for meeting the growing demands of modern society.[1]

Methodology Used

There are several methods that can be used to develop a paradigm of software and systems engineering processes in engineering. Some of these methods include:

An Analysis of existing software and systems engineering processes: This involves analyzing existing software and systems engineering processes to identify their strengths and weaknesses. This can help identify areas for improvement and develop a better understanding of the underlying principles and practices. [4] Surveys and interviews: Surveys and interviews can be used to gather information from software and systems engineers, developers, and other stakeholders. This can provide insights into the challenges and opportunities associated with software and systems engineering processes and can help to identify areas for improvement.[4]

Results Obtained

The result of developing a paradigm of software and systems engineering processes for aerospace engineering is a comprehensive and structured approach to the design, development, testing, and maintenance of software and systems in the aerospace domain. This approach ensures that software and systems meet the necessary requirements, standards, and regulations for safe and reliable operation in a complex and high-risk environment. The development of a paradigm of software and systems engineering processes for aerospace engineering is critical to ensure safe, reliable, and efficient operation of software and systems in the aerospace domain. By following a structured and comprehensive approach, stakeholders can develop, test, and maintain software and systems that meet the necessary requirements, standards, and regulations for aerospace engineering. [3]

Significance and Interpretation of Results

The significance and interpretation of the results of developing a paradigm of software and systems engineering processes for aerospace engineering are that it provides a structured and comprehensive approach to the design, development, testing, and maintenance of software and systems in the aerospace domain. [1] This approach will improve safety, reliability, and efficiency, reduce development time and cost, ensure compliance with industry standards and regulations, and facilitate continuous improvement. [2]

Figure 1. paradigm Engineering

Table 1. system Engineering requirements

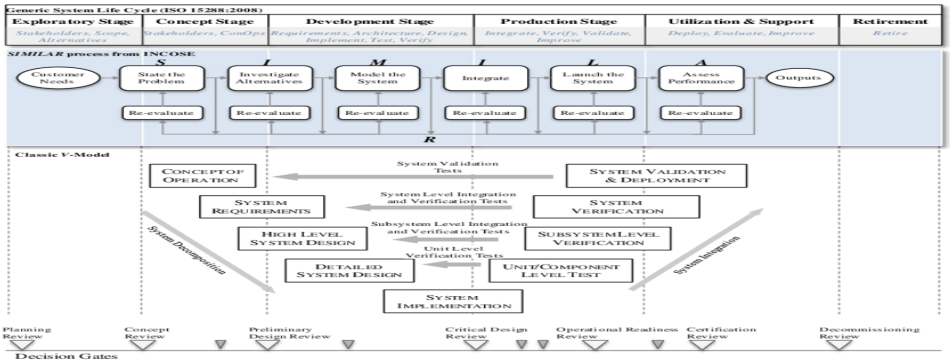

Acknowledgments

[1] "8 Software Development Methodologies Explained." *Easy Agile*, https://www.easyagile.com/blog/software-development-methodologies/.Accessed 24 April 2023.

[2] "Systems Engineering Plan (SEP)." *AcqNotes*, 3 January 2023, https://acqnotes.com/acqnote/acquisitions/systems-engineering-plan. Accessed 24 April 2023.

[3] Nielsen, Paul. "Blog - Systems Engineering and Software Engineering: Collaboratingfor the Smart Systems of the Future." *SEI Blog*, 20 September 2021, https://insights.sei.cmu.edu/blog/systems-engineering-and-software-engineering- collaborating-for-the-smart-systems-of-the-future/. Accessed 24 April 2023.

[4] Brooks, Frederick. "Software paradigm and Software Development Life Cycle (SDLC)." *GeeksforGeeks*, 23 February 2023, https://www.geeksforgeeks.org/software-paradigm-and-software-development-life -cycle-sdlc/. Accessed 24 April 2023.

Electrochemical Detection of Multiple Heavy Metal Ions Using a Metal Organic Framework and Biohybrid Nanocomposite Modified Electrodes

Student Researcher: Kyle A. Preusser

Advisor: Byung-Wook Park

Youngstown State University
Department of Civil/Environmental & Chemical Engineering

Abstract

Heavy metal pollution has become a worldwide problem. Particularly, lead ions (Pb^{2+}) have received growing concerns due to their increased discharge and deleterious effects on the environment as well as human health. Cadmium ions (Cd^{2+}) may cause renal dysfunction and metabolism disorders. Copper ions (Cu^{2+}) is an essential element of biological processes. However, higher concentrations of Cu^{2+} may lead to cancer and genetic disorders. Mercury ions (Hg^{2+}) can interfere with the nervous, immune, and endocrine systems. In this study, a novel biohybrid nanocomposite was fabricated through a simple one-pot hybridization method, and the square wave anodic stripping voltammetry (SWASV) was used as the electrochemical technique for the detection of lead ions. In this study, the developed electrodes using the metal organic framework and cellulose nanocrystals (MOF-CNC) proved to be an effective material to detect leads ions at levels down to sub-ppm in aqueous solutions. Various electrochemical tests such as cyclic voltammetry (CV) and electrochemical impedance spectroscopy (EIS) were performed to characterize the fully modified electrode to compare it with bare glassy carbon electrodes (GCE). The experimental parameters were optimized for detection such as accumulation time and potential range. Research was done to determine the optimal pH of 5 for detection. Selectivity and reproducibility tests indicated an excellent anti interference ability of the electrode to other interfering ions. Individual and simultaneous calibration tests determine linear relationships between the concentration and peak current detected. Real samples such as Mahoning River and tap water were evaluated. The real samples were spiked to determine the electrode's ability to detect ions in them. The MOF-CNC/PEDOT:PSS/GCE electrodes offer portable and efficient methods of safely detecting heavy metals in aqueous media.

Project Objective

In this research project, glassy carbon electrodes (GCEs) were modified with poly(3,4-ethylenedioxythiophene):poly(styrenesulfonate) (PEDOT:PSS), cellulous nanocrystals (CNCs), and metal organic frameworks (MOFs), specifically DUT-67, in order to create a sensitive and selective electrode to determine the presence of certain analytes in aqueous media.[1] PEDOT:PSS is a conductive polymer containing unique properties, such as flexibility, high conductivity, and good water processability.[2] These properties are useful in sensitive detection of multiple heavy metal ions. CNCs are useful for creating conductive pathways between the MOFs and PEDOT:PSS as well as increasing the surface area of the electrode and stabilizing the MOFs to the layer.[2] The MOFs themselves are used to entrap heavy metal ions attracted during accumulation onto the modified electrode due to their porosity and chemical tunability. Recently, the only issue with using them for electrochemical detection has been their poor conductivity, which is solved through the equimolar use of CNC and PEDOT:PSS to create a complete electrochemical sensor.3

Methodology Used/Results Obtained

A simple solution of 800 µL of ethanol, 100 µL of PEDOT:PSS, and 100 µL of CNC was mixed together. This was followed by 1 mg of MOF powder. The mixture was ultrasonicated for 30 seconds. 10 µL of the solution was drop casted onto the surface of a glassy carbon electrode. The solution was left to dry on the electrode for 1 hour to allow for any ethanol to evaporate to leave only the modification layer on the surface of the electrode. The fully modified electrode was used as the working electrode in a model 3-electrode system along with a platinum wire counter electrode and Ag/AgCl as the reference electrode. A Gamry Instrument potentiostat was used for electrochemical measurements in a pH 5 acetate buffer solution.

Figures/Charts

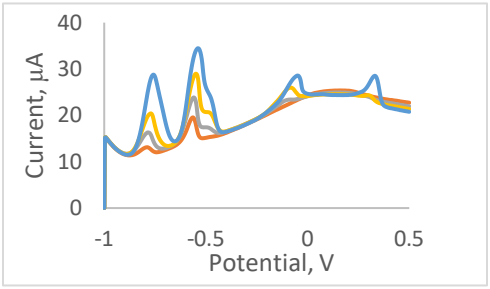

Figure 1. SWASV response of the GCE/PEDOT:PSS/CNC-MOF modified electrode for simultaneous detectio Pb^{2+}, Cu^{2+}, and Hg^{2+} over a small concentration range of 1.3 to 4 µM in an acetate buffer solution.

As shown, the stripping peak currents of the four different heavy metals increased when the concentrations of the ions were increased. The peak potential locations were found to be -0.8 V for Cd^{2+}, -0.6 V for Pb^{2+}, -0.1 V for Cu^{2+}, and 0.35 V for Hg^{2+}. The resulting peak calibration points exhibit a good linear relationship between the concentrations and current peaks. The linear regression for cadmium, lead, copper, and mercury ions were found to be R^2=0.9919, 0.9966, 0.9988, and 0.9881 respectively. The linear detection for lead ions, the ion most favored by the modified electrode, was found to be 5.96 nM.

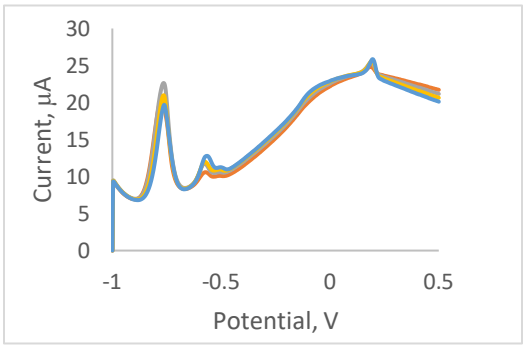

Figure 2. SWASV response of the bare GCE electrode for simultaneous detection of Cd^{2+}, Pb^{2+}, Cu^{2+}, and Hg^{2+} over a small concentration range of 1.3 to 4 µM in an acetate buffer solution.

The current peaks were found to decrease dramatically using a bare GCE. The weak peak observed between Pb^{2+} and Cu^{2+} may be caused by the formation of Pb-Cu intermetallic compounds during deposition. The use of fully modified electrodes increases the current of each heavy metal ion as well as creating sharper peaks.

Significance and Interpretation of Results

The results indicate that the use of the modification layer produces promising improvements to the detection of heavy metal ions in aqueous media. The limit of detection is also low enough for general use in both the detection of lead in drinking water and ground water farming applications, as the maximum allowed concentration of lead in drinking water is 15 µg/L. The maximum allowed lead ion concentration in farmland is around 80 mg/L. With a current LOD of 5.96 nM, both detections are possible with this sensor.

References

1. Geisse et al., Removal of lead ions from water using thiophene-functionalized metal–organic frameworks, *Chem. Commun.*, 2020, 56, 237-240.
2. Yang et al., Recent progress on PEDOT:PSS based polymer blends and composites for flexible electronics and thermoelectric devices, *Mater. Chem. Front.*, 2020,4, 3130-3152.
3. Wang et al., Metal-organic framework and conducting polymer based electrochemical sensor for high performance cadmium ions detection, *J. Mater. Chem. A*, 2017, 5, 8385-8393.

Dynamic Lunar Radiator Design and Optimization

Student Researcher: Jeremy M. Price

Advisor: Dr. Rydge Mulford

University of Dayton
Department of Mechanical Engineering

Abstract

Dynamic radiators are integral thermal control systems for spacecraft that emit excess heat from the craft, keeping internal systems operational. It is important that radiators are dynamic in systems in whichheat output and input can fluctuate widely. A competent dynamic radiator would have the following characteristics, a high turn-down ratio, ease of deployment, ability of scaling, and lightweight. To meetthese goals, a radiator design was pursued that mimics the shape and movement of the square twist origami tessellation. A Python script that uses Monte Carlo Ray Tracing was created to analyze the thermal behavior of an ideal rigidly foldable (RF) and non-rigidly foldable (NRF) versions of the square twist. CAD models of thicker versions of each design were then created, with kinematics identical to theflat model, and FEA was conducted to compare results with the ideal model. It was found that a turn down ratio of at least 4.5 is achievable with the RF model, which actuates with one degree of freedom, and it is expected that the NRF model will have even greater results.

Methodology

A Python script was created to evaluate the heat transfer properties of an ideal square twist shape using Monte-Carlo ray tracing. The Python model only included one complete tessellation of the square twist,or a quarter of what you would find on a folded paper version and has no thickness. To determine the effectiveness of a more realistic design, two square twist designs were created using CAD software. Thefirst was a non-rigidly foldable version of the square twist with thick panels. (Figure 1) The second was arigidly foldable version that was made using the offset panel technique. (Figure 2) [1] The radiative properties of these models were then analyzed in Ansys to characterize the designs. (Figure 3) After initial testing both models were modified to improve the turndown ratio of each and retested. Models of different sizes were 3D printed as well. (Figure 4)

Results and Significance

At this point, we have only done the initial round of testing, mainly focusing on the rigidly foldable design since it is mechanically sound. The non-rigidly foldable design has many mechanical interferences currently, so we have been focusing on fixing those before radiative analysis. However, the rigidly foldable design underwent two stages of testing so far, the first test was with all surfaces of all panels setto radiative with an emissivity of 0.9. Then we selected certain surfaces to be set to an emissivity of 0.1, both because in a real model some of these surfaces likely wouldn't realistically have an emissivity of 0.9and to improve the turndown ratio. Just in that one iteration we were able to increase the turndown ratio from 1.67 to 4.41. A plot of the results from the second iteration are shown in Figure 5. Further testing needs to be done, with confidence that we can continue to increase the performance of the

radiators. The curve for the emitted radiation compared to the angle of articulation is also interesting, with an exponential drop that is not seen very often in the literature. The non-rigidly foldable model isexpected to have even more desirable heat transfer properties, but its mechanical issues will make it difficult to implement a prototype.

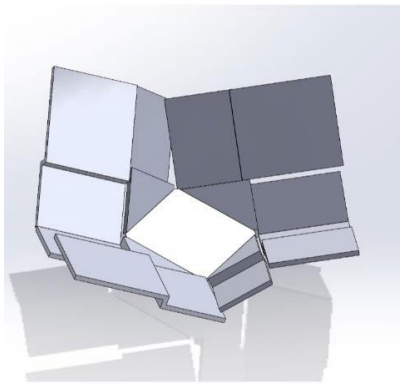

Figure 1. CAD Model of NRF Radiator

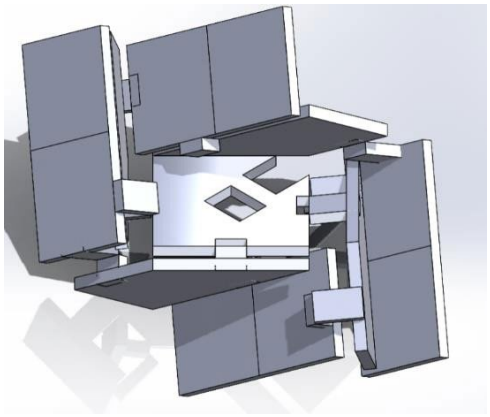

Figure 2. CAD Model of RF Radiator

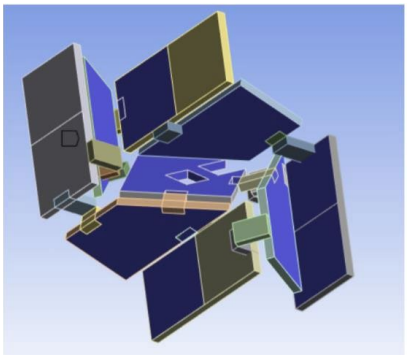

Figure 3. Ansys analysis showing selected emissivity of 0.1

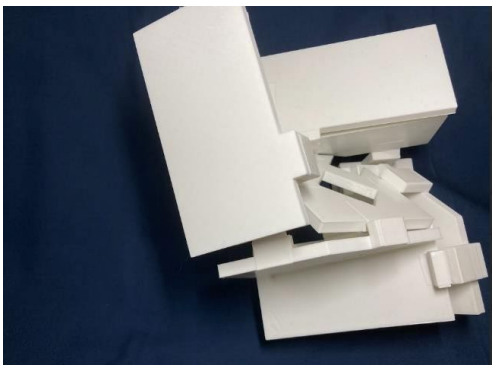

Figure 4. 3D printed model of RF Radiator

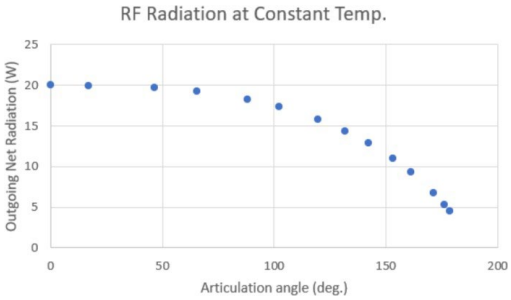

Figure 5. Rigidly Foldable Model, turndown ratio = 4.4

References

[1] Morgan, M. R., Lang, R. J., Magleby, S. P., & Howell, L. L. (2016). Towards developingproduct applications of thick origami using the offset panel technique. *Mechanical Sciences*, *7*(1), 69–77. https://doi.org/10.5194/ms-7-69-2016

Microscopic Dynamics and Rheology of Ionomers: A Molecular Simulation Study

Student Researcher: Ezra J. Ramlo

Advisor: Dr. Fardin Khabaz

University of Akron, Main Campus
Polymer Science

Abstract
Ionomers are polymers in which ionized groups create ionic crosslinks in the intermolecular structure. They are composed of both neutral and ionized repeat units covalently bonded to the polymer backbone as pendant group moieties. The primary effects of ionic functionalization of a polymer are to increase the glass transition temperature, melt viscosity, and characteristic relaxation times. Coarse-grained MD simulations will be used to connect their molecular structure to their macroscopic rheology. In this work, we will create ionomer structures with different architectures and study the network formation at different degrees of electrostatic interactions.

Project Objective
The objective of this project is to determine the effects of ionic percent in an ionomer of a certain length using computer simulations and predetermined constants.

Methodology Used
The process starts by determining the characteristics of the ionomer chain. For this simulation, a polymer chain of a number of single units (monomers), an attraction force, and the percent ionization that will be tested. The ionization percent shows the percentage of monomers that carry a non-neutral charge. For this experiment, a polymer chain of 40, an ε of 0.01, and ionizations of 0, 10, 25, and 40% were used. Each ion will be equally spaced with 25,000 total monomers used in the system.
The first simulation in the process is with set moles, temperature, and pressure while changing volume from the rectangular prism to a square over a set period to allow the chains to reach steady state. Next a simulation is run with set moles, temperature, and volume while changing pressure over a set period to allow time for the chains to reach steady state. These simulations will show how the chains moved over the full course. Calculations are then run to analyze the effects of the simulation. The first is to find the mean square displacement, then to find the radii in between ions.

Results Obtained
For the MSD, results of this can be seen in **Figure 1**. At the beginning of the simulations, each bridge, or ionization percent, tends to be spaced out in order of the ionization. As the simulation progresses, bridge 45 begins to exponentially increase past bridge 20 and approaches bridge 10. This indicates that early on there is not much movement in the bridge 45 system, but as they move throughout the experiment, the ions begin to have a stronger effect as the ions attraction and repulsion forces grow stronger. The graph does cut off before steady state can be reached, indicating that a longer test needs to be run.

For the RDF analysis seen in **Figures 2-4** we can see a spike at lower radii for each pair of ions, but the spike is especially strong for the ion pair of 1 and 2, or positive and negative. That is because this pair has a very strong affinity due to the opposing charges, so we see the highest density at around 1, meaning this is most likely the most stable radii. This spike does decrease as the bridge increases due to less flexibility in the chain in between each ion as there are less monomers in between each ion. This forces the opposing ions to be more spread out. This spike is also much smaller for ions of the same charge, as there is little attraction force in between these monomers.

Figures/Charts

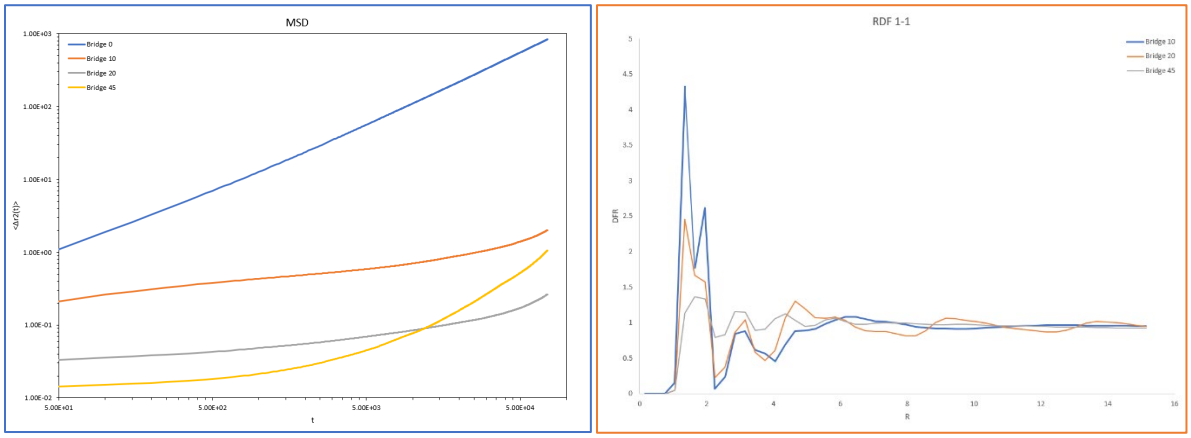

Figure 1. The average change in position of all ionomer chains over the course of the simulation. "Bridge" Represents the ionization percent (ex. "Bridge 10" applies to an ionization of 10%)

Figure 2. The particle density versus radius between positive charges only

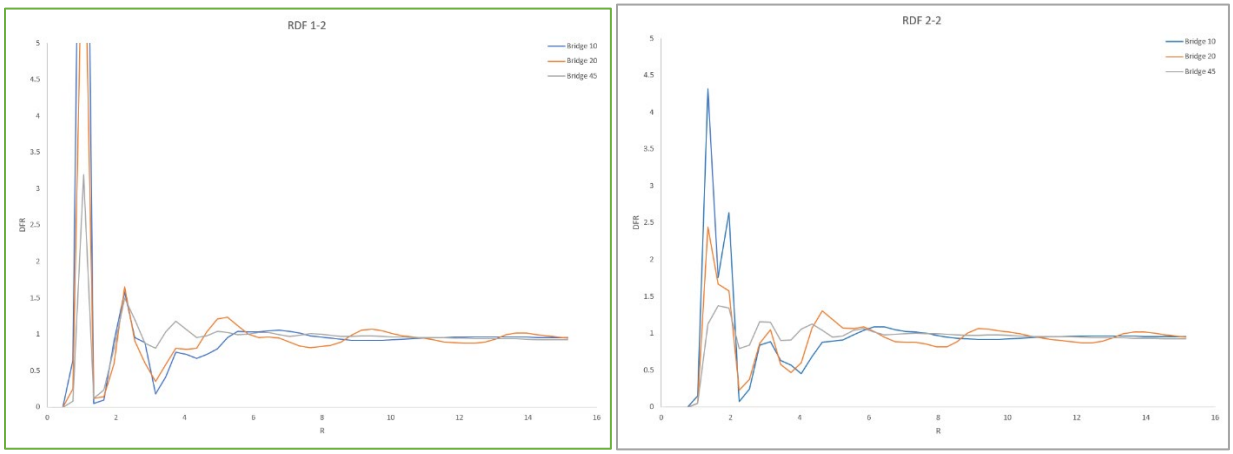

Figure 3. The particle density versus radius between positive and negative charges.

Figure 4. The particle density versus radius between negative charges only.

Acknowledgements and References

[1] Lisa M. Hall, Mark J. Stevens, and Amalie L. Frischknecht
Macromolecules 2012 45 (19), 8097-8108
[2] Janani Sampath, Lisa M. Hall; Impact of ionic aggregate structure on ionomer mechanical properties from coarse-grained molecular dynamics simulations. *J. Chem. Phys.* 7 October 2017; 147 (13): 134901. https://doi.org/10.1063/1.4985904

Thank you Dr. Khabaz and Nazanin Sadeghi for all your help throughout this project. I have learned a lot and gained so much valuable information and experience.

Rimeco CNC Lathe Automation and Industry 4.0 Project

Student Researcher: Nicholas V. Ribic

Advisor: Dr. Andrew Gyekenyesi

Cleveland State University
Department of Mechanical Engineering

Abstract
Industry 4.0 is the idea of adding new technologies, analytics and machine learning into manufacturing facilities. The basic principle of this is collecting data from machines and using that information to improve the manufacturing process. This can be as simple as using sensors to collect data and then manually using that data to increase production and quality or it can be as complex as a robot running a machine and collecting the data and the robot making adjustments based on the data. Industry 4.0 goes hand in hand with automation as automation can be used to collect the data from the machines in the best way possible with minimal human interaction and be used to increase the overall production. Automation will also decrease the number of errors in the industry 4.0 process as there is lower human interaction. Overall, Industry 4.0 and automation are both tools that manufacturing companies can use to increase production, increase quality, and lower waste.

Project Objectives
The project's objective was to do initial research into automation products such as such as sensors, probes and robotics and to then look into ways how to implement them into Rimeco Products' turning department. The second objective of this research industry 4.0 and look for ways Rimeco Products could implement industry 4.0 onto their shop floor while connecting industry 4.0 into the automation implemented in the turning department.

Methodology Used
Research was completed on many automation products that could be used for Rimeco's CNC lathes. One product that was later purchased was a probe that can be placed in the lathe as tool and will measure the part on each run and based on the reading it obtains it will make an automatic offset on the dimension that was not at mean. This probe will also alarm the machine out after making a certain number of offsets on the same tool alerting the operator that the tool needs to be changed. This probe does not fully automate the machine, but it will significantly lower human interaction with each piece and lower the chance of operator error. A Rimeco Lathe tool database was also created which slightly automated the programming process of each job as this database had every in-house tool that is used and significantly lowered programming time as the programmer no longer has to search Mastercam's tool database for the right tool and then modify that tool to what Rimeco has in-house. In terms of industry 4.0 the probe is a good example of industry 4.0 as it collects data from the machine and uses it to make changes to the machine while also presenting it to the operator. Lastly, we researched a torque wrench that you can implement a max torque to ensure that when changing tool, the tool is tightened with same force every time. This may seem like a small tool to implement but it will significantly lower error as there will be less variance between tool life and therefore make the data the machine obtains about tool life more reliable.

Results Obtained
We are still waiting for the probes to arrive, but we implemented the tool database into our everyday programming process and have seen a decrease in programming time. One surprise that occurred was

that the estimated cycle time has been more accurate since creating the tool database. This has led to more accurate schedules being created and an overall increase in production. We believe this occurred because the tool being programmed with are now the exact same tools being used in the machine and not a base Mastercam tool that was changed to be similar to our tools. We also have implemented a few of the torque wrenches that have a max torque and have seen increased tool life as operators can no longer over tighten new tools leading to shorter life. We hope this will lead to more accurate data being collected from the machine when the probes arrive, and we can fully implement industry 4.0 in our lathes by collecting data from the machines using the probes. This will be important because for industry 4.0 to work as its full potential the data from the machines need to be consistent and have minimal variance. Overall, I believe with just these few changes Rimeco has seen an increase in their production as they have met their production goal four weeks in a row and are actually considering increasing their weekly production goal. I believe this is just step one for Rimeco as they work towards fully automating their machine shop and integrating industry 4.0 through the whole shop not just in the turning department.

Figure

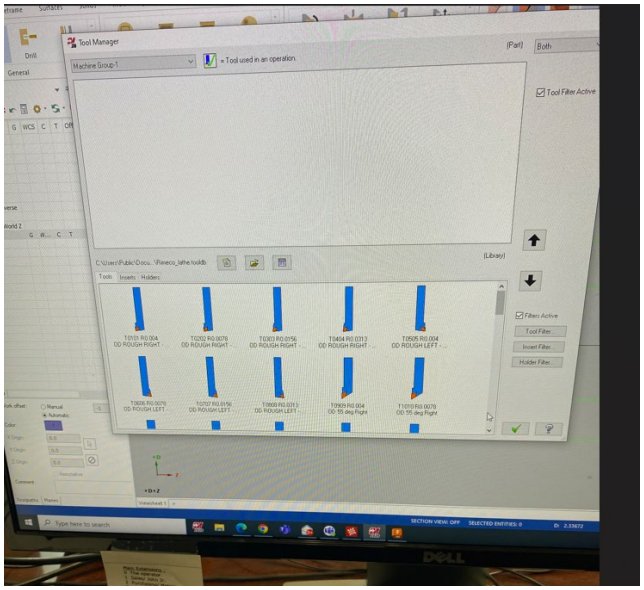

Fig.1- Picture of Partial Rimeco Tool Database

Acknowledgements and Refences

I would like to thank the Ohio Space Grant Consortium and my advisor Dr. Andrew Gyekenyesi as this work would not be possible without their support.

1. IBM. “What Is Industry 4.0?” *Www.ibm.com*, 2022, www.ibm.com/topics/industry-4-0.
2. “Probing.” *Www.haascnc.com*, www.haascnc.com/productivity/probe-system.html.
3. TWI. “What Is Industry 4.0? - the Fourth Industrial Revolution.” *Twi-Global.com*, 2022, www.twi-global.com/what-we-do/research-and-technology/technologies/industry-4-0.

Comparative Studies of Satellite Communication Protocols for Mars Sensor Networks

Student Researcher: Patrick M. Rukundo

Advisor: Deok H. Nam, Ph. D.

Wilberforce University
Department of Electrical Engineering

Abstract

The terraforming of Mars is a hypothetical procedure that consists of a planetary engineering project by transforming Mars from a planet hostile to terrestrial life to one that can sustainably host humans and other lifeforms free of protection or mediation. The Mars environment poses some challenges for communication that can make terrestrial solutions ineffective. Although it is unsuitable for direct replication, it is valuable to study successful terrestrial approaches, evaluate their ability to support the harsh Mars environments and assess how procedures and algorithms can be adapted for efficient Mars communication. In this project, often-used Medium Access Control (MAC) protocols are reviewed, and discussed the challenges of the classifications and performance assessments of MAC protocols for satellite communications, which are faced in the Mars environment

Project Objectives

Communication protocols for mas sensor networks have become life-changing for a decade [15]. People now do everything with wireless connectivity because it makes life easy to communicate with each other, connect quicker, and share the news. We live in a digital electronic most thing is wireless, even the house door, microwave, or coffee maker. Communication became one of the best wireless technologies we used the most. After NASA proves that Mars may have life, earthy people may start thinking about leaving there. If the official statement shows up and people decide to go for Mars, we may need to connect with our loved ones. As NASA wants to give people new green the best way, we find that it will connect Mars and Earth using wireless sensor networks. The best way is to start designing space to communicate with Mars people before people begin to travel there [2]. This work proposed to keep sending the satellite to test Mars, and we continue to examine our future communications to other promised green planets [2]. This project will improve the equipment and more interest in New Planets, and we will be getting more data from the test.

Methodology Used

Since the communication satellite became one of the best constructs and expensive architecture of billions of U.S dollars for one space. The best revolution we can think of is to reduce the price to make it less expensive, so that we can send more designs to our lovely space, and we will be growing the solution of sending more satellites. One of the solutions by Ferre, “the need for more coverage of the IoT networks and the search for cheaper solutions, nanosatellites may be the best answer for the global connectivity that the IoT demands. The nanosatellite standard, the CubeSat with a volume of less than one liter and a weight of less than one kilogram, also offers access to space and satellite development for countries that previously had no experience in space sciences. Nevertheless, the performance of such a solution will depend on the low-level protocols selected for the network architecture”.

Results Obtained

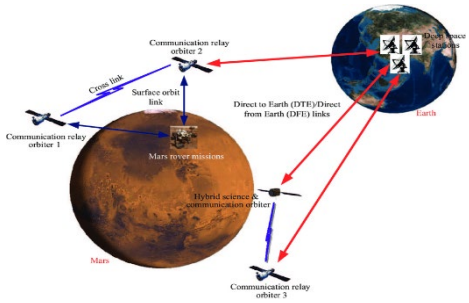

Figure 1. Communication Satellite Architecture

Table 1. Comparison of the Methods along with Distinguished categories

	Category	Strengths	Weaknesses
Protocol of How the satellite communication works	Real-Time Networking (RTN)	Handles diverse types of data about voice, video, and multimedia, designed to handle a range of network topologies	May not be suitable for extensive delays and intermittent connectivity
Consultative Committee for Space Data Systems	Real-Time Networking (RTN)	Low latency communication, a packet-based protocol for efficient and reliable data transmission	May not be suitable for long delays and intermittent connectivity
Internet Protocol	Delay-Tolerant Networking (DTN)	Handles different types of data about voice, video, and multimedia, designed to handle a range of network topologies	May not be suitable for long delays and intermittent connectivity

Acknowledgments and Reference

I am so grateful to Ohio Space Grant Consortium and OAI (Ohio Aerospace Institute) for the academic scholarship program, specially many thanks to Dr. John Sankovic, Mr. Robert Romero, Mr. Tim Hale, and my advisor, Dr. Deok Nam.

[1] Kul B. Bhasin, *Architecting the Communication and Navigation Networks for NASA's Space Exploration Systems*, June 3, 2018 https://ntrs.nasa.gov/api/citations/20070031551/downloads/20070031551.pdf.

[2] Bruce M. Jahosky, “Inventory of CO2 available for terraforming Mars.” *Laboratory for Atmospheric and Space Physics*, https://lasp.colorado.edu/home/maven/files/2018/08/Inventory-of-CO2-available-for-terraforming-Mars.pdf.

[3] J. Sanchez, R. Martines, and M. W. Marcellin, "A survey of MAC protocols for wireless ATM", *IEEE Network*, vol. 11, no. 6, pp. 52-62, Nov. 1997.

Nano-Silver Sintering for Microchip Heat Sink

Student Researcher: Dryana L. Russell

Advisor: Dr. Henry Young

Wright State University
Department of Material Science and Engineering

Abstract
This project focuses on the compression and sintering of silver nano and micro-particles. Multiple processes have been utilized to maximize the density of the silver samples. Tests have been conducted by producing a mixture of di-ionized water, silver nitrate, and silver microparticles. This mixture is placed on silicon wafers and heated at 250℃. Consolidation studies are being conducted with varying silver particle sizes and different concentrations of silver nitrate. This study focused on producing a high packing density of silver particles while analyzing sintering processes. Characterization of resulting solids will be done with SEM.

Project Objectives
The hypothesis of this experiment is to determine whether silver nitrate ($AgNO_{3)}$ will improve diffusion leading to faster necking at lower temperatures. $AgNO_3$ has a low melting temperature. Typically, metal atoms more mobile in liquid phase. Therefore, at accelerated temperatures molten $AgNO_3$ may accelerate the diffusion process. The objective of this research is to quantify the necking and diffusion mechanism of micro-silver particles. Necking occurs when silver atoms diffuse into neighboring silver particles, causing them to become bonded together. Isochronal and isothermal experiments will be conducted to reach our objectives. The ultimate goal is to measure how necking width varies with increased heating time.

Methodology Used
Silver microparticles are being utilized analyze particle necks. For the isochronal experiment, one sample set was produced only including silver micro particles. Another sample set was produced by mixing the silver micro particles, 33% interstitial volume of AgNo3, and small amounts of water. Samples were then heated for 30 minutes at varying temperatures ranging from 150°C - 500°C in 50°C intervals. These samples were then analyzed using the SEM to discern what temperature necking occurred. The isothermal experiment was conducted very similarly to the isochronal tests. Instead of varying the temperature the heating time of the samples was varied. The samples containing $AgNO_3$ were heated at 300°C. The samples only containing silver microparticles were heated at 350°C. The samples were heated for 1 hour, 6 hours, 12 hours, 1 day, 2 days. 4 days, 7 days, and 14 days. SEM analysis was done to observe and measure how necking width changes with increased heating times.

Results Obtained
The isochronal experiment results revealed that $AgNO_3$ does lower the sintering temperature of silver microparticles. The samples not containing $AgNO_3$ exhibited sintering at 350°C, whereas the samples containing $AgNO_3$ started sintering at 300°C. The isothermal experiments show that $AgNO_3$ lead to more extensive sintering. Further analysis needs to be conducted on the necking widths. The $AgNO_3$ starts to decompose past its melting point.

Significance and Interpretation of Results

Silver nitrate aids in the sintering of silver microparticles by lowering the sintering time and temperature. As the next steps the isothermal necking results will be curve fitted to discern the solid-state diffusion mechanism of micro-silver particles. These results will be related to silver nanoparticles. Different salts will be tested to discover their effect on silver particle sintering and diffusion. New methods for applying heat and pressure to silver particles simultaneously will be discovered to improve sintering and further decrease porosity. These results can then be related to utilizing silver nano-particles for more electrical applications such as heat sinks for microchips.

Figures/Charts

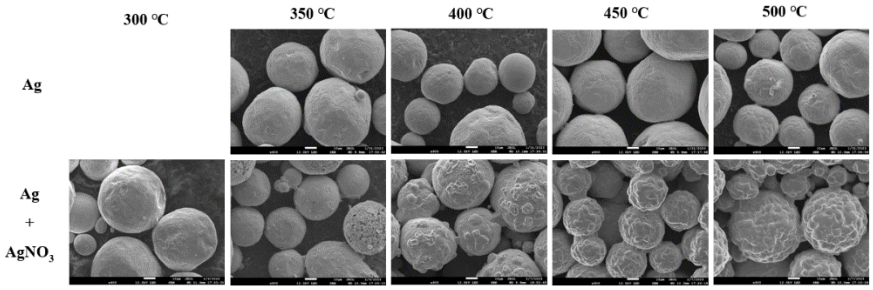

Figure 1: SEM results of the isochronal experiment set.

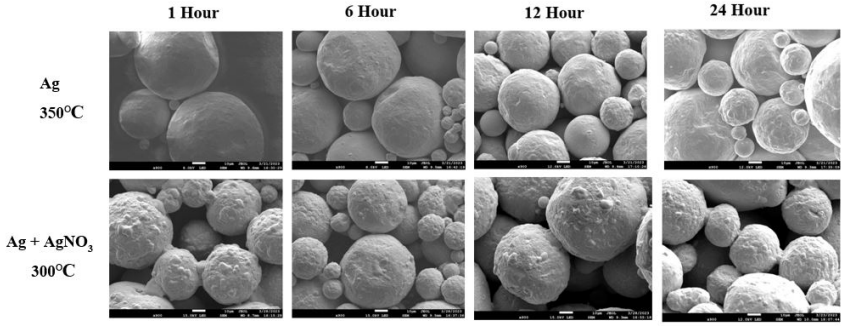

Figure 2: SEM results of the isothermal experiment set.

Acknowledgments and References

Advisor: Dr. Henry Young

Research Partner: Caleb Wasserbeck

OSGC Representative: Dr. Mitch Wolff

Ohio Space Grant Consortium

Ohio Aerospace Institute

Comparison of Flow Attachment with and without Vortex Generators

Student Researcher: Abigail C. Schauer

Advisor: Dr. Jed Marquart

Ohio Northern University
Dr. Carl D. Clay and H. Jane Clay Department of Mechanical Engineering

Abstract
This project will compare flow separation on two identical wings, with the exception that one has vortex generators on it and the other does not. This comparison will be done by placing models in a wind tunnel with smoke and observing the vortices that form around the wing. The lift and drag forces will also be compared. The results will be compared and validated with the results of computational fluid dynamics (CFD) models of the same airfoil.

Project Objective
The objective of this research is to validate the use of vortex generators for improving flow attachment and delaying stall conditions on an airfoil at varying angles of attack. Qualitative and quantitative data will be collected to achieve this.

Methodology Used
The wing model was designed using a CH10 airfoil and a 50% taper ratio. The 3D printed model was altered to incorporate an attachment point for the wind tunnel mount and to maximize the width of the test chamber. Due to manufacturing limitations the models were printed in three pieces and epoxied together. The vortices were also over sized to ensure that they would create a visible effect in the wind tunnel. This model is 16 inches long and was run at 0, 2, and 5 degrees of attack and at 0.02 Mach. This model without the attachment modifications was run in CFD at 2 degrees of attack and at 0.02 Mach with a grid quality of 91% for the non vortex model and 89.5% for the vortex model.

Results Obtained
The lift produced by both airfoils was within 1% of each other at each angle of attack, shown in Figure 1. The drag for the vortex generator case ranged from 3-5% lower, shown in Figure 2. These graphs both show an average of four trials that each included a fifteen second data average. The CFD results are shown in Figures 3 and 4. The CFD vortex model shows a significant delay on when flow separation begins. A significant induced drag forward of the vortices is also observed. Photos of the 5 degree angle of attack are shown in Figures 5 and 6 because they had the best visual of the flow effects.

Significance and Interpretation of Results
At the chosen angles of attack, the vortex generators were not useful in increasing lift. They were, however, useful at decreasing drag despite being oversized. This shows potential for even better results with an optimized vortex generator design. This is also interesting when applied to the CFD results that show high drag forward of the vortex generators. This means that the vortex generators are creating a significant increase in flow attachment to overcome the high induced drag. Figures 3 and 5 show the the control airfoil loses flow attachment about halfway past the airfoil. Figures 4 and 6 show that this is delayed until the trailing edge of the airfoil. This test validated that vortex generators improve the performance of the airfoil. With optimized vortex generator shape and spacing along with higher angles of attack, these effects will likely be improved.

Figures/Charts

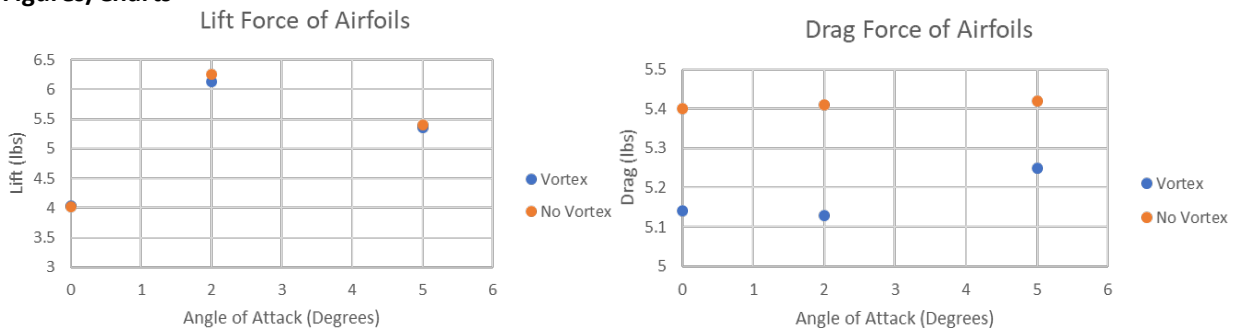

Figures 1 and 2. Lift and Drag Forces from Wind Tunnel Case

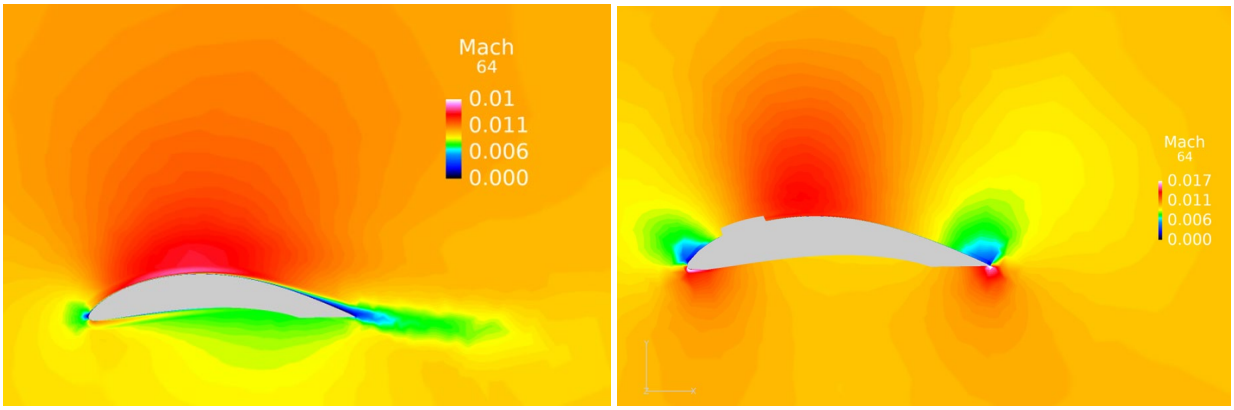

Figures 3 and 4. 2 Degree Angle of Attack CFD Case

Figures 5 and 6. 5 Degree Angle of Attack Wind Tunnel Case

Acknowledgments and References

Thank you to Dr. Marquart for his guidance and mentorship and thank you to the OSGC for the opportunity that they provided.

Effects of Mononitroparaben on Lipid Content of Melanoma Cells

Student Researcher: Julie A. Schlanz

Advisor: Dr. Suzanne Parsons

Marietta College
Department of Chemistry and Biochemistry

Abstract
Parabens are commonly used as preservatives in regularly used topical products, but their safety is under discussion since small amounts of paraben have been found in tumor tissue. Mononitroparaben causes cell death in melanoma cells with an LC_{50} value of 7.02 mM after twelve hours of treatment. This study focused on how mononitroparaben affects the cellular lipid content during induced cell death.
The experiment was conducted by growing the M624 melanoma cells, dissolving the paraben, and then leaving 0 mM, 5 mM, and 10 mM concentrations of paraben on the melanoma cancer cells for twelve hours. The paraben was then removed from the cells, and the cells were lysed. Colorimetric cholesterol assays and ceramide assays were completed to determine the changes in cellular cholesterol and ceramide content and the role of cellular lipids in cell death signaling.

Project Objectives
The objectives of this study included completing cholesterol and ceramide assays on cell lysis samples obtained from melanoma cells treated with 0 mM, 5 mM, and 10 mM concentrations of mononitroparaben. The changes in concentrations of cholesterol and ceramide determined whether apoptosis was occurring in the treated cells. Apoptosis was the desired cell death, and if it was occurring, then mononitroparaben could be a potential treatment for melanoma cancer.

Methodology Used
The concentrations of mononitroparaben that were placed on the cells were 0 mM, 5 mM, and 10 mM concentrations. A stock solution of mononitroparaben was first made by dissolving the mononitroparaben in methanol. Then, aliquots of the stock solution were placed in volumes of cell media to make 0 mM, 5 mM, and 10 mM concentrations of mononitroparaben in the media. The different concentrations of mononitroparaben in medium were placed on the cells for twelve hours. Plates with media that did not contain mononitroparaben were also prepared as controls.
The treated cells were lysed, and then Bradford, cholesterol, and ceramide assays were completed on the cell lysis samples. The Fujifilm Cholesterol E Kit was used for the cholesterol assay, and the AFG Bioscience Human Ceramide (CER) ELISA Kit was used for the ceramide assay.

Results Obtained
Figure 1 showed that as the concentration of mononitroparaben increased, more melanoma cancer cells died. Additionally, from the equation of the trendline in Figure 1, the LC_{50} value for mononitroparaben was calculated to be 7.02 mM. Figure 2 showed that there was no significant difference in cholesterol concentrations in the cells treated with mononitroparaben. However, Figure 3 showed that ceramide concentration increased significantly in the cells treated with 10 mM mononitroparaben compared to 0 mM mononitroparaben.

Significance and Interpretation of Results
Since Figure 1 showed that the cells died when treated with mononitroparaben, the cells were further tested to determine whether apoptosis was occurring. Since the cholesterol concentrations did not significantly change in the cells treated with mononitroparaben, the cholesterol data could not be used to determine

whether apoptosis was occurring. However, the ceramide concentration significantly increased in the cells treated with the 10 mM concentration of mononitroparaben compared to the 0 mM concentration. Ceramide concentrations must increase in the cell to begin the sphingomyelin cycle, which causes apoptosis.[1]
In the sphingomyelin cycle, ceramides act as intracellular messengers that can cause apoptosis and cell differentiation, which slow down the rapid reproduction of cells.[1] The sphingomyelin cycle begins by hydrolyzing sphingomyelin using a ceramide that generates a neutral sphingomyelinase, which causes an increase in the intracellular ceramide levels.[1] Since the intracellular ceramide levels increase, the phosphocholine head-group on a phosphatidylcholine transfers to ceramide to return the ceramide levels back to normal.[1] As a result, sphingomyelin is reproduced, which ends the sphingomyelin cycle and allows it to be completed again.[1] Therefore, since the mononitroparaben caused the ceramide concentration to increase in the cells, apoptosis was occurring through the sphingomyelin cycle. Consequently, mononitroparaben has the potential to be a treatment for melanoma cancer since it initiates apoptosis, which is a controllable cell death.[2]

Figures/Charts

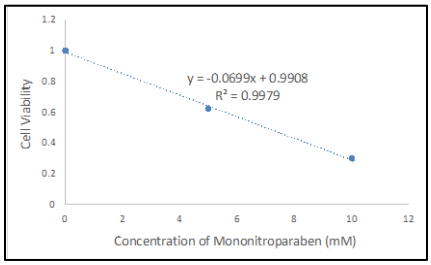

Figure 1. Viability of melanoma cells treated with 0 mM, 5 mM, and 10mM concentrations of mononitroparaben.

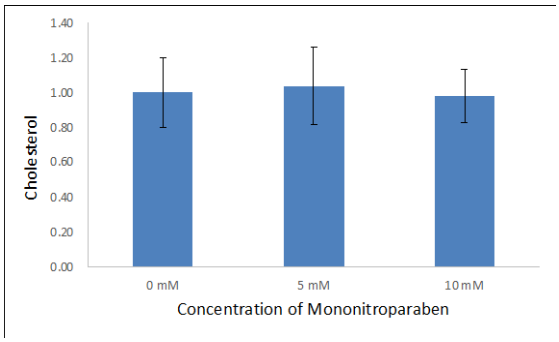

Figure 2. Cholesterol concentrations in treated melanoma cells.

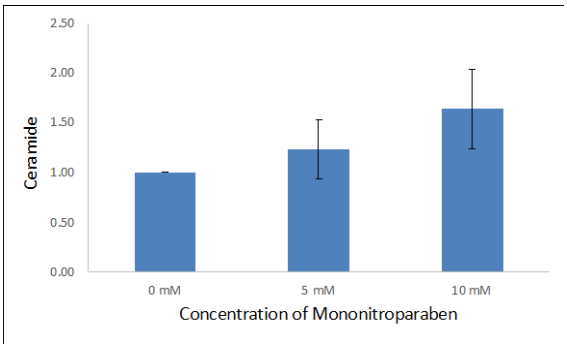

Figure 3. Ceramide concentrations in treated melanoma cells.

Acknowledgements and References
First, the author would like to thank OSGC for funding the project. Additionally, a thank you to Dr. Suzanne Parsons for her guidance and support and to Kennedy Couch for assisting with obtaining the cholesterol assay data. Finally, an appreciation for Dr. Kevin Pate and his organic chemistry research lab for providing the mononitroparaben.

1. Geilen, C. C.; Wieder, T.; Orfanos, C. E. Ceramide Signalling: Regulatory Role in Cell Proliferation, Differentiation and Apoptosis in Human Epidermis. *Arch. Dermatol. Res.* **1997,** *298* (10), 559-566.
2. Galluzzi, L.; Vitale, I. Molecular Mechanisms of Cell Death: Recommendations of the Nomenclature Committee on Cell Death 2018. *Cell Death Differ.* **2018,** *25*, 486-541.

Reduced Modeling of Aerodynamic Temperature Distribution for Hypersonic Vehicles

Student Researcher: James L. Schmitz

Advisor: Dr. Harok Bae

Wright State University
Department of Mechanical and Materials Engineering

Abstract
To develop aerospace vehicles that excel in performance and air superiority, we need to push past traditional designs and models. Models need to be examined early in their development under various operational conditions and design configurations. Reduced models, such as surrogate or machine learning models, can provide important information to aid in decision making and design discovery. This project will seek to develop a hypersonic vehicle structural model to estimate aerodynamic pressure and thermal loads under operational conditions of interest. Using a reduced model built from simulated data, temperature response distributions were able to be predicted. These predicted responses were compared to the original, simulated responses and found to be comparable with high accuracy.

Objectives
This project sought to develop a reduced model to rapidly predict temperature distributions on a Hypersonic Vehicle (HV). To that end, a method was proposed to rapidly predict temperature distributions without having to use a Computational Fluid Dynamic software to simulate the responses. The proposed method can be seen in Figure 1. Each step in that method, aside from the machine learning model, was tested and implemented in order to test the validity of the proposed method.

Methodology
The first step, collecting the response data, was implemented by using NASA's Configuration-Based Aerodynamics (CBAero) software approximate, simulate, and collect temperature response data of a Generic Hypersonic Vehicle (GHV) model under various loading conditions. In total, 189 datasets were simulated. The Mach number, dynamic pressure, and angle of attack was altered for each simulation. All the datasets were then combined into one dataset to prepare for the following steps.

The second step was implemented by developing a MATLAB script to map temperature response data from a design case to a generic case. The script was tested successfully on models with very simple geometry. A second script was used to map the temperature response from the generic case back to the design in order to validate the scripts accuracy. Mapping the response data to a generic model prepares the data for a Principal Component Analysis (PCA). The end goal is to further develop the scripts to work on more complex geometries such as the GHV itself.

The third step, reducing the complexity of the dataset, was implemented by using a PCA on the CBAero data. The PCA reduces the complexity of the dataset while retaining the majority of the dataset's variance.
The last step, predicting the response distributions, was done by using the resulting Principal Component functions from the PCA to predict the temperature distributions on the GHV. The future goal is to use the reduced dataset to train a machine learning model to predict the response distributions.

Results and Discussion
The results of the PCA reveal how a low number of Principal Components (PCs) are required to explain the majority of the variance in the data set. By analyzing Figure 2, it can be seen that using one PC can predict the response data while explaining over 98.6 % of the variance in the whole dataset. By increasing the number of PCs used, more variance can be explained. By using five PCs out the 189 available from the PCA, over 99.9% of the variance is explained. Figure 3 shows how using one PC predicts the data with under 10% global error when compared to the original temperature distribution. When increasing the number of PCs used to five, the global error decreases to the value of 2.7%.

Figures 4 and 5 visualize these results by displaying the original temperature response distribution and the predicted temperature response using five PCs. When compared, the response distributions are remarkably similar. There are some “hot spots” where the temperatures vary by a significant amount, particularly at the wing tip and the end of the body, but the distributions match well globally. Overall, the results demonstrate that a reduced dataset can be used to predict temperature response distributions with high accuracy.

Moving forward, the next steps to improve the proposed methodology are to further develop the mapping function and to train a machine learning model to predict temperature distributions rather than PC functions. Further development of the MATLAB mapping function would allow datasets to be collected from models with varying geometry. This would allow the overall dataset to contain more variance and would cause the proposed methodology to have increasing application to hypersonic design as the geometry of a design vehicle is of more concern than is the varying of load conditions. Additionally, training a machine learning model to predict responses rather than using PC functions, would enable more accurate predictions.

Overall, the conducted study demonstrated the validity of many parts of the proposed methodology. Continued research to improve, test, and implement the methodology will greatly aid future hypersonic vehicle development and design.

Figures/Charts

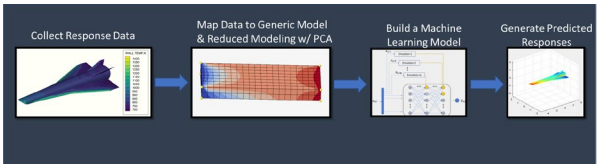

Figure 1: Proposed Method to Predict Temperature Response Distributions of HVs

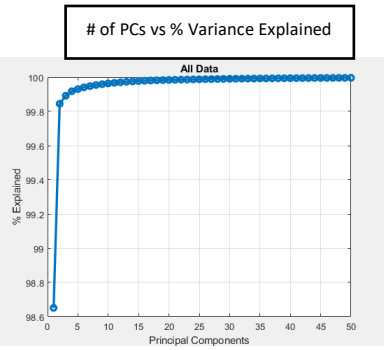

Figure 2: Principal Components Used vs. % Variance Explained

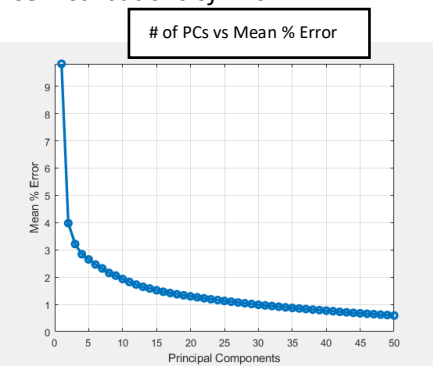

Figure 3: Principal Components Used vs. Mean % Global Error

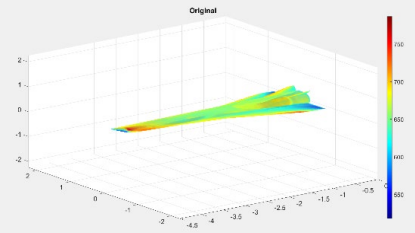

Figure 4: Original Temperature Distribution

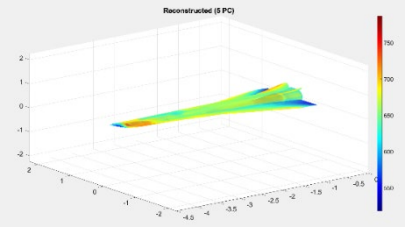

Figure 5: Reconstructed Temperature Distribution Using 5 Principal Components

Acknowledgements

The author would like to thank OSGC for the opportunity to make this research possible, as well as Dr. Harok Bae for their support and guidance provided throughout this project.

Differential Expression of microRNAs in Glioblastoma

Student Researcher: Aubrey C. Strong

Advisor: Dr. Kaleb Pauley

Cedarville University
Department of Science and Mathematics

Abstract

The term "glioma" is used to classify any kind of tumor that originates in brain tissue, including tumors of any neural cell type. Glioblastoma multiforme (GBM) is a tumor of astrocyte cells and is classified as a grade IV glioma. GBM is the most common type of primary brain tumor and accounts for 60% of all brain tumors in adults, mostly affecting men between the ages of 55-60 (Hanif, et al., 2017). According to the World Health Organization, GBM is the most aggressive and invasive type of tumor. Less than 10% of GBM patients survive longer than 5 years after diagnosis (Tan, et al., 2020). 95% of GBM tumors arise from the cerebral region of the brain, typically within white matter. Very few GBM tumors develop in the cerebellum, brain stem, or spinal cord (Hanif, et al., 2017).

MicroRNAs are short, non-coding RNAs that are approximately 22 nucleotides long (Xu, et al., 2019). They play a role in posttranscriptional gene expression and can influence genetic dysregulation that leads to tumor development. MicroRNAs bind to target gene mRNAs to degrade mRNAs or inhibit mRNA translation (Ye, et al., 2019). MiRNAs contribute to angiogenesis, metastasis, tumor growth, and drug resistance in various types of human cancers (Xu, et al., 2019). MiR-145 is commonly known as a tumor suppressor. Low expression of miR-145 in cancer patients is almost always correlated with poor overall survival rates and unfavorable progression free survival (Xu, et al., 2019). High expression of miR-145 is known to correlate with increased sensitivity to chemotherapy and inhibited tumor growth. Because of this, miR-145 shows promising results as a therapeutic target in cancer treatment (Ye, et al., 2019). Restoration of under expressed miR-145 has been shown to increase the efficiency of chemotherapeutic agents against lung carcinomas, breast cancer, ovarian cancer, and pancreatic cancer.

The objective of this study was to determine if miR-145 could serve as a potential therapeutic target to enhance the efficiency of traditional temozolomide (TMZ) chemotherapy against Glioblastoma tumor cells.

Methodology

RNA isolation, reverse transcription, and quantitative real time polymerase chain reaction (qRT-PCR) were performed on one normal human astrocyte (NHA) cell line and two Glioblastoma cell lines: U87 and U251. The cycle threshold values were standardized to compare the relative concentration of NHA cells to the U251 and U87 cells. Then, transfection was used to introduce a negative control mimic to the control group and mimic miR-145 to the experimental group. Following transfection, the cells in the experimental group were treated with 48 hours to temozolomide (TMZ) chemotherapy, and the control group remained untreated. The cellular response was measured using an apoptosis assay.

Figures/Charts

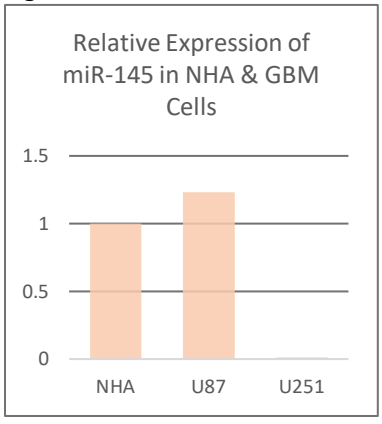

Figure 1: Standardized qRT-PCR data for relative expression of miR-145 in U87 and U251 cell lines compared to NHA cell line

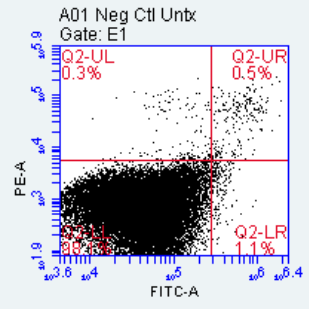

Figure 2: Negative Control Untreated U251 cells apoptosis assay

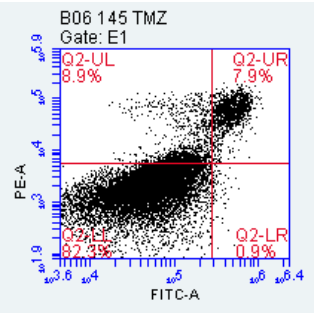

Figure 3: Mimic miR-145 TMZ treated U251 cells apoptosis assay

Significance and Interpretation of Results

Setting the NHA cycle threshold value at a standard value of 1 allows for accurate comparison of relative miR-145 expression between cell lines. From the data in Figure 1, it can be concluded that miR-145 is not differentially expressed in U87 cells compared to NHA cells. However, figure 1 shows that the relative concentration of miR-145 in the U251 cells was 0.015 compared to the standard NHA value of 1. Therefore, miR-145 is significantly under expressed in U251 Glioblastoma cells.

Figures 2 and 3 show two U251 GBM cell populations: one experimental group and one control group. Each individual dot on the graphs represents a single cell in the population. Figure 2 shows the cell population that was treated with a negative control mimic microRNA and experienced no drug treatment. This serves as a control to see how many cells in the population are expected to die without any intervention. Figure 3 shows the GBM cell population that was transfected with mimic miR-145 and treated with TMZ chemotherapy for 48 hours. The hypothesis was that this experimental group would experience a higher percentage of cell death compared to the control group.

The lower left quadrant in each graph represents living cells that do not show any response to treatment. The lower right and upper right quadrants represent apoptotic cells, and the upper left quadrant represents necrotic cells. The cell population in figure 2 only had 1.9% cell death including apoptotic and necrotic cells. When miR-145 levels were restored to normal and the cells were treated with TMZ (in figure 3), cell death increased to 17.7%.

The main conclusion that can be drawn from this data is that by restoring miR-145 to normal levels in GBM cells and treating the cells with TMZ chemotherapy, there was a significant increase in the amount of cell death within the U251 GBM cell population.

References

Hanif, F., Muzaffar, K., Perveen, K., Malhi, S., Simjee, S. (2017). Glioblastoma Multiforme: A Review of its Epidemiology and Pathogenesis through Clinical Presentation and Treatment. *Asian Pacific Journal of Cancer Prevention*, 18(1), 3-9. http://journal.waocp.org/article_42593.html

Tan, A. C., Ashley, D. M., López, G. Y., Malinzak, M., Friedman, H. S., & Khasraw, M. (2020). Management of glioblastoma: State of the art and Future Directions. *CA: A Cancer Journal for Clinicians*, *70*(4), 299–312. https://doi.org/https://doi.org/10.3322/caac.21613

Xu, L., Zhang, Y., Tang, J., Wang, P., Li, L., Yan, X., ... & Xu, M. (2019). The Prognostic Value and Regulatory Mechanisms of microRNA-145 in Various Tumors: A Systematic Review and Meta-analysis of 50 Studies. *Cancer Epidemiology, Biomarkers & Prevention*, *28*(5), 867-881.

Ye D, Shen Z, Zhou S. Function of microRNA-145 and mechanisms underlying its role in malignant tumor diagnosis and treatment. *Cancer Management and Ressearch*. 2019 Jan 22;11:969-979. doi: 10.2147/CMAR.S191696.

Analysis and Modeling of Geological Features with UAS in Southern Ohio

Student Researcher: Andrew T. Swift

Advisor: Dr. John Whitmore

Cedarville University
Department of Science and Mathematics

Abstract
Remote sensing techniques are crucial in the field of planetary geology for terrestrial-based research initiatives. As of now, rovers, and landers on Mars give most of our geological knowledge of the planet. When humans finally set foot on Mars, field geology will be of the utmost importance to understanding where to find evidence of past life and the geological history of the Red Planet. Given present technology, traditional field geology techniques such as those that astronauts have conducted on the Moon will prove difficult due to various factors such as Mars dust and suit mobility. However, the Ingenuity helicopter has recently shown that powered flight similar to drones is possible on Mars. This experimental study will look at small UAV techniques astronauts can use to conduct field geology in a safe and effective manner. A small UAV will be flown over locations in Southern Ohio that are of geological interest. Measurements and images will be taken that will be used to model the topography, structures, and geomorphology of the areas. In the future, these same techniques can be refined and technology improved to conduct field geology using UAVs on Earth, Mars and other planets where in-person field geology is extremely difficult.

Project Objectives
Most scientists in the planetary science community dream of the day when humans will set foot on Mars. Those who study the geological side of planetary science know how important it is to have proper geological field techniques. Current field techniques are mostly done in-person and require much mobility and dexterity to operate tools. These techniques were proven to be difficult on the Apollo missions but in the future, field geology will need to be done on the Moon again and especially on Mars as well. Fortunately, new technologies are on the rise in geoscience for use out in the field. More geologists are turning to unmanned aerial vehicles (UAVs) to survey areas for features of interest and to create 2D and 3D photogrammetry and LiDAR maps for use in the field. This study explores the use of UAVs and remote sensing to conduct field studies in three subjects of geology: structural, geomorphology, and karst. It is possible to encounter all three of these and more on Mars and the field methods needed can be tested in certain areas in Southern Ohio. These three areas are Oakes Quarry Park in Fairborn, Caesar Creek State Park emergency spillway in Waynesville, and an agricultural property in Hillsboro owned by Mr. Roger Epley near Hillsboro.

Methodology Used
For this study, I used a DJI Matrice v200 drone equipped with a Zenmuse X5S camera to conduct photogrammetry surveys. For Oakes Quarry, drone flight was not permitted due to proximity to Wright-Patterson Air Force Base so preexisting Google Earth imagery was used. Using the Measurement tool, I traced each visible joint I could find exposed in the park (Figure 1) and made an electronic note of each joint's directional heading in an Excel spreadsheet. My criteria for a "joint" on Google Earth was any dark linear feature in the surface that most likely indicated vegetation growth. I then added "0" to the second column next to each joint heading. I copied and pasted the two columns into a Stereonet on VisibleGeology.com which created a rose diagram of the data (Figure 2).

For the Caesar Creek spillway, the Matrice drone was flown over the spillway area west of the road in a standard photogrammetry grid pattern. The photographs were then run through Pix4D Mapper software and processed into a 3D mesh (Figure 3) and 2D orthomosaic (Figure 4) to show unique geomorphological features of the spillway.
For the Epley property, the Matrice drone was flown over much of the property in a grid pattern in winter when the tree cover was as minimal as possible. The drone flew a standard grid pattern and the photographs taken were also run through Pix4D software to produce a digital terrain model (DTM) (Figure 5). The DTM was uploaded into ArcGIS Pro where topographic contour lines (Figure 6) and karst depressions were created to identify surface topography and sinkhole location.

Results Obtained

The Oakes Quarry lineament data visually indicates a dominant trend to the northwest and the rose diagram confirms this. The rose diagram would indicate that the majority of joints were trending just north of west.

The 3D mesh of the Caesar Creek spillway generated from Pix4D can be panned and rotated to identify several geological features. Discolored rock along the spillway's cliff face with flow features in the cliff indicated a spring. Geomorphological features could be identified such as surface scouring, small landslides over the cliff face, gravel accumulation, and vegetation zones along the edges of the spillway. The 2D map shows high resolution surface imagery including boulder and gravel size, vegetation, water exiting a spring, and other minute details.

The topographic contour lines and karst depressions on the Epley property were generated but not ideal. There appears to be incorrect elevation data in the DTM forming oddly-shaped ridges that were field-verified to not exist. This elevation data occurs within tree-covered areas but the rest of the surface topography seemed to match reality. The karst depressions were also affected by the faulty elevation data but in open-field areas correctly identified existing depressions. It also featured numerous miniscule false depressions but this was typical.

Significance and Interpretation of Results

For the Oakes Quarry analysis, aerial drone imagery would have been much preferred and higher resolution, allowing for more accurate identification of joints. A higher resolution orthomosaic could then be placed in Google Earth or some similar program to do azimuthal heading measurements for the rose diagram. However, the rose diagram does not quite match the one that was made in previous studies of the park which indicates north-trending joints dominant with a majority of others pointing north of west and north of east. The north of west correlation stands but with much error in the other two directions.

The mesh and orthomosaic for Caesar Creek spillway was ideal. It displayed the landscape accurately and allowed for good identification of features. It could be supplemented with a LiDAR elevation model to better display the topography excluding vegetation but such technology was not available for drone-mounting.

The results from the Epley property were most likely skewed due to vegetation resulting Pix4D DTM output error attempting to correct for it. If a LiDAR elevation dataset were used instead, the results would be vastly improved. The state of Ohio does provide LiDAR datasets for the entire state but the release of the most recent data was pushed back to the summer of 2023 so the only data usable was from 2015 which would not include recent sinkholes that were reported to have developed since then.

Photogrammetry from a drone-mounted camera is easy and efficient to collect high resolution imagery of an area which can then be used for visual identification of strata, structures, and geomorphology for geological mapping. For accurate elevation models, LiDAR and multispectral sensing could potentially supplement photogrammetry for more geologic mapping capability. Therefore, UAVs have potential to be an adequate substitute for traditional in-person field geology methods when the latter is too difficult to conduct. If remote sensing technology continues to improve, so will the accuracy of the analysis and geological mapping capability.

Figures

Figure 1: Oakes Quarry joint lineament map

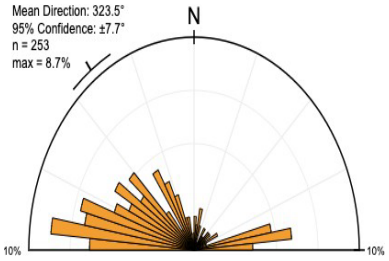

Figure 2: Oakes Quarry joint rose diagram

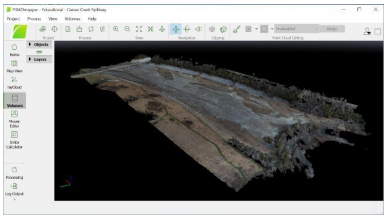

Figure 3: Caesar Creek spillway 3D mesh in Pix4D

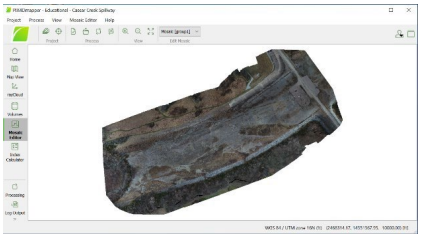

Figure 4: Oakes Quarry spillway 2D orthomosaic

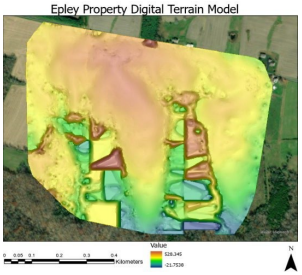

Figure 5: Epley property DTM in ArcGIS Pro

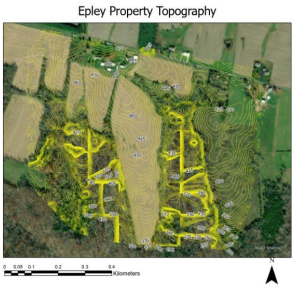

Figure 6: Epley Property topographic contour map

Acknowledgement and References

Thank you to the Ohio Space Grant Consortium for the opportunity to conduct this project, Jess Whitmore for compiling a succinct guide to photogrammetry and post-processing, Dr. John Whitmore for reviewing and approving the project, Thomas Rice for advice and literature review, Dr. Mark Gathany for supplying the Matrice drone, Douglas Aiden of the Ohio Geological Survey for guidance on karst mapping, and Sarah Stone for field assistance and morale support.

Aden, D. J., and Parrick, B.D., (2022, 2021). Karst annual report—Karst mapping of Franklin County, Ohio and adjacent areas: Columbus, Ohio Department of Natural Resources, Division of Geological Survey, p. 17.

Klopfstein, M., Fischer, T. B., & Krekeler, M. P. S. (2011). Mineralogical investigations of wetland soils developed in a disturbed landscape of an emergency spillway at Caesar Creek State Park, southwest Ohio. Abstracts with Programs – Geological Society of America, 43(5), p. 598.

Schumacher, G. A., Angle, M. P., Mott, B.E., and Aden, D. J. (2012). Geology of the Dayton Region in Core and Outcrop--a Workshop and Field Trip for Citizens, Environmental Investigators, Geologists, and Educators. State of Ohio, Department of Natural Resources, Division of Geological Survey.

Whitmore, Jess. (2022). Creating maps and models with drones: how to use drones in geologic field mapping projects using the DJI Mavic Pro. Cedarville University.

Potential Role of AHA2 Protein in *Arabidopsis thaliana* Gravity Response

Student Researcher: Victoria A. Swiler

Advisor: Dr. Sarah Wyatt

Ohio University
Department of Environmental and Plant Biology

Abstract
Following the characterization of differential protein expression in the BRIC-20 spaceflight experiment aboard the International Space Station, AHA2 proteins in *Arabidopsis thaliana* were found to be differentially phosphorylated, or less active, in microgravity compared to ground controls. This project investigates the molecular mechanisms of plant gravitropism signal transduction by researching the importance of AHA2 protein phosphorylation in Arabidopsis. Thus far, Arabidopsis *aha2* mutants lacking the functional *AHA2* gene have been identified and seven AHA2 DNA constructs were developed that biomimic phosphorylation or prevent phosphorylation, causing the protein to stay constantly active or inactive. These DNA constructs are being transformed into the mutant background of Arabidopsis lacking the *AHA2* gene. Once the altered DNA is inserted into the mutants, the transformant's gravity response can be observed. These experiments will show if the phosphorylation of the AHA2 protein is involved in a plant's response to gravity, which will further our knowledge of plant molecular mechanisms and put us another step forward in developing bioregenerative life support and provide food, oxygen, and fuel on spaceflights and habitation.

Project Objectives
A plant's survival is largely impacted by its ability to sense and respond to gravity. Without this gravitropic response, it would not know to bend its shoots upwards to collect sunlight, put its roots in the ground to harvest water and nutrients, or reorient itself if knocked over by wind or precipitation. Typically, gravitropism is broken into gravity sensing, signal transduction, auxin movement, and differential growth response. Although there are many proteins known to be involved in the signal transduction pathway, it is not completely understood. By studying the genes that affect the gravity signaling of plants, we can engineer plants for life support during space flight and habitation.
Following the characterization of differential protein expression in the BRIC-20 spaceflight experiment aboard the International Space Station, Arabidopsis H+ ATPase 2 (AHA2) proteins in *Arabidopsis thaliana* were found to be differentially phosphorylated in microgravity compared to ground controls[1]. When AHA2 is less phosphorylated, it is less active, thus the protein was less active in space[2]. Therefore, AHA2 is suspected to be involved in between auxin and acid growth in the signaling pathway[1], which diminishes auxin's ability to alter proton movement and thus the cell contraction and elongation necessary for gravity response. It is hypothesized that AHA2 protein phosphorylation is the link between auxin and differential growth in the gravity signaling pathway. Also, constitutive phosphorylation (activation) of AHA2 will increase the rate of the differential growth, whereas prevention of phosphorylation (deactivation) will decrease the rate of differential growth.
In spaceflight, the threonine (T) at amino acid position 942 in AHA2 was significantly less phosphorylated[1]. However, another phosphorylation site at T947 is utilized more often by the protein. Seven transgenic Arabidopsis lines are in the process of being developed with altered phosphorylation (activation) sites. The role of AHA2 phosphorylation in gravitropism can be determined by constitutively turning the protein "off" and "on" in the transformants.

Methodology

Confirmation of Homozygous Knockout Arabidopsis Lines: For the first step in this project, an Arabidopsis homozygous *aha2* knockout line was identified, meaning it lacks both *AHA2* genes. Several mutagenized plant lines from the Arabidopsis Biological Resource Center were tested via polymerase chain reaction (PCR) of DNA extractions and gel electrophoresis.

Phenotypic Analysis of aha2 Knockouts: The *aha2* knockout line was phenotyped for altered gravity response with a gravity persistent signaling (GPS) experiment and a root curvature experiment. The GPS experiment involves horizontal reorientation of Arabidopsis with 8-12 cm long shoots in 4°C for one hour. For the root curvature experiments, seedlings were grown vertically on a plate until the roots were 2 cm long, reoriented to a 135-degree angle, and the root's curvature was measured over time.

Development of Transgenic Arabidopsis Lines: PCR was used to develop the seven altered gene constructs with the amino acid threonine (T) changed to alanine (A) to prevent phosphorylation, creating cDNA constructs for three modified AHA2 proteins (T942A, T947A, and T942-947A). Likewise, constructs were developed where each of these sites are constitutively turned "on" by changing the amino acid T to aspartic acid (D) to mimic phosphorylation (T942D, T947D, and T942-947D). Finally, a seventh construct of the original *AHA2* gene was developed to transform the mutant and ensure the WT phenotype is recovered. To insert them into Arabidopsis, they are ligated into a plasmid and transformed into *E. coli* for multiplication of the construct. The plasmid is then isolated and transformed into *Agrobacterium tumefaciens*. These cDNA constructs are finally inserted into the genome of the mutant Arabidopsis lacking the functional *AHA2* gene via *Agrobacterium*-mediated transformation, which will ensure that only the mutant genes are expressed and not the original gene.

Results

For preliminary data, the *aha2* knockout plants lacking functional *AHA2* genes (**Figure 1**) were phenotyped for an altered gravity response. First, they were subjected to a gravity persistent signaling (GPS) experiment, where their shoot curvature was measured after being reoriented in 4°C and then returned to room temperature. The cold temperature allows gravity sensing, but hormone transport and thus curvature is unable to occur. However, when the plants are placed vertically again at room temperature, the signal transduction from gravity sensing persists and shoots will bend horizontally toward the original gravity vector before reorienting to the current one[3]. From this the mutant can be characterized for altered signal transduction[3]. From these experiments, it was concluded that there are significant differences in shoot curvature at 90, 105, and 120 minutes after the return to room temperature and in root curvature at 4 and 24 hours after reorientation when compared to wild-type (WT) Arabidopsis (**Figure 1**).

Thus far, all seven gene constructs have been created for their eventual insertion into Arabidopsis. Three *AHA2* gene constructs with altered phosphorylation sites have been transformed into *Agrobacterium* and have infected the Arabidopsis *aha2* knockouts, and two lines are confirmed to be transformants. The rest of the constructs are in various stages of development and insertion into *Agrobacterium*.

Conclusion

From the preliminary data obtained on the *aha2* knockout mutants showing a reduced gravity response and the study done by Kruse, et al. (2020) where AHA2 had differential phosphorylation in microgravity, it can be inferred that the AHA2 protein likely plays a role in Arabidopsis gravity response. However, to determine the specific role of AHA2 phosphorylation, the transformants described in this paper need to be characterized. Determining the role of more proteins involved in gravity signaling in plants will allow us to develop plants that will thrive in space, allowing us to have both agriculture and bioregenerative life support on long-term manned missions and habitation of other planets.

Figures/Charts

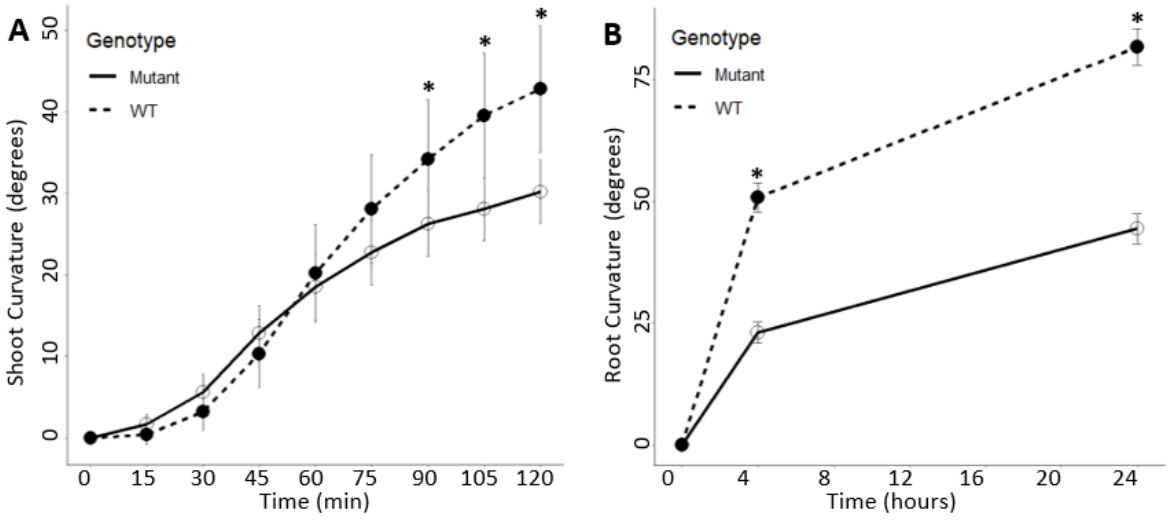

Figure 1 Root and shoots of *aha2* knockout lines have differential curvature compared to WT plants. A) Results of GPS experiment. B) Results of root curvature experiment. * indicates statistical significance ($p<0.05$). Data was analyzed in R programming with ANOVA tests.

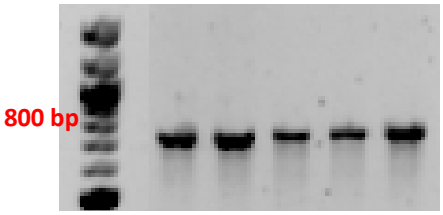

Figure 2 Identification of *aha2* knockout homozygous line. Gel electrophoresis of the DNA from five plants of a mutant line. Bands at ~800 bp indicate *aha2* knockouts.

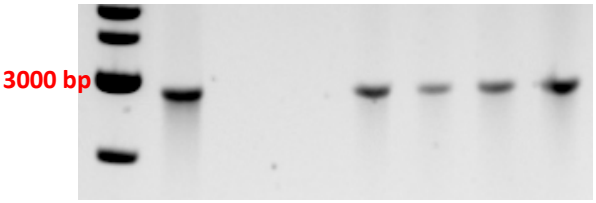

Figure 3 Identification of transformant Arabidopsis lines containing the altered *AHA2* gene, T947D. Gel electrophoresis of the DNA from seven progeny of the floral dipped lines. Bands at ~3000 bp indicate transformants.

Acknowledgements

The author would like to thank the members of Dr. Sarah Wyatt's lab for their help and input on this project, as well as the Ohio University College of Arts and Sciences and the Ohio Space Grant Consortium for project funding.

References

1. Kruse, C. P. S. *et al.* Spaceflight induces novel regulatory responses in Arabidopsis seedling as revealed by combined proteomic and transcriptomic analyses. *BMC Plant Biol.* **20**, 237 (2020).
2. Axelsen, K. B., Venema, K., Jahn, T., Baunsgaard, L. & Palmgren, M. G. Molecular Dissection of the C-Terminal Regulatory Domain of the Plant Plasma Membrane H^+-ATPase AHA2: Mapping of Residues that When Altered Give Rise to an Activated Enzyme. *Biochemistry* **38**, 7227–7234 (1999).
3. Wyatt, S. E., Rashotte, A. M., Shipp, M. J., Robertson, D. & Muday, G. K. Mutations in the Gravity Persistence Signal Loci in Arabidopsis Disrupt the Perception and/or Signal Transduction of Gravitropic Stimuli. *Plant Physiol.* **130**, 1426–1435 (2002).

Feasibility Study on The Use of Geopolymers for Additive Lunar Construction

Student Researcher: Kenneth A. Vigorito

Advisor: Dr. Richard A Deschenes

Youngstown State University
Civil/Environmental and Chemical Engineering

Abstract
The development of building techniques for lunar application is the first step in making the moon habitable. Incorporation of in-situ building materials is vital to the construction of Lunar roads and structures. Additive manufacturing, such as 3-D printing, is a building technique that could be used to construct roads and structures using a lunar regolith-based geopolymer concrete. Creating a geopolymer with adaptable set times and viscosity using aluminosilicate-rich materials, an alkaline activator, and a low water content proved challenging. A fly ash based geopolymer was the closest to the lunar simulant-based geopolymers and was used in this study. The data indicated that printing geopolymer is feasible and requires frequent mix optimization to maintain both printability and strength. The future of lunar habitation is set on the feasibility of 3-D printing geopolymer concrete.

Project Objective
This study aimed to optimize a mix design to allow geopolymer concrete to be extruded using a prototype 3-D printing apparatus. Preliminary research into the variability of the constituents and their effect on set times and printability is required to produce optimum geopolymer characteristics. Producing data that can allow for future 3-D printing geopolymer research to be conducted, focusing on testing the printing, layering, and durability.

Methodology
Compressive strength was the initial criterion for developing the geopolymer concrete mix design. Numerous trial batches were mixed, cured for seven days, and then compression tested to understand the relationships between mixture proportions and compressive strength. Printability was measured using a quarter-inch nozzle and a compression machine to record the force required to print through a nozzle and how this force changed over time. The printability apparatus can be seen in **Figure 1 (A)**.

Results
After testing the fresh properties of the mixture, each batch was oven cured at 45℃ and compression tested at 7 days, 14 days, and 28 days. The mixture was modified and refined based on the data by increasing or decreasing the water content or introducing admixtures such as sucrose to benefit the set time. The data indicates that printing geopolymer requires frequent mix optimization to maintain printability and strength factors. Testing variables like silica fume and sugar allowed for the optimization of the test matrix, furthering the understanding of the printability and strengthening factors. Increasing the set time from 30 minutes to one hour was possible with the addition of sucrose to delay the reaction between the alkaline activator and the fly ash. The geopolymer printing was possible with an auger attached to an electric motor and a prototype hopper and dispenser with attachable nozzles. The printing apparatus can be seen in **Figure 1 (B)**, where a bead of geopolymer concrete is extruded onto a plate. **Figure 1 (C)** shows a cube with the highest silica fume content after seven days in the oven; excessive expansion could be due to entrained air. **Figure 1 (D)** shows the viscometer used to measure the viscosity of a sample.

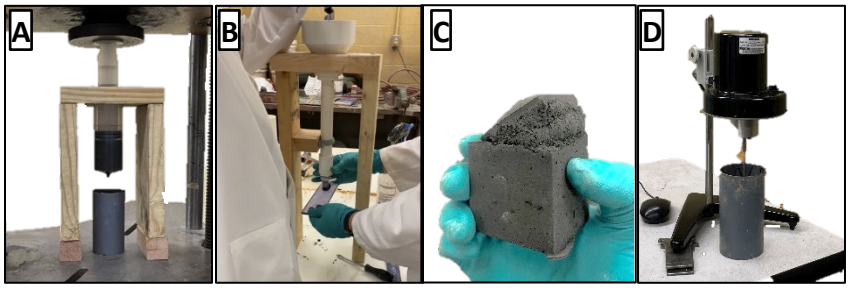

Figure 1. Print force testing apparatus (A), prototype extruder and hopper (B), high silica fume cube at seven days (C), and viscometer testing the viscosity of a batch (D).

Significance and Interpretation of Results

The strength of the optimized geopolymer concrete at 7 days was similar to normal Portland cement concrete at 28 days, roughly 3,000 psi. **Figure 1 (A)** is a summary of the compressive strength over time, noting that the 28-day strength averaged 5,000 psi for Batch 16. **Figure 1 (B)** compares the viscosity over the course of an hour after mixing. The viscosity increases with the decrease in water content in Batch 16. **Figure 1 (C)** shows print force in pounds over time, noting that Batch 16 has a high print force due to the decreased water content.

Figures/Charts

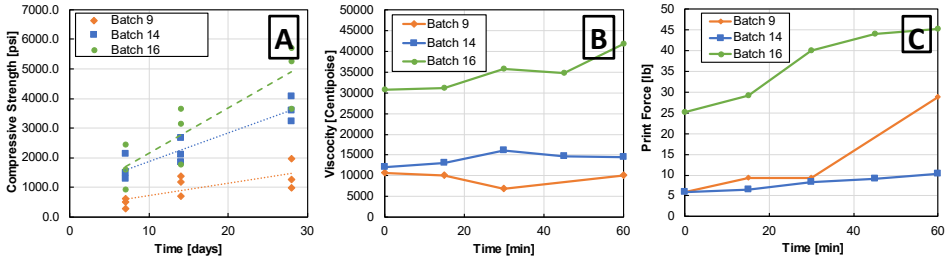

Figure 2. Compressive strength increases over time (A), viscosity with respect to time (B), and print force with respect to time (C).

Conclusion

3-D printing geopolymer proved feasible, with adequate printability, buildability, and strength. Further testing of layered concrete in extreme temperature conditions and its overall durability on the lunar surface is required. The future of lunar habitation is set on the feasibility of 3-D printing geopolymer concrete.

Acknowledgments and References

The research was funded in part by the Ohio Space Grant Consortium and the Youngstown State University Office of Research Services.

[1] Rasuli, M. I., Tajunnisa, Y., Yamamura, A., & Shigeishi, M. (2022). A consideration on the one-part mixing method of alkali-activated material: Problems of sodium silicate solubility and quick setting. Heliyon, 8(1). https://doi.org/10.1016/j.heliyon.2022.e08783

[2] Wang, K.-tuo, Lemougna, P. N., Tang, Q., Li, W., & Cui, X.-min. (2017). Lunar regolith can allow the synthesis of cement materials with near-zero water consumption. Gondwana Research, 44, 1–6. https://doi.org/10.1016/j.gr.2016.11.001

[3] Ryu, G. S., Lee, Y. B., Koh, K. T., & Chung, Y. S. (2013). The mechanical properties of fly ash-based geopolymer concrete with alkaline activators. Construction and Building Materials, 47, 409–418. https://doi.org/10.1016/j.conbuildmat.2013.05.069

Genetic Fuzzy Logic Controller for Explainable AI Asteroids Arcade Game

Student Researcher: Garrison L. Wettengel

Advisor: Dr. Kelly Cohen

University of Cincinnati
Department of Aerospace Engineering & Engineering Mechanics

Advisor

The usage of Genetic Algorithms to train a fuzzy system allows us to optimize the behavior of an AI agent. A fuzzy logic-based controller is developed for the arcade game Asteroids. The controller developed is responsible for target acquisition and object avoidance in a congested asteroid field. The use of fuzzy logic allows for explainable decision making for safety critical processes compared to black box methods. The genetic algorithm trains the input/output functions of the fuzzy system. The controller aims to optimize the bullet accuracy, fuel spent, mission time, and asteroids avoided.

Project Objective

Asteroids is a 2D arcade style game in which a "fighter-style" spaceship has the objective of shooting the asteroids and avoiding them with maneuver. The ship can accelerate forward and backwards, turn left and right, and shoot straight forwards. Asteroids can be between 4 sizes, and each time one is hit, it breaks into 3 of the next smaller size or disappears at the smallest size. Each asteroid shot and hit awards one point to the player. The walls of the "arena" allow for wrapping. This is where asteroids and the ship will teleport from one side of the arena to the other when they hit the edge. This is both a benefit and a hindrance because it allows the ship to get out of situations where it may be trapped against a wall, but it also allows for asteroids to come from all angles.

A controller was developed in Python to control the spaceship. This controller uses fuzzy logic techniques to take inputs such as the position of the ship, the position of the asteroids relative to it, and other variables to output the controls such as turn rate and thrust. The Fuzzy Inference System members are optimized using a Genetic Algorithm to change the member functions.

Methodology

A Fuzzy Inference System gets an asteroid's position relative to the ship, as well as its velocity relative to the ship, and from that a "threat" value is determined. This threat value is a measure of the danger that asteroid poses to the ship. From the threat and its position relative to the ship, we calculate a threat direction. If the ship is in "Firing Mode", meaning it is actively looking for and shooting at asteroids, then the avoidance only controls the forwards and backwards acceleration. The avoidance controller is prevented from interfering with the targeting of the ship as that would hinder its ability to target accurately. If the threat is in front of the ship it goes backwards, if it is behind it then it goes forwards.

If the ship is in "Avoidance Mode", where it is not shooting at asteroids, only evading, the avoidance controller now has control over its turning as well as acceleration. It now turns to the optimal heading to accelerate towards the safe area. It takes the position of the asteroid relative to the ship as well as its direction of travel and calculates a threat vector. This threat vector is calculated for all the asteroids within a certain range and sums up to give us an overall vector that tells us to go in the direction opposite the asteroid with an acceleration determined by its threat level. The system is designed with aggression as a priority. Its first goal is always to take one more asteroid out to reduce the threats. As more asteroids are removed from the system, it becomes easier for the ship to avoid so it wants to remove as many as possible, so it spends as little time with the maximum number of obstacles to avoid.

Results Obtained

When in Firing Mode, the system likes to back away from the closest asteroid. This can be problematic if it is backing up into one that is closer. But it tends to be able to “snap” between the two closest asteroids to clean them up before it is defeated. Currently in Avoidance Mode, the controller likes to stay at the border of our “threat range”, the range at which it calculates asteroids as threats. It does not like to be without information. This allows it to prepare and predict for an asteroid to “warp” from one side to the other, which happens when an asteroid hits a wall.

The system proves able to survive for an extended period in a congested area and is usually able to clear out enough asteroids to no longer be in consistent danger. Its biggest threat is that it is hesitant to “warp”, to use the ability to travel through walls and end up on the other side of the environment. Its biggest challenge in targeting mode is a scenario when 4 asteroids are coming at it directly 90 degrees from each other. Because it is only controlling thrust to avoid, not angle, it will consistently back up into another asteroid until it is sandwiched.

The system is remarkably better than any human at aiming. It is designed to predict the asteroids path and shoots at where it will be, then shoots at another asteroid before the first one is destroyed. This allows it to very quickly clear the arena and have a very high level of accuracy. The system is not as good as a human controller at avoiding obstacles. It tends to put a large amount of weight into avoiding the nearest one or two asteroids but a congested field of asteroids moving in different directions can sandwich it if they are orthogonal to each other.

Significance and Interpretation of Results

The system is remarkably better than any human at aiming. It is designed to predict the asteroids path and shoots at where it will be, then shoots at another asteroid before the first one is destroyed. This allows it to very quickly clear the arena and have a very high level of accuracy. The system is not as good as a human controller at avoiding obstacles. It tends to put a large amount of weight into avoiding the nearest one or two asteroids but a congested field of asteroids moving in different directions can sandwich it if they are orthogonal to each other.

One improvement that could be made in the future is to give the firing-based controller some control over its angle such that it won’t be pinned. This will require sacrifices to be made in accuracy for a period but can be made up for in increased survivability.2

Directivity of Far-Field Noise in Supersonic Rectangular Twin Jets

Student Researcher: Abhilash Yarlagadda

Advisor: Dr. Mo Samimy and Dr. Nathan Webb

The Ohio State University
Department of Mechanical and Aerospace Engineering

Abstract
The directivity of the radiated noise of supersonic rectangular twin jets (SRTJ) over a wide range of Mach numbers was investigated. The flow and acoustic fields of SRTJ are known to couple, generating elevated far-field (FF) noise levels. Large-scale structures (LSS) are responsible for mixing noise, broadband shock-associated noise, screech, and coupling. The primary objective of this research was to examine the differences in the FF noise between the current geometry and that of axisymmetric jets found in the literature, due to the presence of coupling and shielding effects in SRTJ. Measurements were collected at FF polar angles from 0 to 90 degrees along azimuthal angles of 0 and 90 degrees. It was found that the shielding and coupling effects observed in these jets affects the noise at shallow downstream angles but become negligible at the sideline.

Project Objectives
Noise in supersonic jets is an issue for military personnel who spend a great deal of time near these aircraft and communities that live near military bases. For the latter, this is more of an inconvenience. Care must be taken when planning a new installation to place it far enough away from ordinary buildings to avoid noise complaints. On the other hand, jet noise can cause hearing loss and other health problems for the soldiers on deck during launches, particularly in the Navy [1]. This research is part of a broader campaign to study plasma actuator excitation as a method of jet noise reduction, and it is aimed to characterize how SRTJ noise in the far field is different from previous findings about the noise of axisymmetric jets.

Methodology
An anechoic chamber at the Gas Dynamics Turbulence Laboratory at The Ohio State University's Aerospace Research Center was used for this research. Figure 1a shows part of the assembly of the SRTJ and the coordinate system used. A pair of bi-conic, rectangular converging-diverging nozzles (Fig. 1b) with sharp throats and a design Mach number of 1.5 (M_d = 1.5) and aspect ratio of 2 (AR = 2) were used. ϕ is the azimuthal angle of the SRTJ in the y-z plane. The assembly of the SRTJ within the anechoic chamber room is shown in Figure 1b. The angle θ, measured with respect to the downstream jet axis, is the polar angle for the FF acoustic measurements. The stagnation pressure of the flow is set by a computer-controlled valve, which automatically maintains the desired nozzle pressure ratio (NPR). The M_j and NPR for the design conditions are 1.5 and 3.67 respectively. The FF microphone array consists of 8, ¼ in. microphones mounted at polar angles ranging from 30° to 120° and aimed at the origin of the twin jets' coordinate system (Fig. 1a). The SRTJ assembly can be rotated to locate the FF microphone array on the plane of the SRTJs' major axis (ϕ = 0°) or minor axis (ϕ = 90°). The individual microphone distances from the SRTJ origin range from $99D_e$ to $196D_e$. The acoustic data was processed to produce sound pressure level (SPL) spectra, which are in turn integrated across the full frequency range to find the overall sound pressure levels (OASPL).

Significance and Interpretation of Results
The results presented here focus on a subset of all the collected data. The case of M_j = 1.50 was chosen as it is the design Mach, and there was no notable dependency on Mach number other than that of noise levels. In addition, the SPL spectra (Fig. 2a) only show data from microphones at θ = 30°, 40°, 60°, and 90° from top to bottom. Each microphone spectrum is offset by an additional 20dB from the last for readability; thus, only the 30° spectra have numerically accurate SPL values. The OASPL plots (Fig. 2b) exclude data collected beyond θ = 90°.

Potential reasons for the inhomogeneity of radiated noise in SRTJ are the tendency of coupling between the jets to increase noise along the minor axis and the side-by-side positioning of the jets to cause a shielding effect along the major axis, as noted in Samimy et al. [2]. As the polar angle increases, the SPL spectra show that

the different azimuthal angle data begins to collapse, and by θ = 90°, the spectra are nearly identical. This indicates that the coupling and shielding of the jets does not have a significant effect on noise at the sideline and beyond. In contrast, shallower polar angles still have a 1-2dB shift between the two azimuthal configurations, which indicates that these effects likely still play a role at more downstream angles.

Figures

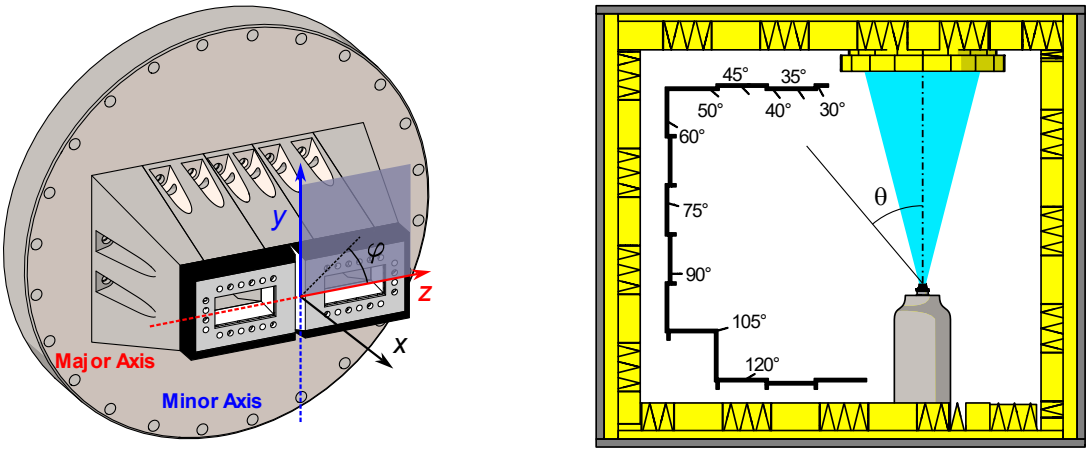

Figure 1. SRTJ assembly with referenced coordinate system (a) and top view of anechoic chamber with FF microphone positions (b).

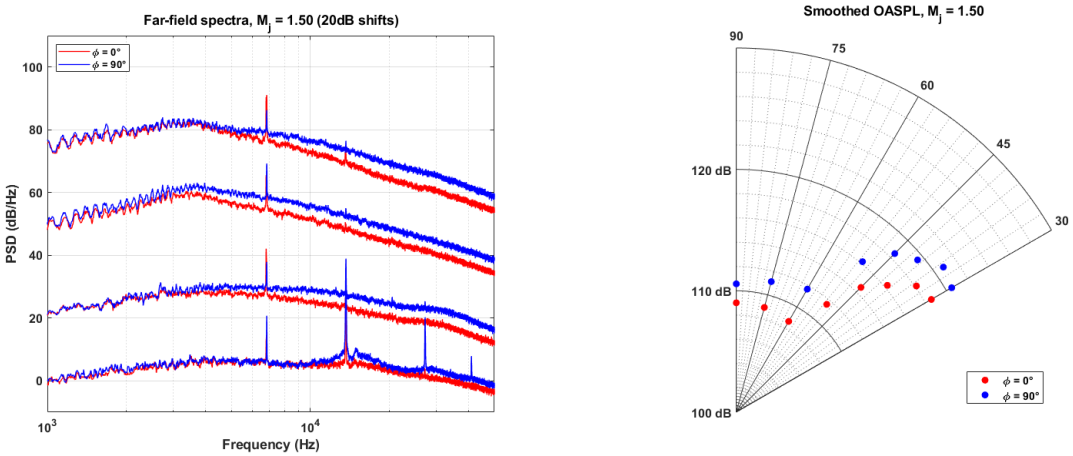

Figure 2. Comparison of FF SPL spectra (a) and polar OASPL (b) along major and minor axes for M_j = 1.50 at several polar angles.

Acknowledgements and References

This work was supported primarily by the Office of Naval Research. However, my experience would not have been possible without the support of the Ohio Space Grant Consortium. In addition, my advisors Dr. Mo Samimy and Dr. Nathan Webb have served as excellent guidance during my time at The Ohio State University's Gas Dynamics and Turbulence Laboratory. Finally, I would like to thank recent PhD graduate Dr. Ata Esfahani, recent Master's graduate Ryan Leahy, and current PhD student Karli Katterle, fellow students who taught and assisted me over the course of the research.

[1] Aubert, A., and McKinley, R. Measurements of Jet Noise Aboard US Navy Aircraft Carriers. Presented at the AIAA Centennial of Naval Aviation Forum "100 Years of Achievement and Progress," Virginia Beach, VA, 2011.
[2] Samimy, M., Webb, N., Esfahani, A., & Leahy, R. "Perturbation-Based Active Flow Control in Overexpanded to Underexpanded Supersonic Rectangular Twin Jets." Journal of Fluid Mechanics, vol. 959, 2023, p. A13., doi:10.1017/jfm.2023.139.

Community College

Spin-on Dopant Semiconductor Process with DC Magnetron Sputtering for Diode Fabrication on 2" Silicon

Student Researcher: Jeffrey A. Burns

Advisors: Johnny Vanderford, Greg Mylnar

Lorain County Community College
Department of Micro-Electromechanical Systems

Abstract
We will examine the methodology and procedures that resulted in successful fabrication of diodes in a community college laboratory setting with a calculated 1.33µm junction depth and forward bias voltages between 0.7 and 1V. These steps included stripping the wafers of their native oxide, applying a dopant, removing the solvents present in the dopant, diffusing the dopant into the wafer, stripping the silicon dioxide again, and using physical vapor deposition (PVD) to coat the doped wafers with aluminum.

Objectives
Our first objective was to devise, utilize, and finally refine a process for fabricating a diode from a silicon semiconductor wafer using equipment accessible to community college level laboratories. Our second objective was to execute the processes and create a diode that functioned in the forward bias.

Methodology
Our work was conducted at Lorain County Community College in a class 10,000 (ISO 7) clean room. Standard gowning for wafer processing calls for smock, hairnet, facemask, and nitrile gloves, though additional personal protective equipment (PPE) was required at different points. We began with four single side polished (SSP), 100 orientation, boron doped, 0-100 Ω resistivity, 2 inch silicon wafers. Our first step was to prepare a 1:1 hydrofluoric (HF) acid-deionized water (DI water) bath inside a fume hood to etch away the native oxide present on all silicon wafers. For this processing step, the additional PPE of elbow length trionic gloves, full body trionic apron, and plastic face mask are strictly required to protect against HF acid exposure. The wafers were submerged in this solution for 60 seconds using a wafer wand with mild agitation. The wafers were then submerged in two separate containers of DI water for approximately 15 seconds each to rinse away any residual HF acid. Each wafer was then thoroughly dried using compressed dry air (CDA).

Using a Laurell WS-650-23B spin coater, we then applied 2ml of Filmtronics P509 phosphosilicate solution (a n-type dopant) using a Pasteur pipette to the center of the wafer and spun them at 4000 RPM for 40 seconds. This resulted in a film of dopant approximately 40nm thick. Two of our wafers were then placed on hot plates set to 150°C for 20 minutes, and two were placed in an exhaust oven at 150°C for 20 minutes. The intention of this process was to drive out the solvents present in the P509 dopant solution to avoid flashing during processing with higher temperatures and to increase the viscosity to allow for better adherence to the silicon wafer substrate.

Assuming the average resistivity of 50 Ω, we calculated the boron doping concentration of the wafer to be 1.9 $x10^{14}$ atoms/cm^3. Our n-type dopant, P509, has a dopant concentration of 1 x 10^{21} atoms/cm^3. Using the calculator here: https://fabweb.ece.illinois.edu/utilities/difcad/default.aspx , we adjusted our time and temperature parameters (3600 seconds and 1050°C, respectively) to achieve a dopant diffusion depth of approximately 1.33µm. We used "large" plot size and 1 diffusion step. The wafers were then placed into a laboratory benchtop diffusion furnace, the temperature allowed to rise to

1050°C and then remained there for 3600 seconds (1 hour). The furnace then cooled to roughly 300°C, at which point the wafers were removed and allowed to further cool in room temperature air. This diffusion process grows silicon dioxide (SiO_2), which was then removed using the same 1:1 HF acid – DI water procedure used above. In a commercial fabrication setting, this Sio_2 growth would be avoided by purging nitrogen gas into the diffusion furnace during diffusion.

While the wafers were cooling, we checked our aluminum target for contamination and flashed the chamber as it was coated with previously used copper. Our target was 4N purity (99.995% pure) aluminum. We then immediately moved two wafers from the HF acid bath (after DI water rinsing and CDA drying) to the sputtering system and placed them into 3D printed jigs that fit closely on the sides of the wafers in an attempt to prevent "wrap around", which could have potentially created an electrical short from the top of the wafer to the bottom. We moved them as quickly as possible to minimize SiO_2 growth on the wafers. Beginning the sputtering process, we did a rough pump to bring the pressure in the chamber down to approximately 1×10^{-2} torr in approximately 5 minutes, then used a turbo pump to bring the pressure down to 4×10^{-5} in 15 minutes. Argon was used as our backfill gas. One of the 3D printed jigs melted and deformed around the wafer, causing it to become stuck in the jig. Our PVD sputtering system has an active cooling system that would have prevented this, but it is currently non-functional.

Results

Diodes	V_F After HF Acid Bath	V_F After AL Sputtering
1	1.25V	N/A
2	0.68V	N/A
3	0.68V	1.1V
4	1.12V	-2.8V

All four wafers functioned as diodes, allowing current to flow in one direction when a continuity test from a DMM was applied. The wafers were placed on a steel tray, the black lead was placed on top of the diode, and the red lead was placed on the steel tray. Inexplicably, diode number 4 functioned in reverse bias after being sputtered with aluminum, only displaying current flow when the lead placements were reversed (black on the steel tray and red on the top of the diode).

Acknowledgements and References

Illinois, ECE. https://fabweb.ece.illinois.edu/utilities/difcad/default.aspx. 2017. 30 March 2023.

Patel, Bhavink, et al. "Investigation of Spin-on Dopants and Curing Temperature Effect on Dopant Activation." 2019.

Thank you to my advisors Johnny Vanderford and Greg Mylnar. Thank you also to Em Williams, Ryan Palmer, John Bukovac, Manaf Alhusayni, and Courtney Tenhover for all of your help and support. And a special thanks to Smart Microsystems for providing deionized water for the project.

Discovering the Distant Universe Using Strong Gravitational Lensing

Student Researcher: Emily R. Bursk

Advisor(s): Dr. Jeremy Huber

Cincinnati State Technical and Community College
Department of Physics

Abstract
The total solar eclipse in May of 1919 confirmed Einstein's theory of general relativity when astronomer Arthur Eddington observed stars were displaced from their normal position as the moon passed in front of the sun. The applications of this discovery have since then aided in many revolutionary scientific discoveries, from gravitational waves to gravitational lensing. Gravitational lensing, more specifically, strong gravitational lensing (SGL), allows a closer look at the distant and early universe, which regular telescopes would not be able to see. This project will examine the use of SGL to study background objects in galaxy clusters and the role of astronomical survey data in these studies.

Project Objective
The central focus of this study is to produce a general understanding of strong gravitational lensing and how galaxy clusters create an ideal lens for such research. This study will also include an explanation of how SGL is classified, as well as the information it provides about the distant universe and what we can learn.

Methodology Used
Through the examination of existing research, I will collect data from existing academic papers, as well as utilize the Sloan Digital Sky Survey to present the applications of SGL. In this case, we will mostly be looking at galaxy clusters acting as the gravitational lens due to their massive size and ability to distort light.

Results Obtained
According to Einstein's theory of general relativity, massive astronomical objects have the ability to distort the fabric of space-time, causing light, which normally travels in a straight path, to curve. This phenomenon can act as a magnifying glass, allowing distant objects to seem closer. In this case, the object acting as the magnifying glass is a galaxy cluster. Galaxy clusters act as an ideal lens due to the fact that they are the most massive objects in the universe, allowing for the greatest distortion of gravity and deflection of light. From our vantage point, we see the light strong gravitational lensing redirects from the background source that would normally be too far and faint to see.

Galaxy clusters represent the densest structures of dark matter; their merging history and evolution shape the properties of their mass distribution (Fox et al., 2022). In this study, galaxy clusters have been chosen as the lens as a result of their lensing strength and ability to magnify some of the earliest galaxies when the Universe was only 10-15% its current age. While the distribution of mass in a cluster is less regular than in a single galaxy, clusters provide a much larger cross-section that produces the desired lensing effect. This makes it much easier to determine the internal properties of the lensed object since clusters also inflate its angular size. The following section provides insight into how SGL is classified and what features determine whether or not the object is a lens.

Gravitational lensing produces different types of images depending on the lensing mass, from an Einstein cross (when the lensed object appears as four points) to an Einstein ring (when the lensed object appears as a smeared circle). The effect galaxy clusters produce from gravitational lensing is sometimes a combination of the two. The image appears as multiple smeared arcs, though it doesn't form a complete circle due to the cluster having an irregular shape. Figures (1) and (2) show the same galaxy cluster from two different telescopes, the Hubble Space Telescope, and the Sloan Digital Sky Survey (a ground-based telescope), presenting smeared arcs from the lensing. The presentation of this image is a major **component in identifying and confirming a strong gravitational lens. Another main standard for** confirming a lens is the spectroscopic verification of multiple redshifts (Rojas et al., 2022). According to Hubble's Law, galaxies further away have greater recessional velocities, resulting in a stronger redshift.

Figure 1. Abell 370 from NASA's Hubble Space Telescope

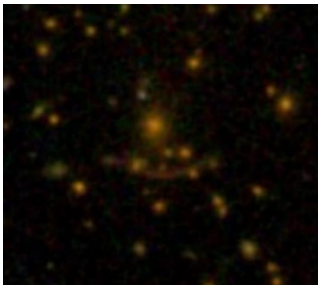

Figure 2. Abell 370 from the Sloan Digital Sky Survey

Therefore, the presentation of multiple redshifts helps distinguish which object is closer (the thing acting as the lens), from the background source. A study on how human experts visually identify strong gravitational lenses concluded that most lenses are reliably identified with an Einstein **radius greater than 1.2 arcseconds (a** measurement of very small angles) (Rojas et al., 2022). When it comes to identifying a lens, it is imperative to identify predictors of lensing strength to increase efficiency in selecting the best natural telescopes (Fox et al., 2022).

Interpretation and Significance of Results

As we have learned, we can now understand some characteristics of the Universe. Using SGL, we are able to study the evolution of galaxy clusters, as well as the earliest galaxies that are magnified and determine their internal properties. This discovery has also allowed us to research the most distant galaxies that are ten times smaller than the Milky Way galaxy.

This review article has presented a general understanding of SGL, as well as the reasoning behind choosing galaxy clusters as a preferable lens, how it is classified/confirmed and what we can learn using gravitational lensing. Now knowing this information, other questions may arise. What about using gravitational lensing to study dark matter or black holes? As science evolves, we are constantly learning new things about the Universe. There may be questions that we don't even know how to ask. There is a wide range of possibilities for future studies using gravitational lensing.

Acknowledgements and References

Fox, Carter, et al. "The Strongest Cluster Lenses: An Analysis of the Relation between Strong Gravitational Lensing Strength and the Physical Properties of Galaxy Clusters." *The Astrophysical Journal*, vol. 928, no. 1, 2022, https://doi.org/10.3847/1538-4357/ac5024.

Rojas, Karina, et al. "The Impact of Human Expert Visual Inspection on the Discovery of Strong Gravitational Lenses." *ArXiv.org*, ArXiv, 9 Jan. 2023, https://arxiv.org/abs/2301.03670v1.

Recycling the Discarded: A More Efficient Approach to Waste

Student Researcher: Ashley C. Meyer

Advisor: Abigail Yee

Cincinnati State Technical and Community College
Chemical Engineering Technology

Abstract

One of the key processes that makes the International Space Station habitable for extended periods of time is the ability to purify and reuse water. This is a process done by multiple filters that remove impurities from waste liquids and discard them into space—but what if those impurities could be separated and repurposed? Urine has all the necessary components to formulate ammonium nitrate, a very effective high-nitrogen fertilizer—which would be used to facilitate fresh food options and limit the number of trips needed to restock resources on ISS.

This separation would occur before the liquids are purified and would be done by size-exclusion chromatography. The urine would travel through a column containing porous beads, separating the molecules by size. The ammonium and nitric acid would then be combined to form ammonium nitrate, and this would be used to fertilize the vegetation on the International Space Station.

Project Objectives

The purpose of this project is to research the plausibility of separating urine into its components to be reused. Using size-exclusion chromatography, nitric acid and ammonia would be isolated and then combined to form ammonium nitrate.

Methodology Used

All information presented in this research is sourced from various articles.

Results Obtained

Size-exclusion chromatography is a process in which porous beads are used to separate molecules by their size. The main chemical composition of urine includes potassium (K^+), urea (CH_4N_2O), uric acid—containing nitric acid ($C_5H_4N_4O_3$), creatine ($C_4H_7N_3O$), ammonium (NH_4^+), calcium (Ca^{2+}), and sodium (Na^+). Using a sealed piston, the liquid would be forced through a column containing a gel filtration resin. Ammonium nitrate has a particle size of about 384 micrometers, and due to its size comparative to other molecules present, would be one of the first particles to exit the column. These would be secured in a container separate from the remaining materials. After traveling through the column, the solution would then proceed through the current ECLSS water recycling system, to be purified into drinking water. The ammonium and nitric acid set aside would then be diluted with purified water and used in the current garden's irrigation system on the International Space Station.

Significance and Interpretation of Results

If size-exclusion chromatography is a functional process in a zero-gravity setting, this would allow for a variety of options with the materials filtered out of wastewater. Being able to separate materials into their individual molecules would help the International Space Station to take one step closer to being a self-sufficient system. In addition to all the possibilities it would open, the ability to nurture the

vegetation aboard the ISS with several nutrients they don't have access to would be vital in helping to sustain growth.

Figure 1. diagram of size-exclusion chromatography process

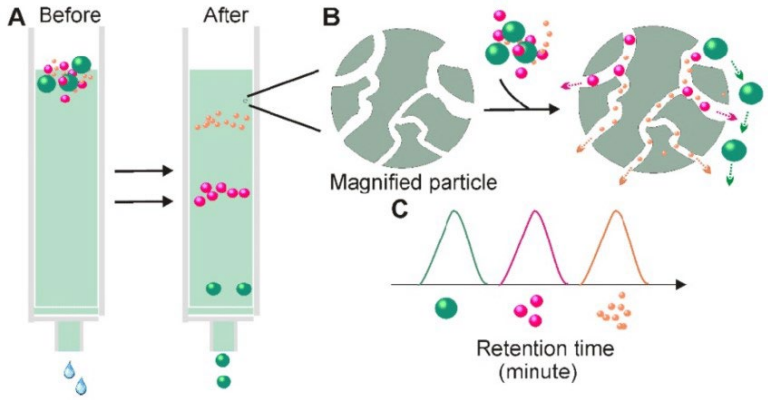

Future Work

The next step in evaluating if this would be a viable process for the International Space Station is performing quantitative, in-lab research. Specifically, the process of extracting chemical compounds from urine via size-exclusion chromatography in a zero-gravity setting. The effectiveness of high-nitrogen fertilizer on vegetation in zero-gravity would need to be tested as well. If both of those tests are effective, an assessment of changes needed to the current irrigation system will need to be conducted. Following that, a full cost analysis would need to be performed in order to evaluate if implementing a vacuum sealed size-exclusion chromatography column would be an effective long-term cost-saving measure.

Acknowledgements

I would like to thank the OSGC, Abigail Yee and Megan Erpelding for their support.

References

[1] Barry, P. L., & Phillips, D. T. (2000, November 1). *Water on the Space Station*. NASA. Retrieved from https://science.nasa.gov/science-news/science-at-nasa/2000/ast02nov_1

[2] Learning Chemistry. (2022, July 3). *Size Exclusion Chromatography*. Learning Chemistry. Retrieved from https://www.priyamstudycentre.com/2022/02/size-exclusion-chromatography.html#google_vignette

[3] Maggi, F., & Garg, P. (2017, January 30). Fragmentation of Ammonium Nitrate Particles under Thermal Cycling. Wiley-VCH Verlag GmbH & Co.

[4] Sarigul, N., Korkmaz, F., & Kurultak, İ. (2019, December 27). *A new artificial urine protocol to better imitate human urine*. Scientific reports. Retrieved from https://www.ncbi.nlm.nih.gov/pmc/articles/PMC6934465/#:~:text=Human%20urine%20is%20composed%20primarily,their%20values%20in%20blood%20plasma.

[5] Wang, T. (n.d.). *Principle for size-exclusion chromatography-based exosome isolation*. ResearchGate. Retrieved from https://www.researchgate.net/figure/Principle-for-Size-exclusion-chromatography-based-exosome-isolation-When-passing-a_fig5_33954493

Education Scholars

Weather Throughout the Year

Student Researcher: Morgan R. Boldt

Advisor: Laura Dell

University of Cincinnati
Early Childhood Education

Abstract
In this lesson, the class will measure weather over the school year. The students will set up a small area outside where they can put their tools to collect data. The class will put a thermometer, barometer, hygrometer, anemometer, and a rain gauge in this area to collect the data. They will have a chance to create some of these tools in the classroom and have their own creations out there. We will have real tools out there to get a more accurate measurement. We will start off by explaining each of the tools that will be used and how to read the measurements. As a class every day, we will take a walk to this area to collect the data. Each student will get a turn to read off the data and graph it on a big chart in the classroom. We will have two charts, one chart will be for that month, and the second one will collect the information for the whole school year. At the end of each month, we will take a moment to look at the data and have a discussion about anything they notice or patterns they see. This will occur every month until the end of the year. At the end of the year, they will look at all the data they have collected. This will conclude with another big discussion with the class about what we learned about weather. This will help the students when they talk about weather in the future, like when they talk about weather patterns on different planets.

Project Objectives
The learning objective of this project is for kindergarten students to understand that weather has short-term and long-term patterns. The students will be creating a graph to help track the weather changes throughout the months of school. This lesson falls under the Kindergarten Ohio Science Standard: K.ESS.1: Weather changes are long-term and short-term.

Methodology Used
This unit will be split up into three parts: the lesson reviewing everything, daily data collection, and an oral assessment at the end of the year. The first part will be reviewing the different types of weather and the tools meteorologists use to measure the weather. The students will be creating the tools to reference throughout the year. The second part occurs throughout the year. We will be graphing the results of the weather on different graphs for each month. The last part will be an oral assessment where the student needs to compare the weather graph. They will need to notice short-term and long-term patterns with the weather.

Results Obtained
I have not yet been able to test out my plan. I plan on using this lesson in the future, hopefully this summer with my daycare class!

Figures/Charts

This is an example of the graph where the students will be tracking the weather.

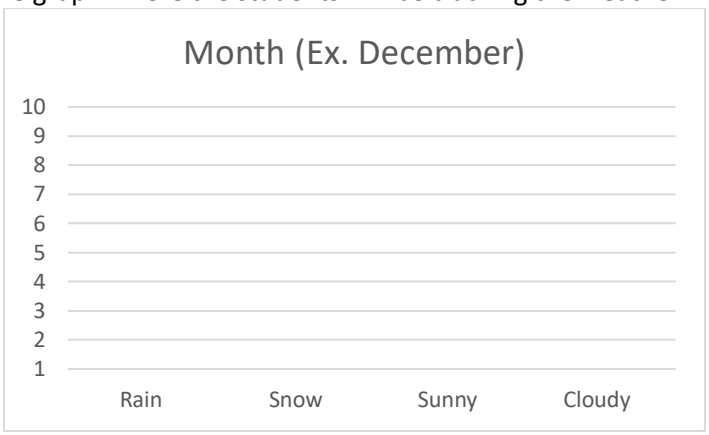

Conclusion

This activity is aimed towards kindergarten, however this can easily be altered for older grade levels as well. The activity helps the students understand how the weather has patterns. Building and utilizing specific tools that measure weather will help them understand how the process works. This activity will give the students a better understanding of weather and will help to apply it to future learning.

Roof Structures: Avoiding Collapse

Student Researcher: Makenna R. Chappell

Advisor: Dr. Todd France

Ohio Northern University
Department of Engineering and Center of Teacher Education

Abstract

Student groups will act as a roof design firm for buildings in northern Ohio. Their design firms need to design new roof systems maximizing peak load and minimizing the overall cost of materials. Many structures have been failing due to increased levels of snowfall, so their roofs will need to support the snow levels expected in their region. The team will design a prototype of a truss system out of the provided materials, and using a force gauge, test how many pounds of force (using a force gauge) the roof can take before collapsing. The teams will then perform a cost analysis of their truss system and retest to find the best combination of strength and cost for their roof.

The goal of this activity is to gain hands-on experience with the engineering design process through prototyping and redesign, as well as mathematics experience in working in scale and performing cost analysis. Students will come out of this activity with knowledge of structural engineering, strengths, trusses, communication and teamwork skills, and more confidence in mathematical modeling.

Project Objectives

Students will be able to explain what engineers consider during long term projects. They will discuss cost, material use, and even how engineers perform life cycle assessments. Students will also be able to explain how engineers work through the engineering design process and create prototypes. THis is crucial for beginning engineering students to learn so they develop the skills of scale modeling and prototyping early on. Students will learn how to use a force gauge and learn about snow loads

Methodology Used

This activity starts with discussion about roof collapses in Ohio during the winter. Students often ask about real world connection, so beginning the activity with such helps with student engagement. A video will be shown of a roof collapse due to increased snow load, and students will discuss why engineers may be involved in developing a solution for this clear issue. Students will then be presented with the materials and presented with the process of building their truss prototype and how to test.

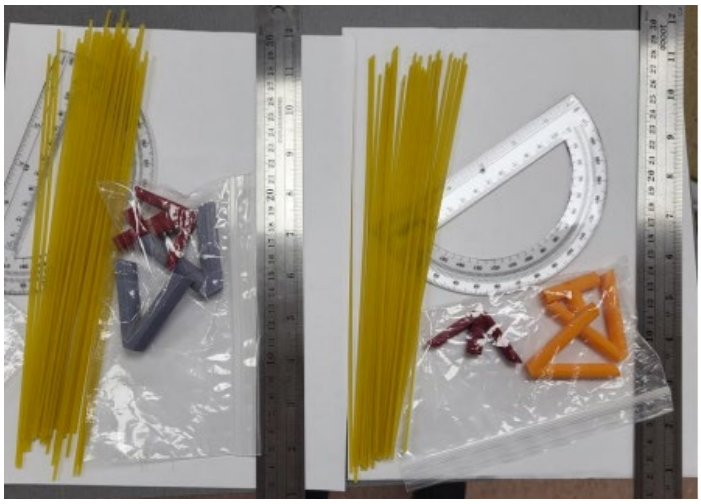

Figure 1. Material kits for students

Results Obtained

This activity was conducted for the first time in December of 2022 with a group of high school freshmen in Wapakoneta high school. Students were engaged with the hands-on activity and thought critically throughout. The following results were obtained from the six student groups in the class and shows the correlations between their truss prototypes' peak load and the total pieces of spaghetti they used in their final prototype.

[redacted]	Peak Load (lb)	Pieces of Spaghetti
Team 1	3.2	8
Team 2	2.57	13
Team 3	1.3	8
Team 4	3.98	8
Team 5	0.71	15
Team 6	1.18	12

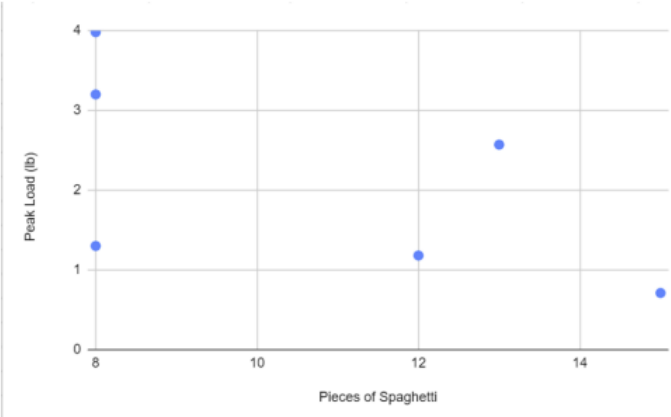

Figure 2. Results from students

Students were then asked to reflect on what they found worked to increase the strength of the truss and what they thought engineers found most important in the engineering design process.

Engineering Exploration Through Rover Tires

Student Researcher: Abigail G. Collins

Advisor: Dr. Todd France

Ohio Northern University
Department of Engineering Education

Abstract

Through this activity, students will build small model rover bases with a DC motor. Using the Engineering Design Process, they will be able to test out the speeds of different designs for the wheels using various materials and sizes. These can be tested for speed on various Mars-like surfaces. This will be simulated with a sandy course, an inclined course, and with rocky terrain. This will encourage students to think like engineers to optimize their design to balance out drawbacks of different applications.

This project can bring up topics such as friction, surface area, size, mass, materials, research, and testing procedures as well as aligning with the SMD. This activity provides a real-world application as their process of modeling and testing is similar to the process engineers had to go through for the Curiosity rover's tires at NASA Glenn. Students can spend time researching beforehand. Students will also have to measure out quantities such as mass, circumference, time, and distance. Friction can also be discussed as they choose materials for their tires. Overall, this activity allows students to dive into a hands-on project, mirroring real engineers, to test and reiterate a rover tire design that they can justify.

Project Objectives

By the end of this activity, students should be able to:

1. Develop a deeper understanding of and explain the Engineering Design Process through an iterative process of brainstorming, designing, building, testing, and reassessing.
2. Collaborate as a team to create a car.
3. State observations and patterns with the data.
4. Share their findings with others.
5. Measure out distance and record time.
6. Complete unit conversions successfully.

Methodology

Students in groups of about four are first given a brief background on NASA's Simulated Lunar Operations (Slope) Lab and the process engineers go through to create tires that can go over rocks, loose surfaces, and uphill. After a brief background on a simple, series circuit consisting of a battery, battery adaptor, motor, and Lego adaptor, students are presented with their challenge for the day. They must create a Lego rover to use as a base for testing. Then, given assorted crafting materials as seen in Figure 1, they must brainstorm unique tire designs without using traditional rubber tires. Demonstrated in Figure 2, group designs must be sketched and planned out before construction could begin.

After creating the base of the rover, testing of the tires started. As shown in Figure 3, a 10-foot ramp with Lego obstacles simulated Slope Lab. Groups would record the time it took the rover to fully climb that ramp. This would be repeated for three tire designs. Groups had to record their data, calculated speed, and observations, as seen in Figure 4. Finally, groups had to communicate their findings with the class: what their group tried, the best speed, why they thought it happened, any observations, and what they would do differently.

Results

Overall, groups found that the rubber bands did the best, and that is most similar to the traditional rubber wheel. As seen in Figure 5, some groups did find that a pipe cleaner design did help them climb over obstacles better. Half of the groups did struggle to fully finish their rover base in time to evaluate and needed assistance.

Significance and Interpretation of Results

In the future, rubber bands can be taken out of the material list in favor of supplies that will force students to think outside the box more. Another change could be giving instructions to students on how to build the base. Overall, this activity can be taught to many ages ranging from middle school to late high school. There are ways to incorporate it into physics classes too by going more in depth into friction calculations, wheel surface area, wheel circumference, and car mass. It can also be done with a ramp using real sand and rocks.

Figures

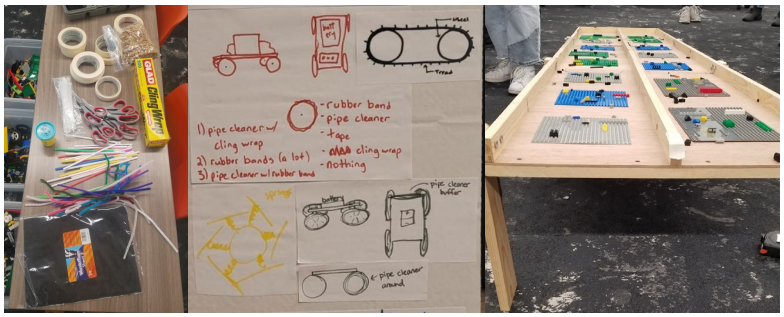

Figures 1-3: Crafting materials, group sketches, and ramp

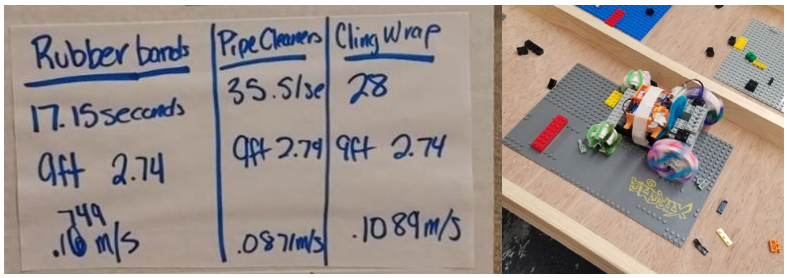

Figures 4 and 5: Group data and rover climbing ramp

Acknowledgments

Thank you to Ohio Northern and Dr. Todd France for providing support and materials for this activity. A special thank you to ONU's chapter of the Society of Women Engineers for their help in the facilitation.

Gravity, The Greatest Debate of All Time and Space

Student Researcher: Jacob T. Cowan

Advisor: Dr. William Theisen

Ohio Northern University
Physics Department

Abstract
This lesson will follow the unit on Universal Gravitation this lesson follows the Ohio Science learning standard of P.F.2: Gravitational force and fields and incorporates standards from multiple other content areas. It will be a short two-day lesson. Students will be split into two groups via a random team generator. One group will research Einstein's version of gravity and another will research Newton's version of gravity. The research will take place for a whole 45-minute class period. On the second day of class, each group will argue why their group has the correct version of gravity. Teachers may need to have guided questions to encourage debate between the class. Students should find that in certain areas it may be better to use Einstein's version and in others, it may be better to use Newton's version.

Project Objectives
Students will be able to identify the Newtonian idea of gravity along with Einstein's idea of gravity. Students will be able to identify similarities and differences between the two ideas allowing them to create discussion or debate between them. This lesson will allow students to understand gravity at a deeper level. Most high school physics classrooms focus on Newtonian physics and do not incorporate any modern physics. I wanted my class to have a little insight into the upper levels of physics without having to deal with high-level math, having a research and debate-style lesson allows students to dig into the material without having to learn high-level math.

Methodology
This lesson is going to be split into 2 days following a unit on Universal gravitation:

- Day 1- Research and Data Analysis
  - This day will consist of splitting students up into two groups. Students will be able to talk to other students within their own group.
  - Students will be able to research using their school devices how to defend their side of the debate while also researching how to prove the other group's defense wrong.
- Day 2- Debate Day
  - Students will debate on what idea of gravity is correct. If the debate comes to a standstill I will ask one of around 12 questions I have prepared to try and spark conversation

These lessons are a mix of learning strategies and strategies that do not get used a lot in STEM classrooms:

- Day 1 the students use social strategies and learn from each other, also students are using the internet to research the two ideas.
- Day 2 the students are going to be using social strategies.

Shirley Simon, Sibel Erduran, & Jonathan Osborn wrote a research paper on the debate style within the class is beneficial to student growth of knowledge. "Learning to Teach Argumentation: Research and Development in the science classroom"

Results

I will be unable to do this lesson in my field placement where I am placed this semester
Because it does not line up with the order of the units. If I am able to teach this lesson in the future, here is how I would plan to assess the students: The students would have an assessment of the universal gravitation unit before this lesson Students will be graded based on multiple different areas including cooperation during the research phase, communication skills with classmates, and debate participation.

Conclusions

This lesson is aimed at high school students. The students may have trouble with the mathematical concepts of general relativity theory but they should understand conceptual ideas. I have very high hopes for this lesson and I think it will be very engaging for the students. I expect students to work on verbal communication skills, critical thinking, and research skills. All of these skills will be used in classes in college and their jobs later in life.

Acknowledgments

I would like to acknowledge the Ohio Space Grant Consortium for my scholarship and the opportunity to participate in and attend each of the conferences. I would also like to thank my advisors for the help I received throughout the process of this project.

Water Conservation

Student Researcher: Mamdouh M. El-Mahdy

Advisor: Dr. Brandi Seither

Baldwin Wallace University
Department of Education

Abstract

Students must learn the importance and applications of water conservation. Fortunately, my students and I live in Ohio, which does not have water shortage issues. However, places worldwide and even within the U.S. are undergoing severe droughts, amplified due to Climate Change. Even if we are not experiencing a water shortage, there is no guarantee that we will not experience one in the future with climate change. Fortunately, when residents see the importance of conserving water, they can limit the effects of droughts. For instance, Cape Town, South Africa was counting down to their last day of water, but when the residents cut back their water usage, they pushed back the date of no water until they eliminated it. Let's teach our students when it is avoidable rather than when it is a necessity.

Project Objectives

By the end of the lesson, the students will be able to:

- ✓ Fill out a data collection chart to track their water usage
- ✓ Detail the importance of water conservation
- ✓ Identify methods of water conservation
- ✓ Apply the methods of water conservation to their own life
- ✓ Predict how the water usage would change when they apply methods of water conservation
- ✓ Discuss with peers their interpretation of results from data provided in images
- ✓ Create a poster that advocates for water conservation

Methodology

1) Students will first track their water usage over a week using a data collection sheet from NASA's educational resources.
2) After collecting the data, the students will learn about water conservation, its importance and how to apply it in their lives.
    a. At this stage, we would use the presentation and supports provided by NASA GPM.
3) From there, they will predict how their tracking results would change if they used what they learned.
4) Then they will re-track their water usage while applying various water conservation skills they have learned in class.
5) They will then analyze their results by comparing the before and after and determine whether their prediction came true.
6) From there, the students may discuss how these small changes can make a difference and potentially advocate for further conservation efforts beyond their own lives to that of their community or beyond.

Results

Unfortunately, I was not able to implement the lesson in my classroom because it is academically above the level of my students. However, there are different methods I would have used for assessing their learning. I would check:

- that they know how to fill out the data collection chart on their water usage.
- that they identified reasons for conserving water.
- that they correctly labeled some methods for conserving water.
- the students' predictions and interpretation of results from applying some water conservation in their life.
- that they can interpret the results from an image.
- that they can create a poster which advocates for water conservation.

Acknowledgements and References

I appreciate NASA GPM for providing the lesson plan and supports. I also thank my advisor Dr. Seither for her guidance.

NASA GPM. (n.d.). Water Conservation. NASA. Retrieved April 20, 2022, from https://gpm.nasa.gov/education/lesson-plans/water-conservation

Creating an Ecosystem on Another Planet

Student Researcher: Cora L. Gill

Advisor: Laura Dell

The University of Cincinnati
Major: Secondary Education Integrated Sciences: ChemistryMinor:
Biological Sciences

Abstract
This lesson would be based on the basic biological factors of life for a freshman biology class. Iwould begin with a lesson on the characteristics of life, teaching the students about the in-depthrequirements for each characteristic. Then over the next two or three days, the students would work in groups of 3-4 to discuss the specific requirements for a complete ecosystem in space.
Each group would be assigned a planet other than Earth, where they would have to design anecosystem based on what is present on that planet (assume a flat surface for gaseous planets).
The groups would have to use what is already at their disposal on their planet and determine
what they need to bring/create or design. Students would then present their findings to the classin a formal presentation using diagrams, PowerPoint, physical models, or any other form of presentation.
It is essential to allow students to think outside the box, giving them a chance to think creativelyabout a problem. This is the best way to learn. Because of this, I made sure that my lesson plan allowed for this creativity of thought and discovery.

Project Objectives
This lesson aims for students to think critically and apply the knowledge they have learned overthe last two years in their science courses.

1. Students will be able to understand and explain the eight characteristics of life
2. Students will be able to explain the requirements of an ecosystem
3. Students will be able to describe the criteria for an ecosystem on another planet

Lesson Plan
This unit is split into two parts, the lesson, and the project.

Lesson: In class, the students will be taught about the eight characteristics of life. They will be given multiple activities in which they will need to use what they have been learning. The discussion of the characteristics of life will take place over three days. The final two days of thatweek will be a review of ecosystems. The students will be reminded of the different kinds of
ecosystems seen on Earth, and there could be time for a small trip outside the school to see someof these ecosystems in action.

The Project: The following week, students will be split into groups of three or four and assigneda planet in our solar system. Using what they learned the week before, they will have to design
an ecosystem that could survive on their planet. Students will also be expected to consult
NASA-published works about the different planets and what is already present there. In the event that an ecosystem cannot be achieved on a planet, the students will be expected to explain why intheir report. The students will have the full week of class to research and gather their information. On the final day of class that week, the groups will present their findings to the
class in a formal presentation using any means they want (PowerPoint, diagrams, videos,physical models, etc.)

Conclusion
For this lesson, I really wanted students to work with their peers and think critically about a problem. I didn't want the answers to be easy to find or obvious. I wanted them to research and really learn about their planet and what would need to happen for life to be sustainable. I haven'thad the opportunity to use this lesson in a classroom, but I hope to have the opportunity to do it in the future.

Research in Space

Student Researcher: Ethan B. Hatch

Advisor: Dr. William Jones

Cedarville University
AYA Science Comprehensive Education

Abstract
The education project "Research in Space" is a project based learning activity using the resources provided on NASA's website. This project allows students the flexibility and scaffolding to explore the world of science using the tools provided by NASA, allowing their creative and scientific minds to explore the universe. During this project students will develop skills like critical thinking, problem solving, collaboration, ingenuity, and presentation skills. The students will be grouped and prompted with the big-picture question "why do research in space?" from there students will be provided scaffolding to help answer this question. Some of the major scaffolding steps include: Why is space so special? What experiments have already been conducted in space? What future research will be conducted in space? How does research in space differ from research on earth? These leading questions will help guide student discovery, providing them the support and direction needed for them to be successful. The students will then collect their findings in an appropriate presentable form of their own choosing and present the material to the class. This process will require students to take ownership of their learning and invest in lifelong skills.

The objectives of this lesson are as follows:

1. Students will synthesize research
2. Students will present information with clarity
3. Students will make applications between terrestrial and astral science
4. Students will be able to explain the effect of gravity on research

Essential Questions:

1. Why is space important?
2. How does scientific research effect humanity?
3. How has technology changed the way we understand space?

Methodology Used
This multi-day activity is based on project based learning (PBL). This form of instruction provides scaffolding and facilitates student independence. It encourages student ownership of learning, which increases engagement and effort. PBL allows students' inquiry to be the driving force behind their own learning. The goal of using complex questions or problems is to develop and enhance student learning

by encouraging critical thinking, problem-solving, teamwork, and self-management. The project's proposed question drives students to make their own decisions, perform their own research, and review their own and fellow students' processes and projects.

Lesson

Students will be assigned groups, preferably groups of 4 students. Each group will choose one of NASA's "Space Station Research Experiments" on their website. The website provides an extensive resource for students to find something that peaks their interest. The research conducted includes Biology and Biochemistry, Earth and Space Science, Educational Activities, Human Resources, Physical Science and Technology. Students will use resources provided by NASA to create a presentation for the class. Students will have to find an experiment, understand and annotate the article provided on the website, use two resources, and explain why this research is being done in space. Students will have two days in class to work on this project and will present on the following day. Students will be graded on their annotated article and research presentation. It will be roughly a 10 minute presentation. Students should have at least two resources: one from the list of NASA projects and an additional source.

Results

I have not been able to formally implement this lesson in a classroom setting. However my expectation is that the lesson would work well in some classrooms. Classrooms with higher levels of independence would be able to thrive during this project. Some classrooms would need additional scaffolding to ensure they will be successful throughout the project.

Conclusion

Using the resources provided by NASA students will be able to explore research in space. The project provides scaffolding and promotes student independence, critical thinking, problem-solving, teamwork, and self-management skills. The lesson plan encourages students to take ownership of their learning and invest in lifelong skills. By using complex questions as the driving force, students are motivated to make their own decisions, perform their own research, and review their own and fellow students' processes and projects.

Acknowledgements and References

What is Project-Based Learning? | PBL Training & Certification | Cultural Exchange, Education, & Professional Development Nonprofit | Educators of America. (2018, August 3). Cultural Exchange, Education, & Professional Development Nonprofit | Educators of America |. https://www.educatorsusa.org/our-programs/professional-development/project-based-learning /?gad=1

Space Station Research: Experimentshttps://www.nasa.gov/mission_pages/station/research/experiments_category/

Will Gravity Impact the Mass of the Class?

Student Researcher: Andrew D. Horton

Advisor: Dr. Brian Boyd

Wright State University
Department of Education

Abstract

This lesson is based on the 8.PS.1 standard in Ohio's Learning Standards for 8th grade science. Before the lesson begins, the teacher will show and articulate the learning objectives to be achieved by the end of class. This lesson begins with students completing an inquiry-based activity. This activity is done after students have watched the short video of astronaut Eugene Cernan jumping on the moon. Students will be prompted to explain what they know and observe from the video. This will be recorded in the K column of the KWL Chart. Next, students will be prompted to ask questions they want to have answered that relate to the video. These questions will be recorded in the W column of the KWL Chart. Then, students will be given the necessary materials to create an air-powered rocket. To create the air-powered rocket, the teacher will display the NASA at Home: Rockets in Motion – Newton's Third Law video. Once students have created their own rocket, students will be placed into partners. Each pair of students will be given a planet in our solar system to research as well as a small poster board. Students will research their planet to find its acceleration due to gravity as well as other characteristics of the planet, such as the planet's estimated mass. While conducting research, students will be given two NASA resources in the form of websites. One of these websites lists numerical data about each planet in our solar system, such as the mass or length of time for one rotation around the sun. The second NASA website lists data that students may find interesting or relevant to the planet like the color, or how many moons the planet has. This information students research and collect will be recorded and designed onto the poster board provided to their pair. After all groups have completed their posters, they will tape their posters along the walls of the classroom with at least 2 feet between each poster. Students will then be provided with the Exploring Mass and Weight on Different Planets data recording sheet. Next, students will stand in a large circle in the middle of the classroom. Students will choose which planet's poster they would like to launch their rocket towards so they may 'land' on that planet. Students will launch their rocket to the planet of their choice. Students will record the new planet's gravitation pull, new planet's mass, and the student's own mass and weight while on the new planet; this will be recorded on the Exploring Mass and Weight on Different Planets Data Recording Sheet. Students will repeat the process of launching to different planets and recording the new planet's gravitation pull, new planet's mass, and the student's own mass and weight while on the new planet 4 more times. Then students will use data from their table to support their answers and claims in the conclusion questions. These conclusion questions prompt students to find patterns or relationships between the planet's gravitational and the student's mass and weight. Also, these conclusion questions prompt students to search for a relationship between the planet's mass and the planet's gravitational pull. Class discussion will be held for students to discuss their answers to the conclusion questions. The teacher may address areas of struggle and misconceptions during the classroom discussion. Lastly, students will complete the L column of the KWL Chart. The L column is for students to write what they learned over the course of the lesson. After the lesson is complete, the teacher will explain how the activities led students to achieve the learning targets.

Project Objectives

By the end of this lesson, students will be able to:

- Calculate their weight on various planets using their mass and the planet's acceleration due to gravity.
- Use data to explain that the gravitational pull of an object is directly related to the mass of that object.
- Utilize data to explain that their weight increases with a stronger gravitational pull and decreases with a weaker gravitational pull.
- Explain the difference between mass and weight by stating that weight must change due to gravity and mass is constant.

Methodology Used

Inquiry based learning is a method of teaching students that involves students exploring a concept by asking questions, investigating the concept, and constructing answers. During inquiry-based learning, students are the leaders in their educational experience while teachers serve as a guide. To act as a guide of inquiry-based learning, teachers have multiple responsibilities. While students ask questions, the teacher can prompt students to ponder content related concepts. Another responsibility the teacher has is to provide helpful insight of what the student should be focusing on or patterns the students should search for while students investigate the concept. To provide this helpful insight, the teacher monitors student progress and gives immediate feedback as and aid. To take ownership of the learning experience, students must make observations and ask questions about a phenomenon. This phenomenon is meant to spark student interest and get students curious about the concept being taught. After posing questions, students actively participate in investigating the concept. Lastly, students use the information gathered during the investigation to create answers to the questions previously posed. Inquiry based learning helps students participate in scientific practices by observing, experimenting, analyzing data, and drawing sound conclusions from that data. Also, inquiry-based learning relates to the theory of constructivism. The theory of constructivism revolves around the student as they construct new knowledge above previous knowledge. As students make observations, experiment, analyze data, and make conclusions, they are constantly building upon their own previous knowledge.

Results Obtained

I have not yet been able to fully teach this lesson to students in a class setting. However, I was able to complete portions of the lesson in a small group of students during an advisory period at my placement for student teaching. I have fully created a lesson that could be completed in one 50 minutes class period but may span an entire block period or two 50-minute class if more trials are done by students as they explore different planets. Because this lesson is inquiry-based, the results of this lesson should conclude in a manner, so students achieve the learning targets through their own discovery.

Acknowledgements

I would like to thank the Ohio Space Grant Consortium for this amazing opportunity and experience.

References

Planetary fact website for students to use as they research their assigned planet.
https://nssdc.gsfc.nasa.gov/planetary/factsheet/
Characteristics of different planets website for students to use as they research their assigned planet.
https://solarsystem.nasa.gov/
NASA STEM channel on YouTube used for students to create their rockets.
https://www.youtube.com/watch?v=-lsTfbigdGk

The Human Impact on Global Climate

Student Researcher: Matthew S. Ripple

Advisor: Dr. Nidaa Makki

The University of Akron
LBJFF School of Education

Abstract
Over time, data trends have shown that human actions have a large, and often negative, impact on Earth's climate. It is extremely important to teach students about this impact so they can make informed decisions in their everyday lives. This lesson is meant to give students an opportunity to learn about the impact of human actions on climate change. The lesson focuses on the effect of greenhouse gasses in Earth's atmosphere on global temperature. Students engage in the scientific practices of using models, planning and carrying out investigations, analyzing and interpreting data, and constructing explanations to learn more about the human impact on the global climate.

Learning Objectives

1. Students can analyze data to determine the impact of carbon dioxide on temperature in a closed system.
2. Students can use a model for the greenhouse effect to gather data and determine the impact that greenhouse gasses have on global temperature.
3. Students can use a model to determine the impact of ice on global temperature and use this to show how a positive feedback loop is developed.
4. Students can use NASA data on global temperature, CO2 concentration, and arctic sea ice to construct an explanation for the impact of atmospheric CO2 concentration on the rise in global temperatures.

Methodology Used
When designing the layout of the lesson, the methods used were meant to provide students with an opportunity to engage with real life data to help them understand the idea of global climate change. The foundation of this method comes from the Next Generation Science Standards' focus on Science and Engineering Practices. These practices help students understand how scientists do science and better equip them to engage in sensemaking as opposed to memorization. This method is supported by research (National Research Council, 2007) that shows that students learn science best when they are able to address their preexisting framework of the topic and interact with data to improve their framework. The activities in this lesson support students' learning progression to improve their understanding of the human impact on the global climate.

Throughout this lesson, students are challenged to apply data gathered through scientific practices to construct explanations regarding the impact of human actions on global climate trends. There are three main ways the students gather evidence to expand their framework of global warming. First, the class investigates the impact of excess carbon dioxide on air temperature through completing an experiment measuring air temperature in an erlenmeyer flask containing air with and without carbon dioxide when both are exposed to light from a lamp. The air temperature will increase more in the flask with carbon dioxide which may be hard for students to grasp because there is no visible difference between the two flasks. In order to better understand this confusing phenomenon, students explore the mechanism

behind the difference in temperature change using online simulations developed by PhET Colorado. The first simulation gives students the opportunity to interact with a model that lets them view the behavior of individual greenhouse gas molecules when exposed to light, which are not visible to the human eye. This will allow students to better understand why greenhouse gasses contribute to an increase in air temperature. In the second simulation, students observe how greenhouse gasses can increase temperature on a global scale. Students also use the Greenhouse Gas simulation to learn about the impact of decreasing arctic sea ice on global temperature. After each of these activities are complete, students create a summary table which details what they learned from each activity and how that contributes to their overall understanding of global warming.

After students use the experiment and models to learn about the mechanisms of global warming, they use data from the NASA Vital Signs website to construct explanations for current global temperature increases. Students will use a Claim Evidence Reasoning (CER) template to support or refute the idea that human activity is increasing global warming. This will allow students to connect the ideas they learned in the activities in this lesson to the current real world data related to global climate change. Students will also use this information to further discuss the push by global leaders to decrease greenhouse gas emissions. Overall, this lesson helps students learn how to use evidence from scientific investigations and real world data to evaluate claims and understand the impact of human actions on the global climate.

Results and Interpretations

I have not been able to teach this lesson in a classroom setting yet, but I am confident that it will serve as a valuable resource for my future teaching endeavors. The overlap of learning from models and learning from real world data will support students as they engage with their preexisting framework of global climate change. Each activity has one learning objective attached so the effectiveness of the lesson would be judged by the degree to which students meet the learning goals as described for each activity. Students who are able to meet the learning objectives would have a better understanding of global climate change and the associated data. They would also be better equipped to work in a team and use data to support a claim.

Acknowledgements and References

Gabra, S. [CEB Cambridge]. (2021, April 2). *Demonstrating the effect of CO2 on global warming* [Video]. Youtube. https://www.youtube.com/watch?v=lSqx0AkmXCs

Global Climate Change: Evidence. (2008, June 15). Retrieved January 14, 2015, from http://climate.nasa.gov/evidence/

National Research Council (2007). *Taking Science to School: Learning and Teaching Science in Grades K-8*. Washington, DC: The National Academies Press. https://doi.org/10.17226/11625.

NGSS Lead States (2013). Appendix F. *Next Generation Science Standards: For States, By State*s. Washington, DC: The National Academies Press.

Levels of Engagement, Prediction, and Discussion for Students with Disabilities When Given a Lesson on Deep Space

Student Researcher: Chaz T. Stump

Advisor: Dr. Stephen Kroeger

University of Cincinnati
College of Education, Criminal Justice, Human Services, and Informational Technology Department of Special Education

Abstract
This lesson was designed in alignment with the Ohio Standards for 5th grade science, using the materials provided by NASA related to deep space. At the beginning of the lesson, background knowledge will be activated by asking students to write on a post-it note what they already know about space and then to make a prediction about what they think deep space is. I will then play a video NASA created about deep space. After this, students will get into groups and select one of the five hazards NASA outlines for them to research further. They have the video that corresponds to each hazard in which they are to watch and select a media to make a presentation on. This can be a PowerPoint, trifold board, or another media of choice. They are to discuss what hazard they selected, how it affects astronauts on an individual level, how it affects the entire team of astronauts, and their overall opinion of the hazard. After each presentation, students will ask each group questions about their presentations to engage in discussion. Students will compare and contrast their predictions from the post-it note and then complete an exit slip at the end to track data on what they learned from the lesson. There is a set of planned supports in place for students to ensure that the lesson is accessible for each student in the class. The contingency plan is designed to provide examples and clarity for students on what is being asked of them, such as providing examples of what opinion they could put in their presentation. In addition, I as the role of the teacher will have a presentation prepared to model for the students so they knowledge about what to do.

Project
Before Phase: Students will make a prediction on what they think deep space is and to write down on a post-it notes what comes to mind when they think of space. (Prediction)

During Phase: Get into groups of 4, watch the NASA overview video on the hazards of deep space, then pick one of the five hazards (Isolation, Environment, Radiation, Distance, Gravity), watch a video on their specific hazard, then create a PowerPoint that answers three questions: How it affects the individual, how it affects the team, and their overall opinion. (Engagement)

After Phase: Students are to present their presentations and then the class will ask 1-2 questions about their work, then they will answer an exit slip related to what they now know about deep space. (Discussion)

Objectives
Given a 5th grade science lesson on deep space, students will be able to use NASA content to engage in explanation, prediction, and discussion through creating a 4-slide presentation, asking questions to each other, and completing an exit slip by the end of the instructional period.

Methodology Used

This was obtained in collaboration with the lesson plan template developed by the University of Cincinnati Department of Special Education. The procedures within this instructional planning incorporate a before phase to gain student attention, activate background knowledge, and pre-teach. The during phase is how students can self-monitor their learning and engage in the learning process. The after phase is how students will remember learning and integrate into existing knowledge. This ensures that there are planned supports within the lesson to make the curriculum accessible to students with learning disabilities, promote self-directed learning, and generalize it into their current knowledge. The planned supports I integrated into the methodology were: Support with spelling, visual schedules, small group setting, explicit instruction, modeling as needed, prompts, AAC device when applicable, support with spelling, extended time, read aloud, teacher modeling, clarity, and rephrasing of questions. I selected this group to participate in this study because the classroom is instructing at the 5th grade level and it is a cluster classroom, meaning there are students on the general education track and students on an IEP track in collaboration with their intervention specialist.

Results Obtained

100% of the students met the objective so my hypothesis was correct. They were able to participate in prediction, engagement, and discussion. The data collection methods are post-it notes as a pre-assessment, the permanent product of the PowerPoint, and the exit slip as a post-assessment.

Significance and Interpretation of Results

Expanding STEM pathways for students with disabilities is an important mission and pillar with this research. By looking at the results, it is evident that these pathways and lessons can be implemented for these students with planned supports to make the content accessible for learners on an IEP. With intervention provided by the intervention specialist, collaborating with the science general education teacher, students are able to experience what STEM education has to offer, and due to the fact that 100% of the students met the objective that is structured with the methodology and the three phases of learning, the research backs that up.

Acknowledgments and References

UC Department of Special Education
Dr. Stephen Kroeger
Ohio Space Grant Consortium
Adams, J. (2021, September 7). *Hazards to deep space astronauts.* NASA. Retrieved April 6, 2023, from https://www.nasa.gov/stem-ed-resources/hazards-to-deep-space-astronauts.html

Bottle Rockets and Trajectory

Student Researcher: Anya zurBurg

Advisor: Ms. Sarah Gilchrist

Cedarville University
Department of Mathematics and Department of Teacher Education

Abstract
This project involves calculating the trajectory of bottle rockets. The lesson is designed for upper middle-school or high school students and could be modified easily to fit the content of a geometry or precalculus/ trigonometry class. The lesson begins by exploring the mathematics behind the calculations used for trajectories of projectiles. Once the students have a grasp on the mathematical part, the project investigates some examples of projectiles, and the students see how accurately they can predict their paths. Finally, the project ends with the students, having already made their predictions, going outside and launching the bottle rockets and seeing how closely their predictions come to the measurements they make.

Objectives
By the end of the unit the students will be able to:

1. Students will be able to use trigonometry to calculate the maximum height of their bottle rocket's trajectory.
2. Students will be able to use trigonometry rules to find the angles and sides of triangles.

Methodology
The primary teaching approach of this lesson is cooperative learning where the students work together in groups to both build the rocket and calculate the maximum height.

- This activity was created using ideas from the NASA lesson plan on "Sine-Cosine-Tangent" in combination with "Water Rocket Construction".
- Students will first learn how to use trigonometry and the data they gather, to calculate the maximum height. The students will work in groups to construct their rockets and do the calculations.
- The students will launch their bottle rockets and use the angle at which they shoot their bottle rockets and the distance from there to where it lands to figure out the maximum height of their rocket.
- Students will be assessed on the lab report that they write in their groups at the end of the experiment.

Discussion Questions

- Comparing with your classmates, what angle of inclination gave your rocket the highest distance? Why do you think this?
- What is the primary trigonometry rule we can use in this experiment?
- What other factors might influence your calculations?